The Dissertation Committee for Aram Lyu Certifies that this is the approved version of the following Dissertation:

Myeloid cells provide critical support for T-ALL in vivo

Committee:

Lauren Ehrlich, Supervisor

Amy Brock

John Digiovanni

George Georgiou

Vishwanath Iyer

Myeloid cells provide critical support for T-ALL in vivo

by

Aram Lyu

Dissertation

Presented to the Faculty of the Graduate School of

The University of Texas at Austin

in Partial Fulfillment

of the Requirements

for the Degree of

Doctor of Philosophy

The University of Texas at Austin

December 2020

Dedication

This dissertation is dedicated to my family

Jinseok, Hyeongsook, and Wooram

who have always been there for me.

Acknowledgements

I am incredibly grateful to have had the opportunity to learn from my advisor Dr. Lauren Ehrlich. She is one of the most passionate scientists I have ever seen. From the moment I first met her, I was inspired by her love for T cells, which guided me to my journey in T-cell leukemia (T-ALL). Her enthusiasm for science has always been motivational for me during my entire PhD training. I am truly thankful for the excellent example she has provided as a good scientist. I appreciate all her contributions of time and ideas to make my PhD training productive. I quite simply cannot imagine a better advisor. Besides my advisor, I would like to thank the rest of my PhD committee, Drs. Brock, Digiovanni, Georgiou, and Iyer, for their professional guidance and comments.

My sincere thanks to the current members of the Ehrlich lab. Hilary for always being very helpful for research and making this lab a great place to work. Yu, Jay, Damaris, and Pablo for being a great source of good advice and friendships. Seohee and Ryan, we are an awesome T-ALL team. Thanks to Seohee for always being willing to help analyze the terrifying in vivo experiments, and Ryan for helping me with my writing. I also thank the past members of the lab: Todd, Jessica, Zicheng, Sanghee, Hiran, and Rachel. Especially, I would like to thank Todd for helping me get up and running when I knew nothing about T-ALL, and Zicheng for his analyses of transcriptional data from pediatric T-ALL patient samples. A special thank you to Wesley for his beautiful immunofluorescence images. I also thank the co-authors of my publication who were not part of the Ehrlich lab, including Chang-Han for contributing to generation of PBMC-derived myeloid cells, Dr. Horton for providing primary pediatric T-ALL samples, and Dhivya for analyzing transcriptional profiling datasets of mouse T-ALL.

My time in Austin has been enjoyable in large part due to the friends I have made here, particularly Seung Kuk and Seung Woo, for all the times we have enjoyed. In addition, to my good friends, Jongcheol and Min Kyu, I am so thankful that I got to share this journey with you all the time.

Last but not least, I would like to express my gratitude to my girlfriend, Heyin, for her moral support and patience over the last 4 years, and my family for all their love and encouragement in all my pursuits. I consider myself nothing without them. Thank you all very much.

Abstract

Myeloid cells provide critical support for T-ALL in vivo

Aram Lyu, Ph.D.

The University of Texas at Austin, 2020

Supervisor: Lauren I. R. Ehrlich

Despite harboring mutations in oncogenes and tumor suppressors that promote tumor growth, T-cell acute lymphoblastic leukemia (T-ALL) cells require exogenous cell types or signals to survive in culture. We previously reported that myeloid cells, particularly dendritic cells, from the thymic tumor microenvironment support the survival and proliferation of primary mouse T-ALL cells in vitro. This dissertation seeks to address two gaps in knowledge in our field. First, it remains to be determined whether tumor-associated myeloid cells promote T-ALL progression in vivo. Second, if so, the molecular mechanisms underlying myeloid-mediated support of T-ALL remain unknown.

In this dissertation, I provide evidence that tumor-associated myeloid cells provide critical support for T-ALL both in mouse models and in patients. First, in vivo depletion of myeloid cells using pharmacologic or genetic means results in a significant reduction in T-ALL burden in multiple organs in two independent mouse models of T-ALL and prolongs survival. Consistent with mouse models, myeloid cells derived from human peripheral blood monocytes support survival of primary patient T-ALL cells in vitro. Furthermore, enriched macrophage gene signatures in published clinical samples correlate with worse outcomes for pediatric T-ALL patients. These results indicate that

tumor-associated myeloid cells promote T-ALL pathogenesis in vivo. Second, transcriptional profiling and functional assays identify activation of IGF1R and integrin signaling as critical components of myeloid-mediated T-ALL support. Consistent with this, acute in vivo myeloid ablation significantly diminishes IGF1R activation in T-ALL cells. In addition, in vivo blockade of integrin-mediated cell adhesion in leukemic mice results in a significant reduction in T-ALL burden. Moreover, enrichment of integrin signaling is associated with elevated myeloid gene signatures and inferior outcomes in pediatric T-ALL patients. These results suggest that IGF1R and integrin signaling plays a critical role in myeloid-mediated T-ALL support. Collectively, the research presented in this dissertation demonstrates that tumor-associated myeloid cells provide signals critical for T-ALL progression in multiple organs in vivo and implicates tumor-associated myeloid cells and associated signals as potential therapeutic targets.

Table of Contents

List of Tables

List of Figures

Chapter 1

Introduction

Cancer is a major public health concern throughout the world and is the second most common cause of death in the United States (Siegel et al., 2020). Although several studies suggest cancer is a modern disease with its risk increased by industrialized diet and lifestyle (Divisi et al., 2006) (Khan et al., 2010), humans have actually walked together with the disease throughout the history. The word "cancer" was first used in 410-360 B.C. by a physician Hippocrates to describe carcinoma, and the oldest record of cancer even dates back to 1600 B.C. (David and Zimmerman, 2010). Tumors initiate when normal cells undergo a series of oncogenic events, causing them to grow out of control (Vogelstein et al., 2013). Cancer can be divided into two main groups: those that form as solid tumors in organs of the body, and those that develop as hematologic malignancies from blood cells in hematopoietic tissues, such as the bone marrow (BM), thymus, lymph nodes (LN), or spleen. Hematologic cancer patients, who account for ~10% of newly diagnosed cancer cases in the United States (Siegel et al., 2020), suffer physically, psychologically, and socially, significantly impacting their quality of life. (Allart-Vorelli et al., 2015). Although recent advances in chemotherapy have increased 5-year survival rates of hematologic malignancy patients, these regimens are toxic and patients who fail to respond to therapies or relapse have inferior outcomes (Ness et al., 2011) (McMahon and Luger, 2019), warranting investigation to determine how to further enhance therapeutic efficacy.

Hematologic malignancies fall into three major categories (Taylor et al., 2017). The first is leukemia, which is a neoplastic transformation of white blood cells within

blood-forming tissues, particularly the BM (Davis et al., 2014). The second is lymphoma, which is a clonal proliferation of lymphocytes at various stages of development in lymphoid tissues, including the LN, spleen, and thymus (Elenitoba-Johnson and Lim, 2018). The last is myeloma, which is a clonal malignancy of plasma cells that produce antibodies (Kumar et al., 2017). Leukemia is the most common cancer in children, and is one of the five leading causes of cancer deaths in patients aged under 40 years (Siegel et al., 2020). Therefore, leukemia is a clinically important disease and improving therapies to increase long-term cures, while minimizing off-target toxicities would have a substantial beneficial impact on convalescent kids' lives.

There are four major subtypes of leukemias diagnosed in the clinic: acute myeloid leukemia (AML), chronic lymphocytic leukemia (CLL), chronic myeloid leukemia (CML), and acute lymphoblastic leukemia (ALL). AML, CLL, and CML almost exclusively impact adults (Davis et al., 2014), while ~80% of ALL occurs in children (Hunger and Mullighan, 2015) (Terwilliger and Abdul-Hay, 2017). ALL is an accumulation and proliferation of lymphoid progenitor cells and occurs in the BM, thymus, or other extramedullary sites (Terwilliger and Abdul-Hay, 2017). After clonal expansion, ALL cells disseminate into multiple organs, including the spleen, BM, LN, liver, and central nervous system (CNS) (Cornell and Palmer, 2012) (Hunger and Mullighan, 2015). Based on the type of lymphocytes from which the tumor originates, ALL is classified as either T-cell ALL (T-ALL) or B-cell ALL (B-ALL) (Terwilliger and Abdul-Hay, 2017) (Sas et al., 2019); T-ALL accounts for 15% and 25% of newly diagnosed ALL cases in children and adults, respectively (Pui et al., 2004) (Vadillo et al., 2018).

Patients with T-ALL used to be categorized as a high-risk leukemia group because of low remission compared to B-ALL patients (Greaves et al., 1981). However,

advanced and intensified cytotoxic therapeutic drugs have significantly improved the prognosis of T-ALL patients over the past 30 years, with 5-year survival rates for pediatric T-ALL reaching ~90% (Möricke et al., 2016) (Siegel et al., 2020). For example, clinical trials have shown that the use of dexamethasone in T-ALL significantly decreased the risk of CNS relapse and increased the survival rates of patients compared to the use of prednisone which had been traditionally used for ALL (Möricke et al., 2016), because of a higher cytotoxic potency, a longer plasma half-life, and better cerebral spinal fluid (CSF) penetration of dexamethasone (Balis et al., 1987) (Ito et al., 1996). Nelarabine, a purine nucleoside analog, provided another advance in inducing remission in patients and was approved for treatments of relapsed or refractory T-ALL (Kadia and Gandhi, 2017). This drug is rapidly metabolized into the active metabolite with a longer plasma half-life, which is more preferentially toxic to T cells than B cells (Cohen et al., 1983). However, benefits of these chemotherapeutic agents are often counterbalanced by high rates of toxicities and long-term morbidity (Ness et al., 2011) (Luskin et al., 2016), including septic toxicity with dexamethasone treatment (Hurwitz et al., 2000) (Möricke et al., 2016) and metabolic disorders, neurotoxicity, and cognitive impairment with the use of nelarabine (Malone and Smith, 2017). Furthermore, ~20% of pediatric patients experience disease relapse (Raetz and Teachey, 2016), typically within 2 years of initial diagnosis, and patients who relapse tend to have resistance to the current chemotherapy (Tzoneva et al., 2013), with survival rates <25% (Nguyen et al., 2008) (Reismüller et al., 2009) (Karrman and Johansson, 2017). These limitations provide a strong rational for identifying novel targets for less toxic and more effective therapies, warranting further studies into the mechanisms underlying T-ALL initiation, progression, and relapse.

Genetic and genomic approaches have identified genetic alterations that are prevalent in T-ALL (Belver and Ferrando, 2016) (Liu et al., 2017). Gain-of-function

mutations in *NOTCH1* (Weng et al., 2004) and loss of the cyclin-dependent kinase inhibitor 2A (*CDKN2A*) loci (Hebert et al., 1994) are present in >60% of T-ALL cases. Activation of transcription factors from rearrangement with the T-cell receptor (TCR) loci is also a common feature of T-ALL. Although a number of preclinical and clinical trials have been ongoing to investigate the efficacy of drugs inhibiting these targets, such as γ-secretase inhibitors (GSIs) to target NOTCH1 activation, these efforts have yet to result in clinically approved therapeutics, largely because of excessive toxicity (McMahon and Luger, 2019). Therefore, it is increasingly recognized that other factors beyond genetic alterations driving T-ALL should be considered for novel targeted drugs.

A growing body of evidence has shown that the tumor microenvironment (TME), which comprises a variety of cell types and soluble factors in the niche surrounding tumors, is essential for survival and progression in both solid tumors and hematologic malignancies (Quail and Joyce, 2013) (Binnewies et al., 2018) (Witkowski et al., 2020). In keeping with the findings that neither mouse nor human T-ALL cells can survive without cytokines or supportive cell types (Armstrong et al., 2009) (Triplett et al., 2016), human thymic epithelial cells (TECs) were shown to support the survival of adult patient T-ALL through release of interleukin 7 (IL-7) in vitro (Scupoli et al., 2003). Moreover, BM endothelial cells have been found to promote leukemic pathogenesis by producing C-X-C motif chemokine ligand 12 (CXCL12) in mouse models of T-ALL (Pitt et al., 2015). Along with these, immune cells, particularly myeloid cells, may be another pro-T-ALL cell type in the TME, because dendritic cells (DCs) are the prototypic antigen-presenting cell type for T cells: they present peptide-major histocompatibility complex (MHC) complexes to activate the TCR, along with costimulatory signals and cytokines that induce full T-cell activation and differentiation (Bassler et al., 2019). Furthermore, macrophages can present antigens to T cells in the periphery and can provide cytokines

that sustain or alter T-cell differentiation and survival (Pozzi et al., 2005). Therefore, myeloid cells could possibly contribute to survival and growth of T-ALL, a malignancy of T cells. More importantly, recent studies have shown that the myeloid compartment became altered in T-ALL mouse models and patients, and survival and proliferation of T-ALL cells was enhanced by co-culture with tumor-associated myeloid cells (Chen et al., 2015) (Triplett et al., 2016). However, the relevance of myeloid cells in promoting T-ALL progression in vivo has remained unknown.

The research presented in this dissertation demonstrates that tumor-associated myeloid cell types provide critical support for T-ALL in vivo and identifies molecular mechanisms underlying myeloid-mediated T-ALL support. The first studies described herein use pharmacologic treatments and genetic mouse models to demonstrate pro-T-ALL activity of myeloid cells using mice and patient samples. These studies also show that tumor-associated myeloid cells support T-ALL survival and progression through activation of insulin-like growth factor 1 receptor (IGF1R) signaling (Chapter 2). The next studies identify integrin signaling as an additional contact-dependent mechanism underlying myeloid-mediated support of T-ALL in mice and in patient samples (Chapter 3). Chapter 4 provides a general discussion of these findings and focuses on questions for future work.

The aim for Chapter 1 is to provide background information for the objectives of this dissertation. This introduction consists of three main sections. The first part introduces the molecular genetics of T-ALL, preclinical models for research, and limitations of the previous genomic studies. The next part provides an overview of the tumor-supportive role of each component of the TME in both solid tumors and hematologic malignancies including T-ALL. It also introduces the current knowledge of

the impact of myeloid cells on T cells and T-ALL. The last part provides an overview of the current gaps in knowledge in the field and how this dissertation will address them.

Overview of T-cell development

T-ALL arises from T-cell progenitors that become transformed as they progress through discrete stages of thymocyte maturation. Therefore, understanding the mechanisms underlying thymocyte development will elucidate the cellular origins and associated molecular signals that promote survival of nascent T-ALL cells (reviewed in (Lancaster et al., 2018); Figure 1.1). When thymic seeding progenitors (TSP) traffic from the BM and enter the thymus via blood vessels at the corticomedullary junction (Lind et al., 2001), cortex-specific vascular endothelial cells support TSP survival and differentiation by providing Kit ligand (KitL) signaling (Buono et al., 2016). Then TSPs give rise to double-negative stage 1 (DN1: $CD3^-CD4^-CD8^-CD25^-CD44^+c\text{-}Kit^+$) and subsequently differentiate into DN2 ($CD3^-CD4^-CD8^-CD25^+CD44^+c\text{-}Kit^+$), which migrate towards the midcortex. DN1 and DN2 interact with cortical TECs (cTECs) which provide CXCL12, IL-7, NOTCH ligands, and KitL (Plotkin et al., 2003) (Rothenberg, 2011) (Shah and Zúñiga-Pflücker, 2014) (Buono et al., 2016), all of which are required for survival, T-lineage specification, and differentiation of DN1 and DN2. After T-lineage commitment, DN2 undergo TCRβ gene rearrangements and differentiate into DN3 ($CD3^-CD4^-CD8^-CD25^+CD44^-c\text{-}Kit^-$), which migrate into subcapsular zone where they are subject to β-selection, in which pre-TCR signaling enables only those cells with productively rearranged TCRβ genes to survive, proliferate, and further differentiate. Survival and proliferation of progenitors are tightly controlled at this point: cells that do not pass β-selection die, while those that pass it proliferate extensively, expanding the pool of progenitors with productive TCRβ rearrangements. Therefore, loss of control of

cell survival and proliferation at this point could result in leukemogenesis, and signals like IL-7 could promote survival of leukemia cells (Boudil et al., 2015). DN3 then differentiate into DN4 ($CD3^-CD4^-CD8^-CD25^-CD44^-c\text{-}Kit^-$), prior to upregulating expression of CD4 and CD8 to become pre-selection double-positive thymocytes (DP: $CD3^-CD4^+CD8^+CD69^-$), which are located throughout the cortex. DP undergo TCRα gene rearrangements and those that successfully make a productive rearrangement are subject to positive selection, ensuring survival of only DP expressing TCRαβ that have the capacity to bind with sufficient affinity the self-peptide-MHC complexes presented by cTECs. Following positive selection, DP upregulate expression of CD69 ($CD3^-CD4^+CD8^+CD69^+$), enter the medulla and subsequently downregulate either CD4 or CD8 to become immature single-positive (SP; immature CD4SP: $CD3^+CD4^+CD8^-CD69^+$; immature CD8SP: $CD3^+CD4^-CD8^+CD69^+$). These SP interact with antigen-presenting cells in the medulla, including medullary TECs (mTECs), DCs, and B cells, enforcing central tolerance in which thymocytes receiving strong TCR signals either undergo apoptosis, called negative selection, or differentiate into regulatory T cells (Treg: $CD3^+CD4^+CD25^+FOXP3^+$). After SP mature further within the medulla, they exit the thymus and move to the periphery.

Hallmarks of T-ALL: genetic alterations in *NOTCH1* and *CDKN2A*

Genetic alterations driving T-ALL have been characterized at the molecular level using genetic and genomic approaches. Among >100 genetic drivers of disease (Girardi et al., 2017) (Liu et al., 2017), *NOTCH1* and *CDKN2A* are the most frequently mutated in T-ALL patients.

NOTCH1

Activating mutations in *NOTCH1* are found in >60% of T-ALL patients (Weng et al., 2004). NOTCH signaling promotes self-renewal and survival of hematopoietic stem cells, and directs T-lineage specification and commitment (Allman et al., 2002) (Ikawa et al., 2006). Among the 4 NOTCH receptors (NOTCH1-4) in humans, which are single-span membrane proteins, NOTCH1 is a key regulator of T-cell commitment. NOTCH1 signaling is activated when a ligand (delta-like ligand 1 (DLL1), DLL2, DLL4, Jagged 1, and Jagged 2) present on adjacent cells binds the NOTCH1 receptor (Steinbuck and Winandy, 2018). Upon ligand binding, a series of proteolytic cleavages occur, resulting in NOTCH1 activation: the first cleavage occurs in the extracellular domain of NOTCH1 by an ADAM-family protease, and the second cleavage occurs in the transmembrane domain of NOTCH1 by the γ-secretase complex. Following these proteolytic events, the intracellular domain of the NOTCH receptor (ICN) is released from the membrane (Struhl and Greenwald, 2001), and translocates to the nucleus to promote the expression of target genes, such as *c-MYC* and *IGF1R*, both of which are essential for T-ALL growth (Weng et al., 2006) (Palomero et al., 2006) (Sharma et al., 2006) (Medyouf et al., 2011) (Figure 1.2). The oncogenic role of *NOTCH1* was initially reported in rare T-ALL cases harboring constitutive activation of NOTCH1 via chromosomal translocation (Ellisen et al., 1991). Later, the ligand independent form of NOTCH1 as a result of gain-of-function mutations was identified in most T-ALL patient samples (Weng et al., 2004). These mutations frequently occur in the heterodimerization domain (HD) and/or the C-terminal PEST domain (Weng et al., 2004). Mutations in the HD region, which links the extracellular tail to ICN, cause ligand-independent activation of NOTCH1, whereas mutations in the PEST domain, responsible for protein degradation, impair the degradation of activated NOTCH1. Because *NOTCH1* is a major driver of T-ALL and its

activation requires proteolytic cleavage events, inhibition of NOTCH1 signaling through GSIs has been extensively tested. Despite promising results in preclinical studies (De Keersmaecker et al., 2008), clinical trials in T-ALL patients showed drug-related toxicity, particularly severe gastrointestinal toxicity (DeAngelo et al., 2006). However, it has been shown that glucocorticoid reversed the GSI-induced gastrointestinal toxicity and induced synergistic anti-leukemic effects with GSIs in preclinical models of glucocorticoid-resistant T-ALL (Samon et al., 2012), suggesting that combination therapies could provide an opportunity for T-ALL treatment with less toxicity. Indeed, some of the GSIs, such as LY3039478, have been clinically evaluated in combination with dexamethasone in patients with T-ALL in a phase I/II study (NCT02518113).

CDKN2A

CDKN2A encodes the tumor suppressors, p16/INK4A and p14/ARF. Loss of the *CDKN2A* locus occurs in >70% of T-ALL patient samples (Hebert et al., 1994). Cell cycle progression is tightly regulated via multiple checkpoints in healthy cells. When cells receive proliferative signals, D-type cyclins (cyclin D1, cyclin D2, and cyclin D3) activate cyclin-dependent kinases (CDK), particularly CDK4 and CDK6, and form cyclin D-CDK4/6 complexes to promote cell cycle progression (Musgrove et al., 2011). p16/INK4A and p14/ARF are negative regulators of cell cycle. The INK4 family of proteins (INK4A, INK4B, INK4C, and INK4D) inhibits the formation and activation of the cyclin D-CDK4/6 complexes (Musgrove et al., 2011), whereas P14/ARF initiates p53-dependent cell cycle arrest (Sherr and Weber, 2000). Previous studies have shown that T cells from CDKN2A-deficient mice exhibited increased proliferation, whereas overexpression of *CDN2A* led to differentiation arrest of thymocytes at DN3 (Sharpless et al., 2001) (Lagresle et al., 2002). During thymocyte development, expression of

CDKN2A is largely activated, but temporarily repressed for extensive proliferation of progenitors with productive TCR rearrangements (Miyazaki et al., 2008). Therefore, deletion of the *CDKN2A* locus leads to the loss of cell cycle control, which could result in T-ALL development. Previous studies have identified inhibition of cyclin D3-CDK4/6 complexes as a potential strategy for T-ALL treatment. For example, cyclin D3-deficient mice were shown to be resistant to NOTCH1-driven T-ALL development, and downregulation of cyclin D3 inhibited proliferation of human T-ALL cell lines (Sicinska et al., 2003). Moreover, acute ablation of cyclin D3 in a mouse model of NOTCH1-induced T-ALL resulted in a significant reduction in leukemic burden and prolonged survival by triggering tumor cell apoptosis (Choi et al., 2012). Consistent with these, pharmacologic inhibition of CDK4/6 activity by PD-0332991 (Palbociclib) validated a reduction of leukemic burden and prolonged survival in mouse and human T-ALL models (Choi et al., 2012). Several clinical trials targeting cyclin D3-CDK4/6 complexes in T-ALL are currently ongoing, such as a phase I study (NCT03792256) investigating the efficacy of Palbociclib in combination with standard chemotherapeutic agents, including doxorubicin, prednisolone, and vincristine, in pediatric patients with relapsed ALL.

Immunophenotypic and molecular characterization of T-ALL

Subgroups of T-ALL have been defined using immunological and genomic approaches. The classification of T-ALL was initially focused on immunophenotype of leukemic blasts reflecting a block at the stages of thymocyte development (Uckun et al., 1997). However, with advances in sequencing techniques, dysregulation of numerous genes, particularly transcription factors, was discovered in T-ALL (Ferrando et al., 2002), revealing greater than expected disease heterogeneity. Recent genome-wide profiling of

T-ALL samples from a large number of pediatric patients has resulted in classification of T-ALL into eight molecular subgroups based on the expression of transcription factor genes (Liu et al., 2017), including the basic helix-loop-helix (bHLH) transcription factors (*TAL1*, *TAL2*, *LYL1*), the LIM-only (LMO) domain transcription factors (*LMO1* and *LMO2*), the HOXA homeobox genes, *TLX1* (*HOX11*), *TLX3*, and *NKX2-1*. Here, an overview of the current classification of T-ALL from the perspective of both immunophenotype and molecular mechanisms is discussed (Figure 1.3).

Early T-lineage progenitor (ETP)-ALL

ETP-ALL is one of the three immunophenotypically distinct T-ALL subgroups. It is associated with a high risk of relapse or remission failure and represents 15-30% of newly diagnosed T-ALL cases (Coustan-Smith et al., 2009) (Allen et al., 2013) (Noronha et al., 2019). By flow cytometry, ETP-ALL blasts are identified phenotypically as $CD1a^{-}CD4^{-}CD5^{lo}CD8^{-}$, suggesting that leukemic transformation occurs at a DN progenitor stage of thymocyte development (Coustan-Smith et al., 2009). The transcription factor genes *LMO2*/*LYL1* or *HOXA* are frequently dysregulated in ETP-ALL (Liu et al., 2017). Interestingly, mutations in *NOTCH1* and *CDKN2A* are not commonly found in ETP-ALL (Liu et al., 2017). Instead, this subgroup aberrantly expresses myeloid and hematopoietic stem cell markers, such as CD13 and CD33, further reflecting an early progenitor origin, prior to T-lineage commitment (Coustan-Smith et al., 2009) (Zhang et al., 2012). Consistent with this, ETP-ALL harbors mutations in genes prevalently altered in hematopoietic malignancies of other lineages, like fms related tyrosine kinase (*FLT3*) and isocitrate dehydrogenase 1 (*IDH1*), both of which are frequently mutated in myeloid leukemias (Zhang et al., 2012), as well as in genes associated with T cell-specific

transcription factors, such as runt related transcription factor 1 (*RUNX1*) and ETS variant 6 (*ETV 6*).

Early cortical T-ALL

Early cortical T-ALL is another subgroup showing relatively favorable outcomes in the clinic (Niehues et al., 1999). It accounts for 30-35% of T-ALL cases (Noronha et al., 2019), and is identified phenotypically by $CD1a^{+}CD4^{+}CD8^{+}$ blasts, reflecting a block at the early cortical stage of thymocyte maturation (Niehues et al., 1999). Early cortical T-ALL is commonly associated with aberrant expression of the *TLX1(HOX11)*, *TLX3*, *NKX2-1*, and *NKX2-2* transcription factor genes (Ferrando et al., 2002) (Homminga et al., 2011) (Liu et al., 2017). Moreover, this subgroup harbors frequent gain-of-function mutations in *NOTCH1* and loss of the *CDKN2A* locus (Liu et al., 2017), and is strongly associated with aberrant expression of genes responsible for cell cycle progression (*E2F7* and cell division cycle 2 (*CDC2*)) (Homminga et al., 2011).

Late cortical T-ALL

Late cortical T-ALL is the most common subgroup, accounting for 35-60% of the patients, and blasts express a more mature cortical thymocyte immunophenotype ($CD3^{+}CD4^{+}CD8^{+}$) (Noronha et al., 2019). It typically is associated with aberrant expression of *TAL1* (Ferrando et al., 2002) (Liu et al., 2017), and clinically shows favorable outcomes, with a trend toward improved event-free survival rates in patients with *TAL1* rearrangements (Kikuchi et al., 1993) (Bash et al., 1993). Although late cortical T-ALL harbors less frequent activating mutations in *NOTCH1*, deletions of *CDKN2A* are commonly found in the leukemia cells (Liu et al., 2017) (Girardi et al., 2017).

T-ALL mouse models

To investigate the molecular mechanisms underlying T-ALL pathogenesis, several mouse models sharing characteristics with human patients, such as dysregulated transcription factors or constitutively activated signaling, have been generated.

TAL1-transgenic mice

Aberrant expression of TAL1 is frequently found in T-ALL (>40% of T-ALL cases; Table 1.1). The leukemogenic role of TAL1 was demonstrated by development of T-ALL in transgenic mice expressing *Tal1* under the control of lymphocyte-specific LCK promoter. ~20% of mice developed T-ALL with 50% penetrance at ~10 months of age (Condorelli et al., 1996). Notably, when these TAL1-transgenic mice were crossed with INK4A- or ARF-deficient mice, all mice developed T-ALL with a median survival period of 5-6 months (Shank-Calvo et al., 2006), suggesting additional genetic alterations are critical for TAL1-mediated leukemogenesis.

LMO2-transgenic mice

Dysregulated LIM domain proteins, particularly LMO2, are prevalent in T-ALL (~10% of T-ALL cases; Table 1.1). Previously, the importance of LMO2 overexpression in human T-ALL development was demonstrated when several X-linked severe combined immunodeficiency (X-SCID) patients who were treated by retrovirus-mediated gene therapy to restore the missing IL-2 receptor gamma gene and rescue T-cell lymphopoiesis developed T-ALL with an insertion of vector into the *LMO2* locus, resulting in uncontrolled clonal proliferation of T cells (Hacein-Bey-Abina et al., 2003) (Hacein-Bey-Abina et al., 2008). The role of constitutively activated LMO2 in T-ALL pathogenesis has been investigated using transgenic mice overexpressing *Lmo2* under the control of T cell-specific CD2 promotor/enhancer. These mice developed T-ALL with

~100% penetrance at a median latency of ~8 months (Smith et al., 2014). Notably, the development of T-ALL was shown to be induced through two independent pathways, one of which is the same as in ETP-ALL (Smith et al., 2014), providing an opportunity to determine the disease mechanisms of the subgroup.

Mice harboring activated NOTCH1

NOTCH1 is constitutively activated by gain-of-function mutations in >60% of T-ALL (Weng et al., 2004). The Role of dysregulated NOTCH1 signaling in T-ALL development has been shown by at least two mouse models. In mice reconstituted with BM cells overexpressing ICN through retroviral transduction, immature DP T cells blasted in the BM, blood, and secondary organs, and T-ALL develops within 2 weeks (Pear et al., 1996). The LN3 mouse model, in which TCRα and β genes were endogenously pre-rearranged in all cells, resulted in premature TCR expression in thymocytes (Serwold et al., 2007). These mice developed T-ALL with ~60% of penetrance by 1 year of age, which was associated with activated NOTCH1 signaling (Serwold et al., 2010) (Triplett et al., 2016).

Aberrant activation of signaling pathways in T-ALL

Transcriptional profiling studies have identified mutations in oncogenic signaling pathways in >60% of T-ALL cases (Liu et al., 2017). Particularly, the Janus kinase-signal transducer and activator of transcription (JAK-STAT) pathway and phosphoinositide 3-kinase (PI3K) pathway are commonly activated in patients, in addition to activated NOTCH1 signaling. Notably, dysregulation of JAK-STAT signaling is associated with ETP-ALL and early cortical T-ALL (Zenatti et al., 2011) (Zhang et al., 2012), whereas

constitutively activated PI3K signaling is associated with late cortical T-ALL (Mendes et al., 2014).

JAK-STAT signaling

IL-7 signaling is critical for T-cell development and the IL-7 receptor (IL-7R) consists of IL-7α and γ_c chains. Upon binding to IL-7, IL-7R induces the activation of tyrosine kinases, particularly JAK1 and JAK3, which subsequently phosphorylate and activate STAT5. Active STAT5 dimers translocate to the nucleus and regulate expression of cell survival genes, such as B-cell lymphoma 2 (*BCL2*) family members. Activating *JAK3* mutations in hematopoietic progenitors were sufficient to drive a T-ALL-like disease in preclinical mouse models (Degryse et al., 2014). Furthermore, activating mutations in *IL-7R*, *JAK1*, *JAK3*, or *STAT5* were found in 25-30% of T-ALL cases (Vicente et al., 2015) (Liu et al., 2017), suggesting that dysregulation of the JAK-STAT pathway is critical for T-ALL pathogenesis. Notably, treatment of Ruxolitinib, a JAK1/2 inhibitor, abrogated hyperactivation of STAT5, resulting in anti-leukemic effects in patient-derived xenograft models of ETP-ALL (Maude et al., 2015). In addition, inhibition of the key downstream molecules, MEK and PI3K, was shown to synergize with JAK inhibitors (Degryse et al., 2018), implicating this signaling as a relevant therapeutic target for treatment of T-ALL. Indeed, several clinical trials targeting JAK-STAT signaling in T-ALL are currently ongoing, such as a phase I/II study (NCT03613428) investigating the efficacy of Ruxolitinib in combination with L-asparaginase, vincristine, and prednisone in adult patients with relapsed and refractory T-ALL (Fattizzo et al., 2020).

PI3K signaling

The PI3K pathway is essential for regulating cell survival and metabolism. PI3K consists of p85, p55, and p110, three of which are plasma membrane-associated lipid kinases, and is activated by CD28 costimulation in T cells and a variety of extracellular stimuli, such as growth factors or cytokines, in tumor cells (Garçon et al., 2008) (Yang et al., 2019). Upon activation, PI3K generates the second messenger phosphatidylinositol-3,4,5-triphosphate (PIP3), thus activating downstream targets, such as AKT and mammalian target of rapamycin (mTOR), which promote cell growth (Sulis and Parsons, 2003) (Yang et al., 2019). Phosphatase and tensin homolog (PTEN), encoding PIP3 phosphatase, is as a major negative regulator of the PI3K signaling cascades (Stambolic et al., 1998). Previous studies have shown that T cell-specific PTEN-deficient mice developed T-ALL (Suzuki et al., 2001), and loss of the *PTEN* locus was observed in ~15% of T-ALL patients, particularly those with a late cortical immunophenotype (Palomero et al., 2007) (Liu et al., 2017). Together, these findings implicate aberrantly activated PI3K signaling in T-ALL leukemogeneis. Notably, pharmacologic inhibition of the PI3K isoforms (PI3Kγ and PI3Kδ) showed strong anti-leukemic effects in PTEN-deficient T-ALL mice (Subramaniam et al., 2012). In addition, NVP-BEZ235, a dual PI3K/mTOR inhibitor, showed cytotoxic effects on patient T-ALL blasts and synergized with chemotherapeutic drugs, including cyclophosphamide, cytarabine, dexamethasone (Chiarini et al., 2010), suggesting that PI3K signaling is a promising target for T-ALL treatment. There are several ongoing clinical trials testing the use of PI3K inhibitors. For example, NCT01756118 is a phase I study evaluating the responses of adult patients with relapsed or refractory acute leukemia to NVP-BEZ235 (Fattizzo et al., 2020).

TME components in T-ALL pathogenesis

Although intensification of cytotoxic chemotherapy has significantly increased survival rates for T-ALL patients (Hunger et al., 2012), there are considerable sides effects, such as neurotoxicity (Malone and Smith, 2017). Even worse, the prognosis of patients who relapse is poor because their leukemia cells become chemoresistant (Tzoneva et al., 2013). Previous studies have shown that selected clones with additional mutations and enhanced leukemia initiating activity are a cause of T-ALL relapse (Clappier et al., 2011). To find novel targets for T-ALL treatment, cell-intrinsic drivers of the disease have been investigated using advanced genome-wide profiling approaches (Liu et al., 2017), and clinical trials targeting frequently aberrant pathways have been ongoing. Although strong anti-leukemic effects were confirmed in in vitro and pre-clinical studies, these approaches have induced considerable systemic side effects in clinical studies. For example, GSIs targeting hyperactivated NOTCH signaling resulted in systemic toxicity in T-ALL patients, particularly in the gastrointestinal tract (DeAngelo et al., 2006) (Papayannidis et al., 2015). Drugs targeting the PI3K signaling also caused significant adverse effects, such as diarrhea and nausea, in patients with acute leukemias (Ragon et al., 2017). These results suggest an urgent need to analyze mechanisms driving T-ALL progression through different lens. Recently, increasing evidence suggests that the TME is essential for survival and progression of leukemia (Witkowski et al., 2020). Because the components in the TME are highly heterogenous, it is essential to understand their distinct role in T-ALL progression for novel targeted agents.

Endothelial cells

Endothelial cells, which line the inner surface of blood and lymphatic vessels, were shown to contribute to progression of solid and hematologic malignancies by

inducing blood vessel formation (angiogenesis) and vascular permeability (Folkman, 2002) (García-Román and Zentella-Dehesa, 2013). Tumor-induced hypoxia and a variety of soluble factors, including platelet derived growth factor (PDGF) and epithelial growth factor (EGF), stimulate tumor cells and other cell types, like fibroblasts, to release signals for angiogenesis and vascular permeabilization, such as vascular endothelial growth factor (VEGF) and nitric oxide (NO). VEGF contributes to the induction of angiogenesis by promoting endothelial cell proliferation and migration (Fukumura et al., 1998) (Neufeld et al., 1999). Previous studies have identified high expression of VEGF in a variety of tumors, particularly solid tumors including breast and colorectal cancers (Hlatky et al., 1994) (Lee et al., 2000). The role of VEGF in endothelial cell-mediated tumor progression has been extensively investigated, and advances in understanding of the VEGF-VEGFR axis have led to the development of anti-angiogenic therapeutic agents which inhibit secretion of VEGF, prevent binding of VEGF to the receptor, or block activation of downstream signaling cascades (Kim et al., 1993) (Goldman et al., 1998). It has been over a decade since the first anti-angiogenic drug, bevacizumab, was approved by the FDA (Muhsin et al., 2004), and clinical trials of several other agents have since been ongoing. NO has been implicated in promoting tumor growth and metastasis by inducing increased vascular leakiness (García-Román and Zentella-Dehesa, 2013) (Rajendran et al., 2013) (Hida et al., 2018). In AML, for example, leukemia cells were shown to increase vascular permeability by elevating NO production in endothelial cells (Passaro et al., 2017).

In addition to inducing angiogenesis and vascular leakiness, endothelial cells have also been shown to promote survival, growth, and migration of tumors, such as B-ALL and AML cells, by producing CXCL12 (Voermans et al., 2002) (Sipkins et al., 2005). Consistent with this, high expression of C-X-C motif chemokine receptor 4 (CXCR4)

correlated with heavy leukemic infiltration and inferior outcomes in patients with B-ALL or AML (Crazzolara et al., 2001) (Schneider et al., 2002) (Spoo et al., 2007). The CXCR4-CXCL12 axis has also been implicated in promoting T-ALL growth. CXCR4 expression by T-ALL modulated the adhesive and migratory properties of leukemic cells towards CXCL12-producing endothelia cells in the BM (Gachet et al., 2013) (Pitt et al., 2015), and targeting this axis inhibited T-ALL survival and progression (Passaro et al., 2015).

Epithelial cells

Transformation of epithelial cells into malignant cells during tumorigenesis and transition of epithelial cells to mesenchymal cells (EMT) in the process of metastasis have been well-demonstrated in a variety of tumors, such as lung, breast, and bladder cancers (Antoniades et al., 1992) (Dimri et al., 2005) (Garg, 2016). However, the question of whether there are tumor-supportive epithelial cells in the TME has remained mostly elusive. Given that a crosstalk between thymocytes and TECs is critical for thymocyte survival and development, and TECs produce NOTCH ligands, IL-7, and CXCL12, all of which have been implicated in T-ALL growth (Scupoli et al., 2003) (Scupoli et al., 2007) (Armstrong et al., 2009) (Silva et al., 2011) (Pitt et al., 2015) (Passaro et al., 2015), TECs could be an essential component of the TME for T-ALL progression. Indeed, recent studies have shown that a transgenic mouse model of T-ALL heterozygous for the FoxN1 transcription factor *nude* null mutation exhibited significantly delayed leukemogenesis (Ghezzo et al., 2018). However, our previous study found that tumor-associated epithelial cells were not necessary for the survival of T-ALL in vitro (Triplett et al., 2016). Furthermore, TECs frequently became ablated during T-ALL progression both in mouse models and in patient samples (Triplett et al., 2016)

(Ghezzo et al., 2018). These results suggest that epithelial cells may contribute to T-ALL development particularly at early stages.

Adipocytes

Several studies have shown that obesity is associated with poor outcomes for patients with solid tumors or leukemias (Basen-Engquist and Chang, 2011) (Castillo et al., 2012) (Orgel et al., 2014) (Orgel et al., 2016), and adipocytes have been thought of as tumor-supportive. Adipocytes produce fatty acids, hormones, and cytokines (adipokines), all of which were shown to promote tumor growth and metastasis in previous studies (Housa et al., 2006) (Pallegar and Christian, 2020). For example, adipocytes produce IL-8 and enhance ovarian tumor cell migration and invasion (Nieman et al., 2011). In addition, survival and growth of these tumor cells were fueled with adipocyte-derived fatty acids transferred by fatty-acid binding protein (FABP) (Nieman et al., 2011). Previous studies have demonstrated that adipocytes promote leukemia pathogenesis by inducing chemotherapy resistance. For example, in B-ALL, adipocytes were shown to impair the anti-leukemic effects of chemotherapy drugs, such as vincristine and L-asparaginase, through several mechanisms. First, adipocytes prevent chemotherapy-induced apoptosis by upregulating the expression of pro-survival genes, *Bcl-2* and *Pim-2* (Behan et al., 2009). Second, they produce counteracting molecules against chemotherapeutic agents, such as glutamine (Ehsanipour et al., 2013). Third, adipocytes absorb and metabolize chemotherapeutic drugs including daunorubicin (Sheng et al., 2017). In AML, adipocytes foster leukemic proliferation through activation of lipolysis by increasing the levels of FABP4 (Shafat et al., 2017). The role of obesity/adipocytes in promoting survival of T-ALL has also been investigated. Using a NOTCH1-induced mouse model and patient samples, fasting was shown to induce differentiation of T-ALL

cells by upregulating the expression of leptin receptor and activating its downstream signaling via the protein PR/SET domain 1 (PRDM1) (Lu et al., 2017).

An overview of myeloid cells and their roles in the TME

Myeloid cells are a heterogenous mixture of immune cells responsible for innate immune responses. Thus, they serve as the frontline defenders against pathogens and cancer. Myeloid cells are largely classified into two classes: mononuclear cells, including macrophages, DCs, and monocytes, and polymorphonuclear cells (granulocytes), including neutrophils, basophils, eosinophils, and mast cells. Although myeloid cells play a critical role in destroying tumor cells or suppressing their growth directly or indirectly by activating anti-tumor T cells and natural killer (NK) cells, ample evidence suggests that these myeloid cells are also a pivotal component of the TME that promotes tumor progression by supporting tumor cell survival directly or establishing pro-tumor environments (Schreiber et al., 2011). For example, it is now well-appreciated that a variety of tumor-derived soluble factors, such as IL-4, IL-10, and transforming growth factor β (TGF-β), reprogram myeloid cells to become tumor-supportive as well as immunosuppressive (Awad et al., 2018) (Hinshaw and Shevde, 2019). The tumor-supportive role of myeloid cells has largely been investigated in solid tumors using two types of approaches: a combination of in vitro functional assays and in vivo animal studies, and immunohistochemical and/or transcriptional analysis-based correlative predictions. For example, a subset of monocyte-derived macrophages was shown to promote breast cancer bone metastasis through IL-4R signaling and macrophage ablation resulted in a significant reduction of metastatic growth (Ma et al., 2020). Furthermore, a strong correlation has been shown between the abundance of tumor-associated macrophages (TAMs) and poor outcomes for breast cancer patients (Zhao et al., 2017).

Recently, evidence of the contribution of myeloid cells to tumor progression has started to emerge for leukemias. In AML, for example, inhibition of colony-stimulating factor 1 receptor (CSF1R), a receptor tyrosine kinase essential for survival and differentiation of myeloid cells, reduced survival of leukemia blasts from patients by suppressing secretion of growth factors such as hepatocyte growth factor (HGF) (Edwards et al., 2019). Moreover, targeting TAMs induced apoptosis on CLL cells in xenograft mice through tumor necrosis factor (TNF) signaling (Galletti et al., 2016). In T-ALL, both TAMs and tumor-associated DCs were shown to promote survival and proliferation of leukemia cells in vitro using several mouse models (Chen et al., 2015) (Triplett et al., 2016), although the relevance of myeloid-mediated T-ALL progression in vivo has yet to be explored. To better understand the objectives of this dissertation, an overview of myeloid cells is provided here.

Macrophage

Macrophages are ubiquitous in the majority of tissues throughout the body. Under normal conditions, these cells carry out immune surveillance, induce inflammation in response to pathogens or damage/stress, and regulate homeostasis in tissues (Davies et al., 2013). Although macrophages used to be thought of as a monocyte-derived population (van Furth et al., 1972), further investigation revealed that macrophages are present in the yolk sac prior to primitive hematopoiesis (Naito et al., 1996) and can proliferate in tissues on their own (Czernielewski and Demarchez, 1987). These results suggest the presence of macrophages with an embryonic origin. Indeed, recent studies using fate mapping techniques have confirmed the presence of yolk sac-derived macrophages in multiple organs, such as the CNS and skin (Ginhoux et al., 2010) (Hoeffel et al., 2012). It is now

well-appreciated that macrophages are ontologically classified into monocyte-derived macrophages and tissue-resident macrophages.

In response to local stimuli, macrophages functionally polarize into various activation states. Although activated macrophages are in a continuum of states (Mosser and Edwards, 2008), they are frequently grouped into two classes using the M1/M2 classification, which represents the extreme ends of the activation states (Biswas and Mantovani, 2010). Similar to T helper type 1 (Th1) and Th2 polarization, macrophages polarize into a pro-inflammatory state (M1-like or classically activated) in response to lipopolysaccharide and interferon γ (IFN-γ) or an anti-inflammatory state (M2-like or alternatively activated) induced by IL-4, IL-10, and IL-13 (Mantovani et al., 2002). Pro-inflammatory macrophages exhibit a high antigen-presenting ability and an enhanced secretion of pro-inflammatory cytokines, such as IL-1, IL-6, and TNF-α, resulting in the induction of a Th1 response against intracellular infections, whereas anti-inflammatory macrophages produce IL-10 and promote a Th2 response to clear parasite infections and facilitate wound healing (Mosser and Edwards, 2008) (Bassler et al., 2019).

In the TME, macrophages have been implicated in promoting survival and progression of several types of tumors, such as breast cancer and AML (Luo et al., 2006) (Jaiswal et al., 2009), and frequently exhibit anti-inflammatory phenotypes (Biswas and Mantovani, 2010). Previous studies have shown that Th2 T cell-derived IL-4 and IL-13 induced anti-inflammatory polarization of macrophages in a mouse model of breast cancer, which supported tumor pathogenesis (DeNardo et al., 2009). TAMs mediate tumor support through multiple mechanisms. First, they directly support tumor growth and metastasis by releasing soluble factors, such as IL-1, TGF-β, VEGF, and matrix metallopeptidase 9 (MMP-9). In mouse models of colon, breast, and lung tumors, elimination of TAMs decreased the levels of TGF-β, VEGF, and MMP-9 in the TME,

resulting in suppression of angiogenesis, and tumor growth and metastasis (Luo et al., 2006). Moreover, TAMs promote tumor progression by inhibiting anti-tumor immune responses through production of inhibitory cytokines, such as IL-10 and TGF-β. Previous studies have shown that anti-inflammatory peritoneal macrophages suppressed T-cell proliferation in vitro by secreting IL-10 and TGF-β (Oishi et al., 2016). TAMs also induce immunosuppression by recruiting Treg to the TME via release of chemokines, including C-C motif chemokine ligand 20 (CCL20) and CCL22. For example, in mouse models of human ovarian cancer, macrophage-derived CCL22 induced migration of Treg into tumor, resulting in the inhibition of T-cell immunity in vivo (Curiel et al., 2004). Additionally, TAMs express the ligands for programmed cell death protein 1 (PD-1; PD-L1 and PD-L2 are the ligands) and cytotoxic T-lymphocyte antigen 4 (CTLA-4; CD80 and CD86 are the ligands) present on activated T cells and B cells. Activation of PD-1 and CTLA-4 inhibits TCR and BCR signaling, resulting in failure of tumor suppression. Macrophage-mediated tumor support through immune checkpoints has been demonstrated using blockade of the ligands with therapeutic antibodies. For example, in a mouse model of human liver cancer, blockade of TAM/monocyte-associated PD-L1 improved anti-tumor T-cell activity and inhibited tumor growth in vivo (Kuang et al., 2009). Lastly, TAMs induce immune evasion of tumor cells by expressing signal regulatory protein α (SIRPα). CD47, the ligand for SIRPα, is frequently overexpressed in tumor cells and the CD47-SIRPα interaction inhibits tumor cell phagocytosis by macrophages. Blockade of the CD47-SIRPα axis using therapeutic antibodies enabled phagocytosis, which resulted in elimination of mouse and human AML cells (Majeti et al., 2009). Consistent with these results, high infiltration of TAMs correlated with worse prognoses for patients with liver and breast cancers (Dong et al., 2016) (Jeong et al., 2019).

Dendritic cell

DCs serve as a bridge between innate and adaptive immunity. After becoming activated at sites of infection or in tumors, DCs mature and traffic to secondary lymphoid organs where they present peptide antigens derived from proteins acquired at the site of infection or from tumors to activate T-cell responses (Engblom et al., 2016). DCs can be subdivided into two major subsets, conventional DCs (cDC: $CD11c^{+}MHCII^{+}$) and plasmacytoid DCs (pDC; mouse: $PDCA1^{+}B220^{+}$ / human: $BDCA2^{+}BDCA4^{+}$) (Guilliams and van de Laar, 2015). cDCs are the predominant subset and are specialized for antigen sampling in tissues and presentation in draining LN to prime T cells (Merad et al., 2013). pDCs are a small DC subset capable of producing type 1 IFN in response to viral infections (Reizis, 2019). cDCs can be further divided into two main subsets, cDC1 (mouse: $CD8^{+}XCR1^{+}CD11b^{lo}$ / human: $CD141^{+}XCR1^{+}CD11b^{-}$) and cDC2 (mouse: $CD11b^{+}SIRP\alpha^{+}$ / human: $CD1c^{+}SIRP\alpha^{+}$) (Guilliams and van de Laar, 2015) (Guilliams et al., 2016). cDC1s were shown to have a superior ability to activate naïve $CD8^{+}$ T cells by cross-presentation of peptides on MHCI (Hildner et al., 2008). cDC2s are specialized in stimulating $CD4^{+}$ T cells through MHCII-mediated antigen presentation (Dudziak et al., 2007), and promote Th2 immune responses (Williams et al., 2013).

In the TME, both cDC1s and cDC2s have been implicated in suppressing tumor growth. The role of cDC1s in eliciting anti-tumor responses has been demonstrated using mouse models of cDC1 ablation. *Batf3*$^{-/-}$ mice deficient in cDC1s failed to reject fibrosarcoma cells and did not respond to immune checkpoint blockade, like anti-PD-1(Hildner et al., 2008) (Salmon et al., 2016). Studies using *Zbtb46*-DTR, which is another cDC1 depletion model, also validated that cDC1s were required for adoptive T-cell therapy for melanoma (Broz et al., 2014). Consistent with this, the abundance of cDC1s was associated with better prognoses for several types of cancer patients, such as breast

cancer, head and neck squamous cell carcinoma, and lung adenocarcinoma (Broz et al., 2014). When it comes to cDC2s, although they had been speculated to play a role in suppressing tumor progression because of their ability to prime $CD4^+$ T cells under other pathological conditions, such as parasitic and viral infections (Gao et al., 2013) (Krishnaswamy et al., 2017), evidence of their contribution to inducing protective anti-tumor immunity has only recently been demonstrated (Binnewies et al., 2019). In this study, cDC2s were shown to stimulate anti-tumor $CD4^+$ T cells, although their functions were susceptible to Treg suppression. Moreover, cDC2 abundance was associated with the frequency of $CD4^+$ T cells and better responsiveness to immune checkpoint blockade, such as anti-PD1, in patients with head and neck squamous cell carcinoma and melanoma. Consistent with this, elevated gene signatures of cDC2 correlated with better survival rates in breast cancer patients (Michea et al., 2018).

Monocyte

Monocytes are a circulating myeloid population in tissues and consist of two main subsets: classical (mouse: $CX3CR1^{lo}CCR2^{+}Ly6C^{hi}$ / human: $CD14^{+}CD16^{-}$) and non-classical (mouse: $CX3CR1^{hi}CCR2^{-}Ly6C^{lo}$ / human: $CD14^{-}CD16^{+}$) (Geissmann et al., 2003) (Movahedi et al., 2010). Classical monocytes are a short-lived cell type, with 1 day of half-life in circulation, and they can either migrate into tissues or convert into non-classical monocytes in the blood (Yona et al., 2013). Upon infection, they were shown to be recruited to inflamed tissues to stimulate naïve $CD8^+$ and $CD4^+$ T cells through antigen presentation on MHCI and MHCII, respectively (Jakubzick et al., 2017). Non-classical monocytes patrol the vascular endothelium in healthy tissues using lymphocyte function-associated antigen 1 (LFA-1) and CX3CR1, and upon tissue damage or infection, they rapidly invade the site, elicit an early immune response, and differentiate into

macrophages (Auffray et al., 2007) (Kapellos et al., 2019). Both monocyte subsets are reservoirs of myeloid precursors and have the ability to differentiate into other myeloid cells, such as macrophages and DCs (Geissmann et al., 2003) (Sander et al., 2017) (Guilliams et al., 2018).

In the TME, classical monocytes have been shown to differentiate into TAMs and promote tumor progression in mouse models of several types of tumors, such as breast, lung, and liver cancers (Qian et al., 2011) (Schmall et al., 2015) (Li et al., 2017), and in lung cancer patient samples (Schmall et al., 2015). For example, genetic or pharmacologic ablation of $CCR2^{+}$ monocytes diminished the frequency of macrophages in lung tumor tissues, resulting in a significant reduction in tumor growth and metastasis in mice (Schmall et al., 2015). After classical monocytes differentiate into TAMs, they support tumor survival through several mechanisms, including T-cell suppression (Li et al., 2017) and angiogenesis (Bonapace et al., 2014). Non-classical monocytes, however, show both pro-tumor and anti-tumor activities in the TME. In mouse models of colorectal cancer, $Ly6C^{lo}$ monocytes promoted tumor growth by driving immunosuppression through CXCL5-mediated recruitment of IL-10-producing neutrophils (Jung et al., 2017). In addition, $TIE2^{+}$ monocytes, a subset of non-classical monocytes (Venneri et al., 2007), were shown to support tumor survival by facilitating angiogenesis (Coffelt et al., 2010). In contrast, in a mouse model of lung metastasis of melanoma, patrolling non-classical monocytes suppressed tumor progression in the lungs through phagocytosis (Headley et al., 2016). In addition, these cells reduced tumor metastasis to the lungs in multiple metastatic tumor models, such as melanoma and breast cancer, by recruiting NK cells via release of CCL3, CCL4, and CCL5 (Hanna et al., 2015). Non-classical monocytes were also shown to inhibit Treg through antibody-dependent cell-mediated cytotoxicity in

melanoma patients who responded to anti-CTLA-4 antibody (Ipilimumab) (Romano et al., 2015).

Granulocyte

Granulocytes, the dominant population among which is neutrophils (mouse: $CD11b^{+}Ly6G^{+}$ / human: $CD14^{-}CD15^{+}CD16^{+}CD66b^{+}$) (Daley et al., 2008) (Dumitru et al., 2012), are one of the primary players responsible for an early innate host defense against bacterial and fungal infections. In response to inflammatory stimuli, they migrate from circulation to the site of infection and phagocytose pathogens. They also release granules containing proteolytic enzymes and microbicidal proteins (Borregaard and Cowland, 1997) as well as chromatin-based extracellular fibers (neutrophil extracellular traps; NETs) to the extracellular space to kill the pathogens (Brinkmann et al., 2004).

In the TME, however, a group of tumor-associated neutrophils (N2 TAN) show a pro-tumor phenotype, whereas the other group is anti-tumor (N1 TAN). N2 TANs were shown to be induced by TGF-β, and ablation of these cells resulted in a significant reduction of lung tumor burden in mice (Fridlender et al., 2009). Furthermore, elevated abundance of neutrophils was associated with poor clinical outcomes for patients with sarcoma (Jiang et al., 2015). Along with TANs, a neutrophil-like cell type, defined as myeloid-derived suppressor cells (MDSCs; mouse: $CD11b^{+}Gr1^{+}$ (Gr1: Ly6C and Ly6G) / human: $CD11b^{+}CD14^{-}CD15^{+}CD16^{+}CD33^{+}CD66b^{+}HLA\text{-}DR^{+}$), is frequently identified both in mice and in patients with several types of tumors (Talmadge and Gabrilovich, 2013) (Solito et al., 2014). There are two subsets of MDSCs: one is monocytic (M-MDSCs), which is mononuclear, and the other is granulocytic (PMN-MDSCs), which is polynuclear (Movahedi et al., 2008). MDSCs were shown to be immunosuppressive by dampening the activation of T cells both in mice and in patients with various types of

tumors, such as lung and breast cancer (Bronte et al., 2000) (Almand et al., 2001). Because MDSCs are immunosuppressive and share the same surface markers ($CD11b^{+}Gr1^{+}$) with neutrophils, it remains to be determined whether MDSCs, particularly PMN-MDSCs, and N2 TANs are different cell types.

Objectives and summary of dissertation

Although previous studies have implicated tumor-associated myeloid cells, particularly macrophages and DCs, in promoting T-ALL survival in vitro (Chen et al., 2015) (Triplett et al., 2016), the relevance in vivo remains unknown. Therefore, the first objective of this dissertation is to determine whether tumor-associated myeloid cells provide critical support for T-ALL using mouse models and human patient samples. The second goal is then to identify the cellular and molecular mechanisms underlying myeloid-mediated T-ALL support. Although IGF1R signaling is critical for T-ALL pathogenesis (Medyouf et al., 2011) and tumor-associated myeloid cells activate the activation of IGF1R in T-ALL in vitro (Triplett et al., 2016), the relevance to T-ALL progression of IGF1R activation by myeloid cells in vivo has remained unclear. Furthermore, close contact between T-ALL cells and tumor-associated stromal cells is required for T-ALL survival (Triplett et al., 2016), suggesting additional mechanisms beyond activation of IGF1R signaling must contribute to myeloid-mediated T-ALL support.

In Chapter 2, I demonstrate that tumor-associated myeloid cells provide critical support of T-ALL in vivo. To tackle this question, I depleted myeloid cells from leukemic mice using pharmacologic and genetic means, which resulted in a significant reduction in leukemia burden and prolonged survival in mouse models of T-ALL. Using a comprehensive flow cytometry panel, I identified candidate tumor-supportive myeloid

subsets, and subsequently tested their ability to support T-ALL survival in vitro. These experiments revealed that several tumor-associated myeloid subsets, including macrophages, monocytes, and cDC2s from multiple organs, promote T-ALL growth in vitro. To determine the cellular and molecular mechanisms of myeloid-mediated support of T-ALL, I analyzed transcriptional profiling datasets to identify activation of the IGF1R pathway as a candidate mechanism of myeloid-mediated T-ALL support, which I tested using in vivo and in vitro pharmacologic assays. Consistent with mouse models, I demonstrated that myeloid cells derived from human peripheral blood monocytes promote survival of patient T-ALL cells, at least partially through IGF1R activation. Moreover, enriched macrophage gene signatures in patients correlated with worse prognoses.

In Chapter 3, I determine that integrin-mediated cell adhesion is critical for myeloid-mediated T-ALL support in vivo. I found that close contact is an essential component of myeloid-mediated T-ALL survival through transwell assays, and subsequently employed transcriptional profiling to identify activation of integrin signaling as a candidate mechanism. To test the contribution of integrins to myeloid-mediated T-ALL support, I inhibited integrin-mediated cell adhesion through genetic or pharmacologic manipulation, which significantly diminished T-ALL burden and conferred a survival benefit in mouse models of T-ALL. Consistent with findings in mouse models, human myeloid cells supported primary patient T-ALL survival through activation of integrins in vitro and elevated gene signatures associated with integrin pathways correlated with inferior patient outcomes. Collectively, the work presented in this dissertation broadens our understanding of the role of tumor-associated myeloid cells in T-ALL survival and progression, and identify potential targets for therapeutic intervention.

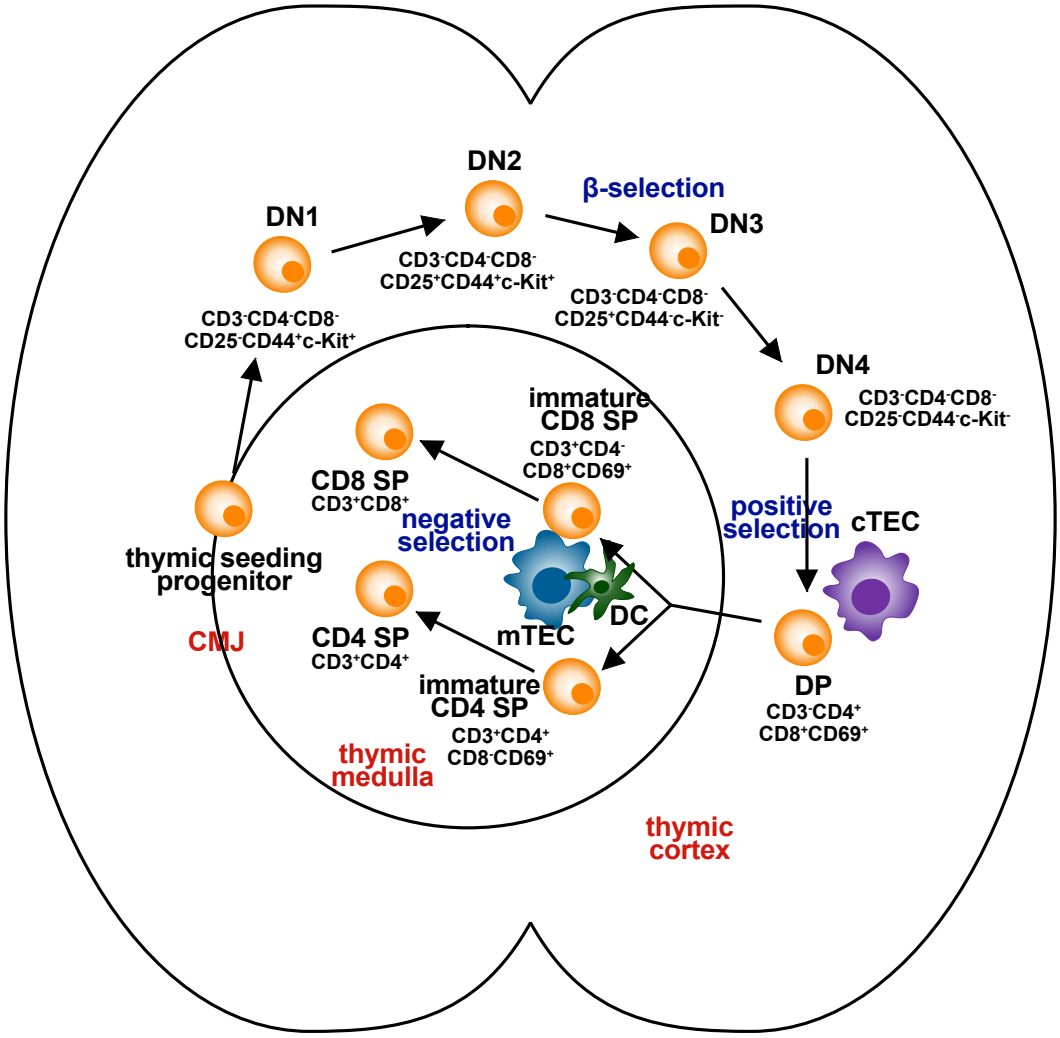

(Figure 1.1 continued on next page)

Figure 1.1. Schematic of T-cell development.

After thymic seeding progenitors traffic from the BM and enter the thymus via blood vessels at the corticomedullary junction (CMJ), they give rise to double-negative stage 1 (DN1: $CD3^-CD4^-CD8^-CD25^-CD44^+c\text{-}Kit^+$) and subsequently differentiate into DN2 ($CD3^-CD4^-CD8^-CD25^+CD44^+c\text{-}Kit^+$). After T-lineage commitment, DN2 undergo TCRβ gene rearrangements and differentiate into DN3 ($CD3^-CD4^-CD8^-CD25^+CD44^-c\text{-}Kit^-$), which migrate into subcapsular zone where they are subject to β-selection, in which pre-TCR signaling enables only those cells with productively rearranged TCRβ genes to survive, proliferate, and further differentiate. DN3 then differentiate into DN4 ($CD3^-CD4^-CD8^-CD25^-CD44^-c\text{-}Kit^-$), prior to upregulating expression of CD4 and CD8 to become pre-selection double-positive thymocytes (DP: $CD3^-CD4^+CD8^+CD69^-$), which are located throughout the cortex. DP undergo TCRα gene rearrangements and those that successfully make a productive rearrangement are subject to positive selection, ensuring survival of only DP expressing TCRαβ that have the capacity to bind with sufficient affinity the self-peptide-MHC complexes presented by cortical thymic epithelial cells (cTECs). Following positive selection, DP upregulate expression of CD69 ($CD3^-CD4^+CD8^+CD69^+$), enter the medulla and subsequently downregulate either CD4 or CD8 to become immature single-positive (SP; immature CD4SP: $CD3^+CD4^+CD8^-CD69^+$; immature CD8SP: $CD3^+CD4^-CD8^+CD69^+$). These SP interact with antigen-presenting cells in the medulla, including medullary TECs (mTECs) and DCs, enforcing central tolerance in which thymocytes receiving strong TCR signals undergo apoptosis called negative selection.

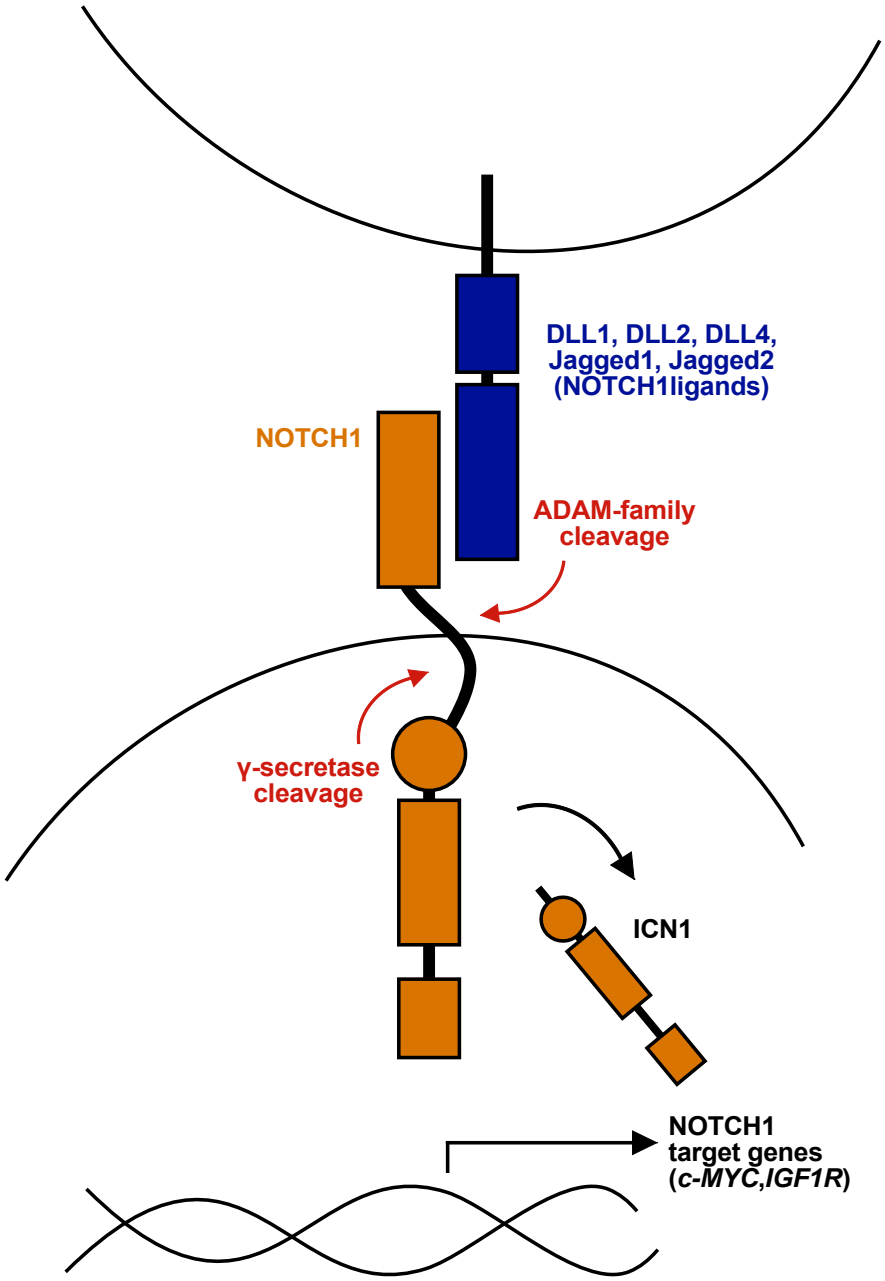

(Figure 1.2 continued on next page)

Figure 1.2. Schematic of NOTCH1 signaling.

NOTCH1 signaling is activated when a ligand (delta-like ligand 1 (DLL1), DLL2, DLL4, Jagged 1, and Jagged 2) present on adjacent cells binds the NOTCH1 receptor. Upon ligand binding, a series of proteolytic cleavages occur, resulting in NOTCH1 activation: the first cleavage occurs in the extracellular domain of NOTCH1 by an ADAM-family protease, and the second cleavage occurs in the transmembrane domain of NOTCH1 by the γ-secretase complex. Following these proteolytic events, the intracellular domain of the NOTCH receptor (ICN) is released from the membrane and translocates to the nucleus to promote the expression of target genes, such as *c-MYC* and *IGF1R*.

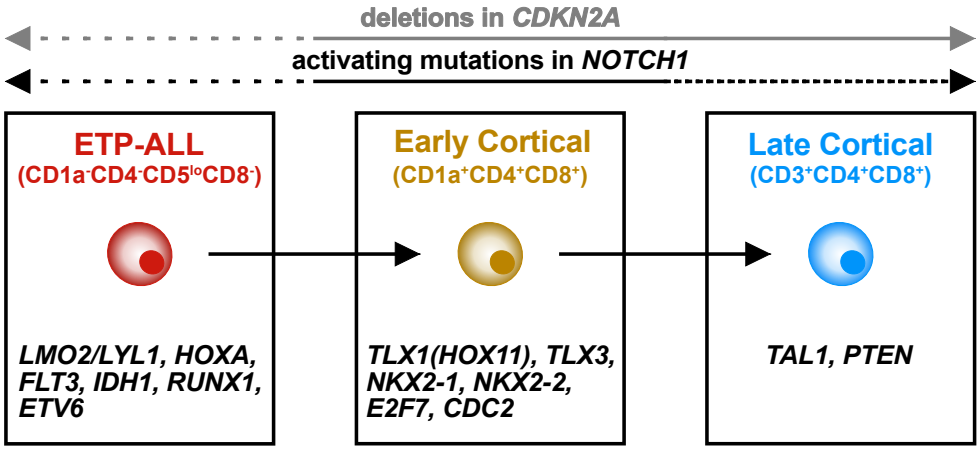

Figure 1.3. Classification of T-ALL.

T-ALL can be divided into three subgroups by immunological and genomic approaches. First, early T-lineage progenitor (ETP)-ALL is identified phenotypically as $CD1a^{-}CD4^{-}CD5^{lo}CD8^{-}$, and the transcription factor genes *LMO2*/*LYL1* or *HOXA* are frequently dysregulated in this subgroup of T-ALL. Although *NOTCH1* and *CDKN2A* are not frequently mutated in ETP-ALL, the leukemia cells harbor mutations in genes prevalently altered in hematopoietic malignancies of other lineages, like fms related tyrosine kinase (*FLT3*) and isocitrate dehydrogenase 1 (*IDH1*), both of which are commonly mutated in myeloid leukemias, as well as in genes associated with T cell-specific transcription factors, such as runt related transcription factor 1 (*RUNX1*) and ETS variant 6 (*ETV 6*). Second, early cortical T-ALL is identified phenotypically by $CD1a^{+}CD4^{+}CD8^{+}$ blasts, and is frequently associated with aberrant expression of the *TLX1(HOX11)*, *TLX3*, *NKX2-1*, and *NKX2-2* transcription factor genes. Moreover, this subgroup harbors frequent gain-of-function mutations in *NOTCH1* and loss of the *CDKN2A* locus, and is strongly associated with aberrant regulation of the cell cycle, such as genetic alterations in *E2F7* and *CDC2*. Last, late cortical T-ALL expresses a more mature cortical thymocyte immunophenotype ($CD3^{+}CD4^{+}CD8^{+}$), and is typically associated with aberrant expression of *TAL1*. Although this subgroup harbors less frequent activating mutations in *NOTCH1*, deletions of *CDKN2A* are commonly found in the leukemia cells.

Transcription factor gene	Frequency (%)	References
TAL1	42	(Bash et al., 1995) (Carroll et al., 1990)
TAL2	4	(Xia et al., 1991)
TLX1(HOX11)	12	(Hatano et al., 1991)
TLX3	9	(Bernard et al., 2001)
HOXA	5	(Soulier, 2005)
LMO1	2	(McGuire et al., 1989)
LMO2	9	(Royer-Pokora et al., 1991)
LYL1	1	(Mellentin et al., 1989)
NKX2-1	7	(Homminga et al., 2011)
c-MYB	8	(Clappier et al., 2007)

Table 1.1. Genetic alterations in oncogenic transcriptional factor genes in T-ALL.
The frequency of each rearrangement was calculated based on (Liu et al., 2017).

Chapter 2

Tumor-associated myeloid cells provide critical support for T-ALL

The work presented in this chapter was published in Lyu and Triplett et al., *Blood*, 2020. A.L. designed and performed experiments, analyzed results, generated figures, and wrote manuscript.

ABSTRACT

Despite harboring mutations in oncogenes and tumor suppressors that promote cancer growth, T-cell acute lymphoblastic leukemia (T-ALL) cells require exogenous cells or signals to survive in culture. We previously reported that myeloid cells, particularly dendritic cells, from the thymic tumor microenvironment support the survival and proliferation of primary mouse T-ALL cells in vitro. Thus, we hypothesized that tumor-associated myeloid cells would support T-ALL in vivo. Consistent with this possibility, in vivo depletion of myeloid cells results in a significant reduction in leukemia burden in multiple organs in 2 distinct mouse models of T-ALL and prolongs survival. The impact of the myeloid compartment on T-ALL growth is not dependent on suppression of anti-tumor T-cell responses. Instead, myeloid cells provide signals that directly support T-ALL cells. Transcriptional profiling, functional assays, and acute in vivo myeloid-depletion experiments identify activation of IGF1R as a critical component of myeloid-mediated T-ALL growth and survival. We identify several myeloid subsets that have the capacity to directly support survival of T-ALL cells. Consistent with mouse models, myeloid cells derived from human peripheral blood monocytes activate IGF1R and directly support survival of primary patient T-ALL cells in vitro. Furthermore, enriched macrophage gene signatures in published clinical samples correlate with inferior outcomes for pediatric T-ALL patients. Collectively, these data reveal that tumor-associated myeloid cells provide signals critical for T-ALL growth in multiple organs in

vivo and implicate tumor-associated myeloid cells and associated signals as potential therapeutic targets.

INTRODUCTION

T-cell acute lymphoblastic leukemia (T-ALL) is a hematologic malignancy that arises from T-cell precursors in the thymus (Belver and Ferrando, 2016) (Terwilliger and Abdul-Hay, 2017). Current treatments have improved survival rates for pediatric patients to ~90%, whereas survival rates for adults remain at ~50%. However, these intensified multiagent chemotherapy regimens are associated with significant long-term morbidity, including metabolic disorders, neurotoxicity, cognitive impairment, secondary cancers, and cardiopathies (Ness et al., 2011) (Iyer et al., 2015). Furthermore, patients refractory to frontline therapy or who relapse have poor outcomes and few alternative therapeutic options (Hefazi and Litzow, 2018) (McMahon and Luger, 2019). Newer agents, such as nelarabine, improve survival for relapsed T-ALL (Kadia and Gandhi, 2017) but often result in neurotoxicity (Malone and Smith, 2017). Thus, development of less toxic effective therapies will be required to improve patient outcomes. Recent efforts to discover new therapeutic strategies for T-ALL have focused on tumor-intrinsic genomic alterations important for T-ALL progression, such as activating mutations in *NOTCH1* (Ferrando, 2018). Although clinical trials are ongoing, such strategies have yet to result in approved therapies that are effective and safe (Terwilliger and Abdul-Hay, 2017) (Hefazi and Litzow, 2018) (McMahon and Luger, 2019), underscoring the need for identification of new therapeutic targets and approaches.

Tumors often modulate cells in their local environments that, in turn, promote cancer survival and progression (Binnewies et al., 2018). Notably, neither murine nor human primary T-ALL cells survive when cultured in the absence of cytokines or cellular

support (Scupoli et al., 2003) (Armstrong et al., 2009) (Triplett et al., 2016), suggesting that the tumor microenvironment (TME) provides signals necessary for T-ALL progression (Passaro et al., 2016). Indeed, interleukin 7 (IL-7) and NOTCH1 ligands, which are expressed by cortical thymic epithelial cells (TECs), have been implicated in promoting T-ALL survival (Armstrong et al., 2009) (Scupoli et al., 2003) (Passaro et al., 2016) (Silva et al., 2011) (Scupoli et al., 2007). However, we and other investigators find that TECs are often ablated during T-ALL progression in mice and humans (Triplett et al., 2016) (Ghezzo et al., 2018), suggesting a role for other factors in the thymic TME. Also, T-ALL results in systemic disease, with leukemic infiltration in the bone marrow (BM), spleen, liver, and other organs (Terwilliger and Abdul-Hay, 2017). The absence of TECs outside of the thymus indicates that other cell types support T-ALL at these secondary leukemia sites. In fact, BM-derived stromal cell lines can support T-ALL (Medyouf et al., 2007) (Winter et al., 2002), possibly through expression of CXCL12 and IL-18 (Passaro et al., 2015) (Pitt et al., 2015) (Uzan et al., 2014). It remains to be determined whether common cell types can support T-ALL in the diverse organs infiltrated with leukemia.

Myeloid cells consist of heterogeneous cells that are often modulated within the TME to support progression, metastasis, and drug resistance of multiple cancer types (Binnewies et al., 2018) (Zilionis et al., 2019) (Tcyganov et al., 2018) (Lavin et al., 2017) (Arlauckas et al., 2017) (Georgoudaki et al., 2016) (Qian et al., 2011). We reported that myeloid cells, particularly dendritic cells (DCs), become more numerous during T-ALL progression in the thymus of mice and patients. We also found that tumor-associated myeloid cells in the thymic TME are necessary and sufficient to support survival of T-ALL cells in vitro. Interestingly, myeloid cells from the thymus of healthy mice were incapable of supporting T-ALL, indicating that the myeloid compartment becomes altered during leukemia progression (Triplett et al., 2016). These findings are consistent

with studies showing that myeloid cells become altered in other organs in a NOTCH1-induced model of T-ALL (Chen et al., 2015) (Yang et al., 2018). Our previous findings also suggest that myeloid cells directly support T-ALL growth (Triplett et al., 2016), rather than relying on indirect mechanisms, such as immunosuppression, modulation of extracellular matrix deposition, or angiogenesis (Binnewies et al., 2018). Although myeloid cells have been shown to support T-ALL in vitro, their role in vivo has yet to be established.

Here, we sought to determine whether myeloid cells are necessary for T-ALL growth in vivo and, if so, to identify relevant myeloid subsets and signals. We find that myeloid cells from multiple leukemic sites have the capacity to support survival of T-ALL cells in vitro. Although our previous data demonstrated an important role for DCs in supporting T-ALL in the thymus (Triplett et al., 2016), DC deficiency does not delay disease progression. However, tumor-associated myeloid cells from DC-deficient mice support T-ALL survival in vitro, suggesting a role for other myeloid subsets. Consistent with this, we show that multiple myeloid cell types can support survival of T-ALL in vitro. Notably, acute depletion of myeloid cells in mice through pharmacologic or genetic manipulation diminishes T-ALL burden in multiple organs and confers a significant survival advantage. Transcriptional profiling and functional assays show the relevance of IGF1R signaling for myeloid-mediated support of T-ALL in vivo. We also find that myeloid cells activate IGF1R and promote survival of human T-ALL cells, and an elevated macrophage gene signature is associated with inferior patient prognosis. Collectively, these studies demonstrate that myeloid cells directly support T-ALL progression in mouse models and in humans.

METHODS

Mice

LN3 (from T. Serwold, Joslin Diabetes Center, Boston, MA) (Serwold et al., 2007) (Serwold et al., 2010), CD2-*Lmo2* transgenic (LMO2; from U. Dave´, Indiana University, Indianapolis, IN) (Smith et al., 2014), C57BL/6J, B6.SJL-Ptprca Pepcb/BoyJ (CD45.1), *Flt3l*$^{-/-}$ (from K. Medina, Mayo Clinic, Rochester, MN) (McKenna et al., 2000), B6.FVB-Tg(ITGAM-DTR/EGFP)34Lan/J (CD11b-DTR) (Duffield et al., 2005), and B6(Cg)-Rag2tm1.1Cgn/J (*Rag2*$^{-/-}$) (Hao and Rajewsky, 2001) mouse strains were bred in-house. Mice were sourced from The Jackson Laboratory, unless otherwise noted. Mice were housed in specific-pathogen-free conditions. All experimental procedures were approved by the Institutional Animal Care and Use Committee at the University of Texas at Austin.

T-ALL transplant model

A total of 5×10^6 T-ALL cells were isolated from leukemic LN3 or LMO2 mice, resuspended in sterile phosphate-buffered saline, and injected intraperitoneally into nonirradiated sex-matched CD45.1$^+$, *Flt3l*$^{-/-}$, CD45.1$^+$CD45.2$^+$CD11b-DTR$^+$, or *Rag2*$^{-/-}$ mice, as indicated. Splenic T-ALL engraftment (CD45.2$^+$CD5$^+$) was evaluated by flow cytometry.

Cell culture media

Complete RPMI culture media consisted of Roswell Park Memorial Institute 1640 (RPMI 1640; Gibco) supplemented with 10% (v/v) fetal bovine serum (FBS; Thermo Scientific Hyclone or Gemini Bio-Products), 55 μM β-mercaptoethanol (Gibco), 1× GlutaMax (2 mM L-alanyl-L-glutamine; Gibco), 1 mM Sodium Pyruvate (Gibco), 1× Penicillin-Streptomycin-Glutamine (100 U/ml Penicillin, 100 μg/ml Streptomycin, 292

μg/ml Glutamine; Gibco), 1× MEM non-essential amino acids (Gibco or Sigma-Aldrich). Cell cultures were carried out at 37 ˚C, 5% CO_2.

Flow cytometric analysis

Tissues were harvested and processed to obtain single-cell suspensions in fluorescence-activated cell sorting (FACS) wash buffer (FWB: 2% BCS (bovine calf serum; GemCell) and 0.5 mM EDTA in PBS). Spleens were mechanically dissociated. Thymuses and lymph nodes were enzymatically dissociated with a cocktail of 0.6 mg/ml (w/v) Liberase™ (Roche, Germany) and 20 U/ml DNase I (Roche) in PBS at 37 ˚C. Tissues were sequentially digested three times with 2 ml cocktail for 12 minutes per digest. Livers were mechanically dissociated, centrifuged at 50 g for 3 minutes, and the supernatant was collected and used for analysis. Bone marrow cells were collected by flushing femurs with 2 ml FWB. All single-cell suspensions samples were subjected to RBC lysis following standard protocols. Cells were filtered using 40 μm filters and immunostained by incubating at 4 ˚C for 30 minutes with fluorescently labeled antibodies with specificity for: CD4 (RM4-5), CD5 (53-7.3), CD8 (53-6.7), CD45.1 (A20), CD45.2 (104), B220 (RA3-6B2), TCRβ (H57-597), CD64 (X54-5/7.1), CD11c (N418), I-A/I-E (M5/114.15.2), SIRPα (P84), XCR1 (ZET), CD11b (M1/70), CD115 (AFS98), Gr1 (RB6-8C5), F4/80 (T45-2342; BD Biosciences). All antibodies were obtained from BioLegend, unless otherwise indicated. After immunostaining, cells were washed twice in FWB and resuspended in FWB containing 1 μg/ml propidium iodide (PI; Enzo Lifesciences) to assess viability.

For intracellular staining of phosphorylated proteins, single-cell suspensions were labeled with LIVE/DEAD™ Fixable Green Dead Cell Stain Kit (Invitrogen) and then treated with FIX & PERM Cell Permeabilization Kit (Invitrogen) according to

manufacturer's methanol-modified protocol. Cells were then immunostained with fluorescently labeled antibodies reactive against CD45.1 (A20), CD45.2 (104), CD5 (53-7.3; all the above from BioLegend), and the following phosphorylated proteins (from BD Biosciences): pIGF1R-AF647 (K74-218; pY1131), pAKT-PE or -BV421 (M89-61; pS473), pERK1/2-PE (20A; pT202/pY204). Mouse IgG1 isotype control antibodies (MOPC-21; BioLegend) were used as negative controls.

For viability analyses, cells were incubated in Annexin V binding buffer (BD Biosciences) containing Annexin V-PE (all from BioLegend), PI and antibodies against CD5 (53-7.3), CD11b (M1/70), CD11c (N418), CD45 (30-F11) according to the manufacturer's protocol. To quantify cellularity, 15 μm Polybead® Microspheres (Polysciences, Inc.) were used.

All flow cytometric data were acquired using an LSR II flow cytometer, a FACSAria or a Fusion (BD Biosciences). Post-acquisition data analysis was performed using FlowJo (v9.9.6, Tree Star, Inc.).

Cytospins

Morphological evaluation of FACS-purified myeloid subsets was determined by resuspending 5×10^4 of each purified myeloid subset in 300 μl of FWB. Cells were centrifuged at 300 rpm with medium acceleration for 6 minutes using a Cytospin 4 cytocentrifuge (Thermo Scientific) onto Superfrost plus microscope slides (Fisher Scientific) using standard protocols. Following centrifugation, slides containing cells were fixed in cold methanol (stored at -20 ˚C) for 15 minutes and stained with May-Grünwald Giemsa solutions (EMD Millipore), according to the manufacturer's protocols. Slides were sealed with Shandon Consul-Mount (Thermo Scientific) and a cover glass (24×50-1.5; Fisher Scientific) prior to imaging on a Leica DMi8 microscope (Leica) with

a 40×/1.30 OIL objective and a Leica DFC450 C digital microscope camera. LAS X software (v3.6.0.20104) was used for image acquisition, and from 5 to 9 fields were imaged and analyzed per slide.

Immunostaining and microscopy

Immunostaining of murine tissue was performed on 7 µm acetone-fixed cryosections according to standard protocols. Sections were immunostained with antibodies with the following specificities: CD45.2-FITC (104), CD11c-biotinylated (N418) and F4/80-AF594 (BM8; all from BioLegend). CD11c signal was amplified using TSA™ Biotin System (PerkinElmer, Inc.) according to manufacturer's protocol, and then stained with Streptavidin-AF647 (Life Technologies). Slides were washed and stained with 4',6-diamidino-2-phenylindole (DAPI; Life Technologies) used at 0.125 µg/ml in PBS to detect nuclei before mounting in ProLong Gold antifade reagent (Thermo Fisher Scientific). Images were obtained on a Leica DMi8 microscope with a 20×/0.7 NA objective and a Leica DFC9000 GTC digital microscope camera, using LAS X software (v3.6.0.20104). Images were processed using ImageJ (v2.0.0-rc-68/1.52g) to create overlays of fluorescent channels, and to adjust exposure uniformly across the images.

In vitro cultures of mouse and human T-ALL cells

Mouse T-ALL cells were enriched from single-cell suspensions from leukemic organs by incubation with biotinylated antibodies against CD11c (N418), CD11b (M1/70), F4/80 (BM8), and I-A/I-E (M5/114.15.2), followed by depletion with MojoSort™ Streptavidin Nanobeads (all from BioLegend), according to the manufacturer's instructions. Myeloid cells were positively enriched from single-cell suspensions by incubation with biotinylated antibodies against CD11c (spleen) or CD11c

and CD11b (liver and BM), followed by passage over MACS columns (Miltenyi Biotec) with Streptavidin Microbeads (Miltenyi Biotec). For co-cultures with specific myeloid subtypes, cells were isolated by FACS. 3×10^5 T-ALL cells were cultured in the presence or absence of $1.5\text{-}2\times10^4$ (spleen and liver) or $1\text{-}1.5\times10^5$ (BM) enriched/purified myeloid cells in 200 µl of complete RPMI in flat-bottom 96-well plates for 6 or 7 days.

To determine if tumor-associated myeloid cells could promote survival of T cells, $CD8^+$ T cells from tumor-free $CD45.1^+$ mice spleens were negatively enriched using the MojoSort™ Mouse CD8 T Cell Isolation Kit (BioLegend), according to manufacturer's instructions and cultured with tumor-associated myeloid cells. To determine if exogenous IGF1 was sufficient for supporting T-ALL survival, leukemia cells were cultured in the presence or absence of 100 ng/ml of recombinant murine IGF1 (PeproTech) for 6 or 7 days either alone or with tumor-associated myeloid cells as described above.

PBMC-derived myeloid cell generation and co-cultures with patient samples

Deidentified primary pediatric T-ALL patient samples were obtained at Texas Children's Hospital (Houston, TX). Sample procurement and analysis were approved by the institutional review board committees at The University of Texas at Austin and Texas Children's Hospital/Baylor College of Medicine. T-ALL cells were isolated via Ficoll density gradient separation, washed, and frozen in RPMI 1640 containing 40% fetal bovine serum and 10% dimethyl sulfoxide (DMSO; v/v) on the day of collection. For preparation of myeloid cells, peripheral blood mononuclear cells (PBMCs) were purified from leukoreduction system chambers from anonymous healthy donors (We Are Blood, Austin, TX) using Histopaque (1.077 g/ml; Sigma-Aldrich) density gradient centrifugation (Lee et al., 2017). $10\text{-}15\times10^6$ PBMCs were seeded into T75 flasks (Corning) in 20 ml of complete RPMI medium and cultured at 37 ˚C, 5% CO_2 for 2 hours

to allow monocyte adhesion. Adherent monocytes were washed twice with complete RPMI media. Monocytes were differentiated for 7 to 9 days in the presence of granulocyte-macrophage colony-stimulating factor (GM-CSF; 50 ng/ml), macrophage colony-stimulating factor (M-CSF; 50 ng/ml), or GM-CSF (100 ng/ml) and IL-4 (50 ng/ml) (Lee et al., 2017) (Repnik et al., 2003) (Lacey et al., 2012) (Hiasa et al., 2009). For co-cultures, 1.25×10^5 patient T-ALL cells were plated alone or with monocyte-derived myeloid cells at a 1:1 ratio in 200 µl of complete RPMI in flat-bottom 96-well plates for 6 days prior to assessing the viability of T-ALL cells by flow cytometry. If the viability of primary pediatric T-ALL cells after thawing was <60%, live cells were enriched on a cushion of Histopaque prior to co-culture.

To determine if survival of mouse or human T-ALL cells co-cultured with myeloid cells requires IGF1R signaling, cells were cultured for 4 days prior to addition of IGF1R inhibitors (AG-1024 and picropodophyllin (PPP); Selleckchem). Viability was assessed by flow cytometry 3 or 4 days after inhibitor addition in comparison to cells treated with vehicle control (DMSO).

To determine if myeloid cells support patient T-ALL cells by activating IGF1R signaling, 1×10^5 T-ALL cells were plated alone or with 5×10^4 PBMC-derived monocytes, or GM-CSF- or M-CSF-derived macrophages in 200 µl of complete RPMI in flat-bottom 96-well plates for 3 or 4 days. T-ALL cells in each group were labeled with LIVE/DEAD™ Fixable Green Dead Cell Stain Kit (Invitrogen) and then treated with FIX & PERM Cell Permeabilization Kit (Invitrogen) according to manufacturer's methanol-modified protocol. Cells were then immunostained with fluorescently labeled antibodies reactive against CD3 (UCHT1), CD5 (UCHT2), CD11b (M1/70), CD14 (M5E2; all the above from BioLegend), CD7 (124-1D1; eBioscience) and pIGF1R-AF647 (K74-218;

pY1131; BD Biosciences). Mouse IgG1 isotype control antibodies (MOPC-21; BioLegend) were used as negative controls.

In vivo depletion of myeloid cells by clodronate liposomes or diphtheria toxin

Mice with established T-ALL (>1% splenic engraftment) were treated with clodronate (dichloromethylene diphosphonate) encapsulated in liposomes (clodlip) from ClodronateLiposomes.org (Amsterdam, The Netherlands; 5 mg/ml) or FormuMax Scientific Inc. (Sunnyvale, CA; neutral, 7 mg/ml). Mice were injected intraperitoneally with 100 or 200 µl of clodlip solution every 3 days, for a total of 4 injections; T-ALL burden was assessed by flow cytometry 48 hours after the final injection. To identify cell types that phagocytose liposomes, control liposomes (devoid of clodronate) that were fluorescently labeled with Dil were injected intraperitoneally, and splenocytes were evaluated by flow cytometry after 24 or 48 hours.

To evaluate the impact of clodlip treatment on the composition of the lymphoid compartment, tumor-free mice were injected once intraperitoneally with 200 µl of clodlip. After 48 hours, splenocytes were immunostained to determine the composition of myeloid and lymphoid subsets by flow cytometric analysis. To evaluate the effects of myeloid depletion on T-ALL burden, cohorts of CD11b-DTR^{+} and CD11b-DTR^{-} littermates were transplanted with primary LN3 T-ALL cells. After splenic chimerism reached 1% to 8%, all mice in the cohort were injected intraperitoneally with 50 ng per g body weight of diphtheria toxin (DT; Sigma-Aldrich) in 200 µl of PBS every 3 days, for 3 total injections. Changes in T-ALL burden were evaluated 48 hours after the final injection.

To determine which signaling pathways were activated in T-ALL cells by tumor-supportive myeloid cells, phosphorylated protein levels were assessed by flow cytometry

in T-ALL cells 48hr after 1 treatment with 200 µl clodlip in mice with >7% splenic T-ALL chimerism as described above. All comparisons within an experiment were performed with age-matched mice (6 to 8 weeks of age) transplanted with the same primary T-ALL sample.

Sample preparation for RNA-seq

To compare the transcriptomes of T-ALL cells and healthy T-lineage cells, splenic and thymic T-ALL cells were isolated from mechanically dissociated spleen and thymus, respectively, of overtly leukemic LN3 mice. For controls, total thymocytes were purified from mechanically dissociated thymuses from C57BL/6J mice, and $CD8^+$ T cells (purity 85 to 95%) were isolated from C57BL/6J spleens using the MojoSort™ Mouse CD8 T Cell Isolation Kit (BioLegend), according to manufacturer's instructions. Total RNA was purified using a RNeasy Mini Kit (Qiagen), and RNA quality and concentration were assessed on an Agilent Bioanalyzer 2100 using the Eukaryote Total RNA Pico/Nano assay. Samples had a range of 8.80 to 10.0 RIN. Poly(A) RNA was enriched from total RNA using the Poly(A)Purist Mag kit (Life Technologies), and libraries were prepared using the NEBNext Ultra II Directional RNA Library Prep kit for Illumina (NEB). 2×150 bp paired-end sequencing was run on a HiSeq 4000 (Illumina) sequencer, with an average of 29.7 million read-pairs per sample.

Analysis for RNA-seq

FastQ files were assessed for quality using FastQC. Reads were then pseudoaligned to the mouse transcriptome (GRCm38) and transcript abundances were estimated using Kallisto (version 0.46.1) (Bray et al., 2016). The transcript-level counts were aggregated to gene-level counts using tximport in R (Soneson et al., 2015),

normalized using DESeq2 (Love et al., 2014) size factors and transformed with variance stabilizing transformation to yield counts that are approximately homoscedastic. Principal Component Analysis (PCA) was performed using 25% of the highest variance genes to look at the underlying structure of the data and identify the largest sources of variance. Genes that correlated significantly (absolute fold change ≥2, adjusted P-value <0.05) to sequencing batch were identified using the likelihood ratio test in DESeq2 and were removed from further analysis. Pairwise comparisons of T-ALL cells vs healthy T-lineage cells in each tissue (thymus and spleen) were run using DESeq2 and differentially expressed genes were identified (absolute fold change ≥1.5, adjusted P-value <0.05). The Gene Set Enrichment Analysis (GSEA) was run using all genes against the BioCarta gene sets using gene set permutations (1000) with default parameters (enrichment statistic: weighted, metric for ranking: signal2noise, gene list sorting model: real, gene list ordering mode: descending, max size: 500, min size:15). The enriched pathways were visualized using the pheatmap package in R.

Bioinformatic analysis for patient T-ALL

Bioinformatic analysis was performed on published RNA-sequencing data of T-ALL samples from 264 patients and the associated clinical outcomes datasets from the TARGET ALL Phase II project (Liu et al., 2017). Patients whose WBC numbers at diagnosis were higher than 200,000/ml were excluded. We used xCell (Aran et al., 2017) to quantify the enrichment score of macrophages, monocytes, natural killer (NK) cells, and B cells from bulk RNA sequencing data. To plot a longitudinal event-free survival of pediatric T-ALL patients, we divided patient data into high and low groups for each cell subset using a cutoff that best separates the bimodal distribution of enrichment scores. Log-rank tests were used to detect the correlation of macrophage, monocyte, NK cell, and

B cell gene scores with the event-free survival time of T-ALL patients. The R code for data downloading and analysis is available on the GitHub (https://github.com/hzc363/SJ_analysis).

To determine if there is a correlation between macrophage signatures and T-ALL subtypes, we binned the samples into molecular subtypes identified in Liu et al. (Liu et al., 2017), and calculated the macrophage enrichment scores across the T-ALL subtypes using xCell (Aran et al., 2017). None of the subtypes were associated with higher macrophage scores by analysis of variance (ANOVA). Furthermore, cox regression indicates that the macrophage signature remains a significant predictor of survival (P=0.0234) when controlling for cancer types.

Statistical analysis

Statistical analyses were performed with Prism (v8.4.2; GraphPad Software) and R (3.5.1; The R Foundation for Statistical Computing). Normality was determined using the D'Agostino & Pearson or Shapiro-Wilk test, as appropriate for sample size. Statistical significance was determined using an unpaired Student t test for normally distributed data; the nonparametric Mann-Whitney test, paired Student t test, or repeated measures one-way ANOVA with the Bonferroni correction for normally distributed data; or the nonparametric Friedman test, repeated measures two-way ANOVA with the Bonferroni correction, or log-rank test, as indicated in the figure legends.

RESULTS

T-ALL infiltrates multiple organs following engraftment in secondary hosts and remains dependent on myeloid cells for in vitro survival

The LN3 mouse strain was cloned from a lymph node (LN) T cell, resulting in endogenously prerearranged TCRα and TCRβ genes in all cells and premature T-cell

receptor expression during thymocyte development (Serwold et al., 2007). LN3 mice spontaneously develop T-ALL, associated with frequent *Notch1* mutations (Triplett et al., 2016), with ~50% penetrance at >6 months of age (Serwold et al., 2010). Our previous studies demonstrated that tumor-associated myeloid cells support survival and proliferation of primary LN3 T-ALL cells in vitro (Triplett et al., 2016). To extend these findings in vivo, we transplanted primary T-ALL cells from leukemic LN3 mice into unconditioned immunocompetent CD45.1^{+} congenic mice. Disease penetrance is 100% following transplantation, and mice within a cohort harboring the same primary leukemia have similar disease kinetics (Figure 2.1A). Transplanted T-ALL cells infiltrate multiple organs, resembling human disease (Figure 2.1B; Figure 2.2). Importantly, T-ALL cells from multiple clinically relevant sites in transplanted mice remain dependent on the presence of myeloid cells from their TMEs to survive in vitro (Figure 2.1C-D; Figure 2.3). Multiple myeloid cell types, including macrophages, conventional DCs (cDC1 and cDC2), monocytes, and granulocytes, become more numerous in leukemic spleens, with an increased frequency of macrophages and Gr1^{lo} monocytes within the myeloid compartment (Figure 2.1E-F; Figure 2.4A). Importantly, this expansion is myeloid specific, as host T-cell (TCRβ^{+}) and B-cell (B220^{+}) counts remain constant, despite increased organ cellularity. Moreover, myeloid cells are intermingled with T-ALL cells in the TME of multiple organs, highlighting their potential to provide growth signals (Figure 2.1G). Collectively, these results demonstrate that, following transplantation into secondary hosts, T-ALL cells modulate the myeloid composition in the TME, and myeloid cells from multiple leukemic organs can support survival of T-ALL cells in vitro.

Other myeloid cells support T-ALL in the absence of DCs

Based on our previous finding that DCs from leukemic thymuses are capable of supporting T-ALL growth in vitro (Triplett et al., 2016), we hypothesized that DCs would contribute to T-ALL progression in vivo. To test this hypothesis, we assessed LN3 T-ALL progression following transplantation into *Flt3l*$^{-/-}$ mice, in which DC differentiation is impaired (McKenna et al., 2000). Flow cytometric evaluation confirmed a selective decrease in cDC1 and cDC2 cellularity in *Flt3l*$^{-/-}$ spleens (Figure 2.5A). Despite this reduction in DCs, *Flt3l*$^{-/-}$ mice succumbed significantly faster to T-ALL than did wild-type (WT) recipients (Figure 2.5B). We next tested whether propagation of T-ALL in DC-attenuated hosts reflected a selective pressure on the leukemia cells to become independent of myeloid support. This was not the case, because T-ALL cells continued to rely on myeloid cells from the TME of *Flt3l*$^{-/-}$ mice for survival in vitro (Figure 2.5C-D). We next confirmed that DCs remained depleted in the spleens of leukemic *Flt3l*$^{-/-}$ mice (Figure 2.5E). To identify myeloid cells likely to support T-ALL, we evaluated the composition of enriched myeloid cells used in co-culture assays and found that macrophages were the most abundant cell type in WT and *Flt3l*$^{-/-}$ spleens (Figure 2.6). These results demonstrate that DCs are not necessary for T-ALL progression in vivo and suggest that other tumor-associated myeloid cell types, such as macrophages, likely contribute to T-ALL growth.

Myeloid cells support T-ALL initiation and progression

To test whether myeloid cells promote T-ALL progression in vivo, we used clodlip to deplete phagocytic cells, including macrophages, DCs, and monocytes (Chow et al., 2011) (Sunderkötter et al., 2004) (van Rooijen and Hendrikx, 2010). We first confirmed that clodlip was internalized by myeloid cells, but not by T-ALL or

lymphocytes (TCRβ$^+$ or B220$^+$) (Figure 2.7A-C). We also confirmed that clodlip treatment does not impact lymphocyte cellularity in healthy mice, indicating that it is not broadly toxic (Figure 2.7D). Next, LN3 T-ALL cells were transferred into congenic recipients; once splenic T-ALL burden reached 1% to 8%, clodlip was administered to half of the cohort over 9 days prior to assessing T-ALL burden (Figure 2.8A). Strikingly, myeloid depletion resulted in fewer circulating T-ALL blasts and diminished T-ALL burden in the spleen, liver, kidney, lung, BM, thymus, and inguinal LN (Figure 2.8B-D). Furthermore, depleting myeloid cells from mice with established T-ALL conferred a significant survival benefit (Figure 2.8E). These results demonstrate that tumor-associated myeloid cells support established T-ALL progression in vivo.

After developing in the thymus, T-ALL cells seed other organs, where local microenvironments must be permissive for successful engraftment. Thus, we tested whether myeloid cells from secondary sites could support T-ALL. Myeloid cells from tumor-free spleens supported T-ALL in vitro, although significantly less efficiently compared with tumor-associated splenic myeloid cells (Figure 2.8F). Furthermore, myeloid depletion prior to T-ALL transplantation resulted in reduced disease penetrance and a significant survival benefit (Figure 2.8G-H). These results demonstrate that myeloid cells in non-leukemic tissues support T-ALL upon engraftment at secondary sites in vivo.

To validate the impact of myeloid support on T-ALL burden, we used CD11b-DTR transgenic mice, in which the diphtheria toxin receptor (DTR) is expressed under the control of the CD11b promoter (Duffield et al., 2005), as an alternate means of depleting myeloid cells. T-ALL cells were transplanted into CD11b-DTR$^+$ mice and transgene-negative littermate controls; once splenic T-ALL burden reached 1% to 8%, diphtheria toxin (DT) was administered to deplete CD11b$^+$ myeloid cells (Figure 2.9A)

(Chow et al., 2011) (Saxena et al., 2007) (Ramachandran et al., 2012). Consistent with clodlip results, myeloid depletion significantly diminished T-ALL burden in several organs, including the spleen and LN, with spleen and liver weights declining to those of tumor-free littermate controls (Figure 2.9B-D).

We also determined whether myeloid cells supported T-ALL in an independent transgenic mouse model in which LIM domain only 2 (*Lmo2*) expression is driven by the human CD2-promoter (Smith et al., 2014). Similar to the LN3 model, LMO2 T-ALL cells remained dependent on tumor-associated myeloid cells for survival in vitro following transplantation into unconditioned recipients (Figure 2.9E-F). Furthermore, myeloid depletion resulted in a significant reduction in T-ALL burden (Figure 2.9G-I). Taken together, these concordant findings using multiple T-ALL models and myeloid-depletion methods demonstrate that myeloid cells provide critical support for T-ALL engraftment and progression in vivo.

Multiple myeloid subsets can directly support T-ALL survival

We reasoned that determining which myeloid subsets were depleted by clodlip or DT would identify candidate cell types that contribute to T-ALL growth. Clodlip treatment resulted in an almost complete depletion of splenic macrophages, as well as a significant reduction in cDC1, cDC2, and monocytes (Figure 2.10A). Although macrophages were also depleted in the BM, we did not detect a significant reduction in myeloid subsets in the thymus or LN (Figure 2.11A) (Winkelmann et al., 2014) (Atibalentja et al., 2011) (Alves-Rosa et al., 2003). In the CD11b-DTR model, administration of DT resulted in a significant decrease in splenic macrophages, cDC1 and cDC2, $Gr1^{hi}$ and $Gr1^{lo}$ monocytes, and granulocytes, whereas only DCs were depleted in the LN (Figure 2.11B). To evaluate the ability of the implicated myeloid subsets to

support T-ALL survival, we used fluorescence-activated cell sorting (FACS) to sort myeloid cells from the spleens and livers of tumor-bearing mice (Figure 2.12A) and verified their cellular identities morphologically (Figure 2.10B) before co-culturing with T-ALL cells. Macrophages from the spleens and livers robustly supported survival of T-ALL cells in vitro, and monocytes and cDC2 were also supportive, albeit to a lesser extent (Figure 2.10C; Figure 2.12B). Thus, multiple myeloid subsets from the TMEs of hematopoietic and nonhematopoietic organs can directly promote T-ALL survival.

Adaptive immunity is not required to reduce T-ALL burden after myeloid depletion

We previously found that thymic tumor-associated myeloid cells express genes associated with an immunosuppressive signature, such as *Arg1*, *Ym1*, *Mmp2*, and *Fizz1* (Mosser and Edwards, 2008) (Triplett et al., 2016). Thus, the reduced T-ALL burden following depletion of tumor-associated myeloid cells could result from relieving suppression of anti-leukemic T-cell responses (Guth et al., 2012). To test this possibility, T-ALL was transplanted into lymphodeficient *Rag2*$^{-/-}$ mice (Hao and Rajewsky, 2001); once T-ALL was established, half of the cohort was treated with clodlip (Figure 2.13A). Flow cytometric analysis revealed that myeloid depletion significantly diminished T-ALL burden, even in the absence of an adaptive immune response (Figure 2.13B-C). Taken together with the finding that myeloid cells support T-ALL survival in vitro, these studies indicate that myeloid cells directly support T-ALL in vivo.

Myeloid cells activate IGF1R signaling to promote T-ALL survival in vivo

To identify mechanisms by which myeloid cells promote T-ALL survival, we carried out transcriptional profiling of T-ALL cells vs healthy T-lineage cells. T cells were chosen as controls because tumor-associated myeloid cells significantly supported

the survival of T-ALL but not T cells (Figure 2.14A). Therefore, we reasoned that T-ALL cells in the leukemic microenvironment would exhibit gene signatures induced by supportive myeloid cells that would not be found in tumor-free T cells. Thus, the transcriptional profiles of primary thymic and splenic T-ALL cells were compared with thymocytes and splenic $CD8^+$ T cells from tumor-free mice by RNA sequencing. Principal component analysis showed that leukemia status was the major driver of transcriptional differences between samples (PC1), followed by tissue-specific signatures (PC2; Figure 2.14B). Pathway analysis showed that "IGF1R" was among the top pathways activated preferentially in T-ALL cells, in the spleen and thymus (Figure 2.14C; Figure 2.15A-B). Consistent with this, *Igf1r* transcripts were elevated in T-ALL cells (Figure 2.14D), and IGF1R was activated in T-ALL cells, but not in T cells from the same leukemic spleens (Figure 2.14E). Experiments were then performed to test whether IGF1R activation is involved in myeloid-mediated support of T-ALL. In vitro co-cultures in the presence of IGF1R inhibitors showed that myeloid-mediated survival of LN3-transplanted T-ALL cells was dependent on IGF1R signaling (Figure 2.15C). Notably, acute myeloid depletion in leukemic mice (Figure 2.14F) resulted in reduced activation of IGF1R (phosphorylated IGF1R [pIGF1R]) and the downstream signaling molecule AKT, but not ERK, in T-ALL cells but not in normal T cells in the same spleens (Figure 2.14G; Figure 2.15D). These results suggest that therapeutic targeting of tumor-associated myeloid cells could specifically reduce survival signals in T-ALL cells, without impairing T cells. We next determined whether IGF1 was sufficient to support T-ALL survival. Although IGF1 was not sufficient to support T-ALL survival, exogenous IGF1 enhanced T-ALL survival in the presence of tumor-associated myeloid cells, indicating that myeloid cells sensitize T-ALL to IGF1R signaling (Figure 2.14H). Collectively,

these studies indicate that tumor-associated myeloid cells support T-ALL, at least in part by activating the IGF1R pathway to promote survival.

Human myeloid cells support primary patient T-ALL cells in vitro and are associated with worse prognosis

To determine whether myeloid cells directly support survival of human T-ALL, primary patient T-ALL cells were co-cultured with monocytes or monocyte-derived myeloid cells from the peripheral blood of healthy donors. Notably, monocytes, M-CSF-derived macrophages, and DCs all supported the survival of primary patient T-ALL cells in vitro (Figure 2.16A; Figure 2.17A). Furthermore, evaluation of published transcriptional datasets from pediatric patient samples (Liu et al., 2017) revealed that an elevated macrophage gene signature correlated with reduced event-free survival rates, with a similar trend observed for elevated monocyte signatures (Figure 2.16B; Table 2.1). In contrast, gene signatures of non-myeloid populations, such as B cells and natural killer (NK) cells, did not correlate with patient outcomes (Figure 2.17B). The association between macrophage signatures and patient outcomes is not confounded by genetic T-ALL subtypes (Figure 2.17C).

M-CSF, which is encoded by *CSF1*, regulates the differentiation and survival of T-ALL-supportive macrophages (Figure 2.16A), and elevated *CSF1* expression is associated with poor prognosis in other cancers (Hume and MacDonald, 2012) (Aharinejad et al., 2013) (Liu et al., 2016). Notably, expression of *CSF1* and macrophage enrichment scores were significantly correlated in T-ALL patients (Figure 2.16C). Because M-CSF-derived macrophages express more *IGF1* than do GM-CSF-derived macrophages (Lacey et al., 2012), we hypothesized that M-CSF-derived macrophages would support human T-ALL by activating IGF1R signaling. After culturing primary

patient T-ALL cells in the presence or absence of myeloid cells, pIGF1R levels were elevated in T-ALL cells only by M-CSF-derived macrophages (Figure 2.16D; Figure 2.17D-E). Furthermore, survival of T-ALL cells co-cultured with M-CSF-derived macrophages was significantly impaired in the presence of IGF1R inhibitors (Figure 2.16E). Collectively, these results indicate that myeloid cells promote progression of human T-ALL, consistent with findings in mouse models, and they do so, in part, by activating IGF1R signaling in T-ALL.

DISCUSSION

Although it has long been recognized that T-ALL cells require external signals to survive in vitro (Armstrong et al., 2009) (Scupoli et al., 2003) (Passaro et al., 2015) (Pitt et al., 2015), the cell types in the TME that promote T-ALL growth in vivo have remained elusive. Because our previous studies indicated a role for DCs in the thymic TME (Triplett et al., 2016), we initially hypothesized that DCs would be required to support T-ALL in vivo. However, *Flt3l*$^{-/-}$ mice succumbed to T-ALL, despite diminished DC cellularity. Because our previous studies showed that CD11b^{+}CD11c^{-} myeloid cells from the thymic TME could also support primary T-ALL in vitro (Triplett et al., 2016), we suspected that other myeloid cell types might compensate for the absence of DCs in *Flt3l*$^{-/-}$ mice. Indeed, enriched myeloid cells from the TME of *Flt3l*$^{-/-}$ mice robustly supported T-ALL survival in vitro. Co-cultures with purified myeloid subsets revealed that macrophages had the most potent pro-T-ALL activity, followed by monocytes and cDC2. Consistent with these results from murine T-ALL models, primary pediatric T-ALL cells were also supported in co-cultures by myeloid cells, including monocytes, M-CSF-derived macrophages, and GM-CSF+IL-4-derived DCs. Collectively, these findings suggested that multiple myeloid subsets could support T-ALL in vivo.

In keeping with a critical role for myeloid cells in supporting T-ALL in vivo, depleting multiple myeloid subsets in mice with established leukemia via pharmacologic or genetic means resulted in a sharp decrease in circulating T-ALL blasts and reduced T-ALL infiltrates in several clinically relevant organs, like the spleen and BM. Notably, although tumor-associated myeloid cells can actively suppress anti-tumor immune responses (Mosser and Edwards, 2008), we found that myeloid depletion reduced T-ALL burden in the absence of adaptive immunity. Together, with the ability of myeloid cells to support T-ALL in co-cultures, these data indicate that myeloid cells in distinct TMEs directly promote T-ALL growth.

Depletion of myeloid cells either before or after T-ALL transfer revealed that myeloid cells promote T-ALL engraftment and progression of established disease. After developing in the thymus, T-ALL cells egress from the thymus and infiltrate secondary organs, including the spleen, liver, BM, and LN. To engraft at these sites, T-ALL cells must encounter a supportive microenvironment. Interestingly, splenic myeloid cells in tumor-free mice, unlike healthy thymic DCs (Triplett et al., 2016), have some capacity to support T-ALL survival, albeit less so than tumor-associated myeloid cells. These findings suggest that T-ALL cells encounter myeloid cells capable of supporting engraftment upon entry into secondary sites. The finding that tumor-free splenic myeloid cells supported T-ALL is also consistent with the result that healthy PBMC-derived myeloid subsets supported survival of patient T-ALL cells. After engrafting, T-ALL cells modify the environment through unknown signals, resulting in recruitment and/or differentiation of myeloid cells with an enhanced capacity to support T-ALL growth. The correlation between increased *CSF1* expression and elevated macrophage signatures in patients suggests that *CSF1* may contribute to altering the myeloid compartment in aggressive T-ALL, because patients with higher macrophage signatures have worse

outcomes. However, the source and cause of increased *CSF1* expression remain to be determined.

Transcriptional profiling data implicated IGF1R signaling in myeloid-mediated T-ALL support, and myeloid cells, including DCs and M2-like macrophages, can be an important source of IGF1 (Spadaro et al., 2017). Our previous studies demonstrated that tumor-associated thymic DCs in LN3 mice with primary T-ALL express and secrete elevated levels of IGF1 relative to DCs from healthy thymuses (Triplett et al., 2016). Thus, we tested whether IGF1R signaling was activated in T-ALL cells in vivo by myeloid cells. Indeed, acute myeloid depletion resulted in a significant reduction in IGF1R and AKT activation in T-ALL cells, and IGF1R signaling was required for survival of mouse and human T-ALL cells co-cultured with leukemic myeloid cells. It remains to be determined whether myeloid cells must produce IGF1 and/or other factors to support T-ALL survival and whether tissue-resident and/or monocyte-derived macrophages promote T-ALL growth. The finding that only M-CSF-derived macrophages induced IGF1R activation in patient T-ALL cells implicates M2-like macrophages as playing a dominant role. The finding that PBMC-derived monocytes supported T-ALL survival but did not activate IGF1R also indicates that additional signals are involved in myeloid-mediated T-ALL support. A more complete understanding of the origin and identity of T-ALL-supportive myeloid cells and their tumor-supportive mechanisms will reveal which subsets and signals would be optimal therapeutic targets.

Collectively, our study demonstrates that myeloid composition and function are altered in multiple organs, such that myeloid cells can directly support T-ALL growth in vivo. Other signals in the TME of different organs likely complement myeloid-dependent signals to promote T-ALL progression. Myeloid depletion delays T-ALL incidence and

improves survival, but most mice still succumb to leukemia. This may partially reflect incomplete myeloid depletion, because the reduction in T-ALL burden was greatest in organs in which clodlip efficiently eliminated multiple myeloid subsets. In addition, previous studies identified a CXCR4-CXCL12 axis as critical for T-ALL survival in the BM (Passaro et al., 2015) (Pitt et al., 2015). Also, IL-7 can support T-ALL and is produced by stromal cells in the LN (Link et al., 2007) (Zamisch et al., 2005). Nevertheless, our studies clearly demonstrate that myeloid cells play a critical role in promoting T-ALL progression in vivo and indicate that a combined therapeutic strategy to target signals provided by myeloid cells and other stromal components may prove efficacious.

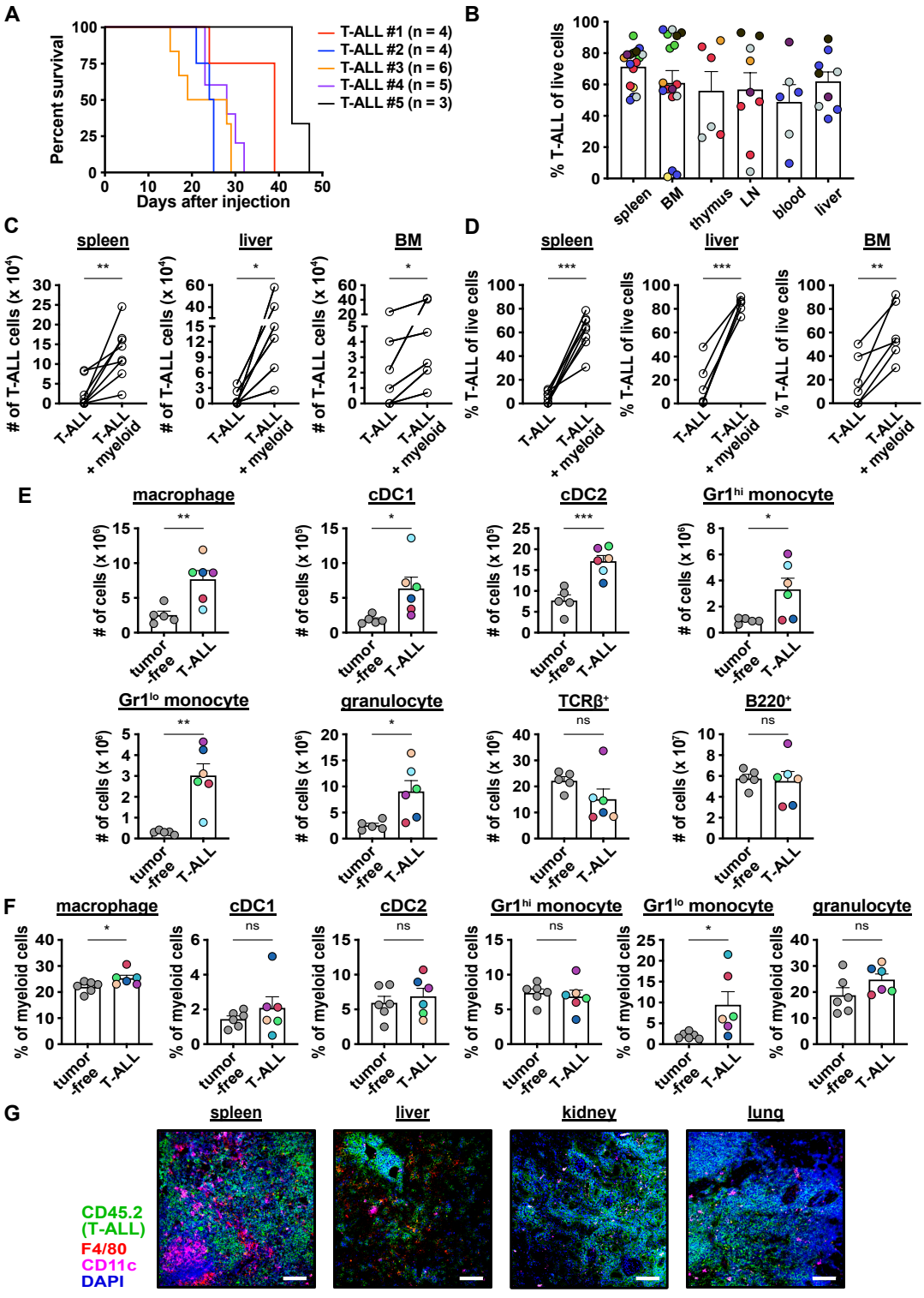

(Figure 2.1 continued on next page)

Figure 2.1. Transplanted T-ALL infiltrates multiple organs, remodels the myeloid compartment, and remains dependent on myeloid support for survival in vitro.

(A) Survival of non-irradiated CD45.1$^+$ mice transplanted with primary LN3 (CD45.2$^+$) T-ALL cells was followed. Each line represents results from a cohort of mice transplanted with a distinct primary T-ALL sample. (B) Quantification of the frequencies of T-ALL cells (CD45.2$^+$) within the indicated organs of leukemic transplant mice. Graph depicts cumulative data from 3 to 8 experiments, each with a distinct color-coded primary T-ALL. Bars represent means + standard error of the mean (SEM); circles represent individual mice. Graphs depict the number (C) and frequency (D) of viable T-ALL cells 6 or 7 days after culture in the presence or absence of enriched myeloid cells from the TME. T-ALL cells and myeloid cells were isolated from the indicated organs of leukemic mice that had been transplanted with primary LN3 T-ALL cells. Graphs depict cumulative data from 6 to 8 experiments, each with a distinct transplanted T-ALL sample; circles represent the average of 2 or 3 technical replicate wells per experiment. Graphs depict the number of cells of the indicated subsets (E) and frequencies of myeloid subsets (F) within the myeloid compartment (CD11b$^+$ and/or CD11c$^+$ cells) of spleens from tumor-free and LN3 T-ALL-transplanted mice. Graphs depict cumulative data from 5 or 6 independent experiments, each with a distinct color-coded primary T-ALL. Bars represent means + SEM; circles represent individual mice. (G) Representative immunofluorescent images of transplanted LN3 T-ALL cells and myeloid cells in the indicated organs. Immunostaining for T-ALL cells (CD45.2; green), F4/80 (red), CD11c (magenta), and DAPI (blue) is shown. Scale bars, 100 μm. *P < .05, **P < .01, ***P < .001, paired (C-D) and unpaired (E-F) Student t test. ns, not significant.

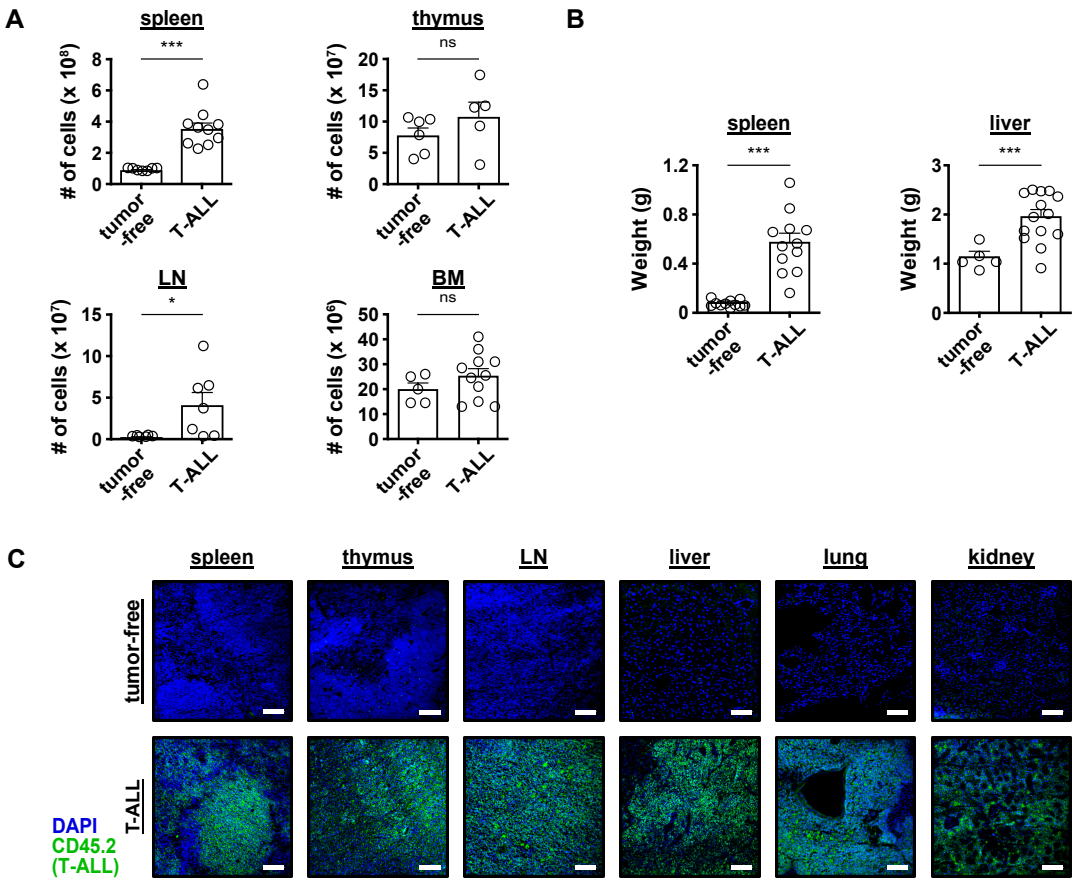

Figure 2.2. Transplanted T-ALL cells infiltrate multiple organs.

(A-B) Quantification of (A) total cell numbers and (B) weights of the indicated organs from tumor-free and overtly leukemic mice following transplantation of primary LN3 T-ALL. Graphs shown are cumulative data from 5 to 12 independent experiments. Bars represent means + standard error of the mean (SEM); circles represent individual mice (spleen (n=7-12), thymus (n=5-6), inguinal lymph nodes (LN; n=6-7), bone marrow (BM; n=5-11), and liver (n=14)). (C) Representative immunofluorescent images of transplanted LN3 T-ALL cells in the indicated organs; immunostained for T-ALL cells (CD45.2; green) with nuclear counterstain (DAPI; blue). Scale bars = 100 μm. *P < .05, ***P < .001, unpaired Student t test (A-B). ns, not significant.

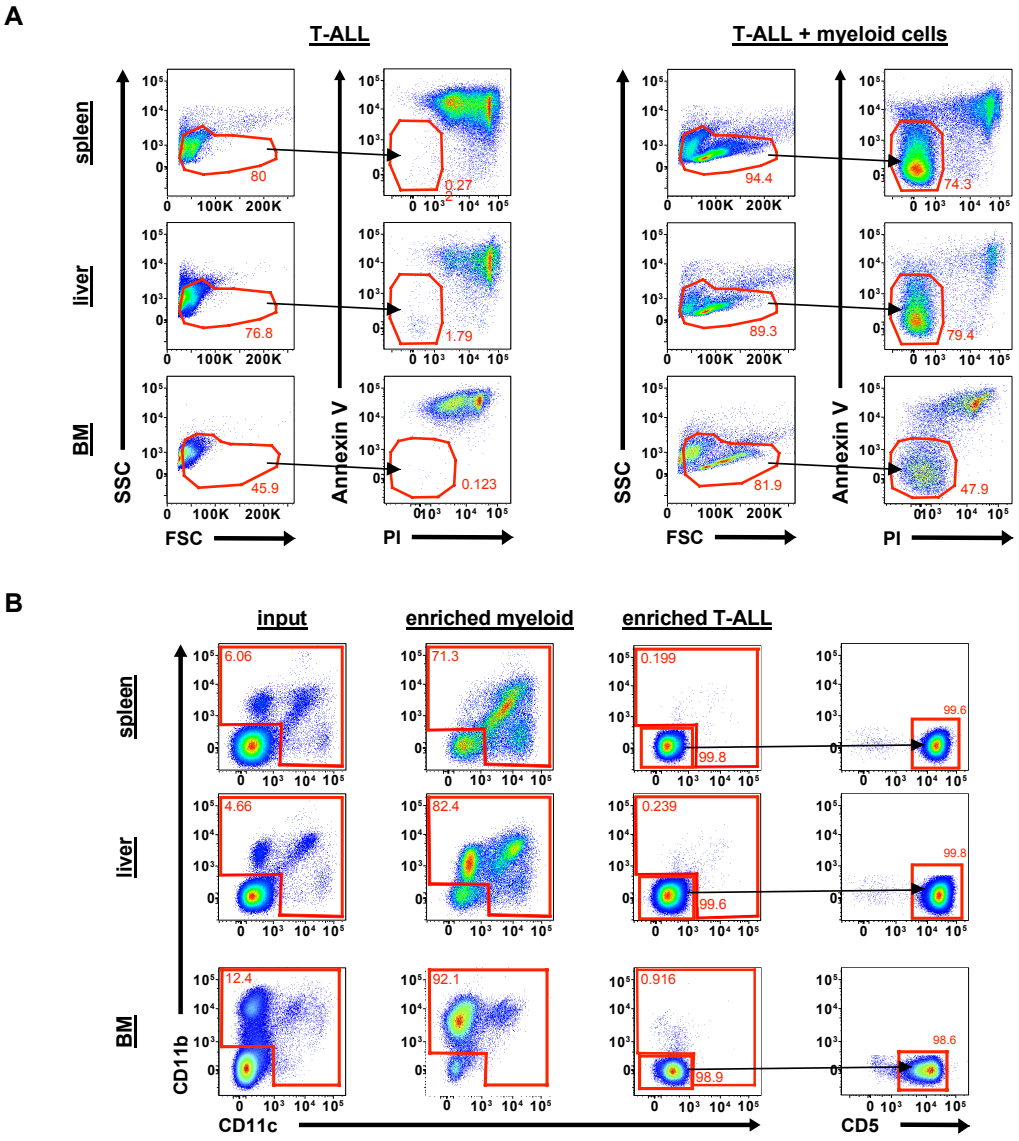

(Figure 2.3 continued on next page)

Figure 2.3. Transplanted T-ALL remains dependent on myeloid cells for survival in vitro.

(A) Representative flow cytometry plots showing the viability of transplanted LN3 T-ALL cells cultured in the presence or absence of paired myeloid cells enriched from the indicated organs. Viable cells were quantified as Annexin V $(AV)^{-}PI^{-}$ cells. (B) Representative flow cytometry plots showing the purity of enriched myeloid ($CD11b^{+}$ and/or $CD11c^{+}$) and T-ALL ($CD11b^{-}CD11c^{-}CD5^{+}$) cells from the indicated organs with sequential gating indicated by arrows. The "input" column shows myeloid composition ($CD11b^{+}$ and/or $CD11c^{+}$) before enrichment. The "enriched myeloid" column shows the percent of myeloid cells following positive enrichment of $CD11c^{+}$ cells from the spleen and enrichment of both $CD11b^{+}$ and $CD11c^{+}$ cells from the liver or bone marrow (BM). The third column shows the low frequency of myeloid ($CD11b^{-}$ and $CD11c^{-}$) cells within the enriched T-ALL population following depletion with antibodies against F4/80, CD11b, I-A/I-E, and CD11c. The fourth column shows expression of the T-lineage marker CD5 on the enriched T-ALL fraction.

A T-ALL spleen / liver myeloid gating strategy

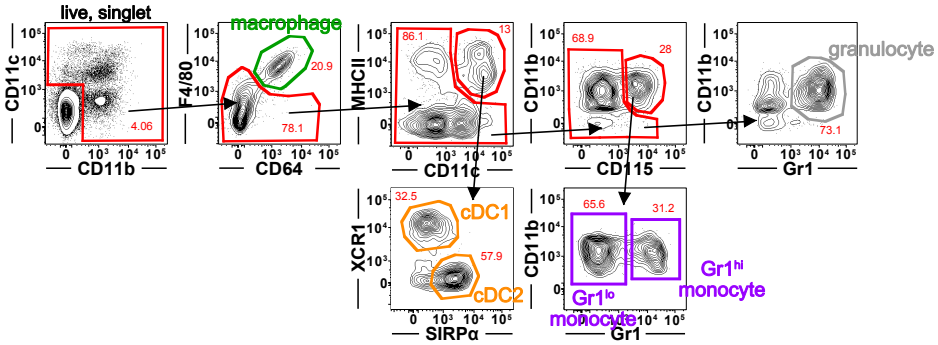

B T-ALL BM myeloid gating strategy

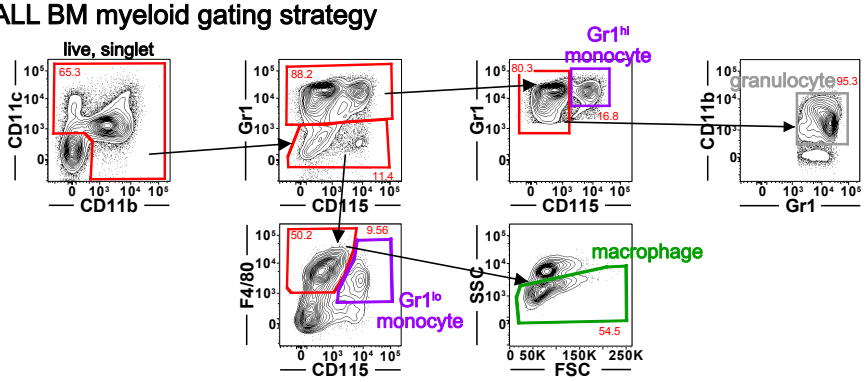

C T-ALL LN myeloid gating strategy

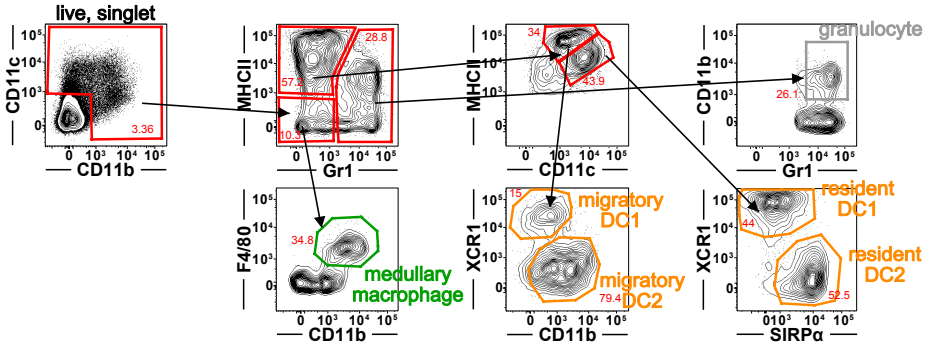

D T-ALL thymus myeloid gating strategy

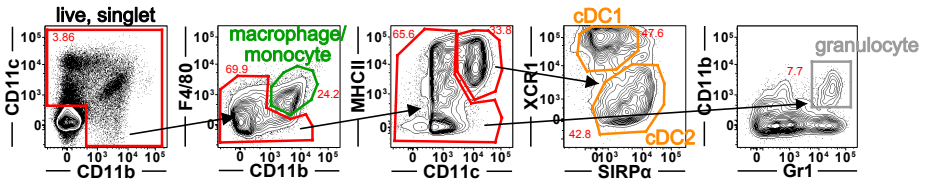

(Figure 2.4 continued on next page)

Figure 2.4. Gating strategies for analyzing the myeloid compartment in multiple organs from mice transplanted with primary T-ALL.

Representative sequential gating schemes for evaluation of the indicated myeloid subsets in mice transplanted with primary LN3 T-ALL in (A) spleen and liver, (B) bone marrow (BM), (C) inguinal lymph nodes (LN), and (D) thymus. The initial plot in each gating scheme is pre-gated on live (PI^-), singlet cells. Sequential gating is indicated by arrows.

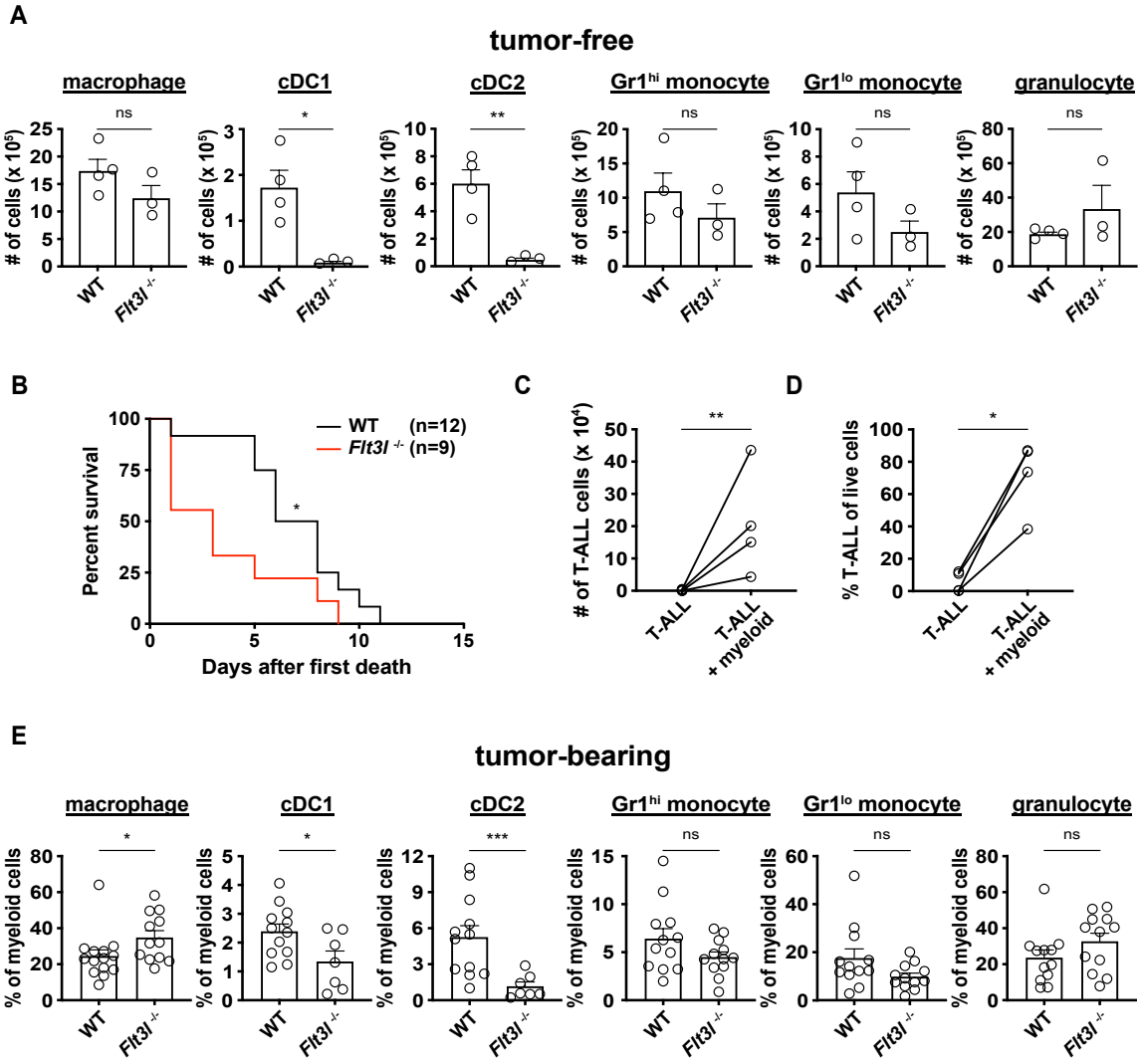

(Figure 2.5 continued on next page)

Figure 2.5. T-ALL growth is independent of DCs in vivo and can be supported by other myeloid subsets.

(A) Quantification of the indicated myeloid cell subsets in spleens of tumor-free WT and *Flt3l*$^{-/-}$ mice. Bars represent means + standard error of the mean (SEM) of 3 independent experiments; circles represent individual mice. (B) Survival of WT and *Flt3l*$^{-/-}$ recipient mice after transplantation with primary LN3 T-ALL cells. Graph displays cumulative survival of WT and *Flt3l*$^{-/-}$ mice from 3 independent experiments, each using distinct primary T-ALL samples. The Kaplan-Meier survival curves were normalized to the first day of death in each experiment. The number (C) and frequency (D) of viable T-ALL cells from the spleens of *Flt3l*$^{-/-}$ mice transplanted with primary LN3 T-ALL were assessed by flow cytometry 6 or 7 days after culture in the presence or absence of tumor-associated myeloid cells. Graphs display cumulative results from 4 independent experiments with distinct primary tumors. Circles represent the mean of 2 or 3 technical replicate wells per experiment. (E) Quantification of the frequencies of the indicated myeloid subsets within the splenic myeloid compartment of primary LN3 T-ALL-bearing WT and *Flt3l*$^{-/-}$ mice. Bars represent means + SEM of cumulative data from 7 to 13 independent primary tumors; circles represent individual mice. **P* < .05, ***P* < .01, ****P* < .001, unpaired Student t test (A,E), log-rank test (B), and paired Student t test (C-D). ns, not significant.

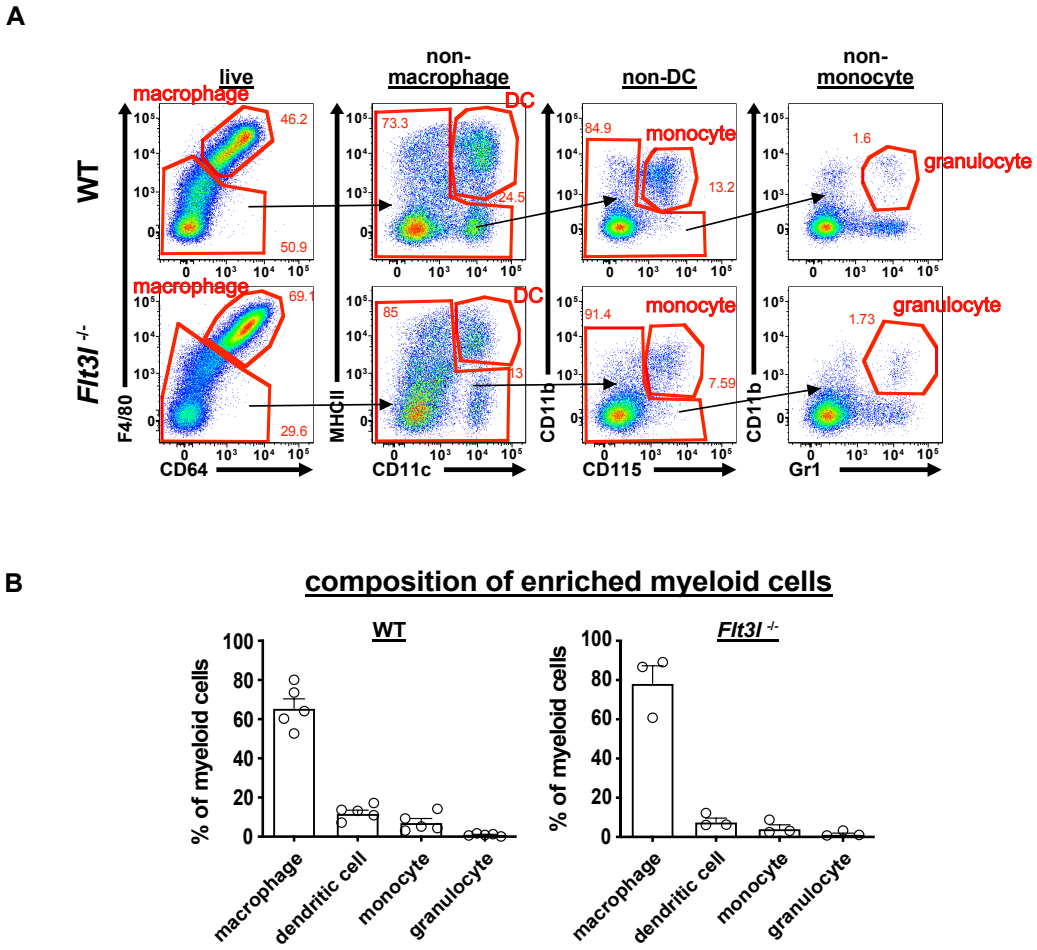

Figure 2.6. Composition of enriched myeloid cells in wild-type and *Flt3l*$^{-/-}$ mice transplanted with primary T-ALL.

(A) Representative flow cytometry plots showing the composition of myeloid subsets in the spleens of LN3 T-ALL-bearing wild-type (WT) and *Flt3l*$^{-/-}$ mice. Sequential gating strategies are shown using arrows. (B) Quantification of the frequency of the indicated subsets within enriched myeloid cells used for co-cultures from WT (Figure 2.1C-D) and *Flt3l*$^{-/-}$ (Figure 2.5C-D) tumor-bearing spleens. Bars represent means + standard error of the mean (SEM) of cumulative data from 3 to 5 independent experiments with distinct tumors; circles represent individual mice from each experiment.

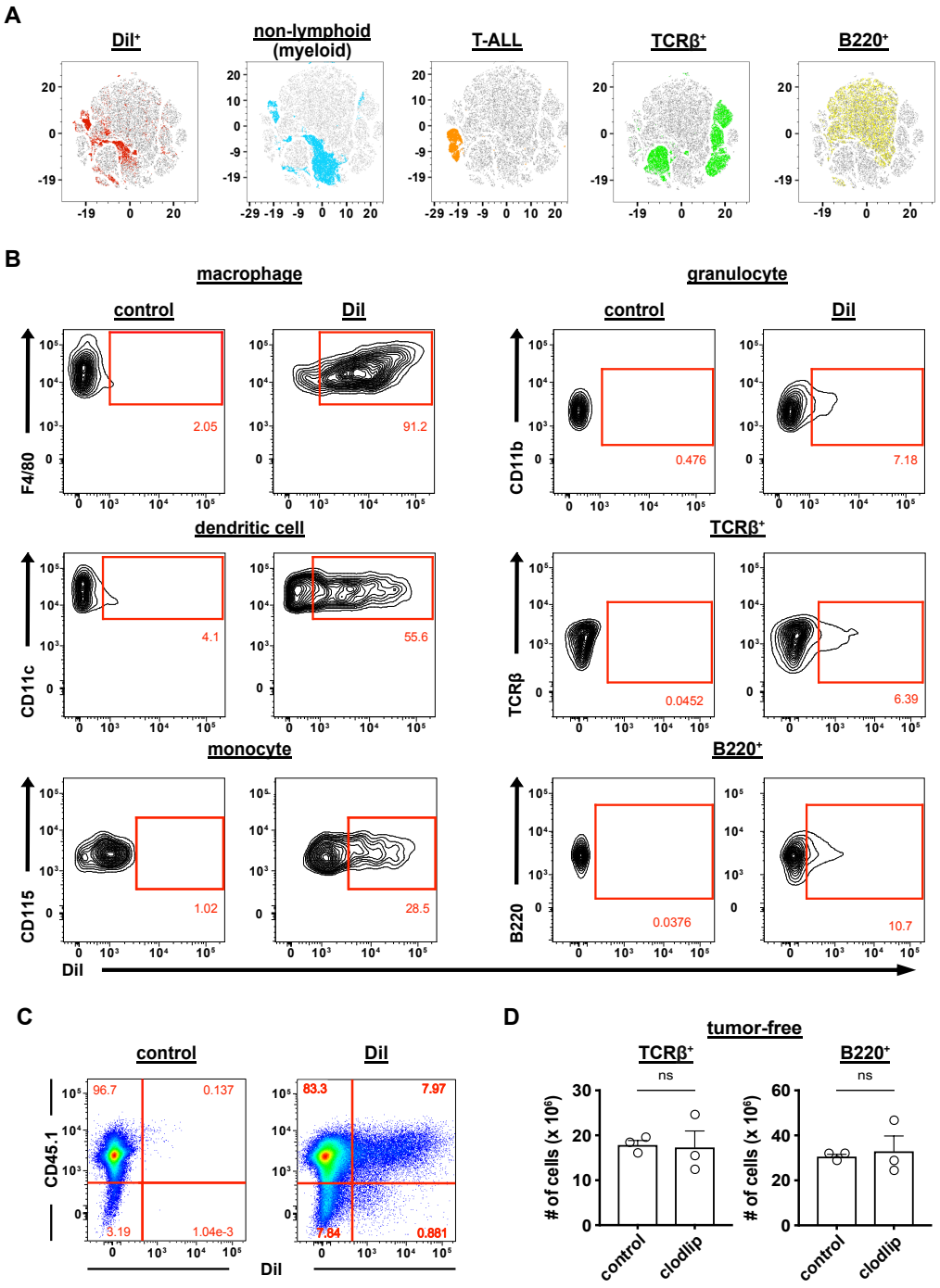

(Figure 2.7 continued on next page)

Figure 2.7. Liposome uptake is specific to myeloid cells and not by lymphocytes or T-ALL cells.

(A-B) Representative (A) t-SNE and (B) flow cytometric plots showing uptake of liposomes (Dil^+) by different cell types in the spleens of LN3 T-ALL-bearing mice following injection with Dil labeled liposomes. (A) t-SNE plots with overlays of cells that took up liposomes (Dil^+), "non-lymphoid" cells ($CD45.1^+TCR\beta^-B220^-$), T-ALL cells ($CD45.2^+$), host T cells ($CD45.1^+TCR\beta^+$), or host B cells ($CD45.1^+B220^+$), as indicated. (B) Splenic macrophages, dendritic cells, and monocytes were identified by flow cytometry using the gating strategy in Figure 2.4A and evaluated for uptake of liposomes (Dil^+). (C) Representative flow cytometry plot showing Dil^+ splenic cells are $CD45.1^+$ host cells, not $CD45.1^-$ T-ALL cells. (D) Quantification of $TCR\beta^+$ or $B220^+$ cells in the spleens following treatment with clodlip in tumor-free mice. Unpaired Student t test (D). ns, not significant.

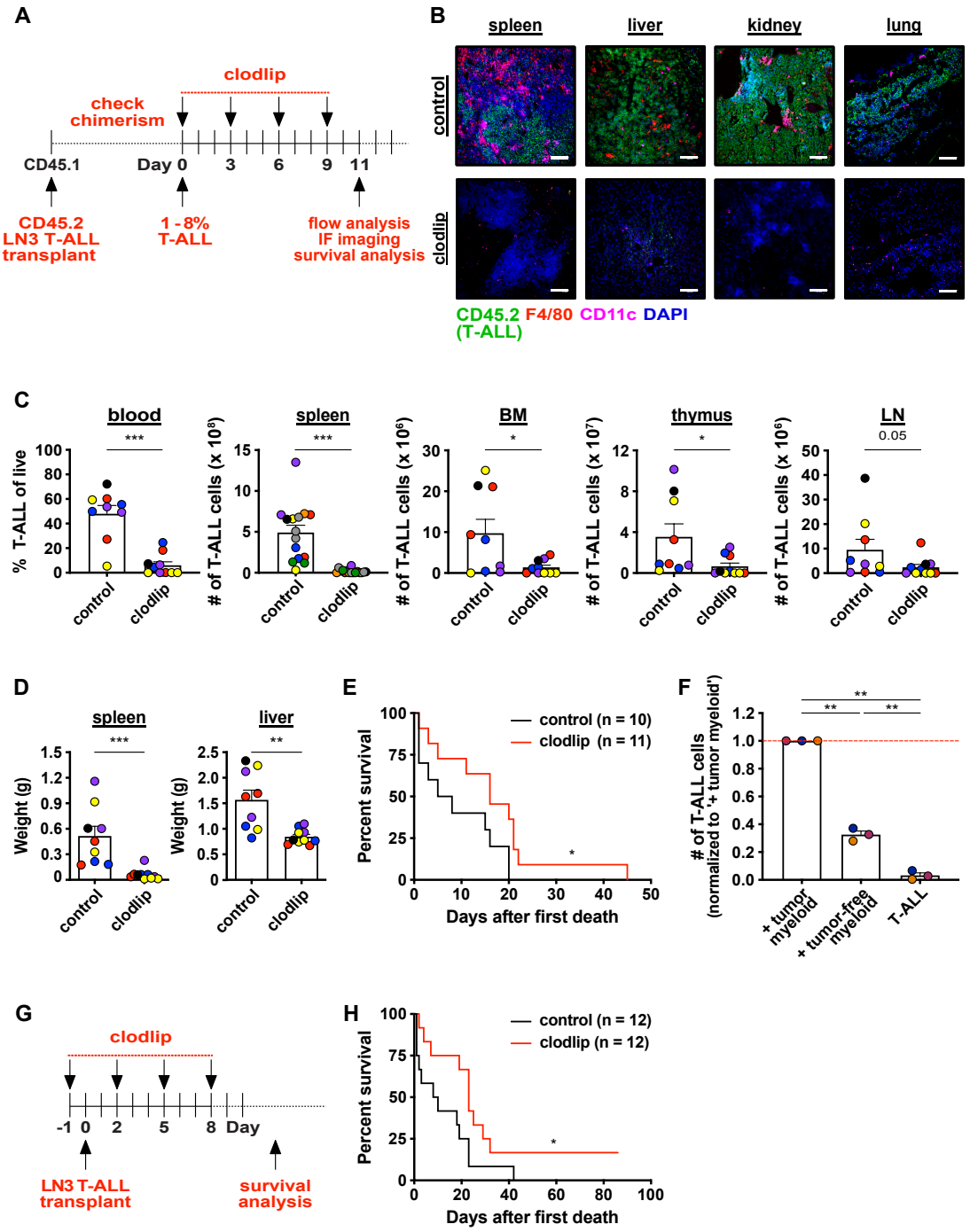

(Figure 2.8 continued on next page)

Figure 2.8. Depletion of phagocytic myeloid subsets results in decreased tumor burden in vivo and prolongs survival.

(A) Schematic diagram depicting the dosing schedule for clodlip treatment to deplete myeloid cells in mice with established transplanted LN3 T-ALL. (B) Representative images from the indicated organs of control or clodlip-treated mice after establishment of T-ALL burden. Immunostaining for T-ALL cells (CD45.2; green), F4/80 (red), CD11c (magenta), and DAPI (blue) is shown. Scale bars, 100 μm. (C) Quantification of the frequency of T-ALL cells in the blood and numbers of T-ALL cells in the spleen, BM, thymus, and inguinal LNs in control and clodlip-treated mice. Bars depict means + standard error of the mean (SEM) of cumulative data from 5 to 8 experiments, each with a distinct color-coded primary T-ALL; circles represent individual mice. (D) Quantification of the weights of spleens and livers from control and clodlip-treated mice from the same experiments as in (C). Bars show means + SEM of cumulative data from 5 independent experiments, each with a distinct color-coded primary T-ALL; circles represent individual mice. (E) Graph displays cumulative survival of control and clodlip-treated mice from 2 independent experiments, each with a different primary LN3 T-ALL, using the treatment regimen in (A). The Kaplan-Meier survival curves were normalized to the first day of death in each experiment. (F) Quantification of viable T-ALL cells, isolated from the spleens of LN3 T-ALL-transplanted mice 6 or 7 days after culture in the presence or absence of enriched myeloid cells from the spleens of tumor-bearing or tumor-free mice. Results were normalized to the viability of T-ALL cells co-cultured with tumor-associated myeloid cells within each experiment (red line). Bars depict means + SEM of cumulative data from 3 experiments, each with a distinct color-coded primary T-ALL; circles represent the mean of 2 or 3 replicate wells per experiment. (G) Schematic diagram depicting the dosing schedule to deplete myeloid cells prior to T-ALL engraftment in congenic recipients. (H) Graph displays cumulative survival of control and clodlip-treated mice from 3 independent experiments, each with a different primary LN3 T-ALL. The Kaplan-Meier survival curves were normalized to the first day of death in each experiment. $*P < .05$, $**P < .01$, $***P < .001$, unpaired Student t test (C-D), log-rank test (E,H), repeated measures one-way ANOVA with the Bonferroni correction (F).

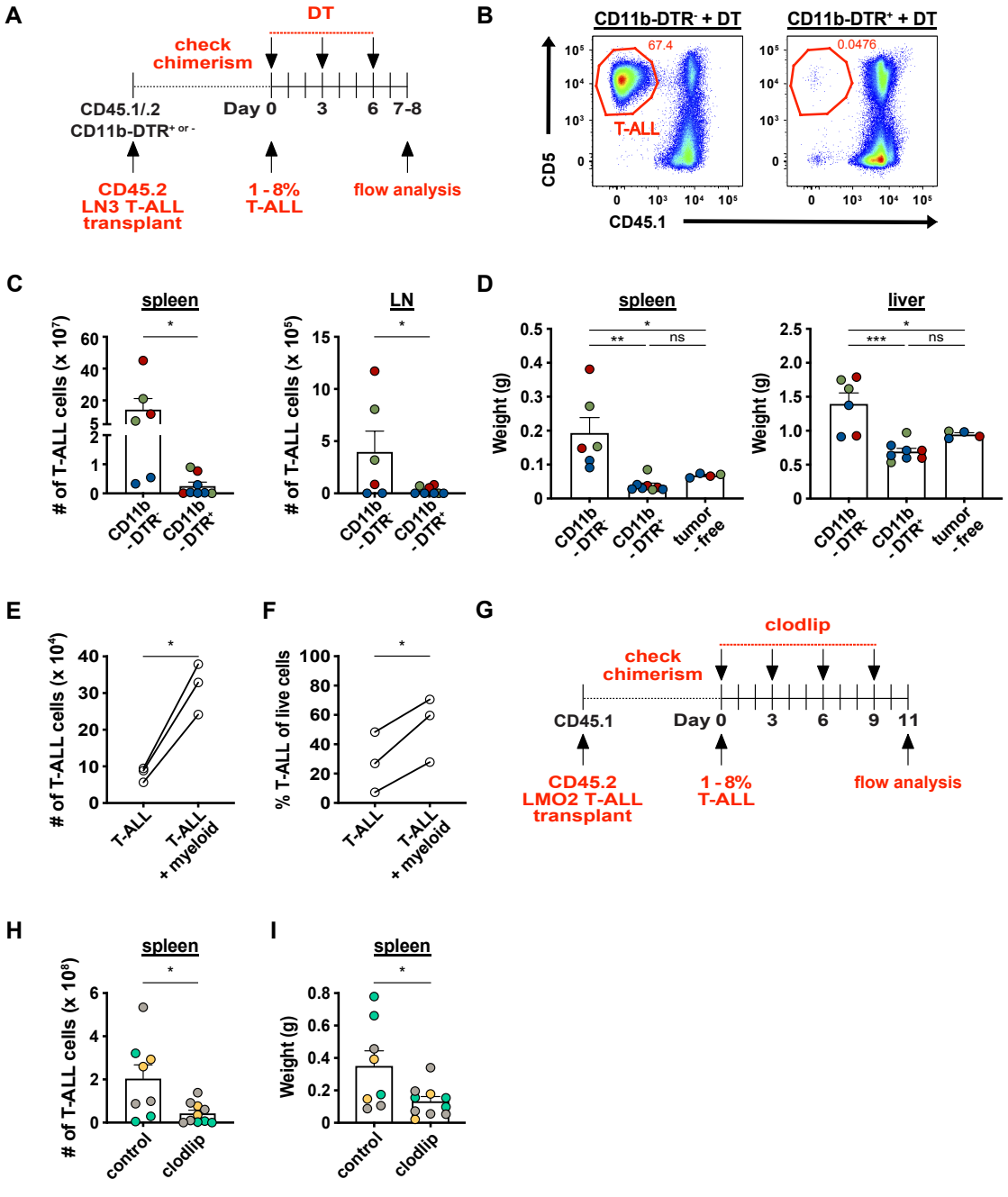

(Figure 2.9 continued on next page)

Figure 2.9. An alternative model of myeloid depletion and an independent mouse T-ALL model confirm that myeloid cells support T-ALL progression in vivo.

(A) Experimental schematic and dosing schedule for diphtheria toxin (DT) treatment to deplete myeloid cells in CD11b-DTR mice with established LN3 T-ALL. Cohorts of CD11b-DTR^{+} and transgene-negative littermate controls were transplanted with primary LN3 TALL cells, and once splenic T-ALL burden reached 1% to 8%, DT was injected in the entire cohort, resulting in myeloid depletion in transgene-positive mice. (B) Representative flow cytometry plots showing a decrease in T-ALL burden in the spleens of LN3 T-ALL-bearing mice treated with DT. (C-D) Quantification of the (C) numbers of T-ALL cells in the spleens and inguinal lymph nodes (LN) and (D) weights of spleens and livers in CD11b-DTR^{+} myeloid-depleted mice and CD11b-DTR^{-} littermate controls. Organ weights of tumor-free littermate controls are included in (D). Bars depict the mean + standard error of the mean (SEM) of cumulative data from 3 experiments, each with a distinct primary T-ALL; circles represent individual mice and each experiment is color-coded. (E-F) Graphs depict the (E) number and (F) frequency of viable LMO2 T-ALL cells cultured in the presence or absence of enriched myeloid cells from the leukemic spleens of mice transplanted with primary LMO2 T-ALL. Graphs show data from 3 independent experiments using distinct primary LMO2 T-ALL, with circles representing the average of 2-3 technical replicate wells per experiment. (G) Experimental schematic and dosing schedule for clodlip treatment to deplete myeloid cells in mice transplanted with primary T-ALL from LMO2 transgenic mice. (H-I) Quantification of the (H) number of T-ALL cells and (I) splenic weights of LMO2 T-ALL-bearing mice in the indicated treatment groups. Bars represent means + SEM of cumulative data from 3 independent experiments with a distinct color-coded primary T-ALL; circles represent individual mice. *P < .05, **P < .01, ***P < .001, unpaired (C,H,I) and paired (E,F) Student t test, repeated measures one-way ANOVA with the Bonferroni correction (D). ns, not significant.

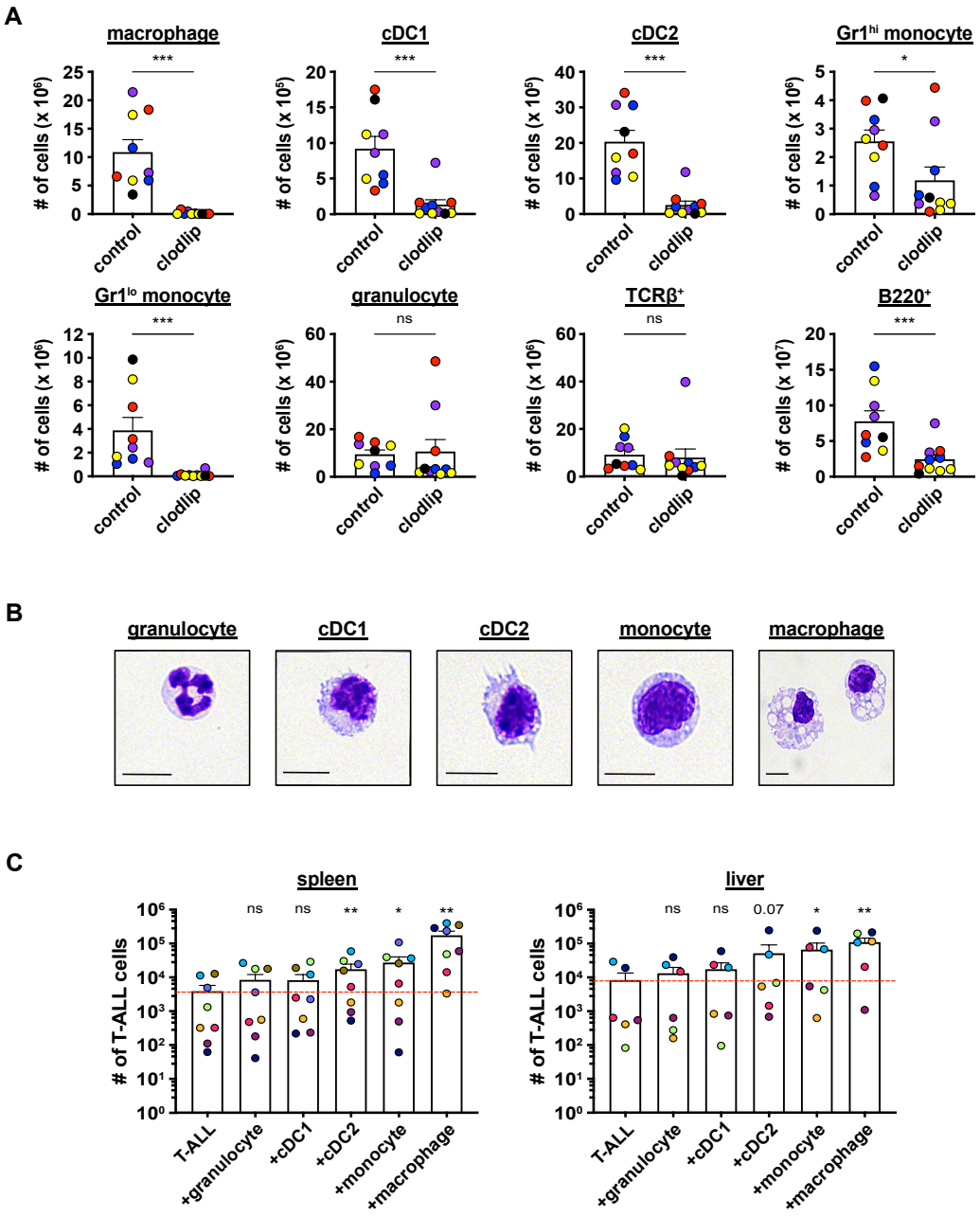

(Figure 2.10 continued on next page)

Figure 2.10. Clodlip treatment depletes multiple myeloid subsets that support T-ALL growth at hematopoietic and nonhematopoietic sites.

(A) Quantification of the number of myeloid cells of the indicated subsets in the spleens of control and clodlip-treated leukemic mice transplanted with primary LN3 T-ALL. Bars show means + standard error of the mean (SEM) from 5 independent experiments (the same as those analyzed in Figure 2.8C), each with a distinct color-coded primary T-ALL; circles represent independent mice. (B) Representative histologic images of FACS-sorted splenic myeloid subsets from primary LN3 T-ALL-transplanted mice, stained with the May-Grünwald Giemsa reagent. Scale bars, 10 μm. (C) Quantification of viable T-ALL cells 6 or 7 days after culture in the presence or absence of the indicated FACS-sorted myeloid subsets from the spleens or livers of transplanted LN3 T-ALL-bearing mice. Bars show means + SEM of cumulative data from 6 to 8 independent experiments, each with a distinct color-coded primary T-ALL; circles represent the average of technical replicate wells per experiment. The red line indicates the mean number of viable T-ALL cells cultured alone. $*P < .05$, $**P < .01$, $***P < .001$, unpaired Student t test (A), repeated measures one-way ANOVA with the Bonferroni correction (C). ns, not significant.

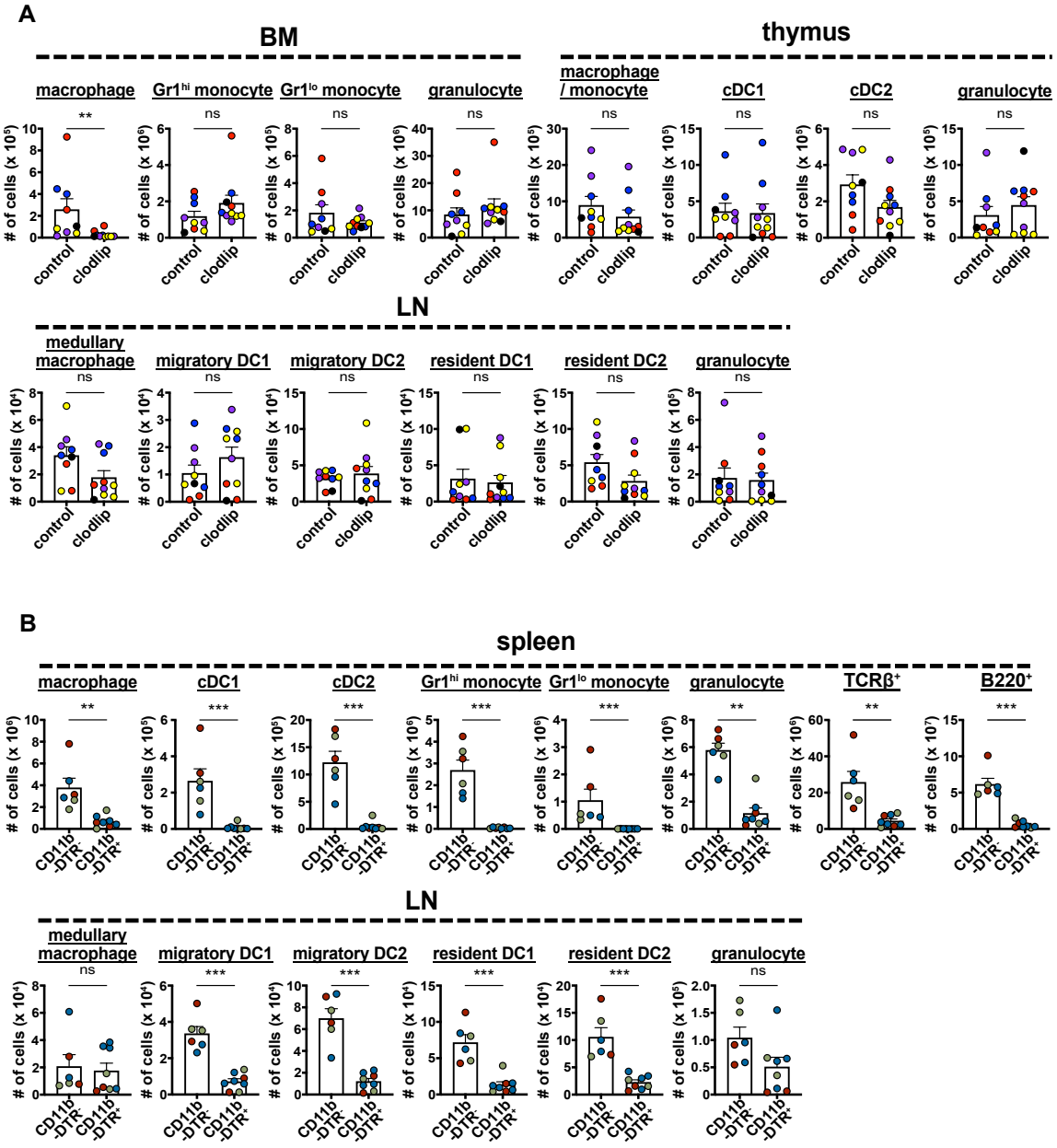

(Figure 2.11 continued on next page)

Figure 2.11. Myeloid subsets are depleted in multiple organs using clodlip or the CD11b-DTR model.

(A) Quantification of the indicated myeloid subsets in the bone marrow (BM), thymus, and inguinal lymph nodes (LN) in control and clodlip-treated mice transplanted with primary LN3 T-ALL (the same mice as in Figure 2.8C). (B) Quantification of the indicated myeloid subsets in the spleens and LN of CD11b-DTR^{-} control and CD11b-DTR^{+} myeloid-depleted mice transplanted with primary LN3 T-ALL (the same mice as in Figure 2.9C). The indicated myeloid subsets in each organ were gated as depicted in Figure 2.4A-D. Bars show the mean + standard error of the mean (SEM) from 3 to 5 independent experiments with a distinct color-coded primary T-ALL; circles represent individual mice. $^{**}P < .01$, $^{***}P < .001$, unpaired Student t test (A,B). ns, not significant.

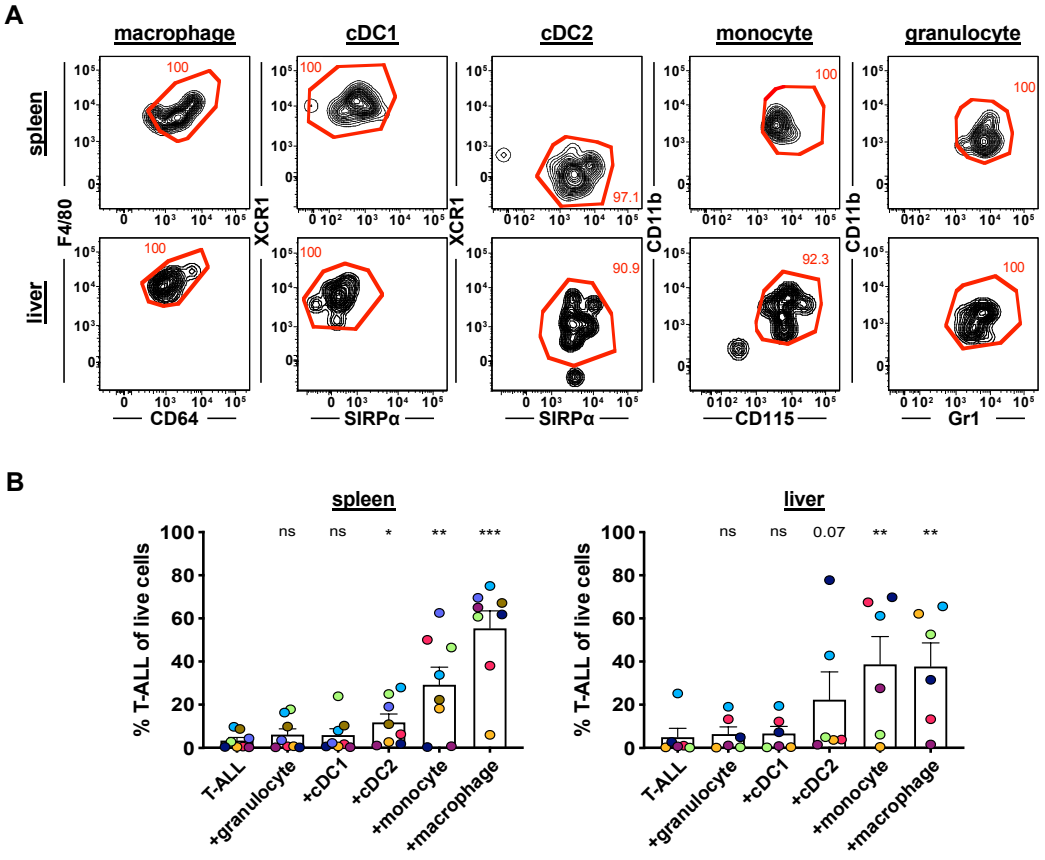

Figure 2.12. Multiple myeloid subsets from the spleen and liver can support T-ALL growth.

(A) Representative flow cytometry plots showing the purity of each myeloid subset after FACS sorting. Myeloid subsets were gated according to the strategy in Figure 2.4A, and the final gate for each subset is shown. (B) Quantification of the percent of viable T-ALL cells 6 or 7 days after culture in the presence or absence of the indicated FACS-sorted myeloid subsets from the spleens or livers of mice transplanted with primary LN3 T-ALL. Bars show the mean + standard error of the mean (SEM) of cumulative results from 6 to 8 independent experiments with a distinct color-coded primary T-ALL; circles represent the average of technical replicate wells per experiment. **P* < .05, ***P* < .01, ****P* < .001, repeated measures one-way ANOVA with the Bonferroni correction (B). ns, not significant.

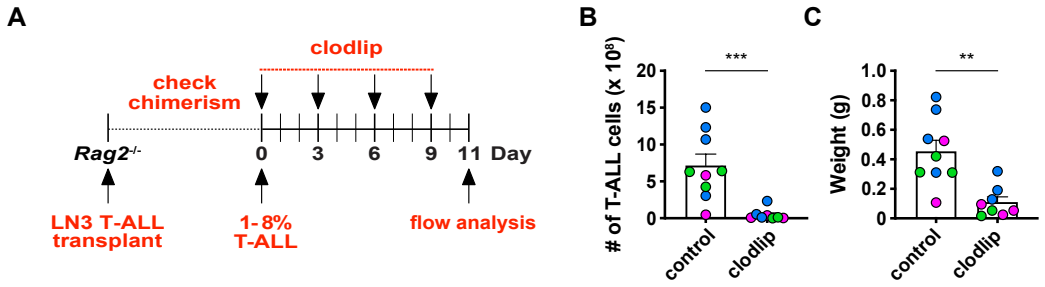

Figure 2.13. Adaptive immune responses are not required for the decrease in leukemia burden following myeloid depletion.

(A) Schematic diagram depicting the dosing schedule for clodlip treatment to deplete myeloid cells in *Rag2*$^{-/-}$ mice transplanted with primary LN3 T-ALL. Quantification of the number of splenic T-ALL cells (B) and weight of spleens (C) from T-ALL-bearing *Rag2*$^{-/-}$ mice in the indicated treatment groups. Bars represent means + standard error of the mean (SEM) of data compiled from 3 independent experiments, each with a distinct color-coded primary T-ALL; circles represent individual mice. $^{**}P < .01$, $^{***}P < .001$, unpaired Student t test (B).

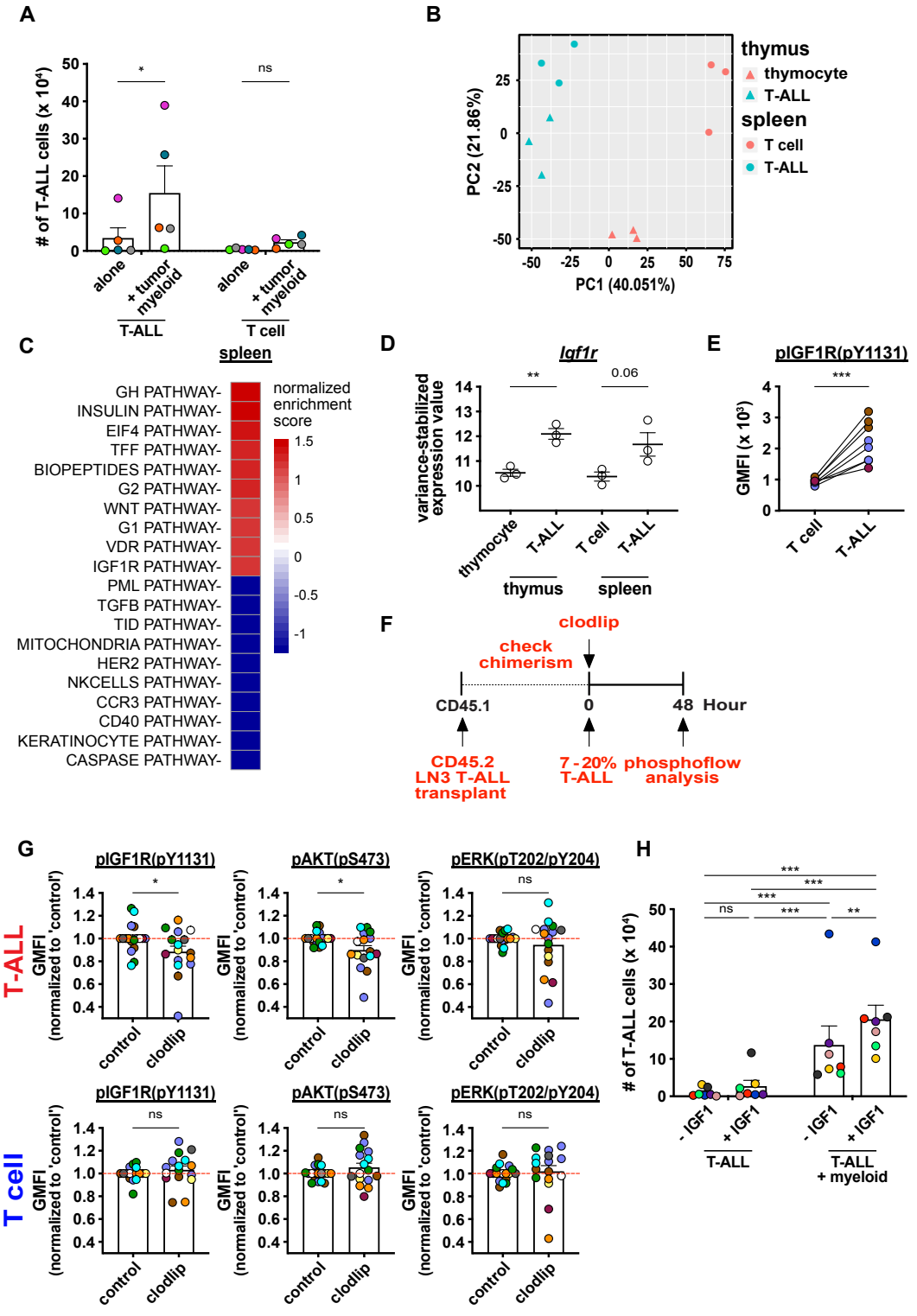

(Figure 2.14 continued on next page)

Figure 2.14. Activation of IGF1R signaling is associated with myeloid-mediated T-ALL survival.

(A) Quantification of viable T-ALL cells and $CD8^+$ T cells, isolated from the spleens of leukemic LN3 mice or tumor-free mice, respectively, 6 or 7 days after culture in the presence or absence of enriched splenic tumor-associated myeloid cells. Bars represent means + standard error of the mean (SEM) of data compiled from 5 independent experiments with a distinct color-coded primary T-ALL; circles represent the average of 2 or 3 technical replicate wells per experiment. (B) Principal component analysis (PCA) of gene-expression profiles of T-ALL cells from the thymus or spleen of LN3 mice, as well as thymocytes or splenic $CD8^+$ T cells from tumor-free mice. Symbols represent individual biologic replicates. (C) The top 10 pathways that were significantly enriched or depleted in splenic T-ALL cells relative to healthy $CD8^+$ T cells were identified by gene set enrichment analysis, using BioCarta gene sets. (D) Variance-stabilized expression values of *Igf1r* from control T-lineage vs T-ALL cells from the thymus and spleen. Bars represent means + SEM; circles represent individual biologic replicates. (E) pIGF1R levels in LN3-transplanted T-ALL cells ($CD45.2^+CD5^+$) relative to host T cells ($CD45.1^+CD5^+$) from the same spleens were quantified by flow cytometry and are displayed as geometric mean fluorescence intensities (GMFI). Data are compiled from 3 independent experiments, each with a distinct color-coded primary T-ALL. Circles represent individual mice. (F) Schematic diagram for acute myeloid depletion in mice with established LN3 T-ALL to assess changes in activation of IGF1R and downstream signals. (G) Levels of pIGF1R and the downstream signaling molecules phosphorylated (p)AKT and pERK were quantified in T-ALL cells (upper panels) and host T cells (lower panels) following acute myeloid depletions, as in (F). GMFIs from clodlip-treated mice were normalized to the mean of control mice in each experiment (red line). Bars represent means + SEM of cumulative data from 9 independent experiments, each with a distinct color-coded primary T-ALL. Circles represent individual mice. (H) Quantification of viable splenic T-ALL cells, isolated from the spleens of primary LN3 T-ALL-transplanted mice, 6 or 7 days after culture in the presence or absence of tumor-associated splenic myeloid cells and in the presence or absence of exogenous IGF1 (100 ng/ml). Bars represent means + SEM of cumulative data from 7 independent experiments with a distinct color-coded primary T-ALL; circles represent the average of 2 or 3 technical replicate wells per experiment. $*P < .05$, $**P < .01$, $***P < .001$, repeated measures two-way ANOVA with the Bonferroni correction (A,H), unpaired (D,G) and paired (E) Student t test. ns, not significant.

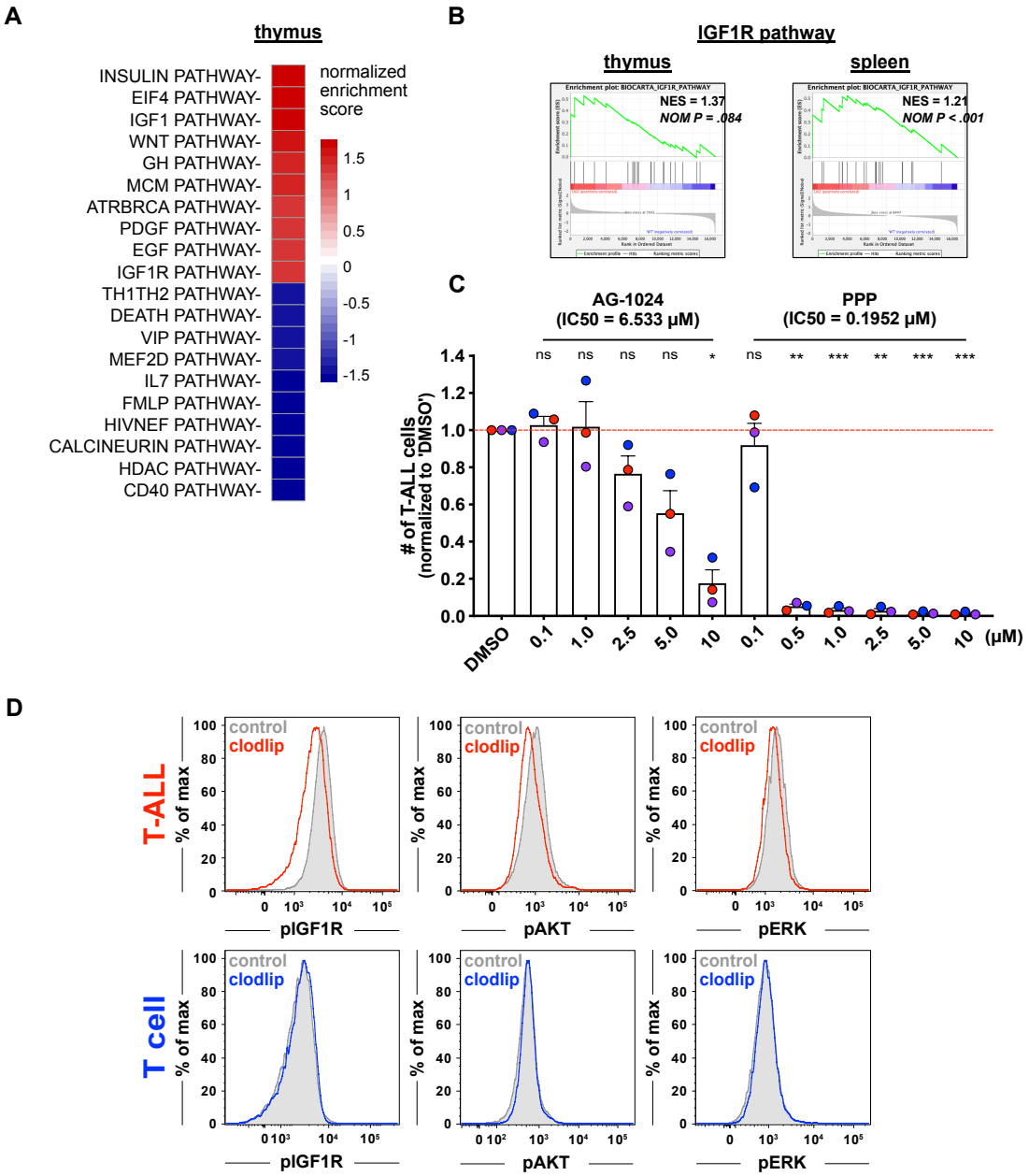

(Figure 2.15 continued on next page)

Figure 2.15. Activation of IGF1R signaling is associated with myeloid-mediated T-ALL survival.

(A) The top 10 pathways significantly enriched or depleted in thymic LN3 T-ALL cells relative to healthy thymocyte controls were identified using the BioCarta gene sets of the Gene Set Enrichment Analysis (GSEA) bioinformatics tool. (B) GSEA enrichment plots for the IGF1R pathway in thymic and splenic T-ALL cells relative to healthy thymocyte and $CD8^+$ T cell controls, respectively, as in (A). Normalized enrichment scores (NES) and nominal P-values are shown. (C) Quantification of viable T-ALL cells, isolated from the spleens of primary LN3 T-ALL-transplanted mice, co-cultured with enriched tumor-associated myeloid cells in the presence of the indicated concentrations of IGF1R inhibitors (AG-1024 or picropodophyllin (PPP)) or vehicle control (DMSO). Results were normalized to DMSO-treated control co-cultures in each experiment (red line). Bars represent means + standard error of the mean (SEM) of cumulative data from 3 independent experiments using distinct color-coded primary T-ALLs. Circles represent the average of 2 or 3 technical replicate wells per experiment. (D) Representative flow cytometry plots of pIGF1R and the downstream signaling molecules pAKT and pERK in LN3-transplanted T-ALL cells (red) and host T cells (blue) from the same leukemic spleens. Clodlip-treated results are indicated in red or blue and controls are shaded in gray. $*P < .05$, $**P < .01$, $***P < .001$, repeated measures one-way ANOVA with the Bonferroni correction (C). ns, not significant.

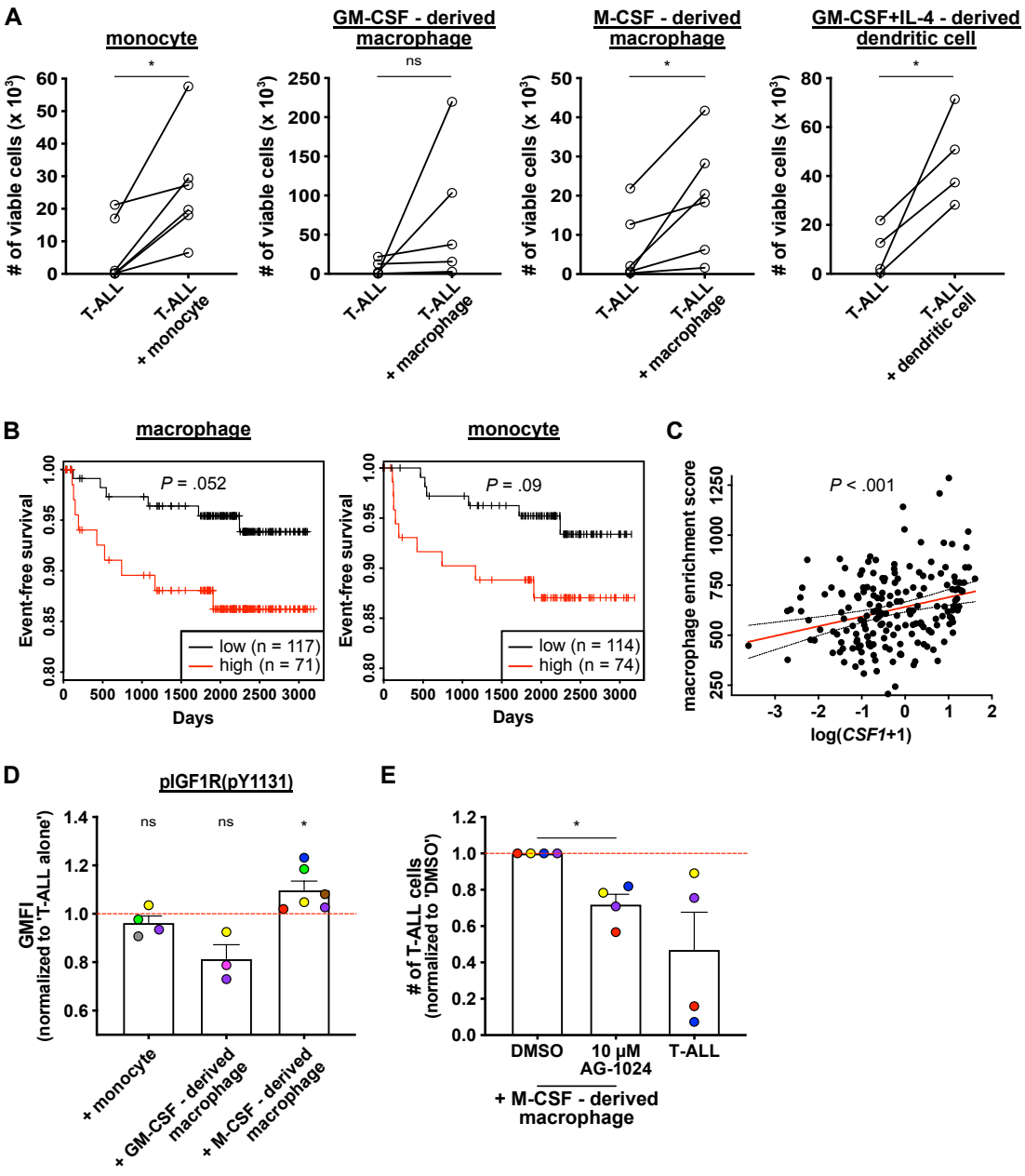

(Figure 2.16 continued on next page)

Figure 2.16. Human myeloid cells promote survival of patient T-ALL cells in vitro, and an elevated macrophage gene signature in patients is associated with worse prognosis.

(A) Quantification of viable primary patient T-ALL cells cultured for 6 or 7 days in the presence or absence of monocytes from healthy donor PBMCs or the indicated monocyte-derived myeloid cells. T-ALL viability was assessed by flow cytometry. Data are compiled from 2 to 4 independent experiments using 4 to 6 distinct patient-derived leukemias. Circle represent the average of 2 or 3 technical replicate wells per experiment. (B) Longitudinal event-free survival is plotted for pediatric T-ALL patients stratified into 2 groups based on their enrichment scores for macrophage or monocyte gene signatures, as indicated. Patient data were analyzed from published datasets from 264 T-ALL patients from the TARGET ALL Phase 2 trial (Liu et al., 2017). (C) Plot depicts the correlation between log-transformed *CSF1* expression values and macrophage enrichment scores in patient samples. The red and dotted lines represent the best-fit line and 95% confidence bands, respectively. Circles represent each patient sample. (D) pIGF1R levels were quantified by flow cytometry in patient T-ALL cells cultured for 3 or 4 days in the presence or absence of PBMC-derived monocytes or the indicated monocyte-derived myeloid cells. Results were normalized to levels in T-ALL cells cultured alone (red line). Bars represent means + standard error of the mean (SEM) of cumulative data from 3 to 5 independent experiments using 3 to 6 distinct color-coded patient-derived T-ALL samples. Circles represent the average of 2 technical replicate wells per experiment. (E) Quantification of viable patient T-ALL cells cultured alone or with M-CSF-derived macrophages in the presence of 10 μM AG-1024 (an IGF1R inhibitor) or DMSO. Results were normalized to DMSO-treated cultures in each experiment (red line). Bars represent means + SEM of cumulative data from 3 independent experiments using 4 of the distinct color-coded patient T-ALL samples used for co-cultures with M-CSF-derived macrophages in (D). Circles represent the average of 2 technical replicate wells per experiment. $*P < .05$, paired Student t test (A), log-rank test (B), simple linear regression analyses (C), one-sample Student t test (D), repeated measures one-way ANOVA with the Bonferroni correction (E). ns, not significant.

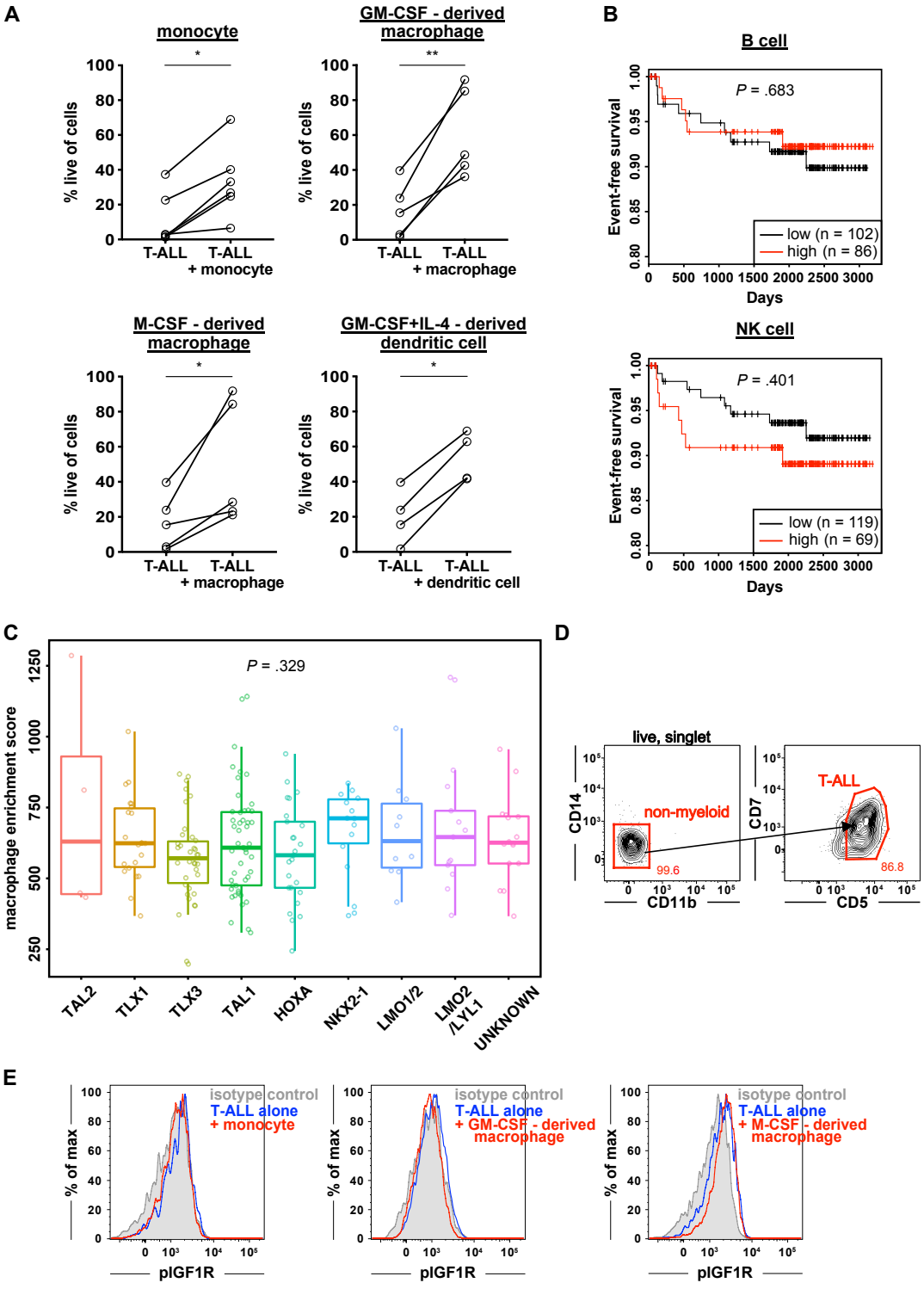

(Figure 2.17 continued on next page)

Figure 2.17. Human myeloid cells, particularly M-CSF-derived macrophages, promote survival of patient T-ALL cells by activating the IGF1R signaling.

(A) Quantification of the percent of viable primary patient T-ALL cells cultured for 6 or 7 days in the presence or absence of monocytes from healthy donor PBMCs or the indicated monocyte-derived myeloid cells. T-ALL viability was assessed by flow cytometry. Data are compiled from 2 to 4 independent experiments using 4 to 6 distinct patient-derived leukemias. Circles represent an average of 2 or 3 technical replicates. (B) Longitudinal event-free survival is plotted for pediatric T-ALL patients stratified into two groups based on their enrichment scores for B cell or natural killer (NK) cell gene signatures, as indicated. Patient data were analyzed from published datasets from 264 T-ALL patients from the TARGET ALL Phase II trial (Liu et al., 2017). (C) Plots depict macrophage enrichment scores stratified by molecular T-ALL subtypes in the same patient datasets as in (B). (D) Representative sequential gating schemes used to identify T-ALL cells so as to evaluate activated IGF1R (pIGF1R) levels. The initial plots are pre-gated on live, singlet cells. (E) Representative flow cytometry histograms of pIGF1R in T-ALL cells cultured alone (blue) or with monocytes or the indicated monocyte-derived macrophages (red) compared to isotype control stained cells (shaded in gray) used for quantification in Figure 2.16D. $*P < .05$, $**P < .01$, paired Student t test (A), log-rank test (B), one-way ANOVA (C). ns, not significant.

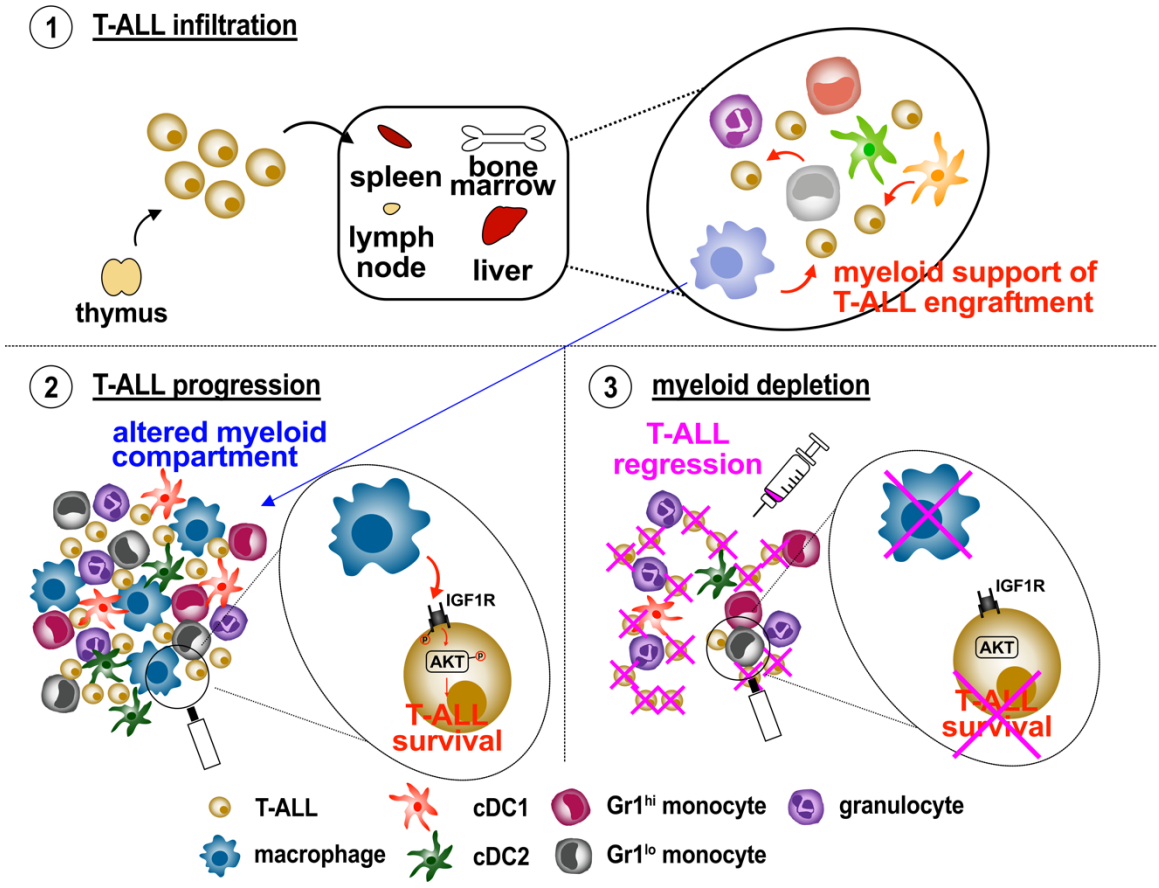

Figure 2.18. Illustrative summary of Chapter 2

① T-ALL cells encounter myeloid cells capable of supporting engraftment upon entry into secondary sites, and modify the environment, resulting in recruitment and/or differentiation of myeloid cells with an enhanced capacity to support T-ALL growth. ②,③ Depletion of multiple myeloid subsets in mice with established T-ALL via pharmacologic or genetic means results in a sharp decrease in circulating T-ALL blasts and reduced T-ALL infiltrates in several clinically relevant organs. Moreover, acute myeloid depletion results in a significant reduction in IGF1R and AKT activation in T-ALL cells, indicating that tumor-associated myeloid cells support T-ALL by activating the IGF1R pathway to promote survival.

Data Sources	Genes																														
BLUEPRINT1	ACP2	ATOX1	ATP6V0C	ATP6V1E1	C1QA	CD9	CD48	CLCN7	CCR1	CRYBB1	CYBB	FCER1G	FDX1	FOLR2	FPR3	FTL	HEXA	HEXB	KCNJ5	LAIR1	M6PR	MDH1	NUBP1	P2RX7	RAC1	CCL8	CCL22	STX4	TCEB1	TYROBP
	VAMP8	MARCO	CD84	ATP6V0E1	ATP6V1F	CD163	CIAO1	LY86	ARHGEF11	HS3ST2	ARPC4	ATP6AP2	BAIAP2	PRDX3	ERP29	LILRB5	SDS	LILRB4	VSIG4	FKBP15	ZZZ3	SIGLEC7	SIGLEC9	ADAMDEC1	ORMDL2	COMMD9	SPG21	MS4A4A	UBE2D4	TRAPPC2L
	TREM2	TMEM70	ARL8B	TMEM126B	SLAMF8	C12orf4	HAMP	GUF1	YIF1B																					
BLUEPRINT2	ACP2	ATOX1	ATP6V0C	ATP6V1E1	C1QA	CD9	CD48	CD63	CLCN7	TPP1	CCR1	CMKLR1	SLC31A1	COX5B	COX7B	COX8A	CRYBB1	CYBA	CYBB	FCER1G	FDX1	FOLR2	FPR3	FTL	GLB1	HEXA	HEXB	KCNJ5	LAIR1	LAMP1
	NUBP1	NDUFB3	NDUFS3	NDUFS6	P2RX7	PCMT1	MAPK13	PSME1	RB1	CCL8	CCL22	SDHD	SUMO3	SNX2	TCEB1	TYROBP	UQCRC2	VAMP8	MARCO	SNX3	CD84	ATP6V0E1	ITGB1BP1	S1PR2	ATP6V1F	CD163	COX5A	CIAO1	LY86	ARHGEF11
	HS3ST2	SCAMP2	ARPC4	ATP6AP2	BAIAP2	PRDX3	ERP29	UQCR11	LILRB5	SDS	LILRB4	VSIG4	STAB1	FKBP15	DNAJC13	CLEC5A	ZZZ3	SIGLEC7	SIGLEC9	ADAMDEC1	ORMDL2	COMMD9	UQCR10	SPG21	MS4A4A	UBE2D4	TRAPPC2L	TREM2	KCTD5	PQLC2
	COMMD8	TMEM70	ARL8B	SLC38A7	NOP10	WDR11	TMEM126B	TMEM99B	SLAMF8	C12orf4	MRS2	HAMP	DNASE2B	GUF1	MS4A6A	MRPL40	PPCS	PMFBP1	YIF1B	ADCK2	HIGD2A									
BLUEPRINT3	ACP2	ATOX1	ATP6V0C	ATP6V1E1	C1QA	CD9	CD48	CD63	CLCN7	CCR1	COX8A	CRYBB1	CYBB	FCER1G	FDX1	FOLR2	FPR3	FTL	HEXA	HEXB	KCNJ5	LAIR1	LAMP1	NDUFB3	NDUFS6	P2RX7	MAPK13	CCL8	CCL22	SNX2
	TCEB1	TYROBP	UQCRC2	VAMP8	MARCO	SNX3	CD84	ATP6V0E1	ITGB1BP1	ATP6V1F	CD163	COX5A	CIAO1	LY86	ARHGEF11	HS3ST2	SCAMP2	ARPC4	ATP6AP2	ERP29	UQCR11	LILRB5	SDS	LILRB4	VSIG4	STAB1	FKBP15	DNAJC13	CLEC5A	ZZZ3
	SIGLEC7	SIGLEC9	ADAMDEC1	ORMDL2	COMMD9	SPG21	MS4A4A	UBE2D4	TREM2	KCTD5	TMEM70	ARL8B	NOP10	WDR11	TMEM126B	SLAMF8	C12orf4	HAMP	GUF1	MS4A6A	MRPL40	PPCS	PMFBP1	YIF1B	ADCK2					
FANTOM1	ACP2	CHIT1	CSF1	CYP19A1	FDX1	HK3	MSR1	CCL22	SLC6A12	CD84	SDS	VSIG4	CLEC5A	ADAMDEC1	HAMP	DNASE2B	MYOZ1													
FANTOM2	ACP2	ADCY3	ALCAM	ABCD1	BPI	CHIT1	CYP19A1	HK3	KCNJ1	KCNMB1	CXCL9	MMP8	MSR1	CCL1	CCL7	CCL22	SLC1A2	SLC6A12	CD84	CD163	SDS	LILRB4	VSIG4	FKBP15	NCAPH	CLEC5A	ADAMDEC1	ATP6V1H	PQLC2	SLAMF8
	HAMP	DNASE2B	MYOZ1	LONRF3	MFSD7																									
FANTOM3	ACP2	ADCY3	ALCAM	ABCD1	ATP6V1A	ATP6V0A1	BPI	CHIT1	SLC31A1	CSF1	CYBB	CYP19A1	FDX1	FGR	HK3	ITGAX	KCNJ1	KCNMB1	CXCL9	MMP8	MMP19	MSR1	P2RX7	MAPK13	CCL1	CCL7	CCL22	SLC1A2	SLC6A12	SLC11A1
	STX4	NUMB	MARCO	CD164	CD84	CD163	CIR1	ARHGEF11	BCAP31	ATP6AP2	SDS	LILRB4	VSIG4	FKBP15	NCAPH	CLEC5A	ADAMDEC1	ATP6V1H	PQLC2	C2CDC58A	PCDHB11	SLAMF8	HAMP	DNASE2B	MYOZ1	LONRF3	MFSD7			
HPCA1	ACADVL	ACP2	ARSB	ATP6V1A	ATP6V0C	ATP6V1C1	CD63	CETN2	CCR1	SLC31A1	COX5B	COX15	CYBB	DBI	ECHS1	FDX1	GRB2	HADHB	HEXA	HEXB	HK3	HMGCL	ITGAX	KIFC3	TNFO1	LAIR1	LAMP1	MGST3	MSR1	NARS
	NDUFA8	NDUFB6	NDUFS8	PRDX1	PEX14	MAPK13	PSMD10	PTPN12	PEX19	QDPR	RAB1A	RAB5C	RALA	RENBP	CLIP1	CCL7	CCL18	SDHB	SRC	STX4	TCEB1	MLX	TRAF3	NSMAF	AGPS	MARCO	SNX4	ATP6V1F	LONP1	GSTO1
	BAG3	CIR1	FEZ2	PDCD6IP	SNUPN	BCAP31	STAM2	IGSF6	ZMPSTE24	TMEM147	VTI1B	TGOLN2	SPIN1	LILRB4	EMILIN1	VSIG4	EFR3A	FKBP15	CLEC5A	IBTK	NPTN	ATP2C1	SIGLEC9	ADAMDEC1	CNIH4	GLRX2	DERA	NDUFAF1	HSD17B12	ZDHHC3
	TNFRSF12A	MS4A4A	ATP6V1D	ATP6V1H	TMBIM4	STYXL1	BTBD1	NUDT9	TMEM33	NOP10	TMEM127	ACTR10	KCMF1	TULP4	C12orf4	RTN4	MKL2	HAMP	DNASE2B	KLHL12	NSUN3	ELOVL1	SLC30A5	MAPKAP1	LONRF3	TCEAL4	CHD9	TM2D1	MFSD7	G6PC3
	TBC1D16	ZDHHC24																												
HPCA2	ACP2	ARSB	ATP6V1A	ATP6V0C	ATP6V1C1	CD63	CETN2	CCR1	SLC31A1	COX5B	COX15	CYBB	DBI	ECHS1	FDX1	HEXB	LAIR1	LAMP1	MGST3	MSR1	NDUFA8	NDUFS8	PRDX1	MAPK13	PSMD10	PTPN12	PEX19	RAB1A	RALA	RENBP
	CCL7	SDHB	STX4	TCEB1	MLX	TRAF3	NSMAF	AGPS	MARCO	ATP6V1F	GSTO1	BCAP31	IGSF6	TMEM147	VTI1B	LILRB4	EMILIN1	VSIG4	EFR3A	CLEC5A	NPTN	ATP2C1	SIGLEC9	ADAMDEC1	CNIH4	GLRX2	DERA	NDUFAF1	ZDHHC3	TNFRSF12A
	MS4A4A	ATP6V1D	ATP6V1H	NUDT9	TMEM33	C12orf4	RTN4	HAMP	DNASE2B	ELOVL1	SLC30A5	MAPKAP1	LONRF3	MFSD7	G6PC3	TBC1D16	10-Sep	ZDHHC24												
HPCA3	ACADVL	ACP2	ARSB	ATP6V1A	ATP6V0C	ATP6V1C1	CD63	CETN2	CCR1	SLC31A1	COX5B	COX15	CYBB	DBI	ECHS1	FDX1	GRB2	HADHB	HCCS	HEXA	HEXB	HK3	HMGCL	ITGAX	TNFO1	LAIR1	LAMP1	MGST3	MSR1	NDUFA8
	NDUFS8	PRDX1	MAPK13	PSMD10	PTPN12	PEX19	QDPR	RAB1A	RALA	RENBP	CLIP1	CCL7	SDHB	SRC	STX4	TCEB1	MLX	TRAF3	UQCRC2	USF2	NSMAF	AGPS	MARCO	SNX4	ATP6V1F	GSTO1	PDCD6IP	BCAP31	STAM2	IGSF6
	ZMPSTE24	CEPT1	TMEM147	VTI1B	TGOLN2	SPIN1	LILRB4	TMEM115	EMILIN1	VSIG4	EFR3A	FKBP15	CLEC5A	NPTN	ATP2C1	TRAPPC3	SIGLEC9	ADAMDEC1	CNIH4	SLC25A24	GLRX2	DERA	NDUFAF1	ZDHHC3	TNFRSF12A	MS4A4A	ATP6V1D	ATP6V1H	BTBD1	NUDT9
	TMEM33	TMEM127	ACTR10	KCMF1	TULP4	C12orf4	RTN4	MKL2	HAMP	DNASE2B	NSUN3	ELOVL1	SLC30A5	C7orf25	MAPKAP1	PANK3	LONRF3	TM2D1	MFSD7	SETD3	G6PC3	TBC1D16	10-Sep	ZDHHC24						
IRIS1	ACP2	ADCY3	ABCD1	ATP6V1A	CHIT1	CLCN7	TPP1	SLC31A1	COX5B	CYP19A1	FDX1	HEXA	HK3	KCNJ1	M6PR	MSR1	SLC6A12	CD163	CD84	LONP1	ATP6AP2	TGOLN2	SDS	LILRB4	VSIG4	FKBP15	CLEC5A	ADAMDEC1	ATP6V1H	STX18
	PQLC2	DNASE2B	MYOZ1	SLC30A5	LONRF3	MFSD7	LDHAL6B																							
IRIS2	ACP2	ADCY3	ALCAM	ABCD1	ARSB	ATOX1	ATP6V1A	ATP6V0C	ATP6V1E1	ATP6V0A1	BPI	TSPO	CD63	CHIT1	CLCN7	TPP1	SLC31A1	COX5B	CSF1	CYBB	CYP19A1	FDX1	HTT	HEXA	HK3	ITGAX	KCNJ1	LAMP1	M6PR	MMP19
	MSR1	MTHFR	P2RX7	MAPK13	PTPRA	RABGGTA	SLC1A2	SLC6A12	STX4	TCEB1	NUMB	CD164	CD84	LONP1	CPNE6	CIR1	TTLL4	ARHGEF11	BCAP31	ATP6AP2	TGOLN2	SDS	LILRB4	VSIG4	FKBP15	CLEC5A	IL17RA	ADAMDEC1	NRBP1	SH3GLB1
	ATP6V1H	STX18	PQLC2	TMEM33	SLC38A7	VPS53	CCDC88A	SLAMF8	HAMP	DNASE2B	MYOZ1	MTMR14	SLC30A5	MUL1	C12orf49	LONRF3	MFSD7	LDHAL6B	ZDHHC24											
IRIS3	ACP2	CHIT1	CSF1	CYP19A1	FDX1	HK3	MSR1	CCL22	SLC6A12	CD84	SDS	VSIG4	CLEC5A	ADAMDEC1	HAMP	DNASE2B	MYOZ1													

Table 2.1. A list of genes used for the macrophage signature to plot longitudinal event-free survival of pediatric T-ALL patients.

Chapter 3

Integrin signaling is critical for myeloid-mediated support of T-ALL

The work presented in this chapter is currently in preparation for manuscript submission. A.L. designed and performed experiments, analyzed results, generated figures, and wrote manuscript.

ABSTRACT

We have recently reported that tumor-associated myeloid cells promote survival and progression of T-ALL both in mouse models and in patient samples, in part by activating IGF1R signaling in the leukemic cells. Tumor-associated myeloid cells sensitize T-ALL cells to exogenous IGF1, whereas IGF1 alone cannot sustain leukemic survival in culture. Thus, we hypothesized that additional mechanisms would contribute to myeloid-mediated support of T-ALL. Here, we report transcriptional profiling and functional assays indicating that integrin signaling is essential for myeloid-mediated support of T-ALL, which is consistent with the finding that T-ALL cells require close contact with myeloid cells to survive. Furthermore, in vivo inhibition of ICAM-1 and VCAM-1 binding through genetic or pharmacologic means results in a significant decrease in T-ALL burden in mouse models and confers a survival advantage. Further pathway analysis reveals activation of the focal adhesion pathway, which is downstream of integrin signaling, as a candidate mechanism of integrin-mediated myeloid support of T-ALL Consistent with this, levels of activated FAK and PYK2 are consistently diminished in T-ALL cells in the presence of blockade of ICAM-1 and VCAM-1. Moreover, in vitro co-cultures in the presence of FAK/PYK2 dual inhibitors show that myeloid-mediated survival of T-ALL is dependent on focal adhesion signaling. Consistent with mouse models, inhibition of integrin-mediated cell adhesion in co-culture of primary patient T-ALL cells with myeloid cells diminishes the viability of leukemia

cells. Moreover, enriched gene signatures of integrin pathways significantly correlate with a poor prognosis for pediatric T-ALL patients. In addition, expression of integrin pathway genes is strongly associated with enriched myeloid gene signatures in T-ALL patients. Collectively, these studies reveal that tumor-associated myeloid cells provide survival signals for T-ALL by activation of integrin signaling, implicating associated integrins and downstream signals as potential therapeutic targets for treatment.

INTRODUCTION

T-cell acute lymphoblastic leukemia (T-ALL) is a hematologic malignancy arising from neoplastic transformation of T-cell progenitors. T-ALL accounts for 15% and 25% of pediatric and adult ALL cases, respectively (Vadillo et al., 2018), and is associated with infiltration of leukemic blasts into multiple organs, including the spleen, bone marrow (BM), lymph nodes (LN), liver, and central nervous system (Hunger and Mullighan, 2015). Although T-ALL was once considered a high risk leukemia with frequent relapses, current intensified chemotherapy regimens have significantly improved prognoses, with 5-year survival rates greater than 90% for pediatric T-ALL (Möricke et al., 2016) (Siegel et al., 2020). However, frontline chemotherapeutics, including nelarabine, etoposide and cyclophosphamide, are associated with long-term morbidities, such as neurological toxicity, cognitive impairments, and metabolic disorders. (Luskin et al., 2016) (Ness et al., 2011). Moreover, outcomes of relapsed patients remain poor, with event-free and overall survival rates less than 25% (Nguyen et al., 2008) (Reismüller et al., 2009) (Karrman and Johansson, 2017). Therefore, there is a critical need to identify targets for development of less toxic and more effective treatments for T-ALL. Previous studies have identified several genetic drivers of disease, including activating mutations in *NOTCH1* (Weng et al., 2004), deletion of the *CDKN2A* locus encoding tumor

suppressors (Hebert et al., 1994) and aberrant expression of T-cell transcription factors (Belver and Ferrando, 2016). Recently, unbiased genome-wide profiling analysis has expanded our understanding of the genetic landscape of T-ALL, identifying novel driver genes and associated molecular mechanisms that promote leukemia (Liu et al., 2017). These efforts have yet to translate into approved therapies, providing rationale to investigate additional leukemia-supportive factors, particularly cell-extrinsic ones, as potential targets.

Numerous studies have shown that the tumor microenvironment (TME), shaped by crosstalk between tumor cells and heterogeneous neighboring cells, plays an essential role in supporting progression of both solid tumors and hematologic malignancies (Binnewies et al., 2018) (Witkowski et al., 2020). Several cell types in the TME have been shown to support T-ALL. For example, vascular endothelial cells promote T-ALL growth via a C-X-C motif chemokine receptor 4 (CXCR4)-CXCL12 axis in the BM (Pitt et al., 2015) (Passaro et al., 2015), and thymic epithelial cells (TECs) support survival of leukemia cells though provision of interleukin 7 (IL-7) and NOTCH ligands (Scupoli et al., 2003) (Armstrong et al., 2009) (Silva et al., 2011). In addition, we and others found that tumor-associated myeloid cells promote T-ALL survival and progression (Triplett et al., 2016) (Lyu et al., 2020) (Yang et al., 2020), at least in part by activating IGF1R signaling (Lyu et al., 2020). However, exogenous IGF1 is not sufficient to support T-ALL survival, although tumor-associated myeloid cells enhance the response of T-ALL cells to IGF1 (Lyu et al., 2020), suggesting a role for additional molecular mechanisms by which myeloid cells promote T-ALL growth.

Integrins are heterodimeric receptors consisting of α and β chains; there are 24 integrin pairs in humans (Giancotti, 2000). Integrins bind a variety of ligands, including extracellular matrix (ECM) components such as fibronectin, collagen, and laminin, and

adhesion molecules present on antigen-presenting cells (APCs) or endothelial cells (Humphries et al., 2006). Upon ligand binding, integrins undergo a conformational change. Then they regulate cytoskeletal structures through talin and actin, and activate kinases downstream of integrins, such as focal adhesion kinase (FAK), proline-rich tyrosine kinase 2 (PYK2), and SRC family kinases, leading to diverse cellular outcomes including cell migration, survival, and proliferation (Cooper and Giancotti, 2019). Integrins are also known to jointly control signaling with growth factor receptors, including IGF1R, to coordinate development of normal cells (Giancotti and Tarone, 2003) (Cooper and Giancotti, 2019). Notably, integrins have been implicated in promoting tumorigenesis, metastasis, and resistance to chemotherapy. Mechanisms underlying integrin-mediated tumor support include production of ECM and recruitment of host cells expressing integrin ligands, such as endothelial cells, fibroblasts, and immune cells, by tumor cells, resulting in overactivation and dysregulation of integrin signaling in tumors (Lu et al., 2012) (Egeblad et al., 2010). Ample evidence suggests dysregulated integrin signaling contributes to tumor progression in multiple malignancies, including breast cancer (Bui et al., 2019), pancreatic cancer (Brannon et al., 2020), and multiple myeloma (Neri et al., 2011). Integrins have also been implicated in T-ALL pathogenesis. For example, BM stroma supports T-ALL cell survival via interactions through intercellular adhesion molecule 1 (ICAM-1) (Winter et al., 2001), and activation of integrin β1 by ECM components induces chemoresistance of T-ALL cells (Berrazouane et al., 2019). Integrin-mediated cell adhesion with antigen-presenting cells is critical for T-cell development, maintenance, and activation (Lancaster et al., 2018) (Walling and Kim, 2018) (Rabb, 2002). We have previously demonstrated that T-ALL cells make more frequent and prolonged contacts with tumor-associated DCs in the thymus relative to healthy thymocytes (Triplett et al., 2016), and tumor-associated myeloid cells provide

critical support for T-ALL in vivo (Lyu et al., 2020). Given that integrins play a key role in enhancing survival signaling by growth factor receptor, supporting tumor progression, and promoting interactions between T cells and APCs, combined with our previous data that myeloid cells promote T-ALL growth through mechanisms involving IGF1R signaling, we hypothesize that integrins play a role in myeloid-mediated support of T-ALL.

Here, we sought to determine whether integrin signaling contributes to myeloid-mediated support of T-ALL. We first determine that survival of T-ALL cells is dependent on close contact with myeloid cells, implicating integrin signaling. Furthermore, transcriptional profiling reveals enhanced integrin signaling in T-ALL cells relative to healthy T-lineage cells. Consistent with this, inhibition of ICAM-1 and/or vascular cell adhesion protein 1 (VCAM-1), both of which are expressed by tumor-associated myeloid cells, or their respective integrin receptors present on T-ALL cells results in a significant decrease in the survival of T-ALL cells in vitro. Notably, inhibition of ICAM-1 and/or VCAM-1 in T-ALL-engrafted mice using genetic or pharmacologic approaches significantly diminishs leukemic burden in multiple organs and confers a significant survival benefit. Transcriptional analysis and functional experiments identify the focal adhesion pathway, which is downstream of integrin signaling, as a target for myeloid-mediated support of T-ALL. We also find that integrin-mediated cell adhesion plays a role in myeloid-mediated support of patient T-ALL cells, and elevated gene signatures of integrin pathways are associated with high enrichment scores of monocytes and macrophages, and inferior patient prognosis. Collectively, these results reveal that myeloid cells promote T-ALL survival and progression via activation of integrin signaling in mouse models and in human patients.

METHODS

Mice

LN3 (Serwold et al., 2007) (Serwold et al., 2010), CD2-*Lmo2* transgenic (Smith et al., 2014), B6.129S4-*Icam1*^{tm1Jcgr}/J (*Icam1*$^{-/-}$) (Xu et al., 1994), C57BL/6J, B6.SJL-*Ptprc*^{a} *Pepc*^{b}/BoyJ (CD45.1) mouse strains were bred in-house and housed in specific-pathogen-free conditions. *Icam1*$^{-/-}$, C57BL/6J, and CD45.1 were sourced from The Jackson Laboratory. All experimental procedures were approved by the Institutional Care Use Committee at the University of Texas at Austin.

Flow cytometric analysis

Organs were harvested and processed as follows: Spleens were mechanically dissociated with fluorescence-activated cell sorting (FACS) wash buffer (FWB: phosphate-buffered saline (PBS) supplemented with 2% (v/v) BCS (Bovine Calf Serum; GemCell) and 0.5 mM EDTA). Bone marrow cells were obtained by flushing a femur with 2 ml of FWB. Inguinal lymph nodes were enzymatically dissociated with a cocktail of 0.6 mg/ml (w/v) Liberase™ and 20 U/ml DNase (both from Roche). These organs were sequentially digested 3 times in 2 ml digest cocktail for 12 minutes per digest. Livers were mechanically dissociated, spun at 50 g for 3 minutes, and the supernatant was collected and analyzed. All single-cell suspensions were filtered using 40 μm filters (Fisher Scientific) and subjected to red blood cell lysis using RBC Lysis Buffer (10×; BioLegend). Cells were immunostained by incubating at 4 ˚C for 30 minutes with fluorescently labeled antibodies against: For staining of the lymphoid compartment, anti-mouse CD4-PerCP/Cy5.5 (RM4-5), -mouse CD5-PE (53-7.3), -mouse CD8a-Pacific Blue (53-6.7), -mouse CD45.1-FITC (A20), -mouse CD45.2-APC/Cy7 (104), -mouse/human B220-Alexa Fluor 700 (RA3-6B2), -mouse TCRβ-PE/Cy7 (H57-597), anti-human CD3-

PE/Cy7 (UCHT1), -human CD5-Pacific Blue (UCHT2), -human CD7-APC eFluor® 780 (124-1D1; eBioscience). For staining of the myeloid compartment, anti-mouse CD64-PE (X54-5/7.1), -mouse CD11c-Pacific Blue (N418), -mouse I-A/I-E-APC/Cy7 (M5/114.15.2), -mouse CD172a-PE/Cy7 (SIRPα; P84), -mouse/rat XCR1-Biotin (ZET), -mouse/human CD11b-Alexa Fluor 700 (M1/70), -mouse CD115-Alexa Fluor 488 (AFS98), -mouse Gr1-Brilliant Violet 510 (RB6-8C5), -mouse F4/80-Alexa Fluor 647 (T45-2342; BD Biosciences), Qdot® 605 streptavidin conjugate (Invitrogen™), anti-human CD14-PerCP/Cy5.5 (M5E2). For staining of integrin components, anti-mouse CD49d-Alexa Fluor 488 (R1-2), -mouse CD11a-FITC (2D7), -mouse/rat CD29-PE (HMβ1-1), -mouse CD18-PE (M18/2), -mouse Integrin α9 (N-19; Santa Cruz Biotechnology), goat anti-mouse IgG-Alexa Fluor 488 (Jackson ImmunoResearch), anti-human CD49d-PE (9F10), -human Integrin α9β1 (Y9A2), -human CD11a-PE (HI111), -human CD29-Alexa Fluor 488 (TS2/16), -human CD18-FITC (TS1/18). For staining of adhesion molecules, anti-mouse CD54-PerCP/Cy5.5 (YN1/1.7.4), -mouse CD106 (429(MVCAM.A)), anti-human CD54 (HA58), -human CD106 (STA). The relevant isotype antibodies (RTK2758, RTK4530, and HTK888) were used as negative controls. All antibodies were purchased from BioLegend, unless otherwise indicated. After staining, cells were washed in FWB and resuspended in FWB containing 1 μg/ml propidium iodide (PI; Enzo Life Sciences) to assess viability.

For intracellular immunostaining of phosphorylated proteins, single-cell suspensions were labeled with LIVE/DEAD™ Fixable Dead Cell Stain Kit (Green or Aqua; Invitrogen™) and then treated with FIX & PERM Fixation & Cell Permeabilization Kit (Invitrogen™) according to the manufacturer's methanol modification procedure. Cells were then stained with fluorescently labeled antibodies against anti-mouse CD45.1-PerCP/Cy5.5 (A20), -mouse CD45.2-APC/Cy7 (104), -

mouse CD5-PE/Cy7 (53-7.3), and antibodies for phosphoflow analysis against pIGF1R-Alexa Fluor 647 (K74-218; pY1131), pAKT-PE or -Brilliant Violet 421 (J24-618; pS473), pPYK2-PE (L68-1256.272; pY402; all the above from BD Biosciences), pFAK (#3284; pY925; Cell Signaling Technology®), and Donkey anti-rabbit IgG-PE (Poly4064). Mouse IgG1 (MOPC-21), Mouse IgG2b, κ-PE (MPC-11), and Purified Rabbit Polyclonal IgG (Poly29108) were used as negative controls. All antibodies were purchased from BioLegend, unless otherwise indicated.

All flow cytometric data were acquired using an LSR II flow cytometer (BD Biosciences). Post-acquisition data analysis was performed using FlowJo (v9.9.6, Tree Star, Inc.).

In vitro cultures of mouse and human T-ALL cells

Complete RPMI cell culture media was made up of Roswell Park Memorial Institute 1640 (RPMI 1640) supplemented with fetal bovine serum (FBS; Gemini Bio-Products), 55 μM β-mercaptoethanol, 1×GlutaMAX™ (2 mM L-alanyl-L-glutamine dipeptide), 1 mM Sodium Pyruvate, 1×MEM Non-essential Amino Acid Solution (Sigma-Aldrich), 1×Penicillin-Streptomycin-Glutamine (100 units of penicillin, 100 μg of streptomycin, and 292 μg/ml of L-glutamine). All reagents were obtained from Gibco, unless otherwise indicated.

For enrichment of mouse T-ALL, single-cell suspensions of leukemic spleens were incubated with biotinylated antibodies against mouse CD11b (M1/70), CD11c (N418), F4/80 (BM8), and I-A/I-E (M5/1114.15.2), and negatively enriched with MojoSort™ Streptavidin Nanobeads (all the above from BioLegend), according to the manufacturer's instructions. For preparation of myeloid cells, single-cell suspensions incubated with biotinylated antibody against CD11c were positively isolated using

Streptavidin Microbeads and MACS LS Columns (both from Miltenyi Biotec). 3×10^5 T-ALL cells were cultured in the presence or absence of 2-2.5×10^4 enriched myeloid cells in 200 µl of complete RMPI in flat-bottom 96-well plates at 37 ˚C, 5% CO_2 for 6 or 7 days.

For culture of human T-ALL cells, deidentified primary pediatric T-ALL samples were obtained from Texas Children's Hospital (Houston, TX). Sample procurement and analysis were approved by the institutional review board committees at The University of Texas at Austin and Texas Children's Hospital/Baylor College of Medicine. T-ALL cells were isolated by density gradient separation using Ficoll, washed, and frozen in RPMI 1640 supplemented with 40% (v/v) FBS and 10% dimethyl sulfoxide (DMSO) upon collection. For preparation of myeloid cells, leukoreduction system chambers were obtained from We Are Blood (Austin, TX) and peripheral blood mononuclear cells (PBMCs) were isolated by density gradient separation using Histopaque (1.077 g/ml; Sigma-Aldrich). For enrichment of monocytes, 40×10^6 PBMCs were plated in 150×15 mm Petri Dish (Corning) in 25 ml of complete RPMI and incubated at 37 ˚C, 5% CO_2 for 2 hours and adherent monocytes were collected using cold PBS and cell scrapers (Fisher Scientific). For better purity, collected monocytes were incubated with biotinylated antibodies against human CD3 (UCHT1) and CD19 (HIB19), and lymphocytes were depleted with MojoSort™ Streptavidin Nanobeads (all of the above from BioLegend), according to the manufacturer's instructions.

To determine whether inhibition of integrin-mediated cell adhesion suppresses myeloid-mediated support of mouse T-ALL, T-ALL cells were co-cultured with myeloid cells in the presence or absence of anti-mouse CD11a (ITGαL; M17/4) and/or -mouse/rat CD29 (ITGβ1; HMβ1-1), or -mouse CD54 (ICAM-1; YN1/1.7.4) and/or -mouse CD106 (VCAM-1; 429(MVCAM.A); all from BioLegend). The relevant isotype antibodies

(RTK2758, RTK4530, HTK888, 53-6.7 (anti-mouse CD8), and 7E.17G9 (anti-mouse CD278 (ICOS))) were used as controls. To determine whether inhibition of integrin-mediated cell adhesion reduces myeloid-mediated support of human T-ALL, primary pediatric T-ALL cells were co-cultured with myeloid cells in the presence or absence of anti-human CD11a (ITGαL; HI111) and -human CD29 (ITGβ1; TS2/16), or -human CD54 (ICAM-1; HCD54; 20 μg/ml) and -human CD106 (VCAM-1; AF809; R&D Systems). The relevant isotype antibodies (MOPC-21 from BioLegend, 31243 from Invitrogen, and OKT-6 (anti-human CD1a) from BioXCell) were used as controls. The final concentration of each antibody was 10 μg/ml, unless otherwise indicated, and all the antibodies above were purchased from BioLegend, unless otherwise indicated. Co-cultures were carried out in 200 μl of complete RMPI in flat-bottom 96-well plates at 37 ˚C, 5% CO_2 for 6 or 7 days.

To determine whether blockade of ICAM-1- and VCAM-1-mediated cell adhesion suppresses sensitization of T-ALL to exogenous IGF1 by tumor-associated myeloid cells, T-ALL cells were co-cultured with myeloid cells at 37 ˚C, 5% CO_2 for 6 or 7 days in the presence or absence of 100 ng/ml of recombinant murine IGF1 (Peprotech) and in the presence or absence of anti-mouse CD54 (ICAM-1; YN1/1.7.4) and -mouse CD106 (VCAM-1; 429(MVCAM.A); both from BioLegend). The relevant isotype antibodies (RTK2758 and RTK4530) were used as controls. The final concentration of each antibody was 10 μg/ml.

To determine whether inhibition of integrin-mediated cell adhesion diminishes IGF1R signaling in T-ALL cells, 1×10^6 T-ALL cells were co-cultured with $7\text{-}8\times10^4$ myeloid cells in the presence of anti-mouse CD54 (ICAM-1; YN1/1.7.4) and -mouse CD106 (VCAM-1; 429(MVCAM.A)), or the relevant isotype controls (RTK2758 and RTK4530), at 10 μg/ml of each antibody in 500 μl of complete RMPI in flat-bottom 48-

well plates. On day 3 or 4 of culture at 37 ˚C, 5% CO_2, cells were immunostained for intracellular phosphorylated proteins as described above.

To determine whether survival of mouse T-ALL cells co-cultured with myeloid cells is dependent on focal adhesion signaling, cells were cultured at 37 ˚C, 5% CO_2 for 4 days prior to addition of FAK/PYK2 dual inhibitors (PF-431396 and PF-562271; Selleckchem). Viability was assessed by flow cytometry 3 or 4 days after inhibitor addition in comparison to cells treated with vehicle control (DMSO).

Transwell assays

T-ALL cells and/or myeloid cells were plated in 12 mm Transwell® with 0.4 μm pore polyester membrane cell culture inserts (Corning®), as indicated. 1×10^6 T-ALL cells or 5×10^4 myeloid cells were added to the upper chamber formed by the inserts, while 3×10^6 T-ALL cells and/or 1.5×10^5 myeloid cells were added to the bottom wells, with 500 μl or 1.5 ml of complete RMPI, respectively. The viability of T-ALL cells in each group was assessed after 6 or 7 days of cultures at 37 ˚C, 5% CO_2. To control for relative differences in surface area, different numbers of cells were added to the upper versus bottom chambers, and results were normalized to the number of input cells in each chamber.

In vivo inhibition of cell-cell adhesion mediated by integrins

Mice with established T-ALL (>1% splenic chimerism) were randomly divided into three groups, which were intraperitoneally administered either 100 μg of InVivoMAb anti-mouse CD54 (YN1/1.7.4), a combination of 100 μg of InVivoMAb anti-mouse CD54 and 100 μg of InVivoMAb anti-mouse CD106 (M/K-2.7), or 100 μg of isotype controls (HRPN and LTF-2; all of the above from BioXCell) in 200 μl of PBS

every 2 days, for 5 total injections. T-ALL burden was evaluated 24 or 48 hours after the final injection. All comparisons within an experiment were carried out with age-matched mice (6 to 8 weeks old) engrafted with the same 5×10^6 primary LN3 T-ALL cells.

Icam1$^{-/-}$ or *Icam1*$^{+/-}$ littermate controls (6 to 8 weeks old) were engrafted intraperitoneally with 5×10^6 primary LN3 T-ALL cells. When tail vein chimerism reached at least 1% in control mice, T-ALL burden was measured by flow cytometry; alternatively, survival of the mice was monitored.

Statistical analysis

Statistical analyses were performed with Prism (v9.0.0; GraphPad Software) and R (3.6.3; The R Foundation for Statistical Computing). Normality was determined using the D'Agostino & Pearson or Shapiro-Wilk tests, as appropriate for sample size. Statistical significance was determined using an unpaired Student t test for normally distributed data or the non-parametric Mann-Whitney test, paired Student t test, repeated measures one-way analysis of variance (ANOVA) with the Holm-Sidak correction for normally distributed data or the non-parametric Friedman test, two-way ANOVA with the Holm-Sidak correction, or Log-rank tests, as indicated in figure legends.

RESULTS

Close contact is required for myeloid-mediated T-ALL support and integrins are candidate mediators of these interactions

We previously found that tumor-associated myeloid cells sensitize T-ALL cells to exogenous IGF1, whereas IGF1 alone is not sufficient for T-ALL survival (Lyu et al., 2020). Because thymic T-ALL cells make frequent and prolonged contacts with tumor-associated DCs in the thymus (Triplett et al., 2016), we hypothesized that T-ALL cells would require close contact with myeloid cells to survive in vitro.

To test this possibility, we isolated T-ALL cells from the spleens of unconditioned immunocompetent CD45.1$^+$ congenic mice engrafted with primary LN3 T-ALL cells, and cultured them in the presence or absence of tumor-associated myeloid cells in transwell plates, such that the two cell types could either contact one another or were separated by micropores through which only soluble factors could pass. Notably, T-ALL cells survived only when co-cultured in the same chamber with myeloid cells (Figure 3.1A), suggesting physical interactions were critical for leukemic survival. To identify candidate mediators of close contact, we evaluated our previously published transcriptional profiling datasets from T-ALL cells versus healthy T-lineage cells isolated from thymuses and spleens (Lyu et al., 2020). Several integrin-associated pathways, including "integrin1 (Integrin β1)" and "ILK (Integrin-linked kinase)", were significantly enriched in T-ALL cells relative to controls from the thymus or spleen (Figure 3.1B-C; Figure 3.2A). Consistent with this pathway analysis, *Itgb1* transcripts were significantly elevated in T-ALL cells from the thymus and spleen relative to healthy T-lineage cells (Figure 3.1D). Furthermore, protein levels of integrin β1 (ITGβ1) at the cell surface were highly elevated on splenic T-ALL cells (CD45.2$^+$CD5$^+$) relative to T cells (CD45.1$^+$CD5$^+$) from the same leukemic environment (Figure 3.1E; Figure 3.2C). Among ITGβ1 heterodimers (Humphries et al., 2006), we hypothesized that ITGα4β1 (VLA-4) and ITGα9β1 could play a role in myeloid-mediated T-ALL support because both bind to VCAM-1, which is expressed by tumor-associated myeloid cells (Figure 3.3) (Barczyk et al., 2010). Indeed, both transcript and protein levels of ITGα9 were significantly higher in T-ALL cells relative to controls, although ITGα4 levels were not significantly different, with a decreasing trend observed for both transcript and protein levels. (Figure 3.1D-E; Figure 3.2B-C) We hypothesized that ITGαLβ2 (LFA-1) could also play a role in myeloid-mediated T-ALL support because binding to APCs through LFA-1 induces

activation of ILK signaling in T cells (Figure 3.1C; Figure 3.2A) (Mak, 2006). Moreover, "cdc42 reg (Regulation of cell division cycle 42 (CDC42) activity)", which is an essential component of LFA-1-mediated T-cell polarity and migration, was among the top pathways activated preferentially in T-ALL cells in the thymus (Figure 3.1B). LFA-1 has also been implicated in T-cell activation upon binding to ICAM-1 (Walling and Kim, 2018), which is expressed by tumor-associated myeloid cells (Figure 3.3). We found protein levels of both ITGαL and ITGβ2 were significantly higher in T-ALL cells relative to controls (Figure 3.1E; Figure 3.2C), despite diminished transcript levels (Figure 3.2B). This discrepancy could be due to other levels of regulation between transcripts and proteins, such as stabilization of active LFA-1 by tension across ITGβ2 upon binding to ICAM-1 (Nordenfelt et al., 2016).

Inhibition of integrin-mediated cell adhesion suppresses myeloid-mediated T-ALL survival by diminishing IGF1R signaling

To test the contribution of ICAM-1 and VCAM-1 to myeloid-mediated T-ALL support, we inhibited cell adhesion between T-ALL cells and myeloid cells using anti-ICAM-1 and/or anti-VCAM-1 antibodies in vitro. Blockade of ICAM-1 or VCAM-1 resulted in a significant reduction in viability of T-ALL cells co-cultured with myeloid cells (Figure 3.4A). Notably, inhibition of both ICAM-1 and VCAM-1 reduced T-ALL survival to the level of T-ALL cells cultured alone (Figure 3.4A; Figure 3.5A-B), indicating that these adhesion ligands are critical for myeloid-mediated support of T-ALL. Isotype-matched blocking antibodies against CD8 (Rat IgG2a, κ) or ICOS (Rat IgG2b, κ), which are expressed on T-ALL cells, did not impact viability of T-ALL cells (Figure 3.5C-D), indicating that the observed reduction in viability of T-ALL cells was due to blockade of ICAM-1 or VCAM-1, not Fc receptor-mediated phagocytosis. To validate

the impact of inhibition of cell adhesion on T-ALL survival, we used blocking antibodies against ITGαL and/or ITGβ1 in culture, which bind ICAM-1 or VCAM-1, respectively. Consistent with blockade of ICAM-1 and/or VCAM-1, viability of T-ALL cells was significantly reduced by inhibiting these integrins (Figure 3.4B). We also determined whether myeloid-mediated T-ALL support through integrin-dependent cell adhesion is a common feature using an independent transgenic mouse model in which LIM domain only 2 (*Lmo2*) expression is driven by the human CD2 promoter (Smith et al., 2014). Although inhibition of both ICAM-1 and VCAM-1 significantly reduced viability of T-ALL cells co-cultured with myeloid cells (Figure 3.4C), leukemia cells from LN3 mice were more susceptible to integrin blockade than those from LMO2 mice, suggesting that there would be additional mechanisms underlying myeloid-mediated support of T-ALL cells from the LMO2 transgenic mouse model.

Because myeloid cells sensitize T-ALL cells to IGF1 (Lyu et al., 2020), we hypothesized that inhibition of integrin-mediated cell adhesion would diminish IGF1R activation in T-ALL by myeloid cells. Consistent with this possibility, levels of phosphorylated (p)IGF1R and the downstream molecule AKT were significantly reduced when T-ALL cells were co-cultured with myeloid cells in the presence of anti-ICAM-1 and anti-VCAM-1 antibodies (Figure 3.4D-E). To determine whether inhibition of adhesion ligands would prevent sensitization of T-ALL cells to IGF1, we co-cultured T-ALL cells with myeloid cells in the presence or absence of anti-ICAM-1 and anti-VCAM-1 antibodies and in the presence or absence of exogenous IGF1. Consistent with our previous findings, addition of IGF1 increased viability of T-ALL cells only in the presence of tumor-associated myeloid cells, and inhibition of ICAM-1 and VCAM-1 diminished survival of T-ALL cells co-cultured with myeloid in the presence of IGF1 (Figure 3.4F). These results demonstrate that integrin activation is required for the full

responsiveness of T-ALL cells to IGF1. Taken together, integrin-mediated cell adhesion between T-ALL cells and tumor-associated myeloid cells plays an essential role in promoting the survival of T-ALL by enabling activation of IGF1R signaling.

Cell adhesion mediated by ICAM-1 and VCAM-1 is critical for T-ALL progression in vivo

Because inhibition of either LFA-1 or ICAM-1 suppresses survival of T-ALL cells co-cultured with myeloid cells in vitro (Figure 3.4A-B), we sought to determine whether ICAM-1 was critical for T-ALL progression in vivo. To this end, primary LN3 T-ALL cells were engrafted into *Icam1*$^{-/-}$ mice and *Icam1*$^{+/-}$ littermate controls. T-ALL burden was assessed once blood T-ALL burden reached 1% to 2% in control mice (Figure 3.6A). ICAM-1 deficiency resulted in a reduction of leukemic burden in the blood, spleen, BM, LN, and liver (Figure 3.6B-C). Furthermore, *Icam1*$^{-/-}$ mice survived significantly longer than littermate controls following transplantation of T-ALL (Figure 3.6D), suggesting that ICAM-1-mediated integrin activation promotes T-ALL initiation and/or progression.

To further test the role of ICAM-1- and VCAM-1-mediated cell adhesion in promoting T-ALL progression in vivo, we administered blocking antibodies against ICAM-1 and/or VCAM-1 to mice in which T-ALL burden reached 1% to 8% in the spleen following engraftment of primary T-ALL cells into CD45.1^{+} congenic mice (Figure 3.6E). Because anti-VCAM-1 alone did not diminish T-ALL burden in pilot experiments (data not shown), leukemic mice were treated with either anti-ICAM-1 antibody alone or a combination of anti-ICAM-1 and anti-VCAM-1 antibodies. Although the use of single anti-ICAM-1 antibody resulted in a diminished T-ALL burden in the blood and LN, reflecting delayed disease progression, leukemic infiltration in the spleen,

BM, and liver was comparable to that of isotype control treated mice (Figure 3.7A), suggesting that the efficacy of anti-ICAM-1 alone is limited. However, when anti-ICAM-1 and anti-VCAM-1 antibodies were administered together, T-ALL burden was significantly diminished in the blood, spleen, BM, LN, and liver (Figure 3.6F-H). The antibodies did not deplete myeloid cells in leukemic mice (Figure 3.7B), indicating that a reduction of T-ALL burden resulted from inhibition of ICAM-1- and VCAM-1-mediated cell adhesion, not Fc receptor-mediated phagocytosis of T-ALL-supportive myeloid cell types, like macrophages. Collectively, ICAM-1 and VCAM-1 play a critical role in promoting T-ALL survival and progression in vivo.

Myeloid cells activate focal adhesion signaling to promote T-ALL survival in vitro

To identify the downstream targets activated by integrins in T-ALL, we further analyzed our published transcriptional profiling datasets using the Enrichr bioinformatics tool (Chen et al., 2013) (Kuleshov et al., 2016) (Lyu et al., 2020). Pathway analysis revealed activation of the focal adhesion pathway, which is downstream of integrin signaling (Huveneers and Danen, 2009), as a candidate mechanism of integrin-mediated myeloid support of T-ALL (Figure 3.8A). Consistent with this, levels of activated FAK and PYK2, the two components of focal adhesion signaling, were consistently diminished when T-ALL cells were co-cultured with myeloid cells in the presence of anti-ICAM-1 and anti-VCAM-1 antibodies (Figure 3.8B). In vitro co-cultures in the presence of FAK/PYK2 dual inhibitors showed that myeloid-mediated survival of both LN3- and LMO2-transplanted T-ALL cells was dependent on focal adhesion signaling (Figure 3.8C-D). Taken together with the finding that blockade of integrin-mediated cell adhesion reduces survival of T-ALL cells co-cultured with tumor-associated myeloid

cells, these studies indicate that integrin signaling plays a pivotal role in promoting T-ALL growth.

Activation of integrins by human myeloid cells promotes primary patient T-ALL growth and is associated with inferior outcomes

We previously demonstrated that human PBMC-derived myeloid cells could support survival of primary patient T-ALL cells (Lyu et al., 2020), and thus hypothesized that integrin-mediated cell adhesion would be critical for myeloid support of human T-ALL cells as well. We first checked surface expression levels of each integrin component and cell adhesion ligands on T-ALL and PBMC-derived monocytes or M-CSF-derived macrophages, respectively. Consistent with mouse models, VLA-4, integrin α9β1, and LFA-1 were expressed on primary pediatric T-ALL cells (Figure 3.9A). As for adhesion molecules, however, ICAM-1 was clearly expressed on both monocytes and M-CSF-derived macrophages, whereas the levels of VCAM-1 were very low on both populations (Figure 3.9B-E). To determine the impact of integrin-mediated cell adhesion on myeloid-mediated support of T-ALL, primary pediatric T-ALL cells were co-cultured with monocytes in the presence or absence of anti-ICAM-1 and anti-VCAM-1 antibodies. Consistent with mouse models, inhibition of these adhesion molecules significantly diminished survival of patient T-ALL cells (Figure 3.10A). In addition, inhibition of anti-ITGαL and anti-ITGβ1 also diminished myeloid-mediated T-ALL survival (Figure 3.10B). To test whether integrin signaling was implicated in patient outcomes, we analyzed published datasets from pediatric T-ALL patients (Liu et al., 2017) and found that an increase in gene signatures of the "(+) regulation of cell adhesion mediated by integrin" and "integrin2" pathways significantly correlated with diminished event-free survival rates (Figure 3.10C). Notably, expression of integrin pathway gene signatures

significantly correlated with enrichment scores of monocytes and macrophages in T-ALL patients (Figure 3.10D-E), suggesting that myeloid cells could activate integrin signaling in patient T-ALL cells. Collectively, these results indicate that myeloid cells support survival of human T-ALL cells via integrin-mediated cell adhesion.

DISCUSSION

Although we previously found that tumor-associated myeloid cells promote T-ALL progression by activating IGF1R signaling (Triplett et al., 2016) (Lyu et al., 2020), which is required for initiation and growth of T-ALL (Medyouf et al., 2011), exogenous IGF1 alone is not sufficient to support T-ALL cell survival. Moreover, PBMC-derived monocytes support survival of primary pediatric T-ALL cells in culture, but they fail to sustain activation of IGF1R in the leukemic cells (Lyu et al., 2020). These findings indicate that myeloid cells employ additional mechanisms to support T-ALL. Because our previous studies showed that, in contrast to thymocytes, T-ALL cells make prolonged and frequent contacts with myeloid cells in the leukemic thymic environment (Triplett et al., 2016), we hypothesized that molecular mediators of cell contact would be involved in myeloid-mediated T-ALL support. Evaluation of transcriptional profiling datasets revealed that gene signatures related to integrin signaling were significantly enriched in T-ALL cells compared to T-lineage cells both in the thymus and spleen, implicating integrins in myeloid support of T-ALL survival. Indeed, inhibition of integrin-mediated cell adhesion between T-ALL cells and tumor-associated myeloid cells using blocking antibodies against either integrins expressed by T-ALL cells or their respective ligands expressed by tumor-associated myeloid cells significantly reduced T-ALL viability in vitro and in vivo. Consistent with these findings from mouse models of T-ALL, the viability of primary patient T-ALL cells co-cultured with monocytes was significantly

reduced by inhibition of integrins or their ligands. Altogether, these results indicate that the activation of integrin signaling by myeloid cells is an essential component of myeloid-mediated support of T-ALL survival and progression.

Consistent with our findings that integrin pathways were enriched in T-ALL cells relative to healthy T-lineage cells, transcriptional profiling data implicated "focal adhesion", which is downstream of integrin signaling, as one of the most significantly enriched pathways in thymic T-ALL cells relative to thymocytes. FAK is a key kinase present at focal adhesion sites and plays a critical role in mediating cell adhesion, migration, and survival (Golubovskaya, 2010). Importantly, FAK positively regulates LFA-1-mediated T-cell adhesion to APCs, implicating that FAK-mediated integrin signaling could play a role in myeloid-mediated T-ALL support (Chapman and Houtman, 2014). Previous studies have shown that high expression and activation of FAK correlate with poor outcomes in several cancer types (Miyazaki et al., 2003) (Jiang et al., 2016) (Li et al., 2018). FAK interacts with several surface receptors, including integrins (Sieg et al., 2000) and IGF1R (Liu et al., 2008). Furthermore, IGF1R and integrins are known to interact cooperatively and induce cell survival, migration, and drug resistance (Kiely et al., 2002) (Sayeed et al., 2013) (Cox et al., 2015). Because myeloid cells were shown to sensitize T-ALL cells to IGF1 (Lyu et al., 2020), and focal adhesion signaling was identified as a candidate mechanism of myeloid-mediated T-ALL support, we hypothesized that inhibition of integrin-mediated cell adhesion between T-ALL cells and myeloid cells would result in a reduction in the activation of IGF1R and focal adhesion signaling in T-ALL cells. Notably, the levels of phosphorylated IGF1R, AKT, FAK, and PYK2 were diminished in T-ALL cells after blocking ICAM-1 and VCAM-1 in co-cultures of T-ALL and myeloid cell. Consistent with this, inhibition of FAK/PYK2 activation diminished survival of T-ALL cells co-cultured with tumor-associated myeloid

cells. Collectively, these results suggest that both IGF1R and focal adhesion pathways play an essential role in integrin-mediated myeloid support of T-ALL.

We found that inhibition of integrin-mediated cell adhesion using a combination of anti-ICAM-1 and anti-VCAM-1 antibodies reduced the viability of both mouse and human T-ALL cells co-cultured with myeloid cells, suggesting that myeloid-mediated support of T-ALL requires cell adhesion. Interestingly, T-ALL cells from LN3 mice were more susceptible to inhibition of integrin-mediated cell adhesion relative to those from LMO2 mice. In keeping with this, LN3 T-ALL cell had higher sensitivity to FAK/PYK2 inhibitors, although the survival of LMO2 T-ALL cells was also dependent on focal adhesion signaling. These results suggest that other adhesion molecules might be involved in myeloid-mediated T-ALL support. Syndecan is one such candidate. Syndecan is a heparan sulfate proteoglycan that binds to several cell adhesion molecules present on myeloid cells, including Mac-1 (ITGαMβ2) and L-selectin (Carey, 1997) (Schittenhelm et al., 2017) (Ivetic et al., 2019). With cooperative interactions with integrins (Morgan et al., 2007), syndecans act as adhesion receptors and promote assembly of focal adhesions (Saoncella et al., 1999) (Rapraeger, 2000) (Kwon et al., 2012). They mediate the activation of survival pathways, including FAK (Wilcox-Adelman et al., 2002) (Shi et al., 2017) and IGF1R (Beauvais et al., 2016), therefore dysregulation of syndecans could result in promoting tumorigenesis and tumor progression. A better understanding of what cell surface receptors are present on T-ALL cells and how tumor-associated myeloid cells activate them to promote leukemic survival will reveal therapeutic targets for T-ALL treatment.

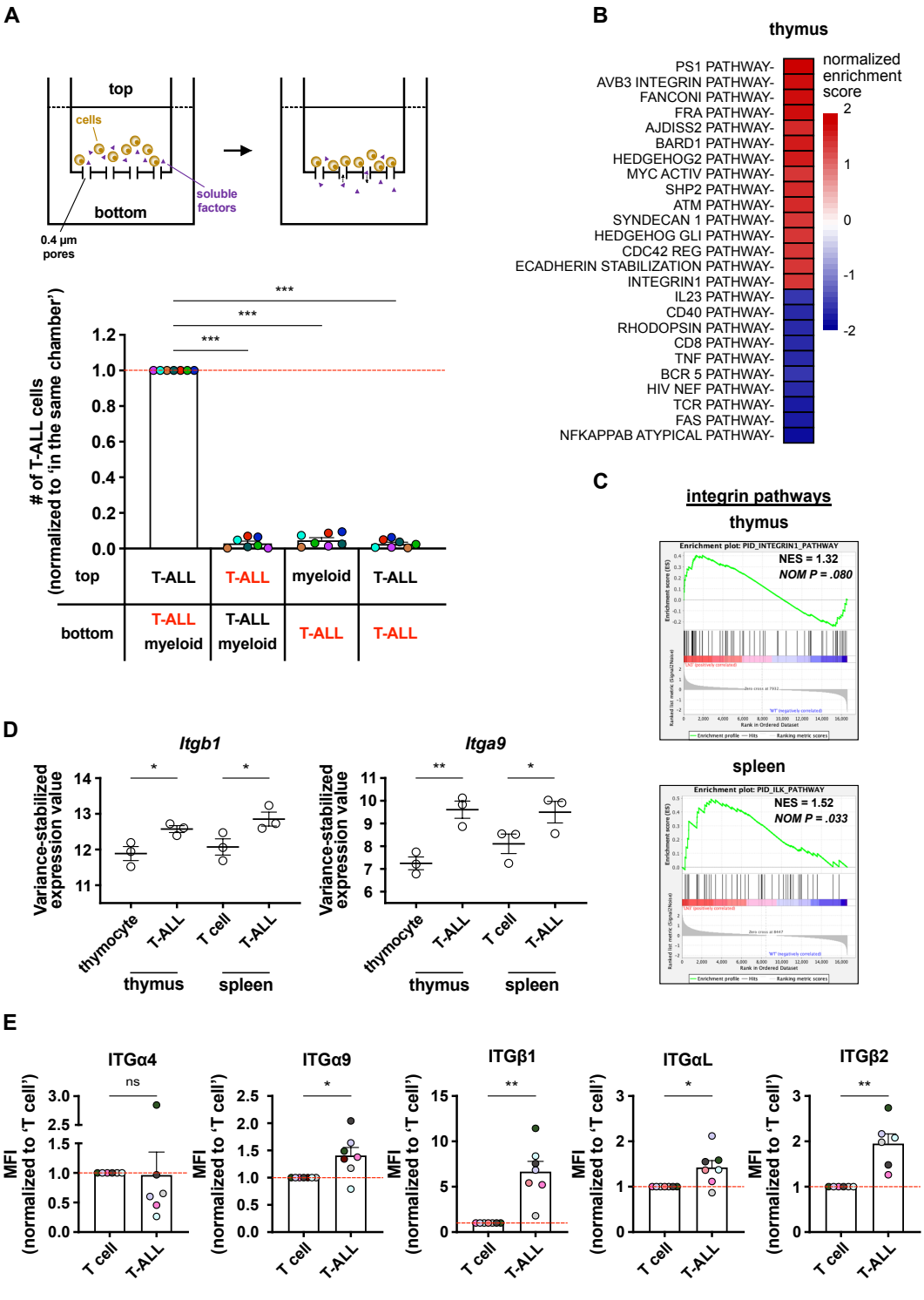

(Figure 3.1 continued on next page)

Figure 3.1. Close contact is critical for myeloid-mediated T-ALL support and several integrin-associated pathways are enriched in T-ALL cells relative to healthy T-lineage cells.

(A) Schematic illustration of transwell assays (top) and quantification of viable T-ALL cells (bottom), isolated from the spleens of LN3 T-ALL-engrafted mice 6 or 7 days after culture in the presence or absence of enriched myeloid cells from the same leukemic spleens in transwell plates, as indicated. Wells analyzed were indicated in red. Results were normalized to the viability of T-ALL cells which could make contacts with tumor-associated myeloid cells in the same chamber within each experiment (red line). Bars depict the mean + standard error of the mean (SEM) of cumulative data from 7 experiments, each with a distinct color-coded primary T-ALL; circles represent the average of 2 or 3 technical replicate wells per experiment. (B) The top 10 to 15 pathways significantly enriched or depleted in thymic LN3 T-ALL cells relative to healthy thymocyte controls were identified using the PID gene sets of the Gene Set Enrichment Analysis (GSEA) bioinformatics tool. (C) GSEA enrichment plots for the INTEGRIN1 (top) and ILK (bottom) pathways in thymic or splenic T-ALL cells relative to healthy thymocyte or $CD8^+$ T cell controls, respectively, as in (B). Normalized enrichment scores (NES) and nominal P-values are shown. (D) Variance-stabilized expression values of *Itgb1* and *Itga9* from control T-lineage vs T-ALL cells from the thymus and spleen. Bars represent means + SEM; circles represent individual biologic replicates. (E) Protein levels of the indicated integrin components in LN3-engrafted T-ALL cells ($CD45.2^+CD5^+$) relative to host T cells ($CD45.1^+CD5^+$) from the same spleen were quantified by flow cytometry and displayed as median fluorescence intensities (MFI). Data are compiled from 6 or 7 independent experiments, each with a distinct color-coded primary T-ALL. Circles represent individual mice. $*P < .05$, $**P < .01$, $***P < .001$, repeated measures one-way ANOVA with the Holm-Sidak correction (A), two-way ANOVA with the Holm-Sidak correction (D), paired Student t test (E). ns, not significant.

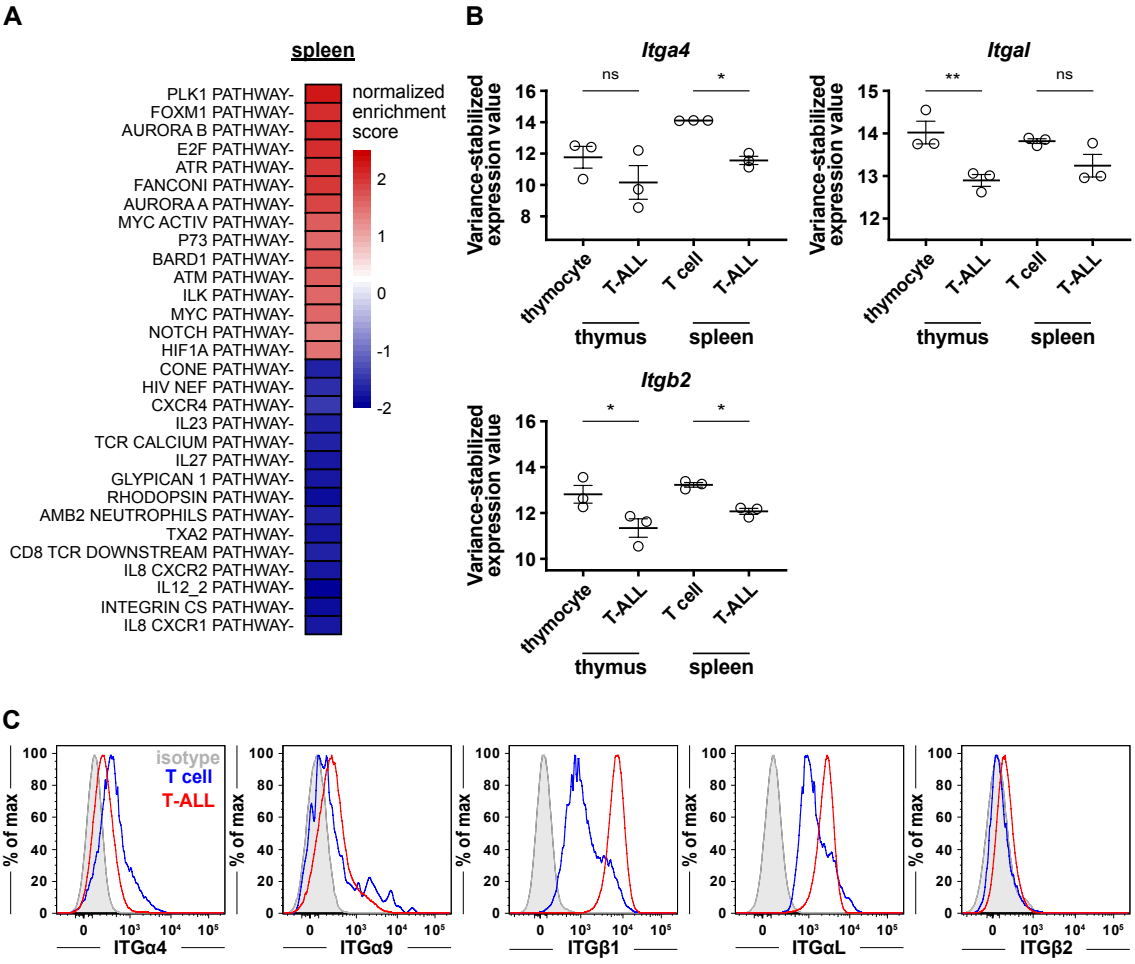

Figure 3.2. Integrin-associated pathways are enriched in T-ALL cells relative to healthy T-lineage cells and expression levels of the indicated integrin components are evaluated.

(A) The top 15 pathways significantly enriched or depleted in splenic LN3 T-ALL cells relative to healthy $CD8^+$ T cells were identified using the PID gene sets of the Gene Set Enrichment Analysis (GSEA) bioinformatics tool. (B) Variance-stabilized expression values of *Itga4*, *Itgal*, and *Itgb2* from control T-lineage vs T-ALL cells from the thymus and spleen. Bars represent means + standard error of the mean (SEM); circles represent individual biologic replicates. (C) Representative flow cytometry plots of the indicated integrin components present on transplanted LN3 T-ALL cells (red) and host T cells (blue) from the same leukemic spleens. Isotype controls are shaded in gray. $*P < .05$, $**P < .01$, two-way ANOVA with the Holm-Sidak correction (B). ns, not significant.

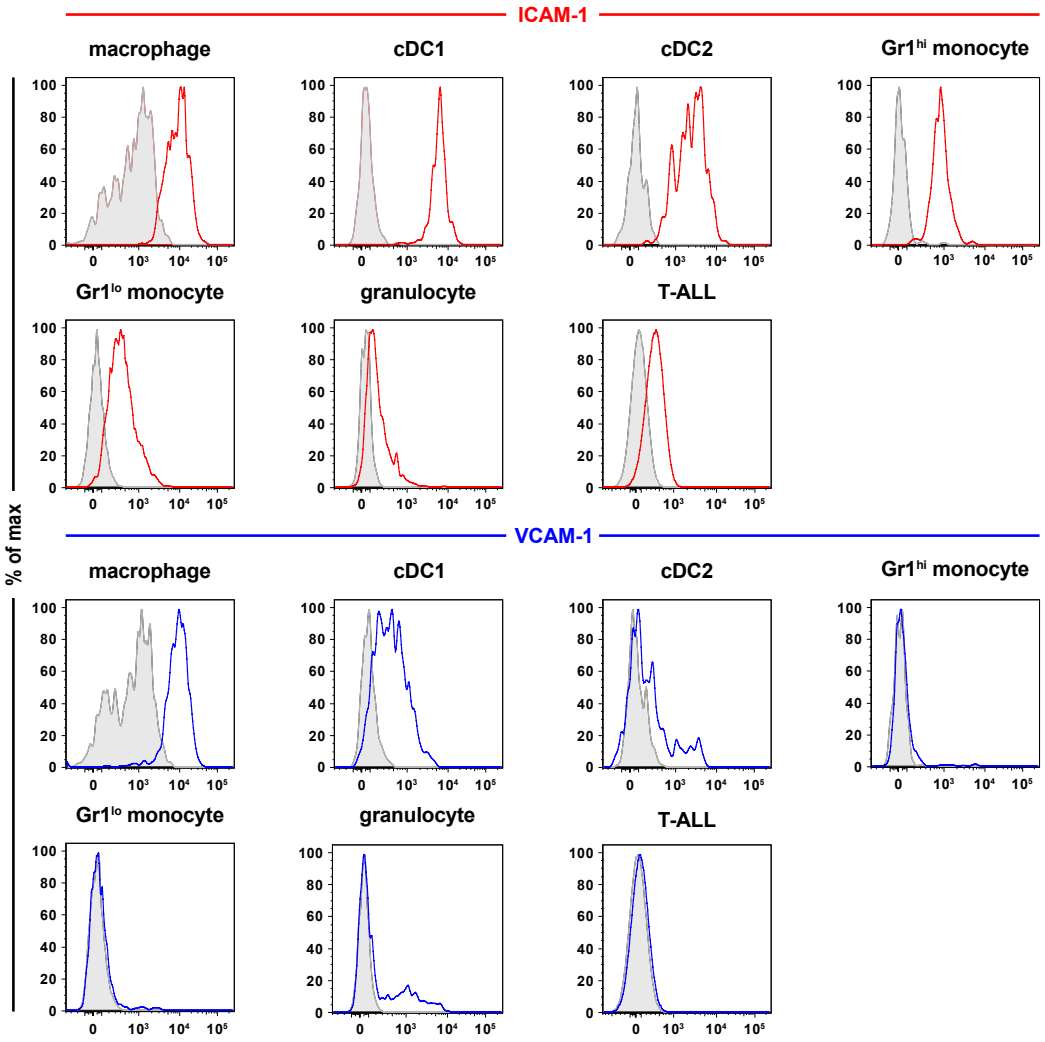

Figure 3.3. ICAM-1 and VCAM-1 are expressed by tumor-associated myeloid cells.

Representative flow cytometry plots of ICAM-1 (red) and VCAM-1 (blue) expressed by the indicated myeloid subsets from the spleens of mice transplanted with primary LN3 T-ALL cells. Each subset was identified by flow cytometry using the gating strategy in Figure 2.4A. Isotype controls are shaded in gray.

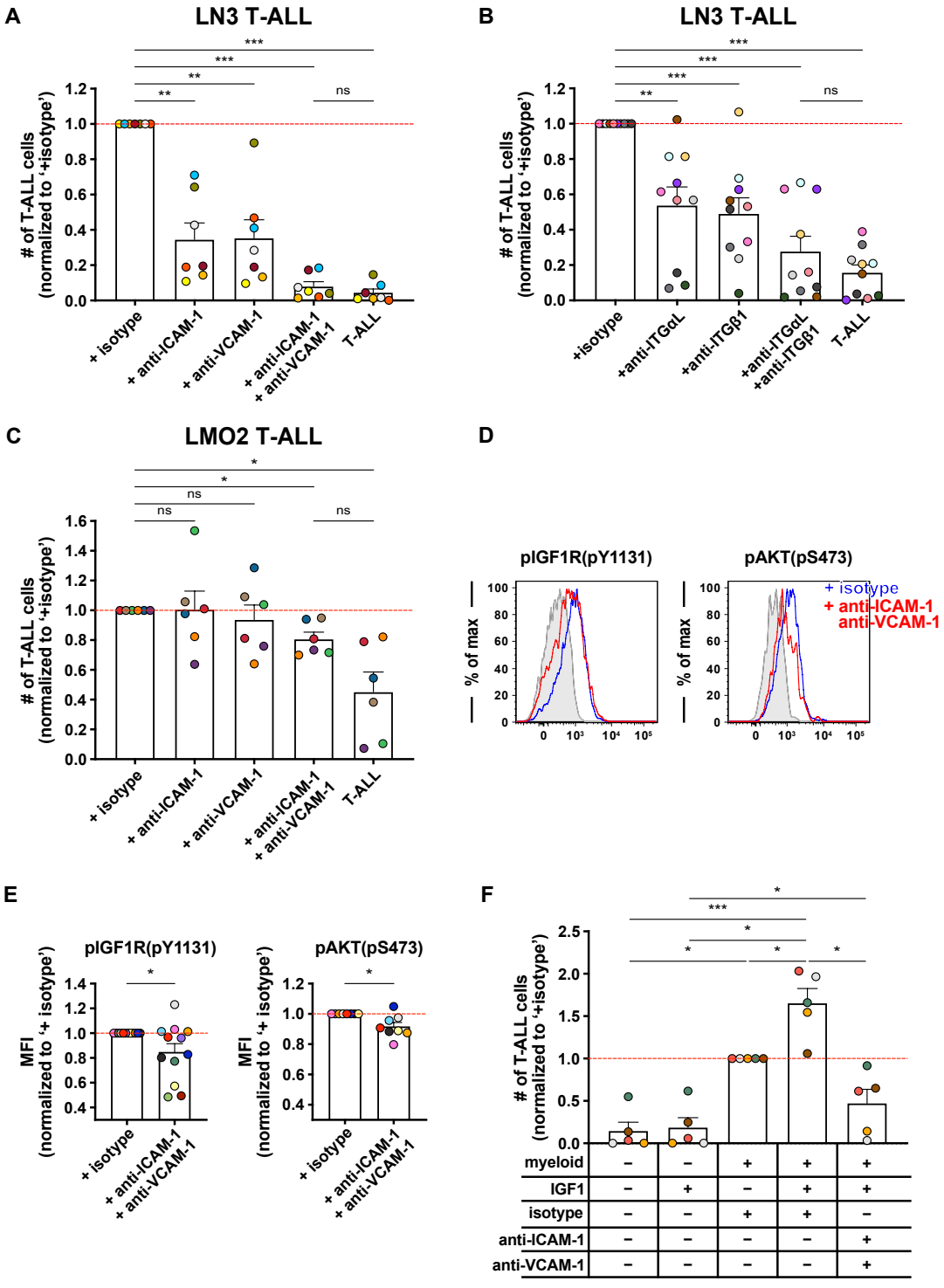

(Figure 3.4 continued on next page)

Figure 3.4. Inhibition of integrin-mediated cell adhesion results in a reduction in viability of T-ALL cells by diminishing IGF1R signaling in vitro.

(A-B) Quantification of viable T-ALL cells, isolated from the spleens of primary LN3 T-ALL-transplanted mice, 6 or 7 days after culture in the presence or absence of enriched tumor-associated splenic myeloid cells and in the presence or absence of (A) anti-ICAM-1 and/or anti-VCAM-1 or (B) anti-integrin αL (ITGαL) and/or anti-ITGβ1 antibodies (10 μg/ml per each). Results were normalized to the viability of T-ALL cells co-cultured with tumor-associated myeloid cells in the presence of isotype control antibodies within each experiment (red line). Bars show means + standard error of the mean (SEM) of cumulative data from 7 to 10 independent experiments, each with a distinct color-coded primary T-ALL; circles represent the average of 2 or 3 technical replicate wells per experiment. (C) Quantification of viable T-ALL cells, isolated from the spleens of primary LMO2 T-ALL-transplanted mice, 6 or 7 days after culture in the presence or absence of enriched tumor-associated splenic myeloid cells and in the presence or absence of anti-ICAM-1 and/or anti-VCAM-1 antibodies (10 μg/ml per each). Results were normalized to the viability of T-ALL cells co-cultured with tumor-associated myeloid cells in the presence of isotype control antibodies within each experiment (red line). Bars show means + SEM of cumulative data from 6 independent experiments, each with a distinct color-coded primary T-ALL; circles represent the average of 2 technical replicate wells per experiment. (D) Representative flow cytometry plots of phosphorylated (p)IGF1R and the downstream signaling molecule pAKT in T-ALL cells, isolated from the spleens of primary LN3 T-ALL-transplanted mice, 4 or 5 days after culture in the presence of enriched tumor-associated splenic myeloid cells and in the presence (red) or absence (blue) of a combination of anti-ICAM-1 and anti-VCAM-1 antibodies (10 μg/ml per each). Controls are shaded in gray. (E) Levels of pIGF1R and pAKT were quantified in T-ALL cells following blockade of both ICAM-1 and VCAM-1, as in (D). MFIs from anti-ICAM-1 and anti-VCAM-1-treated T-ALL cells were normalized to levels in T-ALL cells treated with isotype controls (red line). Bars represent means + SEM of cumulative data from 8 to 12 independent experiments, each with a distinct color-coded primary T-ALL. Circles represent individual experiment. (F) Quantification of viable T-ALL cells, isolated from the spleens of primary LN3 T-ALL-transplanted mice, 6 or 7 days after culture in the presence or absence of tumor-associated splenic myeloid cells, in the presence or absence of exogenous IGF1 (100 ng/ml), and in the presence or absence of anti-ICAM-1 and anti-VCAM-1 antibodies (10 μg/ml per each). Results were normalized to the viability of T-ALL cells co-cultured with myeloid cells in the presence of isotype control antibodies and in the absence of exogenous IGF1 (red line). Bars represent means + SEM of cumulative data from 5 independent experiments with a distinct color-coded primary T-ALL; circles represent the average of 2 or 3 technical replicate wells per experiment. $*P < .05$, $**P < .01$, $***P < .001$, repeated measures one-way ANOVA with the Holm-Sidak correction (A,B,C,F), paired Student t test (E). ns, not significant.

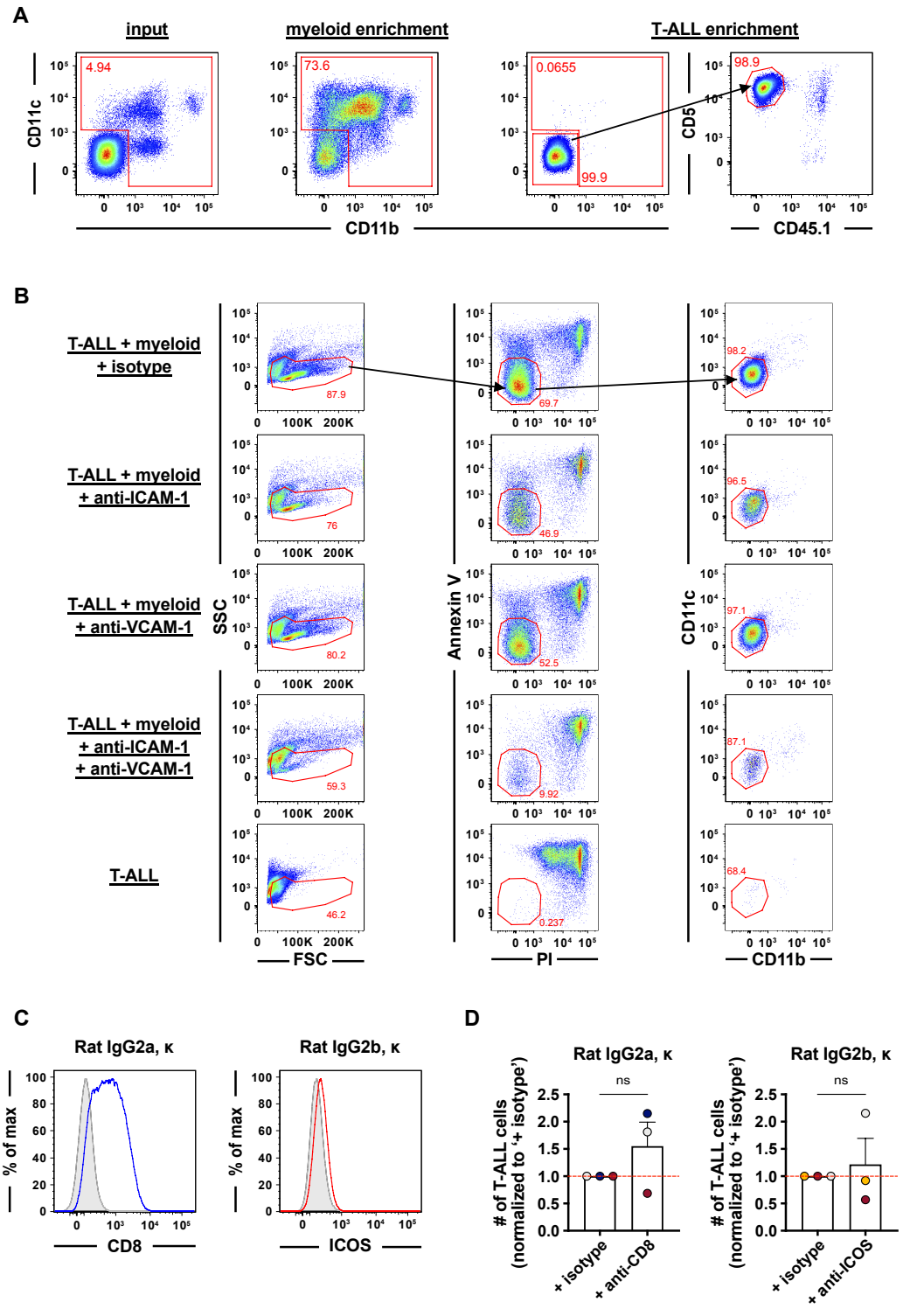

(Figure 3.5 continued on next page)

Figure 3.5. Inhibition of integrin-mediated cell adhesion results in a reduction in viability of T-ALL cells in vitro.

(A) Representative flow cytometry plots showing the purity of enriched myeloid ($CD11b^+$ and/or $CD11c^+$) and T-ALL ($CD11b^-CD11c^-CD45.2^+CD5^+$) cells from the spleen of LN3 T-ALL-transplanted mice with sequential gating indicated by arrows. The "input" column shows myeloid composition ($CD11b^+$ and/or $CD11c^+$) before enrichment. The "myeloid enrichment" column shows the percent of myeloid cells following positive enrichment of $CD11c^+$ cells from the spleen. The third column shows the low frequency of myeloid ($CD11b^-$ and $CD11c^-$) cells within the enriched T-ALL population following depletion with antibodies against F4/80, CD11b, I-A/I-E, and CD11c. The fourth column shows expression of CD45.2 and CD5 on the enriched T-ALL fraction. (B) Representative flow cytometry plots showing the viability of transplanted LN3 T-ALL cells cultured in the presence or absence of enriched myeloid cells from the same spleen and in the presence or absence of anti-ICAM-1 and/or anti-VCAM-1 antibodies. Viable T-ALL cells were quantified as Annexin V $(AV)^-PI^-CD11b^-CD11c^-$ cells. (C) Representative flow cytometry plots of CD8 (blue) and ICOS (red) on leukemia cells ($CD45.2^+CD5^+$) isolated from the spleens of mice transplanted with primary LN3 T-ALL. (D) Quantification of viable T-ALL cells, isolated from the spleens of primary LN3 T-ALL-transplanted mice, 6 or 7 days after culture in the presence of enriched tumor-associated myeloid cells and in the presence or absence of isotype-matched blocking antibodies against CD8 (left; Rat IgG2a, κ) or ICOS (right; Rat IgG2b, κ) (10 μg/ml per each). Results were normalized to the viability of T-ALL cells co-cultured with tumor-associated myeloid cells in the presence of isotype control antibodies within each experiment (red line). Bars show means + standard error of the mean (SEM) of cumulative data from 3 independent experiments, each with a distinct color-coded primary T-ALL; circles represent the average of 2 or 3 technical replicate wells per experiment. Paired Student t test (D). ns, not significant.

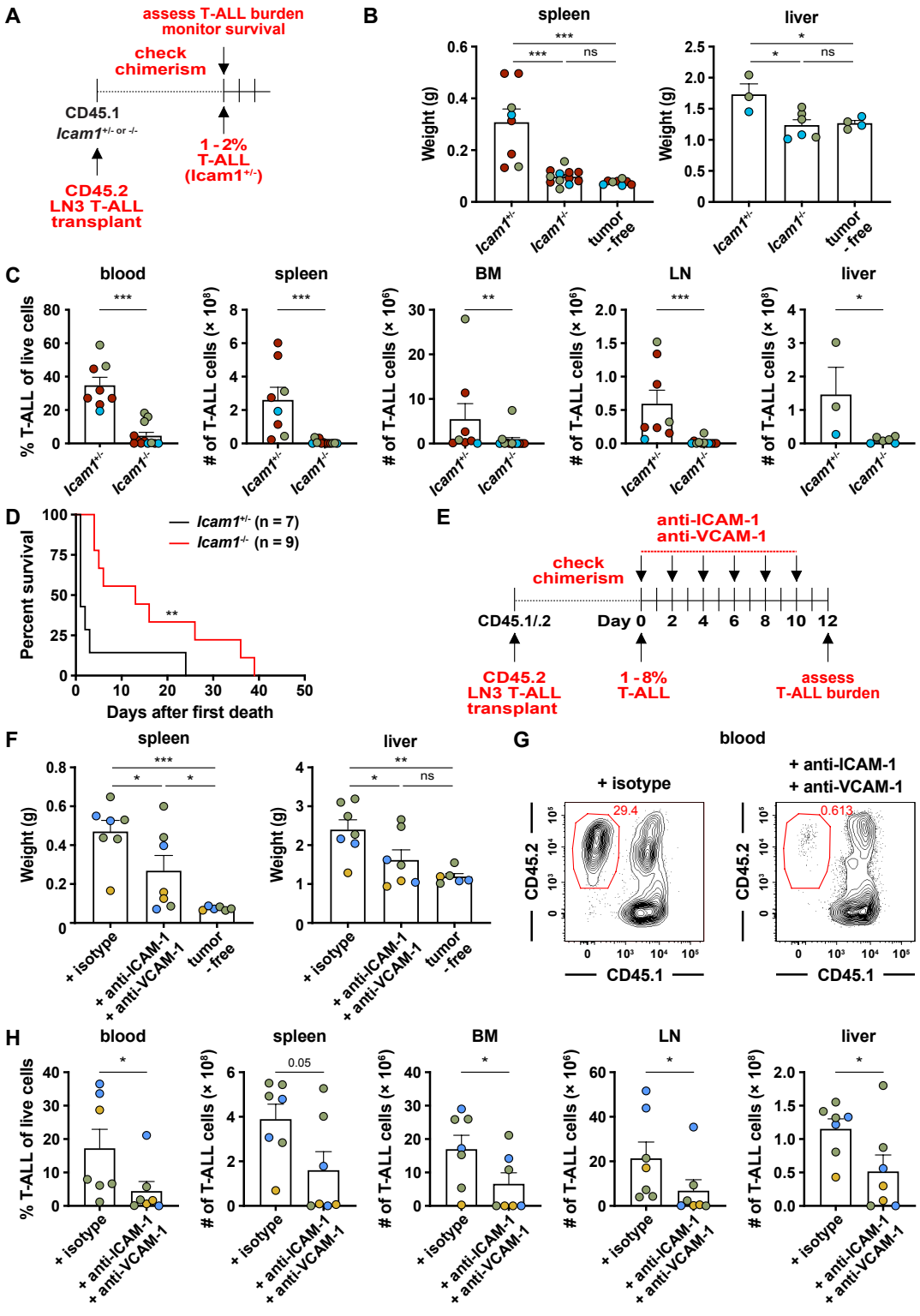

(Figure 3.6 continued on next page)

Figure 3.6. Inhibition of integrin-mediated cell adhesion results in decreased T-ALL burden and prolongs survival in vivo.

(A) Schematic diagram depicting engraftment of primary LN3 T-ALL cells into *Icam1*$^{-/-}$ and *Icam1*$^{+/-}$ littermate controls. Once blood T-ALL burden reached 1% to 2% in control mice, leukemic burden was assessed or survival was monitored. (B) Quantification of the weights of the spleens and livers from *Icam1*$^{+/-}$ and *Icam1*$^{-/-}$ mice transplanted with primary LN3 T-ALL cells. Organ weights of tumor-free littermate controls are included. Bars depict means + standard error of the mean (SEM) of cumulative data from 2 or 3 experiments, each with a distinct color-coded primary T-ALL; circles represent individual mice. (C) Quantification of the frequency of T-ALL cells in the blood and numbers of T-ALL cells in the spleen, BM, inguinal LN, and liver in *Icam1*$^{+/-}$ and *Icam1*$^{-/-}$ mice from the same experiments as in (B). Bars depict means + SEM of cumulative data from 2 or 3 experiments, each with a distinct color-coded primary T-ALL; circles represent individual mice. (D) Graph displays cumulative survival of *Icam1*$^{+/-}$ and *Icam1*$^{-/-}$ leukemic mice from 3 independent experiments, each with a different primary LN3 T-ALL. The Kaplan-Meier survival curves were normalized to the first day of death in each experiment. (E) Schematic diagram depicting the dosing schedule for anti-ICAM-1 and/or anti-VCAM-1 treatment to inhibit integrin-mediated cell adhesion in mice with established transplanted LN3 T-ALL. (F) Quantification of the weights of the spleens and livers from isotype- or anti-ICAM-1 and anti-VCAM-1-treated mice transplanted with primary LN3 T-ALL cells. Organ weights of tumor-free littermate controls are included. Bars depict means + SEM of cumulative data from 3 experiments, each with a distinct color-coded primary T-ALL; circles represent individual mice. (G) Representative flow cytometry plots showing the frequency of T-ALL cells in the blood of LN3 T-ALL-bearing mice treated with isotype (left) or ICAM-1 and VCAM-1 neutralizing antibodies (right). (H) Quantification of the frequency of T-ALL cells in the blood and numbers of T-ALL cells in the spleen, BM, LN, and liver in isotype- or anti-ICAM-1 and anti-VCAM-1-treated mice from the same experiments as in (F). Bars depict means + SEM of cumulative data from 3 experiments, each with a distinct color-coded primary T-ALL; circles represent individual mice. **P* < .05, ***P* < .01, ****P* < .001, repeated measures one-way ANOVA with the Holm-Sidak correction (B,F), unpaired Student t test (C,H), log-rank test (D). ns, not significant.

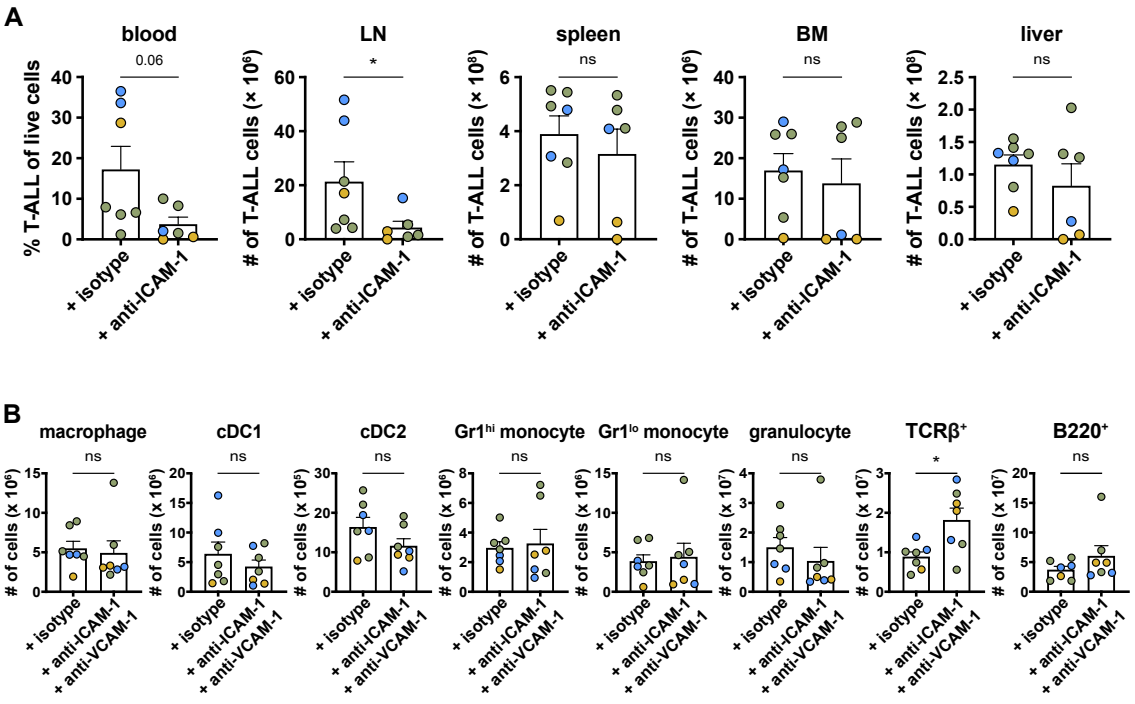

Figure 3.7. Efficacy of anti-ICAM-1 antibody alone is limited and a combination of anti-ICAM1 and anti-VCAM1 does not deplete myeloid cells in T-ALL mice.

(A) Quantification of the frequency of T-ALL cells in the blood and numbers of T-ALL cells in the spleen, BM, inguinal LN, and liver in primary LN3 T-ALL-engrafted mice administered with either isotype (the same isotype-treated mice as in Figure 3.6H) or anti-ICAM-1 neutralizing antibody, using the treatment regimen in Figure 3.6E. Bars depict means + standard error of the mean (SEM) of cumulative data from 3 experiments, each with a distinct color-coded primary T-ALL; circles represent individual mice. (B) Quantification of the indicated myeloid subsets in the spleens of primary LN3 T-ALL-engrafted mice administered with either isotype or a combination of anti-ICAM-1 and anti-VCAM-1 (the same mice as in Figure 3.6H). The indicated myeloid subsets were gated as previously depicted in Figure 2.4A. Bars show means + SEM of cumulative data from 3 independent experiments with a distinct color-coded primary T-ALL; circles represent individual mice. *$P < .05$, unpaired Student t test (A,B). ns, not significant.

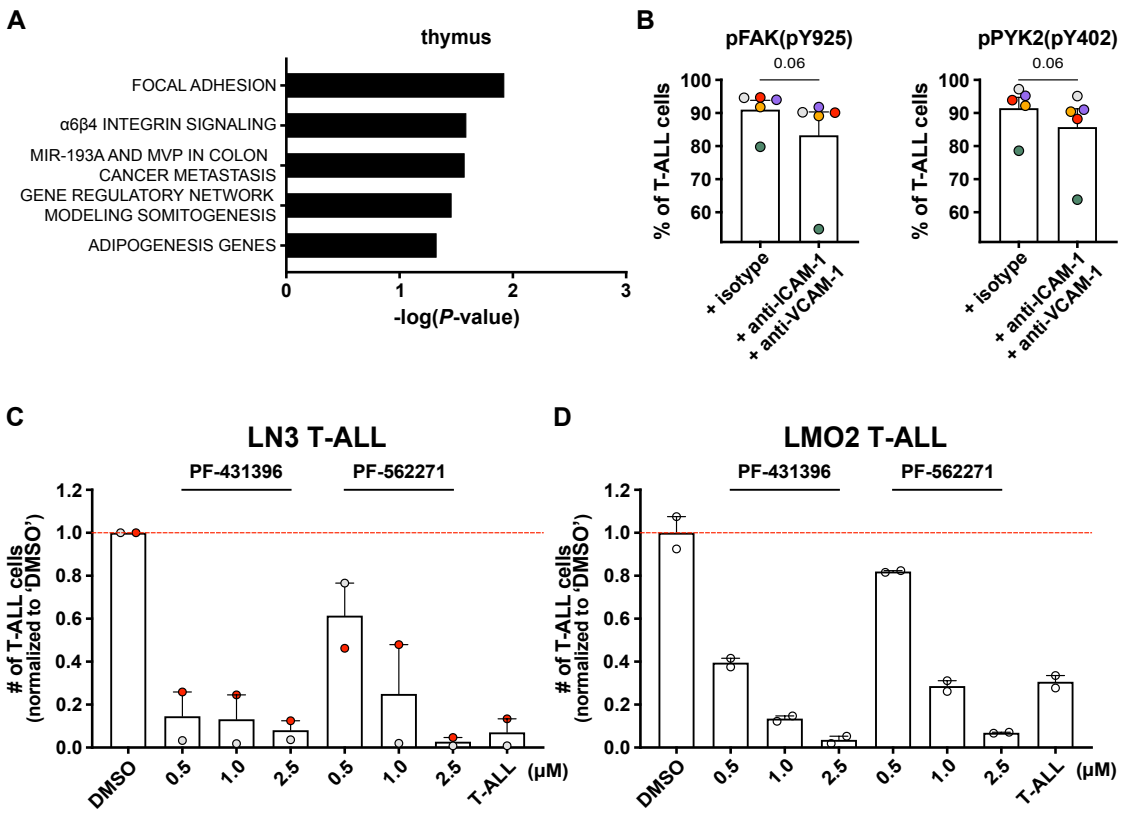

(Figure 3.8 continued on next page)

Figure 3.8. Myeloid-mediated T-ALL survival is dependent on focal adhesion signaling.

(A) The top 5 pathways that were significantly enriched in thymic T-ALL cells relative to healthy T-lineage cells were identified using the WikiPathways 2019 Mouse gene sets of the Enrichr bioinformatics tool. (B) Quantification of the frequencies of $pFAK^+$ or $pPYK2^+$ cells within viable T-ALL cells, isolated from the spleens of primary LN3 T-ALL-engrafted mice, 4 or 5 days after culture in the presence or absence of splenic tumor-associated myeloid cells and in the presence or absence of a combination of anti-ICAM-1 and anti-VCAM-1 (10 μg/ml per each). Bars represent means + standard error of the mean (SEM) of data compiled from 5 independent experiments with a distinct color-coded primary T-ALL; circles represent each experiment. (C-D) Quantification of viable T-ALL cells, isolated from the spleens of primary (C) LN3 or (D) LMO2 T-ALL-transplanted mice, 7 or 8 days after culture in the presence or absence of splenic tumor-associated myeloid cells and in the presence of the indicated concentrations of FAK/PYK2 dual inhibitors (PF-431396 or PF-562271) or vehicle control (DMSO). Results were normalized to DMSO-treated control co-cultures within each experiment (red line). Bars represent means + SEM of cumulative data from 1 or 2 independent experiments using a distinct color-coded primary T-ALL. Circles represent the average of 2 technical replicate wells per experiment. Paired Student t test (B).

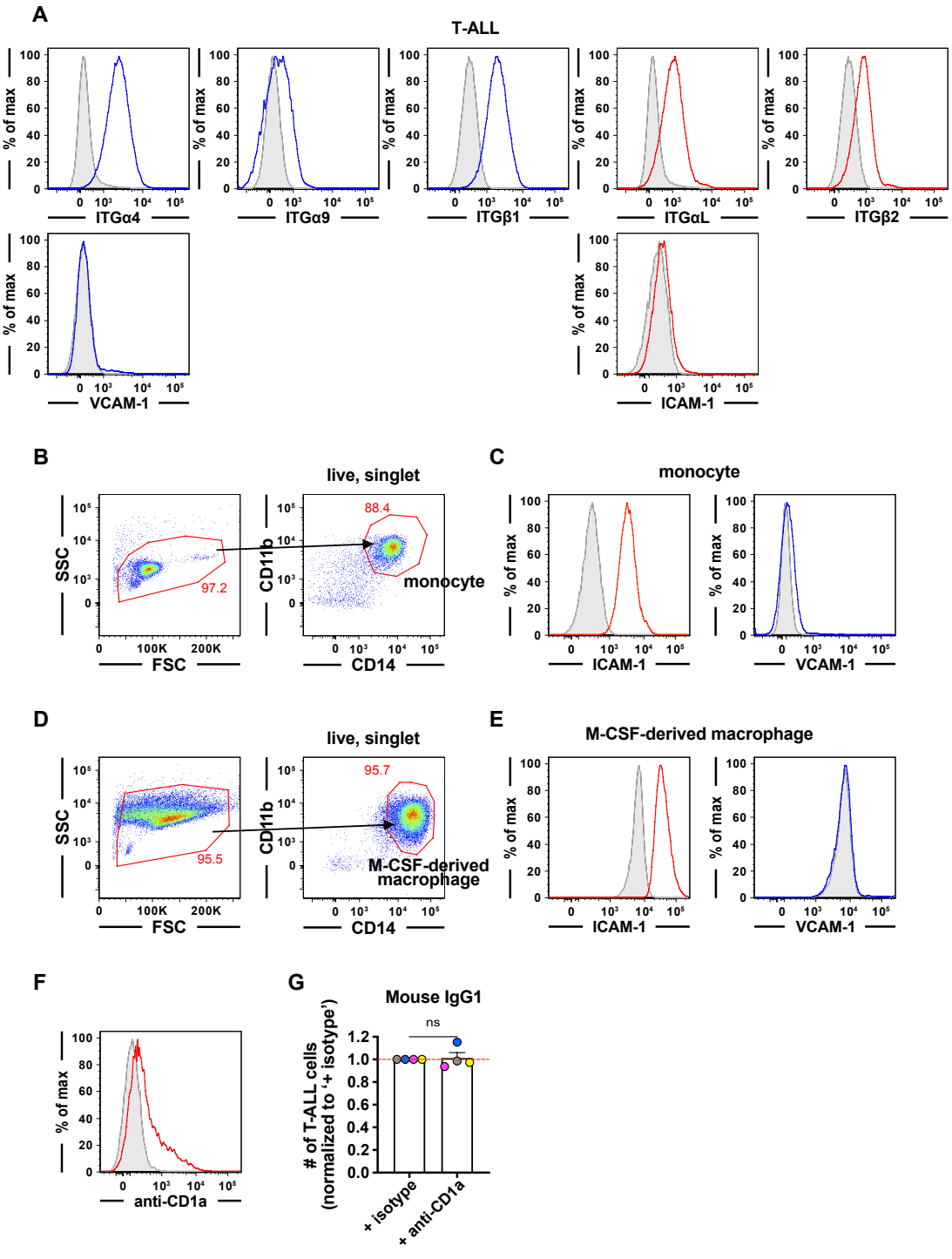

(Figure 3.9 continued on next page)

Figure 3.9. Protein expression levels of integrins and cell adhesion ligands on primary pediatric T-ALL cells and human myeloid cells are evaluated.

(A) Representative flow cytometry plots of the indicated integrin components and cell adhesion ligands on primary pediatric T-ALL cells. (B) Representative sequential gating scheme for evaluation of PBMC-derived monocytes. (C) Representative flow cytometry plots of ICAM-1 (red) and VCAM-1 (blue) on monocytes. Isotype controls are shaded in gray. (D) Representative sequential gating scheme for evaluation of M-CSF-derived macrophages. (E) Representative flow cytometry plots of ICAM-1 (red) and VCAM-1 (blue) on M-CSF-derived macrophages. Isotype controls are shaded in gray. (F) Representative flow cytometry plots of CD1a on primary pediatric T-ALL cells. Isotype control is shaded in gray. (G) Quantification of viable primary pediatric T-ALL cells 6 or 7 days after culture in the presence of monocytes and in the presence of anti-CD1a (30 μg/ml). Results were normalized to the viability of T-ALL cells co-cultured with monocytes in the presence of isotype control antibody (red line). Bars show means + standard error of the mean (SEM) of cumulative data from 4 independent experiments, each with a distinct color-coded primary T-ALL; circles represent the average of 2 technical replicate wells per experiment. Paired Student t test (G). ns, not significant.

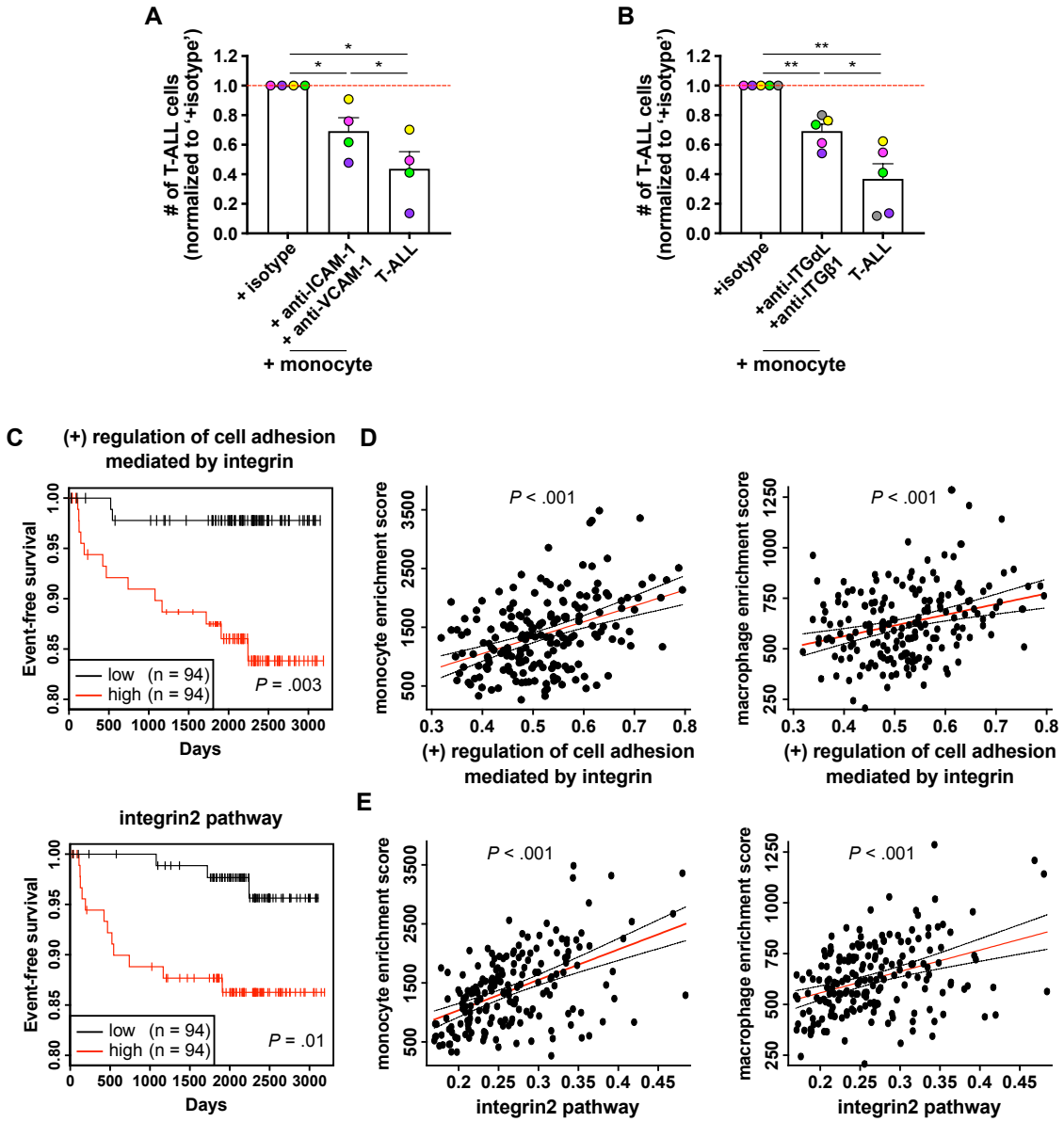

(Figure 3.10 continued on next page)

Figure 3.10. Activation of integrins by human monocytes supports survival of primary pediatric T-ALL cells and enriched gene signatures of integrin signaling pathways are associated with worse outcomes.

(A-B) Quantification of viable primary pediatric T-ALL cells cultured for 6 or 7 days in the presence or absence of PBMC-derived monocytes and in the presence or absence of a combination of (A) anti-ICAM-1 (20 μg/ml) and anti-VCAM-1 (10 μg/ml) antibodies or (B) anti-ITGαL and anti-ITGβ1 antibodies (10 μg/ml per each). T-ALL viability was assessed by flow cytometry. Data are compiled from 2 or 3 independent experiments using 4 or 5 distinct patient-derived T-ALLs. Bars show means + standard error of the mean (SEM) of cumulative data. (C) Longitudinal event-free survival is plotted for pediatric T-ALL patients stratified into 2 groups based on their enrichment scores for "(+) regulation of cell adhesion mediated by integrin" (top) or "integrin2 pathway" (bottom) gene signatures. Patient data were analyzed from published datasets from 264 T-ALL patients from the TARGET ALL Phase II trial (Liu et al., 2017). (D-E) Plot depicts the correlation between (D) enrichment scores for "(+) regulation of cell adhesion mediated by integrin" gene signatures and enrichment scores monocyte (left) or macrophage (right) gene signatures or (E) enrichment scores for "integrin2 pathway" gene signatures and enrichment scores for monocyte (left) or macrophage (right) gene signatures in patient samples. The red and dotted lines represent the best-fit line and 95% confidence bands, respectively. Circles represent each patient sample. $*P < .05$, $**P < .01$, repeated measures one-way ANOVA with the Holm-Sidak correction (A,B), log-rank test (C), simple linear regression analysis (D,E). ns, not significant.

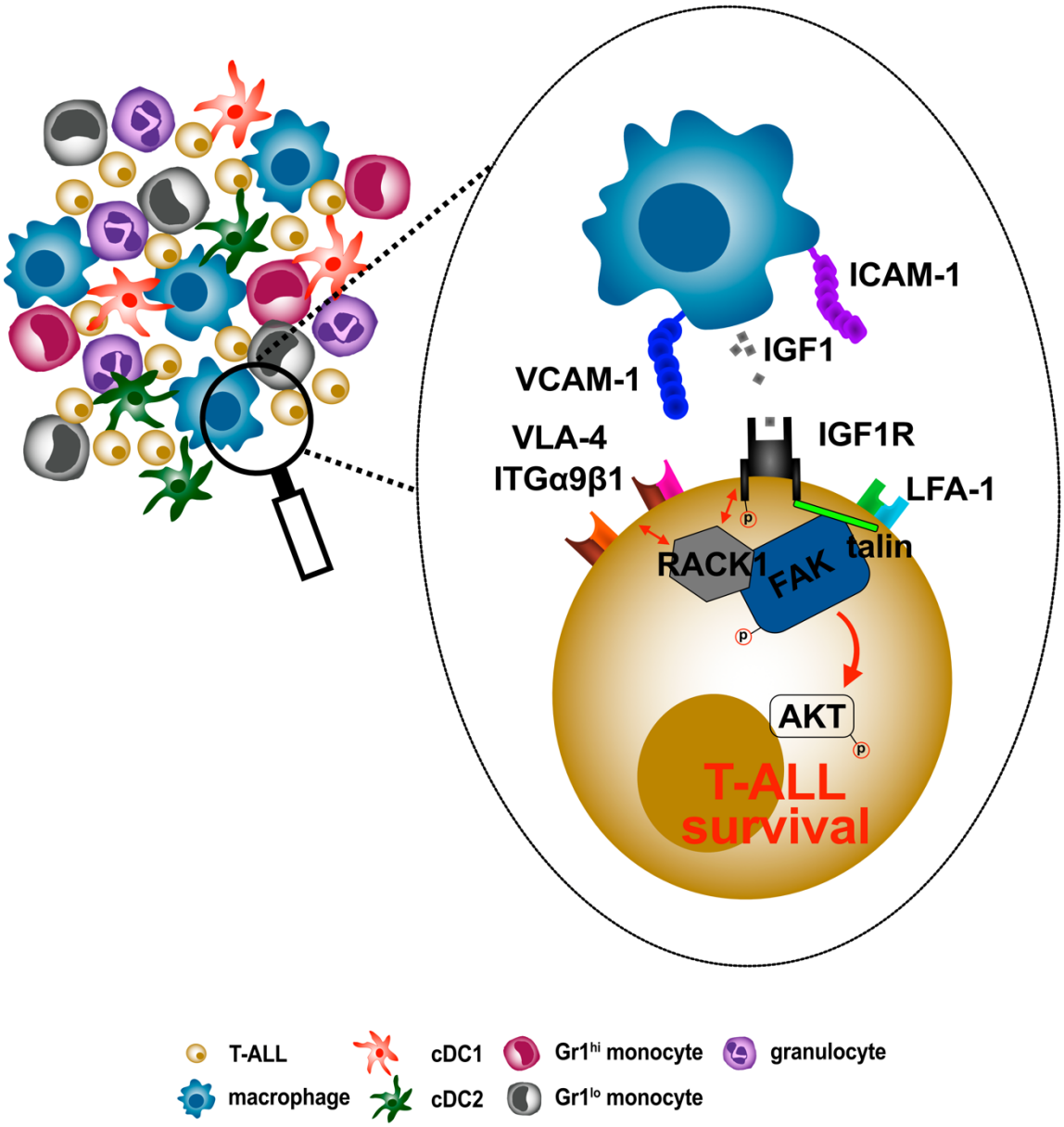

(Figure 3.11 continued on next page)

Figure 3.11. Illustrative summary of Chapter 3

Inhibition of integrin-mediated cell adhesion using genetic or pharmacologic means results in a significant reduction in T-ALL survival in mouse models and in patient samples. Moreover, blockade of cell adhesion ligands (ICAM-1 and VCAM-1) diminishes IGF1R and focal adhesion signaling in T-ALL cells. IGF1R and integrins are known to interact cooperatively (Kiely et al., 2002) (Sayeed et al., 2013) (Cox et al., 2015), and adaptor proteins, such as RACK1, could play a role in mediating the crosstalk (Li and Xie, 2015). These results suggest that myeloid cells promote T-ALL progression by activating integrin signaling.

Chapter 4

Discussion

It is now well-appreciated that the TME plays a pivotal role in promoting tumor survival and progression in both solid and hematologic malignancies (Quail and Joyce, 2013) (Binnewies et al., 2018) (Witkowski et al., 2020). Tumor-associated myeloid cells are a particularly essential component of the TME, responsible for promoting tumor growth and metastases across a wide variety of tumor types, such as lung cancer and AML (Schmall et al., 2015) (Edwards et al., 2019). Emerging evidence suggests that the TME in T-ALL is also critical for leukemia progression both in mouse models and in patients. For example, a contribution of BM vascular endothelial cells to T-ALL progression and migration, via expression of CXCL12, has been elegantly demonstrated using mouse models and patient samples (Pitt et al., 2015) (Passaro et al., 2015). However, although myeloid cells have been shown to support T-ALL survival and proliferation in vitro (Chen et al., 2015) (Triplett et al., 2016), their in vivo contribution to T-ALL progression has remained elusive. Here, in Chapter 2, we present the first studies to demonstrate that myeloid cells play a critical role in T-ALL progression in vivo. Pharmacologic or genetic ablation of myeloid cells results in a significant reduction of T-ALL burden at several leukemic sites and prolongs survival in two distinct mouse models of T-ALL. In addition, PBMC-derived myeloid cells support survival of primary pediatric T-ALL patient samples in vitro, and transcriptional profiling data indicate that macrophage abundance correlates with poor outcomes in pediatric T-ALL patients.

We have also identified two related molecular mechanisms by which myeloid cells support T-ALL progression in vivo. First, in Chapter 2, we report that tumor-associated myeloid cells activate the growth factor receptor IGF1R in T-ALL cells, and

pharmacologic inhibition of IGF1R signaling significantly reduces T-ALL viability in vitro. These results are consistent with previous findings that IGF1R mediates critical survival and growth signals in T-ALL cells (Medyouf et al., 2011) (Gusscott et al., 2016). Furthermore, acute depletion of tumor-associated myeloid cells in vivo significantly diminishes IGF1R signaling in T-ALL cells, but not in host T cells. These results suggest that targeting tumor-associated myeloid cells specifically reduces survival signals in leukemic cells, without impairing healthy T cells that could contribute to anti-leukemic immune responses. Second, in Chapter 3, we report that integrin-mediated cell adhesion is critical for myeloid-mediated T-ALL support. Consistent with transcriptional profiling analyses implicating integrin activation in T-ALL growth, inhibition of integrin-mediated cell adhesion leads to a significant decrease in T-ALL burden in multiple organs and delayed leukemia progression in vivo. Blockade of integrin-mediated close contact results in reduced activation of IGF1R and the downstream molecule AKT in T-ALL cells in vitro, suggesting that integrin signaling and IGF1R signaling are both needed for myeloid-mediated T-ALL survival. Consistent with mouse models, blockade of integrin-mediated cell adhesion also suppresses monocyte-mediated support of primary pediatric T-ALL cell survival. Furthermore, enriched gene signatures associated with integrin signaling correlate with worse prognosis in T-ALL patients. Although previous studies have shown that integrin signaling has been implicated in promoting T-ALL survival by BM stroma or ECM (Winter et al., 2001) (You et al., 2015), the contribution of integrin-mediated cell adhesion to myeloid-mediated support of T-ALL has remained unexplored. Collectively, the results of this dissertation expand our understanding of the role of the TME, particularly tumor-associated myeloid cells, in T-ALL pathogenesis, and identify putative targets for therapeutic intervention.

Are macrophages the major myeloid player in T-ALL progression in vivo?

TAMs have been implicated in supporting tumor growth in multiple cancer types, such as breast, colon, melanoma, and lung cancers (DeNardo et al., 2009) {Kiura:2015iv} (Georgoudaki et al., 2016) (Loyher et al., 2018). TAMs can directly trigger tumor progression and metastasis either by releasing soluble factors or by expressing ligands on their cell surfaces that signal to tumor cells to promote survival, proliferation, and/or migration. For example, macrophages provide survival signals in breast cancer cells by activating ITGα4β1 and ITGα4β7 on the tumor cells, resulting in increased metastasis to the lungs (Chen et al., 2011). TAMs can also promote tumor growth by producing a variety of cytokines, chemokines, and growth factors that have direct or indirect effects on tumor growth. In a mouse model of breast cancer, TAMs were shown to secrete angiogenic factors, such as VEGF and MMP-9, resulting in an establishment of dense vasculature supplying oxygen and nutrition to tumor cells (Lin and Pollard, 2007). Co-cultures of T-ALL cells with FACS-sorted tumor-associated myeloid subsets, revealed that TAMs are the most potent T-ALL-supportive myeloid subset, although monocytes and cDC2 also support leukemic survival (Lyu et al., 2020). Additionally, evaluation of transcriptional datasets from pediatric T-ALL patients (Liu et al., 2017) indicates that an abundance of macrophages correlates with poor outcomes for patients (Lyu et al., 2020). Therefore, macrophages could be the major myeloid player in T-ALL pathogenesis in vivo; if so, targeting TAMs could be a potential therapeutic strategy for T-ALL treatment. The work presented in this dissertation used pharmacologic or genetic ablation of multiple myeloid subsets, including macrophages, monocytes, and cDCs, to demonstrate that myeloid cells provide essential support for T-ALL. Thus, it remains to be determined whether TAMs are necessary and sufficient for T-ALL growth in vivo. To tackle this question, we could utilize mouse genetic models specific for macrophage depletion. For

example, previous studies showed that targeting of cells expressing both the macrophage colony-stimulating factor receptor (*Csf1r*) and lysozyme (*LysM*) results in ablation of macrophages in multiple organs, such as the spleen, liver, lung, and peritoneum, without reducing monocyte or DC cellularity (*LysM*^{Cre}×*Csf1r*$^{LsL\text{-}DTR}$ mice; (Schreiber et al., 2013)).

T-ALL-supportive macrophages: monocyte-derived or tissue-resident?

Our findings reveal that macrophages (F4/80^{+}CD64^{+}) isolated from the spleen and liver have the ability to support T-ALL survival. However, these cells are not homogenous; they can be divided into monocyte-derived macrophages and tissue-resident macrophages, which seed the tissues during ontogeny (Ginhoux et al., 2010) (Hoeffel et al., 2012). Thus, investigation of whether tumor-supportive TAMs are monocyte-derived or tissue-resident using mouse models of T-ALL and pediatric T-ALL samples would determine whether a unique subset of macrophages is tumor-supportive, potentially revealing more specific therapeutic targets for T-ALL treatment.

Macrophages are present in most tissues throughout the body, and historically, they were thought to originate from circulating monocytes (van Furth et al., 1972). However, recent studies using genetic fate-mapping approaches and parabiotic techniques have elegantly shown that tissue-resident macrophages originate from embryonic progenitors and are maintained by self-renewal in tissues throughout life (Ginhoux et al., 2010) (Hashimoto et al., 2013) (Epelman et al., 2014). Under normal conditions, both subsets of macrophages serve as the first line of defense; they generate innate immune responses to pathogens, shape the environment for tissue development, and maintain tissue homeostasis by clearing dead cells and promoting tissue repair (Davies et al., 2013) (Italiani and Boraschi, 2014). In response to pathogens, circulating monocytes are

recruited to the site of infection, where they differentiate into inflammatory monocyte-derived macrophages, while tissue-resident macrophages clear the pathogens and repair the tissues (Watanabe et al., 2019) (Mu et al., 2020). Although studies are still ongoing to discriminate between the contributions of each macrophage subset to tumor progression, there are a few studies investigating the role of monocyte-derived macrophages versus tissue-resident Kupffer cells during liver tumorigenesis. During the onset of liver cancer, Kupffer cells were shown to promote tumor pathogenesis by inducing inflammatory responses via production of cytokines, such as IL-1β, IL-6, and TNF-α, as well as through expression of the proinflammatory myeloid cell surface receptor TREM-1 (Wu et al., 2012). Elimination of *Trem1* diminished activation of Kupffer cells, resulting in attenuation of liver tumorigenesis in mice. On the other hand, monocyte-derived macrophages play a role in progression and metastasis of liver cancer at later stages. In patients with liver cancer, monocyte-derived macrophages induced NK-cell dysfunction through the CD48/2b4 axis, resulting in immunosuppression (Wu et al., 2013). Moreover, high infiltration of macrophages was associated with poor prognosis in patients with liver cancer after resection (Ding et al., 2009). In terms of a role for monocyte-derived macrophages in T-ALL progression, our finding that M-CSF-derived macrophages are capable of supporting survival of primary pediatric T-ALL cells suggests that monocyte-derived macrophages are likely to be pro-T-ALL in vivo. Indeed, monocyte-derived TAMs were recently shown to facilitate extramedullary infiltration of T-ALL cells through CCL8-CCR1/CCR2 and CCL9/10-CCR1 signaling in a NOTCH1-induced mouse model of T-ALL (Yang et al., 2020). In this study, genetic ablation of CCR2 or therapeutic blockade of CCR1 and CCR2 significantly delayed T-ALL progression in vivo (Yang et al., 2020). However, it remains to be determined whether tissue-resident macrophages promote T-ALL growth. This possibility could be explored in vitro by

carrying out co-cultures of T-ALL cells with tissue-resident macrophages, such as Kupffer cells ($F4/80^{+}CD64^{+}Clec4F^{+}Tim4^{+}Ly6C^{-}Ly6G^{-}$; (Scott et al., 2018)) isolated from T-ALL-engrafted organs. Additionally, a role for tissue-resident macrophages in T-ALL progression could be investigated in vivo by specific depletion of the population. Previously, administration of clodlip (Gehring et al., 2006) (Tavares et al., 2017) or Gadolinium chloride (GdCl3) (Hardonk et al., 1992) (Adding et al., 2001) was used to ablate Kupffer cells. However, clodlip broadly depletes phagocytes without specificity for Kupffer cells (Lanthier et al., 2010), and mice are relatively resistant to GdCl3 (Gehring et al., 2006). Instead, genetic ablation using mouse models may be a more reliable option. Previously, Kupffer cells were genetically ablated using the Clec4F-DTR mouse model (Scott et al., 2016). Expression of *Clec4f* was determined to be restricted to Kupffer cells, and DT administration preferentially depleted Kupffer cells in the liver, but did not impact other tissue-resident macrophages, such as lung alveolar or splenic red pulp (Scott et al., 2016).

T-ALL-supportive monocytes: classical or non-classical?

We found that monocytes ($CD11b^{+}CD11c^{-}CD64^{-}CD115^{+}F4/80^{+}MHCII^{-}$) isolated from the leukemic spleen and liver are also capable of promoting survival of T-ALL cells. Because monocytes comprise two major subsets, classical and non-classical, it remains to be determined which subset exhibits more potent activity in T-ALL progression.

Classical monocytes are the major subset recruited to sites of infection in response to inflammatory stimuli (Jakubzick et al., 2017). It is now well-documented that classical monocytes are tumor-supportive in a variety of tumors, such as breast, lung, and liver cancers (Qian et al., 2011) (Schmall et al., 2015) (Li et al., 2017). For example, in mouse models of breast cancer, $Gr1^{+}$ classical monocytes were recruited to lung metastases via

the CCR2-CCL2 axis (Qian et al., 2011). In this study, therapeutic neutralization of CCL2 inhibited recruitment of classical monocytes, resulting in a significant reduction of metastasis in vivo. Moreover, elimination of tumor cell-derived CCL2 was shown to suppress metastatic seeding (Qian et al., 2011). Recently, classical monocytes were shown to play a pathologic role in T-ALL progression in vivo using mouse models (Yang et al., 2020). This study determined that $Ly6C^{+}$ classical monocytes differentiate into $Ly6C^{+}$ macrophages which induce inflammation and contribute to broader distribution of T-ALL cells within organs. Moreover, inhibition of classical monocyte infiltration using genetic or pharmacologic means significantly delayed extramedullary infiltration of T-ALL (Yang et al., 2020). However, it remains to be investigated whether classical monocytes are capable of supporting T-ALL growth directly. Co-cultures of T-ALL cells with this subset of monocytes ($CX3CR1^{lo}CCR2^{+}Ly6C^{hi}$) isolated from the spleen or liver of leukemic mice could fill this gap in knowledge.

A more intriguing question is whether non-classical monocytes contribute to T-ALL pathogenesis in vivo. In response to infections, non-classical monocytes, which generally patrol the vascular endothelium in tissues, rapidly migrate into the inflamed sites, induce immune responses, and differentiate into macrophages (Auffray et al., 2007) (Kapellos et al., 2019). Previous studies have shown that these non-classical monocytes can have pro-tumor or anti-tumor activities. In mouse models of colorectal and lung cancers, non-classical monocytes have been implicated in promoting tumor progression with induction of immunosuppression and angiogenesis (Jung et al., 2017) (Venneri et al., 2007). On the contrary, in mouse models of melanoma and breast cancer, non-classical monocytes were shown to suppress tumor metastasis through phagocytosis and activation of anti-tumor immune responses (Hanna et al., 2015). Although the role of non-classic monocytes in T-ALL growth has yet to be investigated, our results presented in this

dissertation suggest they could be tumor-supportive. First, we found $Gr1^{lo}$ non-classical monocytes drastically expand in the spleens of T-ALL-engrafted mice, not only in numbers, but also in frequencies of the total myeloid compartment ($CD11b^{+}$ and/or $CD11c^{+}$). These monocytes show the highest increase in frequencies compared to other myeloid subsets, suggesting they could play a critical role in T-ALL progression. Moreover, in the spleens of leukemic mice injected with clodlip, where T-ALL burden significantly reduced, macrophages and $Gr1^{lo}$ non-classical monocytes were almost completed ablated, whereas $Gr1^{hi}$ classical monocytes were not greatly impacted. The contribution of non-classical monocytes to T-ALL survival in vitro could be tested by co-cultures of T-ALL cells with isolated monocytes ($CX3CR1^{hi}CCR2^{-}Ly6C^{lo}$) from the spleen or liver of leukemic mice. Ablation of non-classical monocytes via mouse models, such as NR4A1-deficient mice in which $Ly6C^{-}$ monocytes are absent, (Hanna et al., 2011), could be used to validate their roles in vivo. However, results should be interpreted with caution, because T-cell development can also be impacted in this model (Nowyhed et al., 2015).

Is activation of PDGFRβ in T-ALL mediated by macrophage-fibroblast crosstalk?

Evaluation of transcriptional profiling revealed that the expression of *Pdgfrb* is significantly upregulated in T-ALL cells from the spleen and thymus of leukemic mice, relative to organ-matched tumor-free T-lineage cells. Consistent with this, T-ALL cells examined ex vivo showed significantly higher levels of activated PDGFRβ compared to tumor-free thymocytes (Triplett et al., 2016). This study also showed that tumor-associated DCs alone were not sufficient to sustain PDGFRβ activation in vitro (Triplett et al., 2016). Our preliminary data indicated that ablation of myeloid cells using clodlip slightly decrease activation of PDGFRβ in T-ALL cells from leukemic spleen, whereas

host T cells are not impacted (unpublished). In addition, re-analysis of published transcriptional datasets of pediatric T-ALL patients (Liu et al., 2017) revealed that there is a significant correlation between enriched gene signatures of macrophages and PDGFR signaling (P-value = 2×10^{-16}; unpublished). Therefore, it is possible that myeloid cells promote T-ALL survival by activating PDGFRβ in vivo, potentially with the help of other components in the TME.

Previously, a macrophage-fibroblast cell circuit has been characterized using computational and functional approaches (Zhou et al., 2018). In this study, proliferation of BM-derived macrophages and mouse embryonic fibroblasts in vitro was dependent on CSF1 and PDGFB, respectively, and the reciprocal growth factor receptors (*Csf1r, Pdgfrb*) were expressed by macrophages and fibroblasts, respectively (Zhou et al., 2018). Notably, macrophages and fibroblasts were shown to express high levels of *Pdgfb* and *Csf1*, respectively, which is consistent with previous publications (Ryan et al., 2001) (Lavin et al., 2014), suggesting these two cell types could promote each other's growth. Co-cultures of macrophages and fibroblasts confirmed that there was reciprocal proliferation of these two cell types, and the mechanism was validated using CSF1-deficient fibroblasts and PDGFB-deficient macrophages (Zhou et al., 2018). Thus, bi-directional crosstalk between macrophages and fibroblasts could play a role in promoting T-ALL progression, and PDGFB could promote survival not only of fibroblasts but also of T-ALL cells, which express high levels of PDGFRβ. Evaluation of changes in the viability of T-ALL cells and/or the levels of activated PDGFRβ in T-ALL cells in co-cultures of T-ALL cells with tumor-associated myeloid cells in the presence or absence of embryonic fibroblasts could be a way to explore this possibility. Moreover, the role of the macrophage-fibroblast interaction in T-ALL pathogenesis in vivo could be validated by ablation of fibroblasts using α-smooth muscle actin (α-SMA)-TK mice (LeBleu et al.,

2013) in the presence or absence of pharmacologic or genetic myeloid depletion. In addition, BM chimeras in which hematopoietic cells lacked expression of *Pdgfb* could also be used.

Validation of myeloid-mediated T-ALL support through integrins in vivo

Our studies have shown that blockade of integrin-mediated close contact between T-ALL cells and tumor-associated myeloid cells from the spleen robustly suppresses the survival of leukemia cells in vitro. Moreover, elimination of *Icam1* results in a significant decrease in T-ALL burden at multiple leukemic sites, and prolongs survival. Additionally, therapeutic neutralization of both ICAM-1 and VCAM-1 in mice with established T-ALL significantly delays leukemic progression. We confirmed that neutralization of these adhesion molecules did not deplete myeloid cells in the spleen, indicating that inhibition of ICAM-1- and VCAM-1 blocks integrin signaling in T-ALL cells that drives leukemia growth and progression. However, these in vivo experiments do not allow us to determine whether ICAM-1/VCAM-1 expression by myeloid cells, as opposed to other cell types, is essential for T-ALL progression. Previous studies have shown that normal BM stromal cells, consisting of endothelial and mesenchymal cells, support survival of patient-derived T-ALL cells through ICAM-1- and VCAM-1-mediated cell adhesion events (Winter et al., 2001). Expression of ICAM-1 by endothelial cells and fibroblasts (Dustin et al., 1988) and VCAM-1 by endothelial cells (Frenette et al., 1998) (Ulyanova et al., 2005) have been demonstrated in the BM. ICAM-1 and VCAM-1 are also expressed by epithelial cells in the thymus (Salomon et al., 1997), which is the primary site of T-ALL initiation. Therefore, BM stromal cells and TECs could play a role in promoting T-ALL growth through ICAM-1- and VCAM-1-mediated interactions in vivo. It remains to be determined whether inhibition of integrin-mediated close contact

between T-ALL cells and tumor-associated myeloid cells is sufficient to suppress leukemic progression in vivo. To this end, genetic ablation of the adhesion molecules in myeloid cells using mouse models could be utilized. Myeloid-specific ablation of ICAM-1 and VCAM-1 in mice established with T-ALL (LysM-Cre ER^{T2}×$Icam1^{fl/fl}$;$Vcam1^{fl/fl}$; (Canli et al., 2017)) provides an appealing option.

Collectively, the research presented in this dissertation demonstrates that tumor-associated myeloid cells provide critical support for T-ALL in vivo through activation of IGF1R signaling and integrin signaling in T-ALL cells, and indicates that a combined therapeutic strategy to target signals provided by myeloid cells and other components in the TME may prove efficacious. However, although myeloid depletion or blockade of integrin-mediated cell adhesion delays T-ALL progression, most mice still succumb to leukemia, suggesting that additional mechanisms need to be resolved. In addition, further studies allowing a deep understanding of the contribution of tumor-associated myeloid cells to T-ALL pathogenesis in other clinically relevant sites, such as the CNS, will be required.

References

Adding, L.C., Bannenberg, G.L., and Gustafsson, L.E. (2001). Basic experimental studies and clinical aspects of gadolinium salts and chelates. Cardiovasc Drug Rev. *19*, 41–56.

Aharinejad, S., Salama, M., Paulus, P., Zins, K., Berger, A., and Singer, C.F. (2013). Elevated CSF1 serum concentration predicts poor overall survival in women with early breast cancer. Endocr Relat Cancer. *20*, 777–783.

Allart-Vorelli, P., Porro, B., Baguet, F., Michel, A., and Cousson-Gélie, F. (2015). Haematological cancer and quality of life: a systematic literature review. Blood Cancer J. *5*, e305–e305.

Allen, A., Sireci, A., Colovai, A., Pinkney, K., Sulis, M., Bhagat, G., and Alobeid, B. (2013). Early T-cell precursor leukemia/lymphoma in adults and children. Leuk Res. *37*, 1027–1034.

Allman, D., Aster, J.C., and Pear, W.S. (2002). Notch signaling in hematopoiesis and early lymphocyte development. Immunol Rev. *187*, 75–86.

Almand, B., Clark, J.I., Nikitina, E., van Beynen, J., English, N.R., Knight, S.C., Carbone, D.P., and Gabrilovich, D.I. (2001). Increased production of immature myeloid cells in cancer patients: a mechanism of immunosuppression in cancer. J Immunol. *166*, 678–689.

Alves-Rosa, F., Vermeulen, M., Cabrera, J., Stanganelli, C., Capozzo, A., Narbaitz, M., van Rooijen, N., Palermo, M., and Isturiz, M.A. (2003). Macrophage depletion following liposomal-encapsulated clodronate (LIP-CLOD) injection enhances megakaryocytopoietic and thrombopoietic activities in mice. Br J Haematol. *121*, 130–138.

Antoniades, H.N., Galanopoulos, T., Neville-Golden, J., and O'Hara, C.J. (1992). Malignant epithelial cells in primary human lung carcinomas coexpress in vivo platelet-derived growth factor (PDGF) and PDGF receptor mRNAs and their protein products. Proc Natl Acad Sci U S A. *89*, 3942–3946.

Aran, D., Hu, Z., and Butte, A.J. (2017). xCell: digitally portraying the tissue cellular heterogeneity landscape. Genome Biol. *18*, 220.

Arlauckas, S.P., Garris, C.S., Kohler, R.H., Kitaoka, M., Cuccarese, M.F., Yang, K.S., Miller, M.A., Carlson, J.C., Freeman, G.J., Anthony, R.M., et al. (2017). In vivo imaging reveals a tumor-associated macrophage-mediated resistance pathway in anti-PD-1 therapy. Sci Transl Med. *9*, eaal3604.

Armstrong, F., la Grange, de, P.B., Gerby, B., Rouyez, M.-C., Calvo, J., Fontenay, M., Boissel, N., Dombret, H., Baruchel, A., Landman-Parker, J., et al. (2009). NOTCH is a

key regulator of human T-cell acute leukemia initiating cell activity. Blood. *113*, 1730–1740.

Atibalentja, D.F., Murphy, K.M., and Unanue, E.R. (2011). Functional redundancy between thymic CD8α+ and Sirpα+ conventional dendritic cells in presentation of blood-derived lysozyme by MHC class II proteins. J Immunol. *186*, 1421–1431.

Auffray, C., Fogg, D., Garfa, M., Elain, G., Join-Lambert, O., Kayal, S., Sarnacki, S., Cumano, A., Lauvau, G., and Geissmann, F. (2007). Monitoring of blood vessels and tissues by a population of monocytes with patrolling behavior. Science. *317*, 666–670.

Awad, R.M., De Vlaeminck, Y., Maebe, J., Goyvaerts, C., and Breckpot, K. (2018). Turn Back the TIMe: Targeting Tumor Infiltrating Myeloid Cells to Revert Cancer Progression. Front Immunol. *9*, 1977.

Balis, F.M., Lester, C.M., Chrousos, G.P., Heideman, R.L., and Poplack, D.G. (1987). Differences in cerebrospinal fluid penetration of corticosteroids: possible relationship to the prevention of meningeal leukemia. J Clin Oncol. *5*, 202–207.

Barczyk, M., Carracedo, S., and Gullberg, D. (2010). Integrins. Cell Tissue Res. *339*, 269–280.

Basen-Engquist, K., and Chang, M. (2011). Obesity and cancer risk: recent review and evidence. Curr Oncol Rep. *13*, 71–76.

Bash, R.O., Crist, W.M., Shuster, J.J., Link, M.P., Amylon, M., Pullen, J., Carroll, A.J., Buchanan, G.R., Smith, R.G., and Baer, R. (1993). Clinical features and outcome of T-cell acute lymphoblastic leukemia in childhood with respect to alterations at the TAL1 locus: a Pediatric Oncology Group study. Blood. *81*, 2110–2117.

Bash, R.O., Hall, S., Timmons, C.F., Crist, W.M., Amylon, M., Smith, R.G., and Baer, R. (1995). Does activation of the TAL1 gene occur in a majority of patients with T-cell acute lymphoblastic leukemia? A pediatric oncology group study. Blood. *86*, 666–676.

Bassler, K., Schulte-Schrepping, J., Warnat-Herresthal, S., Aschenbrenner, A.C., and Schultze, J.L. (2019). The Myeloid Cell Compartment-Cell by Cell. Annu Rev Immunol. *37*, 269–293.

Beauvais, D.M., Jung, O., Yang, Y., Sanderson, R.D., and Rapraeger, A.C. (2016). Syndecan-1 (CD138) Suppresses Apoptosis in Multiple Myeloma by Activating IGF1 Receptor: Prevention by SynstatinIGF1R Inhibits Tumor Growth. Cancer Res. *76*, 4981–4993.

Behan, J.W., Yun, J.P., Proektor, M.P., Ehsanipour, E.A., Arutyunyan, A., Moses, A.S., Avramis, V.I., Louie, S.G., Butturini, A., Heisterkamp, N., et al. (2009). Adipocytes impair leukemia treatment in mice. Cancer Res. *69*, 7867–7874.

Belver, L., and Ferrando, A. (2016). The genetics and mechanisms of T cell acute lymphoblastic leukaemia. Nat Rev Cancer. *16*, 494–507.

Bernard, O.A., Busson-LeConiat, M., Ballerini, P., Mauchauffé, M., Valle, Della, V., Monni, R., Nguyen Khac, F., Mercher, T., Penard-Lacronique, V., Pasturaud, P., et al. (2001). A new recurrent and specific cryptic translocation, t(5;14)(q35;q32), is associated with expression of the Hox11L2 gene in T acute lymphoblastic leukemia. Leukemia. *15*, 1495–1504.

Berrazouane, S., Boisvert, M., Salti, S., Mourad, W., Al-Daccak, R., Barabé, F., and Aoudjit, F. (2019). Beta1 integrin blockade overcomes doxorubicin resistance in human T-cell acute lymphoblastic leukemia. Cell Death Dis. *10*, 357.

Binnewies, M., Mujal, A.M., Pollack, J.L., Combes, A.J., Hardison, E.A., Barry, K.C., Tsui, J., Ruhland, M.K., Kersten, K., Abushawish, M.A., et al. (2019). Unleashing Type-2 Dendritic Cells to Drive Protective Antitumor CD4+ T Cell Immunity. Cell. *177*, 556–571.e16.

Binnewies, M., Roberts, E.W., Kersten, K., Chan, V., Fearon, D.F., Merad, M., Coussens, L.M., Gabrilovich, D.I., Ostrand-Rosenberg, S., Hedrick, C.C., et al. (2018). Understanding the tumor immune microenvironment (TIME) for effective therapy. Nat Med. *24*, 541–550.

Biswas, S.K., and Mantovani, A. (2010). Macrophage plasticity and interaction with lymphocyte subsets: cancer as a paradigm. Nat Immunol. *11*, 889–896.

Bonapace, L., Coissieux, M.-M., Wyckoff, J., Mertz, K.D., Varga, Z., Junt, T., and Bentires-Alj, M. (2014). Cessation of CCL2 inhibition accelerates breast cancer metastasis by promoting angiogenesis. Nature. *515*, 130–133.

Borregaard, N., and Cowland, J.B. (1997). Granules of the human neutrophilic polymorphonuclear leukocyte. Blood. *89*, 3503–3521.

Boudil, A., Matei, I.R., Shih, H.-Y., Bogdanoski, G., Yuan, J.S., Chang, S.G., Montpellier, B., Kowalski, P.E., Voisin, V., Bashir, S., et al. (2015). IL-7 coordinates proliferation, differentiation and Tcra recombination during thymocyte β-selection. Nat Immunol. *16*, 397–405.

Brannon, A., Drouillard, D., Steele, N., Schoettle, S., Abel, E.V., Crawford, H.C., and Pasca di Magliano, M. (2020). Beta 1 integrin signaling mediates pancreatic ductal adenocarcinoma resistance to MEK inhibition. Sci Rep. *10*, 11133.

Bray, N.L., Pimentel, H., Melsted, P., and Pachter, L. (2016). Erratum: Near-optimal probabilistic RNA-seq quantification. Nat Biotechnol. *34*, 888.

Brinkmann, V., Reichard, U., Goosmann, C., Fauler, B., Uhlemann, Y., Weiss, D.S., Weinrauch, Y., and Zychlinsky, A. (2004). Neutrophil extracellular traps kill bacteria. Science. *303*, 1532–1535.

Bronte, V., Apolloni, E., Cabrelle, A., Ronca, R., Serafini, P., Zamboni, P., Restifo, N.P., and Zanovello, P. (2000). Identification of a CD11b(+)/Gr-1(+)/CD31(+) myeloid progenitor capable of activating or suppressing CD8(+) T cells. Blood. *96*, 3838–3846.

Broz, M.L., Binnewies, M., Boldajipour, B., Nelson, A.E., Pollack, J.L., Erle, D.J., Barczak, A., Rosenblum, M.D., Daud, A., Barber, D.L., et al. (2014). Dissecting the tumor myeloid compartment reveals rare activating antigen-presenting cells critical for T cell immunity. Cancer Cell. *26*, 638–652.

Bui, T., Rennhack, J., Mok, S., Ling, C., Perez, M., Roccamo, J., Andrechek, E.R., Moraes, C., and Muller, W.J. (2019). Functional Redundancy between β1 and β3 Integrin in Activating the IR/Akt/mTORC1 Signaling Axis to Promote ErbB2-Driven Breast Cancer. Cell Rep. *29*, 589–602.e6.

Buono, M., Facchini, R., Matsuoka, S., Thongjuea, S., Waithe, D., Luis, T.C., Giustacchini, A., Besmer, P., Mead, A.J., Jacobsen, S.E.W., et al. (2016). A dynamic niche provides Kit ligand in a stage-specific manner to the earliest thymocyte progenitors. Nat Cell Biol. *18*, 157–167.

Canli, Ö., Nicolas, A.M., Gupta, J., Finkelmeier, F., Goncharova, O., Pesic, M., Neumann, T., Horst, D., Löwer, M., Sahin, U., et al. (2017). Myeloid Cell-Derived Reactive Oxygen Species Induce Epithelial Mutagenesis. Cancer Cell. *32*, 869–883.e5.

Carey, D.J. (1997). Syndecans: multifunctional cell-surface co-receptors. Biochem J. *327 (Pt 1)*, 1–16.

Carroll, A.J., Crist, W.M., Link, M.P., Amylon, M.D., Pullen, D.J., Ragab, A.H., Buchanan, G.R., Wimmer, R.S., and Vietti, T.J. (1990). The t(1;14)(p34;q11) is nonrandom and restricted to T-cell acute lymphoblastic leukemia: a Pediatric Oncology Group study. Blood. *76*, 1220–1224.

Castillo, J.J., Reagan, J.L., Ingham, R.R., Furman, M., Dalia, S., Merhi, B., Nemr, S., Zarrabi, A., and Mitri, J. (2012). Obesity but not overweight increases the incidence and

mortality of leukemia in adults: a meta-analysis of prospective cohort studies. Leuk Res. *36*, 868–875.

Chapman, N.M., and Houtman, J.C.D. (2014). Functions of the FAK family kinases in T cells: beyond actin cytoskeletal rearrangement. Immunol Res. *59*, 23–34.

Chen, E.Y., Tan, C.M., Kou, Y., Duan, Q., Wang, Z., Meirelles, G.V., Clark, N.R., and Ma'ayan, A. (2013). Enrichr: interactive and collaborative HTML5 gene list enrichment analysis tool. BMC Bioinformatics. *14*, 128.

Chen, Q., Zhang, X.H.-F., and Massagué, J. (2011). Macrophage binding to receptor VCAM-1 transmits survival signals in breast cancer cells that invade the lungs. Cancer Cell. *20*, 538–549.

Chen, S.Y., Yang, X., Feng, W.L., Liao, J.F., Wang, L.N., Feng, L., Lin, Y.M., Ren, Q., and Zheng, G.G. (2015). Organ-Specific Microenvironment Modifies Diverse Functional and Phenotypic Characteristics of Leukemia-Associated Macrophages in Mouse T Cell Acute Lymphoblastic Leukemia. J Immunol. *194*, 2919–2929.

Chiarini, F., Grimaldi, C., Ricci, F., Tazzari, P.L., Evangelisti, C., Ognibene, A., Battistelli, M., Falcieri, E., Melchionda, F., Pession, A., et al. (2010). Activity of the novel dual phosphatidylinositol 3-kinase/mammalian target of rapamycin inhibitor NVP-BEZ235 against T-cell acute lymphoblastic leukemia. Cancer Res. *70*, 8097–8107.

Choi, Y.J., Li, X., Hydbring, P., Sanda, T., Stefano, J., Christie, A.L., Signoretti, S., Look, A.T., Kung, A.L., Boehmer, von, H., et al. (2012). The requirement for cyclin D function in tumor maintenance. Cancer Cell. *22*, 438–451.

Chow, A., Lucas, D., Hidalgo, A., Méndez-Ferrer, S., Hashimoto, D., Scheiermann, C., Battista, M., Leboeuf, M., Prophete, C., van Rooijen, N., et al. (2011). Bone marrow CD169+ macrophages promote the retention of hematopoietic stem and progenitor cells in the mesenchymal stem cell niche. J Exp Med. *208*, 261–271.

Clappier, E., Cuccuini, W., Kalota, A., Crinquette, A., Cayuela, J.M., Dik, W.A., Langerak, A.W., Montpellier, B., Nadel, B., Walrafen, P., et al. (2007). The C-MYB locus is involved in chromosomal translocation and genomic duplications in human T-cell acute leukemia (T-ALL), the translocation defining a new T-ALL subtype in very young children. Blood. *110*, 1251–1261.

Clappier, E., Gerby, B., Sigaux, F., Delord, M., Touzri, F., Hernandez, L., Ballerini, P., Baruchel, A., Pflumio, F., and Soulier, J. (2011). Clonal selection in xenografted human T cell acute lymphoblastic leukemia recapitulates gain of malignancy at relapse. J Exp Med. *208*, 653–661.

Cohen, A., Lee, J.W., and Gelfand, E.W. (1983). Selective toxicity of deoxyguanosine and arabinosyl guanine for T-leukemic cells. Blood. *61*, 660–666.

Coffelt, S.B., Tal, A.O., Scholz, A., De Palma, M., Patel, S., Urbich, C., Biswas, S.K., Murdoch, C., Plate, K.H., Reiss, Y., et al. (2010). Angiopoietin-2 regulates gene expression in TIE2-expressing monocytes and augments their inherent proangiogenic functions. Cancer Res. *70*, 5270–5280.

Condorelli, G.L., Facchiano, F., Valtieri, M., Proietti, E., Vitelli, L., Lulli, V., Huebner, K., Peschle, C., and Croce, C.M. (1996). T-cell-directed TAL-1 expression induces T-cell malignancies in transgenic mice. Cancer Res. *56*, 5113–5119.

Cooper, J., and Giancotti, F.G. (2019). Integrin Signaling in Cancer: Mechanotransduction, Stemness, Epithelial Plasticity, and Therapeutic Resistance. Cancer Cell. *35*, 347–367.

Cornell, R.F., and Palmer, J. (2012). Adult acute leukemia. Dis Mon. *58*, 219–238.

Coustan-Smith, E., Mullighan, C.G., Onciu, M., Behm, F.G., Raimondi, S.C., Pei, D., Cheng, C., Su, X., Rubnitz, J.E., Basso, G., et al. (2009). Early T-cell precursor leukaemia: a subtype of very high-risk acute lymphoblastic leukaemia. Lancet Oncol. *10*, 147–156.

Cox, O.T., O'Shea, S., Tresse, E., Bustamante-Garrido, M., Kiran-Deevi, R., and O'Connor, R. (2015). IGF-1 Receptor and Adhesion Signaling: An Important Axis in Determining Cancer Cell Phenotype and Therapy Resistance. Front Endocrinol (Lausanne). *6*, 106.

Crazzolara, R., Kreczy, A., Mann, G., Heitger, A., Eibl, G., Fink, F.M., Möhle, R., and Meister, B. (2001). High expression of the chemokine receptor CXCR4 predicts extramedullary organ infiltration in childhood acute lymphoblastic leukaemia. Br J Haematol. *115*, 545–553.

Curiel, T.J., Coukos, G., Zou, L., Alvarez, X., Cheng, P., Mottram, P., Evdemon-Hogan, M., Conejo-Garcia, J.R., Zhang, L., Burow, M., et al. (2004). Specific recruitment of regulatory T cells in ovarian carcinoma fosters immune privilege and predicts reduced survival. Nat Med. *10*, 942–949.

Czernielewski, J.M., and Demarchez, M. (1987). Further evidence for the self-reproducing capacity of Langerhans cells in human skin. J Invest Dermatol. *88*, 17–20.

Daley, J.M., Thomay, A.A., Connolly, M.D., Reichner, J.S., and Albina, J.E. (2008). Use of Ly6G-specific monoclonal antibody to deplete neutrophils in mice. J Leukoc Biol. *83*, 64–70.

David, A.R., and Zimmerman, M.R. (2010). Cancer: an old disease, a new disease or something in between? Nat Rev Cancer. *10*, 728–733.

Davies, L.C., Jenkins, S.J., Allen, J.E., and Taylor, P.R. (2013). Tissue-resident macrophages. Nat Immunol. *14*, 986–995.

Davis, A.S., Viera, A.J., and Mead, M.D. (2014). Leukemia: an overview for primary care. Am Fam Physician. *89*, 731–738.

De Keersmaecker, K., Lahortiga, I., Mentens, N., Folens, C., Van Neste, L., Bekaert, S., Vandenberghe, P., Odero, M.D., Marynen, P., and Cools, J. (2008). In vitro validation of gamma-secretase inhibitors alone or in combination with other anti-cancer drugs for the treatment of T-cell acute lymphoblastic leukemia. Haematologica. *93*, 533–542.

DeAngelo, D.J., Stone, R.M., Silverman, L.B., Stock, W., Attar, E.C., Fearen, I., Dallob, A., Matthews, C., Stone, J., Freedman, S.J., et al. (2006). A phase I clinical trial of the notch inhibitor MK-0752 in patients with T-cell acute lymphoblastic leukemia/lymphoma (T-ALL) and other leukemias. J Clin Oncol. *24*, 6585–6585.

Degryse, S., de Bock, C.E., Cox, L., Demeyer, S., Gielen, O., Mentens, N., Jacobs, K., Geerdens, E., Gianfelici, V., Hulselmans, G., et al. (2014). JAK3 mutants transform hematopoietic cells through JAK1 activation, causing T-cell acute lymphoblastic leukemia in a mouse model. Blood. *124*, 3092–3100.

Degryse, S., de Bock, C.E., Demeyer, S., Govaerts, I., Bornschein, S., Verbeke, D., Jacobs, K., Binos, S., Skerrett-Byrne, D.A., Murray, H.C., et al. (2018). Mutant JAK3 phosphoproteomic profiling predicts synergism between JAK3 inhibitors and MEK/BCL2 inhibitors for the treatment of T-cell acute lymphoblastic leukemia. Leukemia. *32*, 788–800.

DeNardo, D.G., Barreto, J.B., Andreu, P., Vasquez, L., Tawfik, D., Kolhatkar, N., and Coussens, L.M. (2009). CD4(+) T cells regulate pulmonary metastasis of mammary carcinomas by enhancing protumor properties of macrophages. Cancer Cell. *16*, 91–102.

Dimri, G., Band, H., and Band, V. (2005). Mammary epithelial cell transformation: insights from cell culture and mouse models. Breast Cancer Res. *7*, 171–179.

Ding, T., Xu, J., Wang, F., Shi, M., Zhang, Y., Li, S.-P., and Zheng, L. (2009). High tumor-infiltrating macrophage density predicts poor prognosis in patients with primary hepatocellular carcinoma after resection. Hum Pathol. *40*, 381–389.

Divisi, D., Di Tommaso, S., Salvemini, S., Garramone, M., and Crisci, R. (2006). Diet and cancer. Acta Biomed. *77*, 118–123.

Dong, P., Ma, L., Liu, L., Zhao, G., Zhang, S., Dong, L., Xue, R., and Chen, S. (2016). $CD86^+/CD206^+$, Diametrically Polarized Tumor-Associated Macrophages, Predict Hepatocellular Carcinoma Patient Prognosis. Int J Mol Sci. *17*, 320.

Dudziak, D., Kamphorst, A.O., Heidkamp, G.F., Buchholz, V.R., Trumpfheller, C., Yamazaki, S., Cheong, C., Liu, K., Lee, H.-W., Park, C.G., et al. (2007). Differential antigen processing by dendritic cell subsets in vivo. Science. *315*, 107–111.

Duffield, J.S., Forbes, S.J., Constandinou, C.M., Clay, S., Partolina, M., Vuthoori, S., Wu, S., Lang, R., and Iredale, J.P. (2005). Selective depletion of macrophages reveals distinct, opposing roles during liver injury and repair. J Clin Invest. *115*, 56–65.

Dumitru, C.A., Moses, K., Trellakis, S., Lang, S., and Brandau, S. (2012). Neutrophils and granulocytic myeloid-derived suppressor cells: immunophenotyping, cell biology and clinical relevance in human oncology. Cancer Immunol Immunother. *61*, 1155–1167.

Dustin, M.L., Staunton, D.E., and Springer, T.A. (1988). Supergene families meet in the immune system. Immunol Today. *9*, 213–215.

Edwards, D.K., Watanabe-Smith, K., Rofelty, A., Damnernsawad, A., Laderas, T., Lamble, A., Lind, E.F., Kaempf, A., Mori, M., Rosenberg, M., et al. (2019). CSF1R inhibitors exhibit antitumor activity in acute myeloid leukemia by blocking paracrine signals from support cells. Blood. *133*, 588–599.

Egeblad, M., Nakasone, E.S., and Werb, Z. (2010). Tumors as Organs: Complex Tissues that Interface with the Entire Organism. Dev Cell. *18*, 884–901.

Ehsanipour, E.A., Sheng, X., Behan, J.W., Wang, X., Butturini, A., Avramis, V.I., and Mittelman, S.D. (2013). Adipocytes cause leukemia cell resistance to L-asparaginase via release of glutamine. Cancer Res. *73*, 2998–3006.

Elenitoba-Johnson, K.S.J., and Lim, M.S. (2018). New Insights into Lymphoma Pathogenesis. Annu Rev Pathol. *13*, 193–217.

Ellisen, L.W., Bird, J., West, D.C., Soreng, A.L., Reynolds, T.C., Smith, S.D., and Sklar, J. (1991). TAN-1, the human homolog of the Drosophila notch gene, is broken by chromosomal translocations in T lymphoblastic neoplasms. Cell. *66*, 649–661.

Engblom, C., Pfirschke, C., and Pittet, M.J. (2016). The role of myeloid cells in cancer therapies. Nat Rev Cancer. *16*, 447–462.

Epelman, S., Lavine, K.J., and Randolph, G.J. (2014). Origin and functions of tissue macrophages. Immunity. *41*, 21–35.

Fattizzo, B., Rosa, J., Giannotta, J.A., Baldini, L., and Fracchiolla, N.S. (2020). The Physiopathology of T- Cell Acute Lymphoblastic Leukemia: Focus on Molecular Aspects. Front Oncol. *10*, 273.

Ferrando, A. (2018). Can one target T-cell ALL? Best Pract Res Clin Haematol. *31*, 361–366.

Ferrando, A.A., Neuberg, D.S., Staunton, J., Loh, M.L., Huard, C., Raimondi, S.C., Behm, F.G., Pui, C.-H., Downing, J.R., Gilliland, D.G., et al. (2002). Gene expression signatures define novel oncogenic pathways in T cell acute lymphoblastic leukemia. Cancer Cell. *1*, 75–87.

Folkman, J. (2002). Role of angiogenesis in tumor growth and metastasis. Semin Oncol. *29*, 15–18.

Frenette, P.S., Subbarao, S., Mazo, I.B., Andrian, von, U.H., and Wagner, D.D. (1998). Endothelial selectins and vascular cell adhesion molecule-1 promote hematopoietic progenitor homing to bone marrow. Proc Natl Acad Sci U S A. *95*, 14423–14428.

Fridlender, Z.G., Sun, J., Kim, S., Kapoor, V., Cheng, G., Ling, L., Worthen, G.S., and Albelda, S.M. (2009). Polarization of tumor-associated neutrophil phenotype by TGF-beta: "N1" versus “N2” TAN. Cancer Cell. *16*, 183–194.

Fukumura, D., Xavier, R., Sugiura, T., Chen, Y., Park, E.C., Lu, N., Selig, M., Nielsen, G., Taksir, T., Jain, R.K., et al. (1998). Tumor induction of VEGF promoter activity in stromal cells. Cell. *94*, 715–725.

Gachet, S., Genescà, E., Passaro, D., Irigoyen, M., Alcalde, H., Clémenson, C., Poglio, S., Pflumio, F., Janin, A., Lasgi, C., et al. (2013). Leukemia-initiating cell activity requires calcineurin in T-cell acute lymphoblastic leukemia. Leukemia. *27*, 2289–2300.

Galletti, G., Scielzo, C., Barbaglio, F., Rodriguez, T.V., Riba, M., Lazarevic, D., Cittaro, D., Simonetti, G., Ranghetti, P., Scarfò, L., et al. (2016). Targeting Macrophages Sensitizes Chronic Lymphocytic Leukemia to Apoptosis and Inhibits Disease Progression. Cell Rep. *14*, 1748–1760.

Gao, Y., Nish, S.A., Jiang, R., Hou, L., Licona-Limón, P., Weinstein, J.S., Zhao, H., and Medzhitov, R. (2013). Control of T helper 2 responses by transcription factor IRF4-dependent dendritic cells. Immunity. *39*, 722–732.

García-Román, J., and Zentella-Dehesa, A. (2013). Vascular permeability changes involved in tumor metastasis. Cancer Lett. *335*, 259–269.

Garçon, F., Patton, D.T., Emery, J.L., Hirsch, E., Rottapel, R., Sasaki, T., and Okkenhaug, K. (2008). CD28 provides T-cell costimulation and enhances PI3K activity at the immune

synapse independently of its capacity to interact with the p85/p110 heterodimer. Blood. *111*, 1464–1471.

Garg, M. (2016). Epithelial plasticity in urothelial carcinoma: Current advancements and future challenges. World J Stem Cells. *8*, 260–267.

Gehring, S., Dickson, E.M., San Martin, M.E., van Rooijen, N., Papa, E.F., Harty, M.W., Tracy, T.F., and Gregory, S.H. (2006). Kupffer cells abrogate cholestatic liver injury in mice. Gastroenterology. *130*, 810–822.

Geissmann, F., Jung, S., and Littman, D.R. (2003). Blood monocytes consist of two principal subsets with distinct migratory properties. Immunity. *19*, 71–82.

Georgoudaki, A.-M., Prokopec, K.E., Boura, V.F., Hellqvist, E., Sohn, S., Östling, J., Dahan, R., Harris, R.A., Rantalainen, M., Klevebring, D., et al. (2016). Reprogramming Tumor-Associated Macrophages by Antibody Targeting Inhibits Cancer Progression and Metastasis. Cell Rep. *15*, 2000–2011.

Ghezzo, M.N., Fernandes, M.T., Pacheco-Leyva, I., Rodrigues, P.M., Machado, R.S., Araújo, M.A.S., Kalathur, R.K., Futschik, M.E., Alves, N.L., and Santos, Dos, N.R. (2018). FoxN1-dependent thymic epithelial cells promote T-cell leukemia development. Carcinogenesis. *39*, 1463–1476.

Giancotti, F.G. (2000). Complexity and specificity of integrin signalling. Nat Cell Biol. *2*, E13–E14.

Giancotti, F.G., and Tarone, G. (2003). Positional control of cell fate through joint integrin/receptor protein kinase signaling. Annu Rev Cell Dev Biol. *19*, 173–206.

Ginhoux, F., Greter, M., Leboeuf, M., Nandi, S., See, P., Gokhan, S., Mehler, M.F., Conway, S.J., Ng, L.G., Stanley, E.R., et al. (2010). Fate mapping analysis reveals that adult microglia derive from primitive macrophages. Science. *330*, 841–845.

Girardi, T., Vicente, C., Cools, J., and De Keersmaecker, K. (2017). The genetics and molecular biology of T-ALL. Blood. *129*, 1113–1123.

Goldman, C.K., Kendall, R.L., Cabrera, G., Soroceanu, L., Heike, Y., Gillespie, G.Y., Siegal, G.P., Mao, X., Bett, A.J., Huckle, W.R., et al. (1998). Paracrine expression of a native soluble vascular endothelial growth factor receptor inhibits tumor growth, metastasis, and mortality rate. Proc Natl Acad Sci U S A. *95*, 8795–8800.

Golubovskaya, V.M. (2010). Focal adhesion kinase as a cancer therapy target. Anticancer Agents Med Chem. *10*, 735–741.

Greaves, M.F., Janossy, G., Peto, J., and Kay, H. (1981). Immunologically defined subclasses of acute lymphoblastic leukaemia in children: their relationship to presentation features and prognosis. Br J Haematol. *48*, 179–197.

Guilliams, M., and van de Laar, L. (2015). A Hitchhiker's Guide to Myeloid Cell Subsets: Practical Implementation of a Novel Mononuclear Phagocyte Classification System. Front Immunol. *6*, 406.

Guilliams, M., Dutertre, C.-A., Scott, C.L., McGovern, N., Sichien, D., Chakarov, S., Van Gassen, S., Chen, J., Poidinger, M., De Prijck, S., et al. (2016). Unsupervised High-Dimensional Analysis Aligns Dendritic Cells across Tissues and Species. Immunity. *45*, 669–684.

Guilliams, M., Mildner, A., and Yona, S. (2018). Developmental and Functional Heterogeneity of Monocytes. Immunity. *49*, 595–613.

Gusscott, S., Jenkins, C.E., Lam, S.H., Giambra, V., Pollak, M., and Weng, A.P. (2016). IGF1R Derived PI3K/AKT Signaling Maintains Growth in a Subset of Human T-Cell Acute Lymphoblastic Leukemias. PLoS One. *11*, e0161158.

Guth, A.M., Hafeman, S.D., and Dow, S.W. (2012). Depletion of phagocytic myeloid cells triggers spontaneous T cell- and NK cell-dependent antitumor activity. Oncoimmunology. *1*, 1248–1257.

Hacein-Bey-Abina, S., Kalle, Von, C., Schmidt, M., McCormack, M.P., Wulffraat, N., Leboulch, P., Lim, A., Osborne, C.S., Pawliuk, R., Morillon, E., et al. (2003). LMO2-associated clonal T cell proliferation in two patients after gene therapy for SCID-X1. Science. *302*, 415–419.

Hacein-Bey-Abina, S., Garrigue, A., Wang, G.P., Soulier, J., Lim, A., Morillon, E., Clappier, E., Caccavelli, L., Delabesse, E., Beldjord, K., et al. (2008). Insertional oncogenesis in 4 patients after retrovirus-mediated gene therapy of SCID-X1. J Clin Invest. *118*, 3132–3142.

Hanna, R.N., Carlin, L.M., Hubbeling, H.G., Nackiewicz, D., Green, A.M., Punt, J.A., Geissmann, F., and Hedrick, C.C. (2011). The transcription factor NR4A1 (Nur77) controls bone marrow differentiation and the survival of Ly6C- monocytes. Nat Immunol. *12*, 778–785.

Hanna, R.N., Cekic, C., Sag, D., Tacke, R., Thomas, G.D., Nowyhed, H., Herrley, E., Rasquinha, N., McArdle, S., Wu, R., et al. (2015). Patrolling monocytes control tumor metastasis to the lung. Science. *350*, 985–990.

Hao, Z., and Rajewsky, K. (2001). Homeostasis of peripheral B cells in the absence of B cell influx from the bone marrow. J Exp Med. *194*, 1151–1164.

Hardonk, M.J., Dijkhuis, F.W., Hulstaert, C.E., and Koudstaal, J. (1992). Heterogeneity of rat liver and spleen macrophages in gadolinium chloride-induced elimination and repopulation. J Leukoc Biol. *52*, 296–302.

Hashimoto, D., Chow, A., Noizat, C., Teo, P., Beasley, M.B., Leboeuf, M., Becker, C.D., See, P., Price, J., Lucas, D., et al. (2013). Tissue-resident macrophages self-maintain locally throughout adult life with minimal contribution from circulating monocytes. Immunity. *38*, 792–804.

Hatano, M., Roberts, C.W., Minden, M., Crist, W.M., and Korsmeyer, S.J. (1991). Deregulation of a homeobox gene, HOX11, by the t(10;14) in T cell leukemia. Science. *253*, 79–82.

Headley, M.B., Bins, A., Nip, A., Roberts, E.W., Looney, M.R., Gerard, A., and Krummel, M.F. (2016). Visualization of immediate immune responses to pioneer metastatic cells in the lung. Nature. *531*, 513–517.

Hebert, J., Cayuela, J.M., Berkeley, J., and Sigaux, F. (1994). Candidate tumor-suppressor genes MTS1 (p16INK4A) and MTS2 (p15INK4B) display frequent homozygous deletions in primary cells from T- but not from B-cell lineage acute lymphoblastic leukemias. Blood. *84*, 4038–4044.

Hefazi, M., and Litzow, M.R. (2018). Recent Advances in the Biology and Treatment of T Cell Acute Lymphoblastic Leukemia. Curr Hematol Malig Rep. *13*, 265–274.

Hiasa, M., Abe, M., Nakano, A., Oda, A., Amou, H., Kido, S., Takeuchi, K., Kagawa, K., Yata, K., Hashimoto, T., et al. (2009). GM-CSF and IL-4 induce dendritic cell differentiation and disrupt osteoclastogenesis through M-CSF receptor shedding by up-regulation of TNF-alpha converting enzyme (TACE). Blood. *114*, 4517–4526.

Hida, K., Maishi, N., Annan, D.A., and Hida, Y. (2018). Contribution of Tumor Endothelial Cells in Cancer Progression. Int J Mol Sci. *19*, 1272.

Hildner, K., Edelson, B.T., and Murphy, K.M. (2008). *Batf3 Deficiency Reveals a Critical Role for CD8α+ Dendritic Cells in Cytotoxic T Cell Immunity*. Science. *322*, 1097–1100.

Hinshaw, D.C., and Shevde, L.A. (2019). The Tumor Microenvironment Innately Modulates Cancer Progression. Cancer Res. *79*, 4557–4566.

Hlatky, L., Tsionou, C., Hahnfeldt, P., and Coleman, C.N. (1994). Mammary fibroblasts may influence breast tumor angiogenesis via hypoxia-induced vascular endothelial growth factor up-regulation and protein expression. Cancer Res. *54*, 6083–6086.

Hoeffel, G., Wang, Y., Greter, M., See, P., Teo, P., Malleret, B., Leboeuf, M., Low, D., Oller, G., Almeida, F., et al. (2012). Adult Langerhans cells derive predominantly from embryonic fetal liver monocytes with a minor contribution of yolk sac-derived macrophages. J Exp Med. *209*, 1167–1181.

Homminga, I., Pieters, R., Langerak, A.W., de Rooi, J.J., Stubbs, A., Verstegen, M., Vuerhard, M., Buijs-Gladdines, J., Kooi, C., Klous, P., et al. (2011). Integrated transcript and genome analyses reveal NKX2-1 and MEF2C as potential oncogenes in T cell acute lymphoblastic leukemia. Cancer Cell. *19*, 484–497.

Housa, D., Housová, J., Vernerová, Z., and Haluzík, M. (2006). Adipocytokines and cancer. Physiol Res. *55*, 233–244.

Hume, D.A., and MacDonald, K.P.A. (2012). Therapeutic applications of macrophage colony-stimulating factor-1 (CSF-1) and antagonists of CSF-1 receptor (CSF-1R) signaling. Blood. *119*, 1810–1820.

Humphries, J.D., Byron, A., and Humphries, M.J. (2006). Integrin ligands at a glance. J Cell Sci. *119*, 3901–3903.

Hunger, S.P., and Mullighan, C.G. (2015). Acute Lymphoblastic Leukemia in Children. N Engl J Med. *373*, 1541–1552.

Hunger, S.P., Lu, X., Devidas, M., Camitta, B.M., Gaynon, P.S., Winick, N.J., Reaman, G.H., and Carroll, W.L. (2012). Improved survival for children and adolescents with acute lymphoblastic leukemia between 1990 and 2005: a report from the children's oncology group. J Clin Oncol. *30*, 1663–1669.

Hurwitz, C.A., Silverman, L.B., Schorin, M.A., Clavell, L.A., Dalton, V.K., Glick, K.M., Gelber, R.D., and Sallan, S.E. (2000). Substituting dexamethasone for prednisone complicates remission induction in children with acute lymphoblastic leukemia. Cancer. *88*, 1964–1969.

Huveneers, S., and Danen, E.H.J. (2009). Adhesion signaling - crosstalk between integrins, Src and Rho. J Cell Sci. *122*, 1059–1069.

Ikawa, T., Kawamoto, H., Goldrath, A.W., and Murre, C. (2006). E proteins and Notch signaling cooperate to promote T cell lineage specification and commitment. J Exp Med. *203*, 1329–1342.

Italiani, P., and Boraschi, D. (2014). From Monocytes to M1/M2 Macrophages: Phenotypical vs. Functional Differentiation. Front Immunol. *5*, 514.

Ito, C., Evans, W.E., McNinch, L., Coustan-Smith, E., Mahmoud, H., Pui, C.H., and Campana, D. (1996). Comparative cytotoxicity of dexamethasone and prednisolone in childhood acute lymphoblastic leukemia. J Clin Oncol. *14*, 2370–2376.

Ivetic, A., Hoskins Green, H.L., and Hart, S.J. (2019). L-selectin: A Major Regulator of Leukocyte Adhesion, Migration and Signaling. Front Immunol. *10*, 1068.

Iyer, N.S., Balsamo, L.M., Bracken, M.B., and Kadan-Lottick, N.S. (2015). Chemotherapy-only treatment effects on long-term neurocognitive functioning in childhood ALL survivors: a review and meta-analysis. Blood. *126*, 346–353.

Jaiswal, S., Jamieson, C.H.M., Pang, W.W., Park, C.Y., Chao, M.P., Majeti, R., Traver, D., van Rooijen, N., and Weissman, I.L. (2009). CD47 is upregulated on circulating hematopoietic stem cells and leukemia cells to avoid phagocytosis. Cell. *138*, 271–285.

Jakubzick, C.V., Randolph, G.J., and Henson, P.M. (2017). Monocyte differentiation and antigen-presenting functions. Nat Rev Immunol. *17*, 349–362.

Jeong, H., Hwang, I., Kang, S.H., Shin, H.C., and Kwon, S.Y. (2019). Tumor-Associated Macrophages as Potential Prognostic Biomarkers of Invasive Breast Cancer. J Breast Cancer. *22*, 38–51.

Jiang, H., Hegde, S., Knolhoff, B.L., Zhu, Y., Herndon, J.M., Meyer, M.A., Nywening, T.M., Hawkins, W.G., Shapiro, I.M., Weaver, D.T., et al. (2016). Targeting focal adhesion kinase renders pancreatic cancers responsive to checkpoint immunotherapy. Nat Med. *22*, 851–860.

Jiang, L., Jiang, S., Situ, D., Lin, Y., Yang, H., Li, Y., Long, H., and Zhou, Z. (2015). Prognostic value of monocyte and neutrophils to lymphocytes ratio in patients with metastatic soft tissue sarcoma. Oncotarget. *6*, 9542–9550.

Jung, K., Heishi, T., Khan, O.F., Kowalski, P.S., Incio, J., Rahbari, N.N., Chung, E., Clark, J.W., Willett, C.G., Luster, A.D., et al. (2017). Ly6Clo monocytes drive immunosuppression and confer resistance to anti-VEGFR2 cancer therapy. J Clin Invest. *127*, 3039–3051.

Kadia, T.M., and Gandhi, V. (2017). Nelarabine in the treatment of pediatric and adult patients with T-cell acute lymphoblastic leukemia and lymphoma. Expert Rev Hematol. *10*, 1–8.

Kapellos, T.S., Bonaguro, L., Gemünd, I., Reusch, N., Saglam, A., Hinkley, E.R., and Schultze, J.L. (2019). Human Monocyte Subsets and Phenotypes in Major Chronic Inflammatory Diseases. Front Immunol. *10*, 2035.

Karrman, K., and Johansson, B. (2017). Pediatric T-cell acute lymphoblastic leukemia. Genes Chromosomes Cancer. *56*, 89–116.

Khan, N., Afaq, F., and Mukhtar, H. (2010). Lifestyle as risk factor for cancer: Evidence from human studies. Cancer Lett. *293*, 133–143.

Kiely, P.A., Sant, A., and O'Connor, R. (2002). RACK1 is an insulin-like growth factor 1 (IGF-1) receptor-interacting protein that can regulate IGF-1-mediated Akt activation and protection from cell death. J Biol Chem. *277*, 22581–22589.

Kikuchi, A., Hayashi, Y., Kobayashi, S., Hanada, R., Moriwaki, K., Yamamoto, K., Fujimoto, J., Kaneko, Y., and Yamamori, S. (1993). Clinical significance of TAL1 gene alteration in childhood T-cell acute lymphoblastic leukemia and lymphoma. Leukemia. *7*, 933–938.

Kim, K.J., Li, B., Winer, J., Armanini, M., Gillett, N., Phillips, H.S., and Ferrara, N. (1993). Inhibition of vascular endothelial growth factor-induced angiogenesis suppresses tumour growth in vivo. Nature. *362*, 841–844.

Krishnaswamy, J.K., Gowthaman, U., Zhang, B., Mattsson, J., Szeponik, L., Liu, D., Wu, R., White, T., Calabro, S., Xu, L., et al. (2017). Migratory CD11b+ conventional dendritic cells induce T follicular helper cell-dependent antibody responses. Sci Immunol. *2*, eaam9169.

Kuang, D.-M., Zhao, Q., Peng, C., Xu, J., Zhang, J.-P., Wu, C., and Zheng, L. (2009). Activated monocytes in peritumoral stroma of hepatocellular carcinoma foster immune privilege and disease progression through PD-L1. J Exp Med. *206*, 1327–1337.

Kuleshov, M.V., Jones, M.R., Rouillard, A.D., Fernandez, N.F., Duan, Q., Wang, Z., Koplev, S., Jenkins, S.L., Jagodnik, K.M., Lachmann, A., et al. (2016). Enrichr: a comprehensive gene set enrichment analysis web server 2016 update. Nucleic Acids Res. *44*, W90–W97.

Kumar, S.K., Rajkumar, V., Kyle, R.A., van Duin, M., Sonneveld, P., Mateos, M.-V., Gay, F., and Anderson, K.C. (2017). Multiple myeloma. Nat Rev Dis Primers. *3*, 17046.

Kwon, M.-J., Jang, B., Yi, J.Y., Han, I.-O., and Oh, E.S. (2012). Syndecans play dual roles as cell adhesion receptors and docking receptors. FEBS Lett. *586*, 2207–2211.

Lacey, D.C., Achuthan, A., Fleetwood, A.J., Dinh, H., Roiniotis, J., Scholz, G.M., Chang, M.W., Beckman, S.K., Cook, A.D., and Hamilton, J.A. (2012). Defining GM-CSF- and

macrophage-CSF-dependent macrophage responses by in vitro models. J Immunol. *188*, 5752–5765.

Lagresle, C., Gardie, B., Eyquem, S., Fasseu, M., Vieville, J.-C., Pla, M., Sigaux, F., and Bories, J.-C. (2002). Transgenic Expression of the p16INK4a Cyclin-Dependent Kinase Inhibitor Leads to Enhanced Apoptosis and Differentiation Arrest of CD4−CD8− Immature Thymocytes. J Immunol. *168*, 2325–2331.

Lancaster, J.N., Li, Y., and Ehrlich, L.I.R. (2018). Chemokine-Mediated Choreography of Thymocyte Development and Selection. Trends Immunol. *39*, 86–98.

Lanthier, N., Horsmans, Y., and Leclercq, I.A. (2010). Clodronate liposomes: all sites of injection are not equal. Hepatology. *51*, 721–722–author reply 722.

Lavin, Y., Kobayashi, S., Leader, A., Amir, E.-A.D., Elefant, N., Bigenwald, C., Remark, R., Sweeney, R., Becker, C.D., Levine, J.H., et al. (2017). Innate Immune Landscape in Early Lung Adenocarcinoma by Paired Single-Cell Analyses. Cell. *169*, 750–765.e17.

Lavin, Y., Winter, D., Blecher-Gonen, R., David, E., Keren-Shaul, H., Merad, M., Jung, S., and Amit, I. (2014). Tissue-resident macrophage enhancer landscapes are shaped by the local microenvironment. Cell. *159*, 1312–1326.

LeBleu, V.S., Taduri, G., O'Connell, J., Teng, Y., Cooke, V.G., Woda, C., Sugimoto, H., and Kalluri, R. (2013). Origin and function of myofibroblasts in kidney fibrosis. Nat Med. *19*, 1047–1053.

Lee, C.-H., Romain, G., Yan, W., Watanabe, M., Charab, W., Todorova, B., Lee, J., Triplett, K., Donkor, M., Lungu, O.I., et al. (2017). IgG Fc domains that bind C1q but not effector Fcγ receptors delineate the importance of complement-mediated effector functions. Nat Immunol. *18*, 889–898.

Lee, J.C., Chow, N.H., Wang, S.T., and Huang, S.M. (2000). Prognostic value of vascular endothelial growth factor expression in colorectal cancer patients. Eur J Cancer. *36*, 748–753.

Li, J.-J., and Xie, D. (2015). RACK1, a versatile hub in cancer. Oncogene. *34*, 1890–1898.

Li, M., Hou, F., Zhao, J., Zhang, T., Li, D., Wu, W., Liu, X., and Xu, L. (2018). Focal adhesion kinase is overexpressed in thymic epithelial tumors and may serve as an independent prognostic biomarker. Oncol Lett. *15*, 3001–3007.

Li, X., Yao, W., Yuan, Y., Chen, P., Li, B., Li, J., Chu, R., Song, H., Xie, D., Jiang, X., et al. (2017). Targeting of tumour-infiltrating macrophages via CCL2/CCR2 signalling as a therapeutic strategy against hepatocellular carcinoma. Gut. *66*, 157–167.

Lin, E.Y., and Pollard, J.W. (2007). Tumor-associated macrophages press the angiogenic switch in breast cancer. Cancer Res. *67*, 5064–5066.

Lind, E.F., Prockop, S.E., Porritt, H.E., and Petrie, H.T. (2001). Mapping Precursor Movement through the Postnatal Thymus Reveals Specific Microenvironments Supporting Defined Stages of Early Lymphoid Development. J Exp Med. *194*, 127–134.

Link, A., Vogt, T.K., Favre, S., Britschgi, M.R., Acha-Orbea, H., Hinz, B., Cyster, J.G., and Luther, S.A. (2007). Fibroblastic reticular cells in lymph nodes regulate the homeostasis of naive T cells. Nat Immunol. *8*, 1255–1265.

Liu, H., Zhang, H., Shen, Z., Lin, C., Wang, X., Qin, J., Qin, X., Xu, J., and Sun, Y. (2016). Increased Expression of CSF-1 Associates With Poor Prognosis of Patients With Gastric Cancer Undergoing Gastrectomy. Medicine (Baltimore). *95*, e2675.

Liu, W., Bloom, D.A., Cance, W.G., Kurenova, E.V., Golubovskaya, V.M., and Hochwald, S.N. (2008). FAK and IGF-IR interact to provide survival signals in human pancreatic adenocarcinoma cells. Carcinogenesis. *29*, 1096–1107.

Liu, Y., Easton, J., Shao, Y., Maciaszek, J., Wang, Z., Wilkinson, M.R., McCastlain, K., Edmonson, M., Pounds, S.B., Shi, L., et al. (2017). The genomic landscape of pediatric and young adult T-lineage acute lymphoblastic leukemia. Nat Genet. *49*, 1211–1218.

Love, M.I., Huber, W., and Anders, S. (2014). Moderated estimation of fold change and dispersion for RNA-seq data with DESeq2. Genome Biol. *15*, 550.

Loyher, P.-L., Hamon, P., Laviron, M., Meghraoui-Kheddar, A., Goncalves, E., Deng, Z., Torstensson, S., Bercovici, N., Baudesson de Chanville, C., Combadière, B., et al. (2018). Macrophages of distinct origins contribute to tumor development in the lung. J Exp Med. *215*, 2536–2553.

Lu, P., Weaver, V.M., and Werb, Z. (2012). The extracellular matrix: a dynamic niche in cancer progression. J Cell Biol. *196*, 395–406.

Lu, Z., Xie, J., Wu, G., Shen, J., Collins, R., Chen, W., Kang, X., Luo, M., Zou, Y., Huang, L.J.-S., et al. (2017). Fasting selectively blocks development of acute lymphoblastic leukemia via leptin-receptor upregulation. Nat Med. *23*, 79–90.

Luo, Y., Zhou, H., Krueger, J., Kaplan, C., Lee, S.-H., Dolman, C., Markowitz, D., Wu, W., Liu, C., Reisfeld, R.A., et al. (2006). Targeting tumor-associated macrophages as a novel strategy against breast cancer. J Clin Invest. *116*, 2132–2141.

Luskin, M.R., Ganetsky, A., Landsburg, D.J., Loren, A.W., Porter, D.L., Nasta, S.D., Svoboda, J., Luger, S.M., and Frey, N.V. (2016). Nelarabine, cyclosphosphamide and

etoposide for adults with relapsed T-cell acute lymphoblastic leukaemia and lymphoma. Br J Haematol. *174*, 332–334.

Lyu, A., Triplett, T.A., Nam, S.H., Hu, Z., Arasappan, D., Godfrey, W.H., Ames, R.Y., Sarang, A., Selden, H.J., Lee, C.-H., et al. (2020). Tumor-associated myeloid cells provide critical support for T-ALL. Blood. *136*, 1837–1850.

Ma, R.-Y., Zhang, H., Li, X.-F., Zhang, C.-B., Selli, C., Tagliavini, G., Lam, A.D., Prost, S., Sims, A.H., Hu, H.-Y., et al. (2020). Monocyte-derived macrophages promote breast cancer bone metastasis outgrowth. J Exp Med. *217*, 2315.

Majeti, R., Chao, M.P., Alizadeh, A.A., Pang, W.W., Jaiswal, S., Gibbs, K.D., van Rooijen, N., and Weissman, I.L. (2009). CD47 is an adverse prognostic factor and therapeutic antibody target on human acute myeloid leukemia stem cells. Cell. *138*, 286–299.

Mak, T.W. (2006). The Immune Response (Elsevier).

Malone, A., and Smith, O.P. (2017). Nelarabine toxicity in children and adolescents with relapsed/refractory T-ALL/T-LBL: can we avoid throwing the baby out with the bathwater? Br J Haematol. *179*, 179–181.

Mantovani, A., Sozzani, S., Locati, M., Allavena, P., and Sica, A. (2002). Macrophage polarization: tumor-associated macrophages as a paradigm for polarized M2 mononuclear phagocytes. Trends Immunol. *23*, 549–555.

Maude, S.L., Dolai, S., Delgado-Martin, C., Vincent, T., Robbins, A., Selvanathan, A., Ryan, T., Hall, J., Wood, A.C., Tasian, S.K., et al. (2015). Efficacy of JAK/STAT pathway inhibition in murine xenograft models of early T-cell precursor (ETP) acute lymphoblastic leukemia. Blood. *125*, 1759–1767.

McGuire, E.A., Hockett, R.D., Pollock, K.M., Bartholdi, M.F., O'Brien, S.J., and Korsmeyer, S.J. (1989). The t(11;14)(p15;q11) in a T-cell acute lymphoblastic leukemia cell line activates multiple transcripts, including Ttg-1, a gene encoding a potential zinc finger protein. Mol Cell Biol. *9*, 2124–2132.

McKenna, H.J., Stocking, K.L., and Peschon, J.J. (2000). Mice lacking flt3 ligand have deficient hematopoiesis affecting hematopoietic progenitor cells, dendritic cells, and natural killer cells. Blood. *95*, 3489–3497.

McMahon, C.M., and Luger, S.M. (2019). Relapsed T Cell ALL: Current Approaches and New Directions. Curr Hematol Malig Rep. *14*, 83–93.

Medyouf, H., Alcalde, H., Berthier, C., Guillemin, M.C., Santos, Dos, N.R., Janin, A., Decaudin, D., de Thé, H., and Ghysdael, J. (2007). Targeting calcineurin activation as a therapeutic strategy for T-cell acute lymphoblastic leukemia. Nat Med. *13*, 736–741.

Medyouf, H., Gusscott, S., Wang, H., Tseng, J.-C., Wai, C., Nemirovsky, O., Trumpp, A., Pflumio, F., Carboni, J., Gottardis, M., et al. (2011). High-level IGF1R expression is required for leukemia-initiating cell activity in T-ALL and is supported by Notch signaling. J Exp Med. *208*, 1809–1822.

Mellentin, J.D., Smith, S.D., and Cleary, M.L. (1989). lyl-1, a novel gene altered by chromosomal translocation in T cell leukemia, codes for a protein with a helix-loop-helix DNA binding motif. Cell. *58*, 77–83.

Mendes, R.D., Sarmento, L.M., Canté-Barrett, K., Zuurbier, L., Buijs-Gladdines, J.G.C.A.M., Póvoa, V., Smits, W.K., Abecasis, M., Yunes, J.A., Sonneveld, E., et al. (2014). PTEN microdeletions in T-cell acute lymphoblastic leukemia are caused by illegitimate RAG-mediated recombination events. Blood. *124*, 567–578.

Merad, M., Sathe, P., Helft, J., Miller, J., and Mortha, A. (2013). The dendritic cell lineage: ontogeny and function of dendritic cells and their subsets in the steady state and the inflamed setting. Annu Rev Immunol. *31*, 563–604.

Michea, P., Noël, F., Zakine, E., Czerwinska, U., Sirven, P., Abouzid, O., Goudot, C., Scholer-Dahirel, A., Vincent-Salomon, A., Reyal, F., et al. (2018). Adjustment of dendritic cells to the breast-cancer microenvironment is subset specific. Nat Immunol. *19*, 885–897.

Miyazaki, M., Miyazaki, K., Itoi, M., Katoh, Y., Guo, Y., Kanno, R., Katoh-Fukui, Y., Honda, H., Amagai, T., van Lohuizen, M., et al. (2008). Thymocyte Proliferation Induced by Pre-T Cell Receptor Signaling Is Maintained through Polycomb Gene Product Bmi-1-Mediated Cdkn2a Repression. Immunity. *28*, 231–245.

Miyazaki, T., Kato, H., Nakajima, M., Sohda, M., Fukai, Y., Masuda, N., Manda, R., Fukuchi, M., Tsukada, K., and Kuwano, H. (2003). FAK overexpression is correlated with tumour invasiveness and lymph node metastasis in oesophageal squamous cell carcinoma. Br J Cancer. *89*, 140–145.

Morgan, M.R., Humphries, M.J., and Bass, M.D. (2007). Synergistic control of cell adhesion by integrins and syndecans. Nat Rev Mol Cell Biol. *8*, 957–969.

Mosser, D.M., and Edwards, J.P. (2008). Exploring the full spectrum of macrophage activation. Nat Rev Immunol. *8*, 958–969.

Movahedi, K., Guilliams, M., Van den Bossche, J., Van den Bergh, R., Gysemans, C., Beschin, A., De Baetselier, P., and van Ginderachter, J.A. (2008). Identification of discrete tumor-induced myeloid-derived suppressor cell subpopulations with distinct T cell-suppressive activity. Blood. *111*, 4233–4244.

Movahedi, K., Laoui, D., Gysemans, C., Baeten, M., Stangé, G., Van den Bossche, J., Mack, M., Pipeleers, D., In't Veld, P., De Baetselier, P., et al. (2010). Different tumor microenvironments contain functionally distinct subsets of macrophages derived from Ly6C(high) monocytes. Cancer Res. *70*, 5728–5739.

Möricke, A., Zimmermann, M., Valsecchi, M.G., Stanulla, M., Biondi, A., Mann, G., Locatelli, F., Cazzaniga, G., Niggli, F., Aricò, M., et al. (2016). Dexamethasone vs prednisone in induction treatment of pediatric ALL: results of the randomized trial AIEOP-BFM ALL 2000. Blood. *127*, 2101–2112.

Mu, X., Li, Y., and Fan, G.-C. (2020). Tissue-Resident Macrophages in the Control of Infection and Resolution of Inflammation. Shock. Online ahead of print.

Muhsin, M., Graham, J., and Kirkpatrick, P. (2004). Bevacizumab. Nat Rev Drug Discov. *3*, 995–996.

Musgrove, E.A., Caldon, C.E., Barraclough, J., Stone, A., and Sutherland, R.L. (2011). Cyclin D as a therapeutic target in cancer. Nat Rev Cancer. *11*, 558–572.

Naito, M., Umeda, S., Yamamoto, T., Moriyama, H., Umezu, H., Hasegawa, G., Usuda, H., Shultz, L.D., and Takahashi, K. (1996). Development, differentiation, and phenotypic heterogeneity of murine tissue macrophages. J Leukoc Biol. *59*, 133–138.

Neri, P., Ren, L., Azab, A.K., Brentnall, M., Gratton, K., Klimowicz, A.C., Lin, C., Duggan, P., Tassone, P., Mansoor, A., et al. (2011). Integrin β7-mediated regulation of multiple myeloma cell adhesion, migration, and invasion. Blood. *117*, 6202–6213.

Ness, K.K., Armenian, S.H., Kadan-Lottick, N., and Gurney, J.G. (2011). Adverse effects of treatment in childhood acute lymphoblastic leukemia: general overview and implications for long-term cardiac health. Expert Rev Hematol. *4*, 185–197.

Neufeld, G., Cohen, T., Gengrinovitch, S., and Poltorak, Z. (1999). Vascular endothelial growth factor (VEGF) and its receptors. Faseb J. *13*, 9–22.

Nguyen, K., Devidas, M., Cheng, S.-C., La, M., Raetz, E.A., Carroll, W.L., Winick, N.J., Hunger, S.P., Gaynon, P.S., Loh, M.L., et al. (2008). Factors influencing survival after relapse from acute lymphoblastic leukemia: a Children's Oncology Group study. Leukemia. *22*, 2142–2150.

Niehues, T., Kapaun, P., Harms, D.O., Burdach, S., Kramm, C., Körholz, D., Janka-Schaub, G., and Göbel, U. (1999). A classification based on T cell selection-related phenotypes identifies a subgroup of childhood T-ALL with favorable outcome in the COALL studies. Leukemia. *13*, 614–617.

Nieman, K.M., Kenny, H.A., Penicka, C.V., Ladanyi, A., Buell-Gutbrod, R., Zillhardt, M.R., Romero, I.L., Carey, M.S., Mills, G.B., Hotamisligil, G.S., et al. (2011). Adipocytes promote ovarian cancer metastasis and provide energy for rapid tumor growth. Nat Med. *17*, 1498–1503.

Nordenfelt, P., Elliott, H.L., and Springer, T.A. (2016). Coordinated integrin activation by actin-dependent force during T-cell migration. Nat Commun. *7*, 13119.

Noronha, E.P., Marques, L.V.C., Andrade, F.G., Thuler, L.C.S., Terra-Granado, E., Pombo-de-Oliveira, M.S., Brazilian Collaborative Study Group of Acute Leukemia (2019). The Profile of Immunophenotype and Genotype Aberrations in Subsets of Pediatric T-Cell Acute Lymphoblastic Leukemia. Front Oncol. *9*, 316.

Nowyhed, H.N., Huynh, T.R., Blatchley, A., Wu, R., Thomas, G.D., and Hedrick, C.C. (2015). The nuclear receptor nr4a1 controls CD8 T cell development through transcriptional suppression of runx3. Sci Rep. *5*, 9059.

Oishi, S., Takano, R., Tamura, S., Tani, S., Iwaizumi, M., Hamaya, Y., Takagaki, K., Nagata, T., Seto, S., Horii, T., et al. (2016). M2 polarization of murine peritoneal macrophages induces regulatory cytokine production and suppresses T-cell proliferation. Immunology. *149*, 320–328.

Orgel, E., Genkinger, J.M., Aggarwal, D., Sung, L., Nieder, M., and Ladas, E.J. (2016). Association of body mass index and survival in pediatric leukemia: a meta-analysis. Am J Clin Nutr. *103*, 808–817.

Orgel, E., Tucci, J., Alhushki, W., Malvar, J., Sposto, R., Fu, C.H., Freyer, D.R., Abdel-Azim, H., and Mittelman, S.D. (2014). Obesity is associated with residual leukemia following induction therapy for childhood B-precursor acute lymphoblastic leukemia. Blood. *124*, 3932–3938.

Pallegar, N.K., and Christian, S.L. (2020). Adipocytes in the Tumour Microenvironment. Adv Exp Med Biol. *1234*, 1–13.

Palomero, T., Lim, W.K., Odom, D.T., Sulis, M.L., Real, P.J., Margolin, A., Barnes, K.C., O'Neil, J., Neuberg, D., Weng, A.P., et al. (2006). NOTCH1 directly regulates c-MYC and activates a feed-forward-loop transcriptional network promoting leukemic cell growth. Proc Natl Acad Sci U S A. *103*, 18261–18266.

Palomero, T., Sulis, M.L., Cortina, M., Real, P.J., Barnes, K., Ciofani, M., Caparros, E., Buteau, J., Brown, K., Perkins, S.L., et al. (2007). Mutational loss of PTEN induces resistance to NOTCH1 inhibition in T-cell leukemia. Nat Med. *13*, 1203–1210.

Papayannidis, C., DeAngelo, D.J., Stock, W., Huang, B., Shaik, M.N., Cesari, R., Zheng, X., Reynolds, J.M., English, P.A., Ozeck, M., et al. (2015). A Phase 1 study of the novel gamma-secretase inhibitor PF-03084014 in patients with T-cell acute lymphoblastic leukemia and T-cell lymphoblastic lymphoma. Blood Cancer J. *5*, e350.

Passaro, D., Di Tullio, A., Abarrategi, A., Rouault-Pierre, K., Foster, K., Ariza-McNaughton, L., Montaner, B., Chakravarty, P., Bhaw, L., Diana, G., et al. (2017). Increased Vascular Permeability in the Bone Marrow Microenvironment Contributes to Disease Progression and Drug Response in Acute Myeloid Leukemia. Cancer Cell. *32*, 324–341.E6.

Passaro, D., Irigoyen, M., Catherinet, C., Gachet, S., Da Costa De Jesus, C., Lasgi, C., Quang, C.T., and Ghysdael, J. (2015). CXCR4 Is Required for Leukemia-Initiating Cell Activity in T Cell Acute Lymphoblastic Leukemia. Cancer Cell. *27*, 769–779.

Passaro, D., Quang, C.T., and Ghysdael, J. (2016). Microenvironmental cues for T-cell acute lymphoblastic leukemia development. Immunol Rev. *271*, 156–172.

Pear, W.S., Aster, J.C., Scott, M.L., Hasserjian, R.P., Soffer, B., Sklar, J., and Baltimore, D. (1996). Exclusive development of T cell neoplasms in mice transplanted with bone marrow expressing activated Notch alleles. J Exp Med. *183*, 2283–2291.

Pitt, L.A., Tikhonova, A.N., Hu, H., Trimarchi, T., King, B., Gong, Y., Sanchez-Martin, M., Tsirigos, A., Littman, D.R., Ferrando, A.A., et al. (2015). CXCL12-Producing Vascular Endothelial Niches Control Acute T Cell Leukemia Maintenance. Cancer Cell. *27*, 755–768.

Plotkin, J., Prockop, S.E., Lepique, A., and Petrie, H.T. (2003). Critical role for CXCR4 signaling in progenitor localization and T cell differentiation in the postnatal thymus. J Immunol. *171*, 4521–4527.

Pozzi, L.-A.M., Maciaszek, J.W., and Rock, K.L. (2005). Both dendritic cells and macrophages can stimulate naive CD8 T cells in vivo to proliferate, develop effector function, and differentiate into memory cells. J Immunol. *175*, 2071–2081.

Pui, C.-H., Relling, M.V., and Downing, J.R. (2004). Acute lymphoblastic leukemia. N Engl J Med. *350*, 1535–1548.

Qian, B.-Z., Li, J., Zhang, H., Kitamura, T., Zhang, J., Campion, L.R., Kaiser, E.A., Snyder, L.A., and Pollard, J.W. (2011). CCL2 recruits inflammatory monocytes to facilitate breast-tumour metastasis. Nature. *475*, 222–225.

Quail, D.F., and Joyce, J.A. (2013). Microenvironmental regulation of tumor progression and metastasis. Nat Med. *19*, 1423–1437.

Rabb, H. (2002). The T cell as a bridge between innate and adaptive immune systems: implications for the kidney. Kidney Int. *61*, 1935–1946.

Raetz, E.A., and Teachey, D.T. (2016). T-cell acute lymphoblastic leukemia. Hematology Am Soc Hematol Educ Program. *2016*, 580–588.

Ragon, B.K., Kantarjian, H., Jabbour, E., Ravandi, F., Cortes, J., Borthakur, G., DeBose, L., Zeng, Z., Schneider, H., Pemmaraju, N., et al. (2017). Buparlisib, a PI3K inhibitor, demonstrates acceptable tolerability and preliminary activity in a phase I trial of patients with advanced leukemias. Am J Hematol. *92*, 7–11.

Rajendran, P., Rengarajan, T., Thangavel, J., Nishigaki, Y., Sakthisekaran, D., Sethi, G., and Nishigaki, I. (2013). The vascular endothelium and human diseases. Int J Biol Sci. *9*, 1057–1069.

Ramachandran, P., Pellicoro, A., Vernon, M.A., Boulter, L., Aucott, R.L., Ali, A., Hartland, S.N., Snowdon, V.K., Cappon, A., Gordon-Walker, T.T., et al. (2012). Differential Ly-6C expression identifies the recruited macrophage phenotype, which orchestrates the regression of murine liver fibrosis. Proc Natl Acad Sci U S A. *109*, E3186–E3195.

Rapraeger, A.C. (2000). Syndecan-regulated receptor signaling. J Cell Biol. *149*, 995–998.

Reismüller, B., Attarbaschi, A., Peters, C., Dworzak, M.N., Pötschger, U., Urban, C., Fink, F.-M., Meister, B., Schmitt, K., Dieckmann, K., et al. (2009). Long-term outcome of initially homogenously treated and relapsed childhood acute lymphoblastic leukaemia in Austria--a population-based report of the Austrian Berlin-Frankfurt-Münster (BFM) Study Group. Br J Haematol. *144*, 559–570.

Reizis, B. (2019). Plasmacytoid Dendritic Cells: Development, Regulation, and Function. Immunity. *50*, 37–50.

Repnik, U., Knezevic, M., and Jeras, M. (2003). Simple and cost-effective isolation of monocytes from buffy coats. J Immunol Methods. *278*, 283–292.

Romano, E., Kusio-Kobialka, M., Foukas, P.G., Baumgaertner, P., Meyer, C., Ballabeni, P., Michielin, O., Weide, B., Romero, P., and Speiser, D.E. (2015). Ipilimumab-

dependent cell-mediated cytotoxicity of regulatory T cells ex vivo by nonclassical monocytes in melanoma patients. Proc Natl Acad Sci U S A. *112*, 6140–6145.

Rothenberg, E.V. (2011). T cell lineage commitment: identity and renunciation. J Immunol. *186*, 6649–6655.

Royer-Pokora, B., Loos, U., and Ludwig, W.D. (1991). TTG-2, a new gene encoding a cysteine-rich protein with the LIM motif, is overexpressed in acute T-cell leukaemia with the t(11;14)(p13;q11). Oncogene. *6*, 1887–1893.

Ryan, G.R., Dai, X.M., Dominguez, M.G., Tong, W., Chuan, F., Chisholm, O., Russell, R.G., Pollard, J.W., and Stanley, E.R. (2001). Rescue of the colony-stimulating factor 1 (CSF-1)-nullizygous mouse (Csf1(op)/Csf1(op)) phenotype with a CSF-1 transgene and identification of sites of local CSF-1 synthesis. Blood. *98*, 74–84.

Salmon, H., Idoyaga, J., Rahman, A., Leboeuf, M., Remark, R., Jordan, S., Casanova-Acebes, M., Khudoynazarova, M., Agudo, J., Tung, N., et al. (2016). Expansion and Activation of CD103(+) Dendritic Cell Progenitors at the Tumor Site Enhances Tumor Responses to Therapeutic PD-L1 and BRAF Inhibition. Immunity. *44*, 924–938.

Salomon, D.R., Crisa, L., Mojcik, C.F., Ishii, J.K., Klier, G., and Shevach, E.M. (1997). Vascular cell adhesion molecule-1 is expressed by cortical thymic epithelial cells and mediates thymocyte adhesion. Implications for the function of alpha4beta1 (VLA4) integrin in T-cell development. Blood. *89*, 2461–2471.

Samon, J.B., Castillo-Martin, M., Hadler, M., Ambesi-Impiobato, A., Paietta, E., Racevskis, J., Wiernik, P.H., Rowe, J.M., Jakubczak, J., Randolph, S., et al. (2012). Preclinical analysis of the γ-secretase inhibitor PF-03084014 in combination with glucocorticoids in T-cell acute lymphoblastic leukemia. Mol Cancer Ther. *11*, 1565–1575.

Sander, J., Schmidt, S.V., Cirovic, B., McGovern, N., Papantonopoulou, O., Hardt, A.-L., Aschenbrenner, A.C., Kreer, C., Quast, T., Xu, A.M., et al. (2017). Cellular Differentiation of Human Monocytes Is Regulated by Time-Dependent Interleukin-4 Signaling and the Transcriptional Regulator NCOR2. Immunity. *47*, 1051–1066.e12.

Saoncella, S., Echtermeyer, F., Denhez, F., Nowlen, J.K., Mosher, D.F., Robinson, S.D., Hynes, R.O., and Goetinck, P.F. (1999). Syndecan-4 signals cooperatively with integrins in a Rho-dependent manner in the assembly of focal adhesions and actin stress fibers. Proc Natl Acad Sci U S A. *96*, 2805–2810.

Sas, V., Moisoiu, V., Teodorescu, P., Tranca, S., Pop, L., Iluta, S., Pasca, S., Blag, C., Man, S., Roman, A., et al. (2019). Approach to the Adult Acute Lymphoblastic Leukemia Patient. J Clin Med. *8*, 1175.

Saxena, V., Ondr, J.K., Magnusen, A.F., Munn, D.H., and Katz, J.D. (2007). The countervailing actions of myeloid and plasmacytoid dendritic cells control autoimmune diabetes in the nonobese diabetic mouse. J Immunol. *179*, 5041–5053.

Sayeed, A., Fedele, C., Trerotola, M., Ganguly, K.K., and Languino, L.R. (2013). IGF-IR promotes prostate cancer growth by stabilizing α5β1 integrin protein levels. PLoS One. *8*, e76513.

Schittenhelm, L., Hilkens, C.M., and Morrison, V.L. (2017). β2 Integrins As Regulators of Dendritic Cell, Monocyte, and Macrophage Function. Front Immunol. *8*, 1866.

Schmall, A., Al-Tamari, H.M., Herold, S., Kampschulte, M., Weigert, A., Wietelmann, A., Vipotnik, N., Grimminger, F., Seeger, W., Pullamsetti, S.S., et al. (2015). Macrophage and cancer cell cross-talk via CCR2 and CX3CR1 is a fundamental mechanism driving lung cancer. Am J Respir Crit Care Med. *191*, 437–447.

Schneider, P., Vasse, M., Bayati, Al, A., Lenormand, B., and Vannier, J.-P. (2002). Is high expression of the chemokine receptor CXCR-4 of predictive value for early relapse in childhood acute lymphoblastic leukaemia? Br J Haematol. *119*, 579–580.

Schreiber, H.A., Loschko, J., Karssemeijer, R.A., Escolano, A., Meredith, M.M., Mucida, D., Guermonprez, P., and Nussenzweig, M.C. (2013). Intestinal monocytes and macrophages are required for T cell polarization in response to Citrobacter rodentium. J Exp Med. *210*, 2025–2039.

Schreiber, R.D., Old, L.J., and Smyth, M.J. (2011). Cancer immunoediting: integrating immunity's roles in cancer suppression and promotion. Science. *331*, 1565–1570.

Scott, C.L., T'Jonck, W., Martens, L., Todorov, H., Sichien, D., Soen, B., Bonnardel, J., De Prijck, S., Vandamme, N., Cannoodt, R., et al. (2018). The Transcription Factor ZEB2 Is Required to Maintain the Tissue-Specific Identities of Macrophages. Immunity. *49*, 312–325.e315.

Scott, C.L., Zheng, F., De Baetselier, P., Martens, L., Saeys, Y., De Prijck, S., Lippens, S., Abels, C., Schoonooghe, S., Raes, G., et al. (2016). Bone marrow-derived monocytes give rise to self-renewing and fully differentiated Kupffer cells. Nat Commun. *7*, 10321.

Scupoli, M.T., Perbellini, O., Krampera, M., Vinante, F., Cioffi, F., and Pizzolo, G. (2007). Interleukin 7 requirement for survival of T-cell acute lymphoblastic leukemia and human thymocytes on bone marrow stroma. Haematologica. *92*, 264–266.

Scupoli, M.T., Vinante, F., Krampera, M., Vincenzi, C., Nadali, G., Zampieri, F., Ritter, M.A., Eren, E., Santini, F., and Pizzolo, G. (2003). Thymic epithelial cells promote

survival of human T-cell acute lymphoblastic leukemia blasts: the role of interleukin-7. Haematologica. *88*, 1229–1237.

Serwold, T., Hochedlinger, K., Inlay, M.A., Jaenisch, R., and Weissman, I.L. (2007). Early TCR expression and aberrant T cell development in mice with endogenous prerearranged T cell receptor genes. J Immunol. *179*, 928–938.

Serwold, T., Hochedlinger, K., Swindle, J., Hedgpeth, J., Jaenisch, R., and Weissman, I.L. (2010). T-cell receptor-driven lymphomagenesis in mice derived from a reprogrammed T cell. Proc Natl Acad Sci U S A. *107*, 18939–18943.

Shafat, M.S., Oellerich, T., Mohr, S., Robinson, S.D., Edwards, D.R., Marlein, C.R., Piddock, R.E., Fenech, M., Zaitseva, L., Abdul-Aziz, A., et al. (2017). Leukemic blasts program bone marrow adipocytes to generate a protumoral microenvironment. Blood. *129*, 1320–1332.

Shah, D.K., and Zúñiga-Pflücker, J.C. (2014). An overview of the intrathymic intricacies of T cell development. J Immunol. *192*, 4017–4023.

Shank-Calvo, J.A., Draheim, K., Bhasin, M., and Kelliher, M.A. (2006). p16Ink4a or p19Arf loss contributes to Tal1-induced leukemogenesis in mice. Oncogene. *25*, 3023–3031.

Sharma, V.M., Calvo, J.A., Draheim, K.M., Cunningham, L.A., Hermance, N., Beverly, L., Krishnamoorthy, V., Bhasin, M., Capobianco, A.J., and Kelliher, M.A. (2006). Notch1 contributes to mouse T-cell leukemia by directly inducing the expression of c-myc. Mol Cell Biol. *26*, 8022–8031.

Sharpless, N.E., Bardeesy, N., Lee, K.-H., Carrasco, D., Castrillon, D.H., Aguirre, A.J., Wu, E.A., Horner, J.W., and DePinho, R.A. (2001). Loss of p16 Ink4a with retention of p19 Arf predisposes mice to tumorigenesis. Nature. *413*, 86–91.

Sheng, X., Parmentier, J.-H., Tucci, J., Pei, H., Cortez-Toledo, O., Dieli-Conwright, C.M., Oberley, M.J., Neely, M., Orgel, E., Louie, S.G., et al. (2017). Adipocytes Sequester and Metabolize the Chemotherapeutic Daunorubicin. Mol Cancer Res. *15*, 1704–1713.

Sherr, C.J., and Weber, J.D. (2000). The ARF/p53 pathway. Curr Opin Genet Dev. *10*, 94–99.

Shi, S., Zhong, D., Xiao, Y., Wang, B., Wang, W., Zhang, F., and Huang, H. (2017). Syndecan-1 knockdown inhibits glioma cell proliferation and invasion by deregulating a c-src/FAK-associated signaling pathway. Oncotarget. *8*, 40922–40934.

Sicinska, E., Aifantis, I., Le Cam, L., Swat, W., Borowski, C., Yu, Q., Ferrando, A.A., Levin, S.D., Geng, Y., Boehmer, von, H., et al. (2003). Requirement for cyclin D3 in lymphocyte development and T cell leukemias. Cancer Cell. *4*, 451–461.

Sieg, D.J., Hauck, C.R., Ilic, D., Klingbeil, C.K., Schaefer, E., Damsky, C.H., and Schlaepfer, D.D. (2000). FAK integrates growth-factor and integrin signals to promote cell migration. Nat Cell Biol. *2*, 249–256.

Siegel, R.L., Miller, K.D., and Jemal, A. (2020). Cancer statistics, 2020. CA Cancer J Clin. *70*, 7–30.

Silva, A., Laranjeira, A.B.A., Martins, L.R., Cardoso, B.A., Demengeot, J., Yunes, J.A., Seddon, B., and Barata, J.T. (2011). IL-7 contributes to the progression of human T-cell acute lymphoblastic leukemias. Cancer Res. *71*, 4780–4789.

Sipkins, D.A., Wei, X., Wu, J.W., Runnels, J.M., Côté, D., Means, T.K., Luster, A.D., Scadden, D.T., and Lin, C.P. (2005). In vivo imaging of specialized bone marrow endothelial microdomains for tumour engraftment. Nature. *435*, 969–973.

Smith, S., Tripathi, R., Goodings, C., Cleveland, S., Mathias, E., Hardaway, J.A., Elliott, N., Yi, Y., Chen, X., Downing, J., et al. (2014). LIM domain only-2 (LMO2) induces T-cell leukemia by two distinct pathways. PLoS One. *9*, e85883.

Solito, S., Marigo, I., Pinton, L., Damuzzo, V., Mandruzzato, S., and Bronte, V. (2014). Myeloid-derived suppressor cell heterogeneity in human cancers. Ann N Y Acad Sci. *1319*, 47–65.

Soneson, C., Love, M.I., and Robinson, M.D. (2015). Differential analyses for RNA-seq: transcript-level estimates improve gene-level inferences. F1000Res. *4*, 1521.

Soulier, J. (2005). HOXA genes are included in genetic and biologic networks defining human acute T-cell leukemia (T-ALL). Blood. *106*, 274–286.

Spadaro, O., Camell, C.D., Bosurgi, L., Nguyen, K.Y., Youm, Y.-H., Rothlin, C.V., and Dixit, V.D. (2017). IGF1 Shapes Macrophage Activation in Response to Immunometabolic Challenge. Cell Rep. *19*, 225–234.

Spoo, A.C., Lübbert, M., Wierda, W.G., and Burger, J.A. (2007). CXCR4 is a prognostic marker in acute myelogenous leukemia. Blood. *109*, 786–791.

Stambolic, V., Suzuki, A., la Pompa, de, J.L., Brothers, G.M., Mirtsos, C., Sasaki, T., Ruland, J., Penninger, J.M., Siderovski, D.P., and Mak, T.W. (1998). Negative regulation of PKB/Akt-dependent cell survival by the tumor suppressor PTEN. Cell. *95*, 29–39.

Steinbuck, M.P., and Winandy, S. (2018). A Review of Notch Processing With New Insights Into Ligand-Independent Notch Signaling in T-Cells. Front Immunol. *9*, 1230.

Struhl, G., and Greenwald, I. (2001). Presenilin-mediated transmembrane cleavage is required for Notch signal transduction in Drosophila. Proc Natl Acad Sci U S A. *98*, 229–234.

Subramaniam, P.S., Whye, D.W., Efimenko, E., Chen, J., Tosello, V., De Keersmaecker, K., Kashishian, A., Thompson, M.A., Castillo, M., Cordon-Cardo, C., et al. (2012). Targeting nonclassical oncogenes for therapy in T-ALL. Cancer Cell. *21*, 459–472.

Sulis, M.L., and Parsons, R. (2003). PTEN: from pathology to biology. Trends Cell Biol. *13*, 478–483.

Sunderkötter, C., Nikolic, T., Dillon, M.J., van Rooijen, N., Stehling, M., Drevets, D.A., and Leenen, P.J.M. (2004). Subpopulations of mouse blood monocytes differ in maturation stage and inflammatory response. J Immunol. *172*, 4410–4417.

Suzuki, A., Yamaguchi, M.T., Ohteki, T., Sasaki, T., Kaisho, T., Kimura, Y., Yoshida, R., Wakeham, A., Higuchi, T., Fukumoto, M., et al. (2001). T cell-specific loss of Pten leads to defects in central and peripheral tolerance. Immunity. *14*, 523–534.

Talmadge, J.E., and Gabrilovich, D.I. (2013). History of myeloid-derived suppressor cells. Nat Rev Cancer. *13*, 739–752.

Tavares, A.J., Poon, W., Zhang, Y.-N., Dai, Q., Besla, R., Ding, D., Ouyang, B., Li, A., Chen, J., Zheng, G., et al. (2017). Effect of removing Kupffer cells on nanoparticle tumor delivery. Proc Natl Acad Sci U S A. *114*, E10871–E10880.

Taylor, J., Xiao, W., and Abdel-Wahab, O. (2017). Diagnosis and classification of hematologic malignancies on the basis of genetics. Blood. *130*, 410–423.

Tcyganov, E., Mastio, J., Chen, E., and Gabrilovich, D.I. (2018). Plasticity of myeloid-derived suppressor cells in cancer. Curr Opin Immunol. *51*, 76–82.

Terwilliger, T., and Abdul-Hay, M. (2017). Acute lymphoblastic leukemia: a comprehensive review and 2017 update. Blood Cancer J. *7*, e577–e577.

Triplett, T.A., Cardenas, K.T., Lancaster, J.N., Hu, Z., Selden, H.J., Jasso, G.J., Balasubramanyam, S., Chan, K., Li, L., Chen, X., et al. (2016). Endogenous dendritic cells from the tumor microenvironment support T-ALL growth via IGF1R activation. Proc Natl Acad Sci U S A. *113*, E1016–E1025.

Tzoneva, G., Perez-Garcia, A., Carpenter, Z., Khiabanian, H., Tosello, V., Allegretta, M., Paietta, E., Racevskis, J., Rowe, J.M., Tallman, M.S., et al. (2013). Activating mutations

in the NT5C2 nucleotidase gene drive chemotherapy resistance in relapsed ALL. Nat Med. *19*, 368–371.

Uckun, F.M., Gaynon, P.S., Sensel, M.G., Nachman, J., Trigg, M.E., Steinherz, P.G., Hutchinson, R., Bostrom, B.C., Sather, H.N., and Reaman, G.H. (1997). Clinical features and treatment outcome of childhood T-lineage acute lymphoblastic leukemia according to the apparent maturational stage of T-lineage leukemic blasts: a Children's Cancer Group study. J Clin Oncol. *15*, 2214–2221.

Ulyanova, T., Scott, L.M., Priestley, G.V., Jiang, Y., Nakamoto, B., Koni, P.A., and Papayannopoulou, T. (2005). VCAM-1 expression in adult hematopoietic and nonhematopoietic cells is controlled by tissue-inductive signals and reflects their developmental origin. Blood. *106*, 86–94.

Uzan, B., Poglio, S., Gerby, B., Wu, C.-L., Gross, J., Armstrong, F., Calvo, J., Cahu, X., Deswarte, C., Dumont, F., et al. (2014). Interleukin-18 produced by bone marrow-derived stromal cells supports T-cell acute leukaemia progression. EMBO Mol Med. *6*, 821–834.

Vadillo, E., Dorantes-Acosta, E., Pelayo, R., and Schnoor, M. (2018). T cell acute lymphoblastic leukemia (T-ALL): New insights into the cellular origins and infiltration mechanisms common and unique among hematologic malignancies. Blood Rev. *32*, 36–51.

van Furth, R., Cohn, Z.A., Hirsch, J.G., Humphrey, J.H., Spector, W.G., and Langevoort, H.L. (1972). The mononuclear phagocyte system: a new classification of macrophages, monocytes, and their precursor cells. Bull World Health Organ. *46*, 845–852.

van Rooijen, N., and Hendrikx, E. (2010). Liposomes for specific depletion of macrophages from organs and tissues. Methods Mol Biol. *605*, 189–203.

Venneri, M.A., De Palma, M., Ponzoni, M., Pucci, F., Scielzo, C., Zonari, E., Mazzieri, R., Doglioni, C., and Naldini, L. (2007). Identification of proangiogenic TIE2-expressing monocytes (TEMs) in human peripheral blood and cancer. Blood. *109*, 5276–5285.

Vicente, C., Schwab, C., Broux, M., Geerdens, E., Degryse, S., Demeyer, S., Lahortiga, I., Elliott, A., Chilton, L., La Starza, R., et al. (2015). Targeted sequencing identifies associations between IL7R-JAK mutations and epigenetic modulators in T-cell acute lymphoblastic leukemia. Haematologica. *100*, 1301–1310.

Voermans, C., van Heese, W.P.M., de Jong, I., Gerritsen, W.R., and van Der Schoot, C.E. (2002). Migratory behavior of leukemic cells from acute myeloid leukemia patients. Leukemia. *16*, 650–657.

Vogelstein, B., Papadopoulos, N., Velculescu, V.E., Zhou, S., Diaz, L.A., and Kinzler, K.W. (2013). Cancer genome landscapes. Science. *339*, 1546–1558.

Walling, B.L., and Kim, M. (2018). LFA-1 in T Cell Migration and Differentiation. Front Immunol. *9*, 952.

Watanabe, S., Alexander, M., Misharin, A.V., and Budinger, G.R.S. (2019). The role of macrophages in the resolution of inflammation. J Clin Invest. *129*, 2619–2628.

Weng, A.P., Ferrando, A.A., Lee, W., Morris, J.P., Silverman, L.B., Sanchez-Irizarry, C., Blacklow, S.C., Look, A.T., and Aster, J.C. (2004). Activating mutations of NOTCH1 in human T cell acute lymphoblastic leukemia. Science. *306*, 269–271.

Weng, A.P., Millholland, J.M., Yashiro-Ohtani, Y., Arcangeli, M.L., Lau, A., Wai, C., del Bianco, C., Rodriguez, C.G., Sai, H., Tobias, J., et al. (2006). c-Myc is an important direct target of Notch1 in T-cell acute lymphoblastic leukemia/lymphoma. Genes Dev. *20*, 2096–2109.

Wilcox-Adelman, S.A., Denhez, F., and Goetinck, P.F. (2002). Syndecan-4 modulates focal adhesion kinase phosphorylation. J Biol Chem. *277*, 32970–32977.

Williams, J.W., Tjota, M.Y., Clay, B.S., Vander Lugt, B., Bandukwala, H.S., Hrusch, C.L., Decker, D.C., Blaine, K.M., Fixsen, B.R., Singh, H., et al. (2013). Transcription factor IRF4 drives dendritic cells to promote Th2 differentiation. Nat Commun. *4*, 2990.

Winkelmann, E.R., Widman, D.G., Xia, J., Johnson, A.J., van Rooijen, N., Mason, P.W., Bourne, N., and Milligan, G.N. (2014). Subcapsular sinus macrophages limit dissemination of West Nile virus particles after inoculation but are not essential for the development of West Nile virus-specific T cell responses. Virology. *450-451*, 278–289.

Winter, S.S., Sweatman, J., Shuster, J.J., Link, M.P., Amylon, M.D., Pullen, J., Camitta, B.M., and Larson, R.S. (2002). Bone marrow stroma-supported culture of T-lineage acute lymphoblastic leukemic cells predicts treatment outcome in children: a Pediatric Oncology Group study. Leukemia. *16*, 1121–1126.

Winter, S.S., Sweatman, J.J., Lawrence, M.B., Rhoades, T.H., Hart, A.L., and Larson, R.S. (2001). Enhanced T-lineage acute lymphoblastic leukaemia cell survival on bone marrow stroma requires involvement of LFA-1 and ICAM-1. Br J Haematol. *115*, 862–871.

Witkowski, M.T., Kousteni, S., and Aifantis, I. (2020). Mapping and targeting of the leukemic microenvironment. J Exp Med. *217*, 126.

Wu, J., Li, J., Salcedo, R., Mivechi, N.F., Trinchieri, G., and Horuzsko, A. (2012). The proinflammatory myeloid cell receptor TREM-1 controls Kupffer cell activation and development of hepatocellular carcinoma. Cancer Res. *72*, 3977–3986.

Wu, Y., Kuang, D.-M., Pan, W.-D., Wan, Y.-L., Lao, X.-M., Wang, D., Li, X.-F., and Zheng, L. (2013). Monocyte/macrophage-elicited natural killer cell dysfunction in hepatocellular carcinoma is mediated by CD48/2B4 interactions. Hepatology. *57*, 1107–1116.

Xia, Y., Brown, L., Yang, C.Y., Tsan, J.T., Siciliano, M.J., Espinosa, R., Le Beau, M.M., and Baer, R.J. (1991). TAL2, a helix-loop-helix gene activated by the (7;9)(q34;q32) translocation in human T-cell leukemia. Proc Natl Acad Sci U S A. *88*, 11416–11420.

Xu, H., Gonzalo, J.A., St Pierre, Y., Williams, I.R., Kupper, T.S., Cotran, R.S., Springer, T.A., and Gutierrez-Ramos, J.C. (1994). Leukocytosis and resistance to septic shock in intercellular adhesion molecule 1-deficient mice. J Exp Med. *180*, 95–109.

Yang, F., Feng, W., Wang, H., Wang, L., Liu, X., Wang, R., Chen, C., Yang, X., Zhang, D., Ren, Q., et al. (2020). Monocyte-Derived Leukemia-Associated Macrophages Facilitate Extramedullary Distribution of T-cell Acute Lymphoblastic Leukemia Cells. Cancer Res. *80*, 3677–3691.

Yang, J., Nie, J., Ma, X., Wei, Y., Peng, Y., and Wei, X. (2019). Targeting PI3K in cancer: mechanisms and advances in clinical trials. Mol Cancer. *18*, 26–28.

Yang, X., Feng, W., Wang, R., Yang, F., Wang, L., Chen, S., Chen, C., Ren, Q., and Zheng, G. (2018). Hepatic leukemia-associated macrophages exhibit a pro-inflammatory phenotype in Notch1-induced acute T cell leukemia. Immunobiology. *223*, 73–80.

Yona, S., Kim, K.-W., Wolf, Y., Mildner, A., Varol, D., Breker, M., Strauss-Ayali, D., Viukov, S., Guilliams, M., Misharin, A., et al. (2013). Fate mapping reveals origins and dynamics of monocytes and tissue macrophages under homeostasis. Immunity. *38*, 79–91.

You, D., Xin, J., Volk, A., Wei, W., Schmidt, R., Scurti, G., Nand, S., Breuer, E.-K., Kuo, P.C., Breslin, P., et al. (2015). FAK mediates a compensatory survival signal parallel to PI3K-AKT in PTEN-null T-ALL cells. Cell Rep. *10*, 2055–2068.

Zamisch, M., Moore-Scott, B., Su, D.-M., Lucas, P.J., Manley, N., and Richie, E.R. (2005). Ontogeny and regulation of IL-7-expressing thymic epithelial cells. J Immunol. *174*, 60–67.

Zenatti, P.P., Ribeiro, D., Li, W., Zuurbier, L., Silva, M.C., Paganin, M., Tritapoe, J., Hixon, J.A., Silveira, A.B., Cardoso, B.A., et al. (2011). Oncogenic IL7R gain-of-

function mutations in childhood T-cell acute lymphoblastic leukemia. Nat Genet. *43*, 932–939.

Zhang, J., Ding, L., Holmfeldt, L., Wu, G., Heatley, S.L., Payne-Turner, D., Easton, J., Chen, X., Wang, J., Rusch, M., et al. (2012). The genetic basis of early T-cell precursor acute lymphoblastic leukaemia. Nature. *481*, 157–163.

Zhao, X., Qu, J., Sun, Y., Wang, J., Liu, X., Wang, F., Zhang, H., Wang, W., Ma, X., Gao, X., et al. (2017). Prognostic significance of tumor-associated macrophages in breast cancer: a meta-analysis of the literature. Oncotarget. *8*, 30576–30586.

Zhou, X., Franklin, R.A., Adler, M., Jacox, J.B., Bailis, W., Shyer, J.A., Flavell, R.A., Mayo, A., Alon, U., and Medzhitov, R. (2018). Circuit Design Features of a Stable Two-Cell System. Cell. *172*, 744–757.e17.

Zilionis, R., Engblom, C., Pfirschke, C., Savova, V., Zemmour, D., Saatcioglu, H.D., Krishnan, I., Maroni, G., Meyerovitz, C.V., Kerwin, C.M., et al. (2019). Single-Cell Transcriptomics of Human and Mouse Lung Cancers Reveals Conserved Myeloid Populations across Individuals and Species. Immunity. *50*, 1317–1334.e10.